frontiers | Research Topics

Circulating molecular biomarkers: Next-generation tools for monitoring minimal residual disease in cancer patients

Edited by
Rana Jahanban-Esfahlan, Zohreh Amoozgar and Mehdi - Jaymand

Published in
Frontiers in Oncology

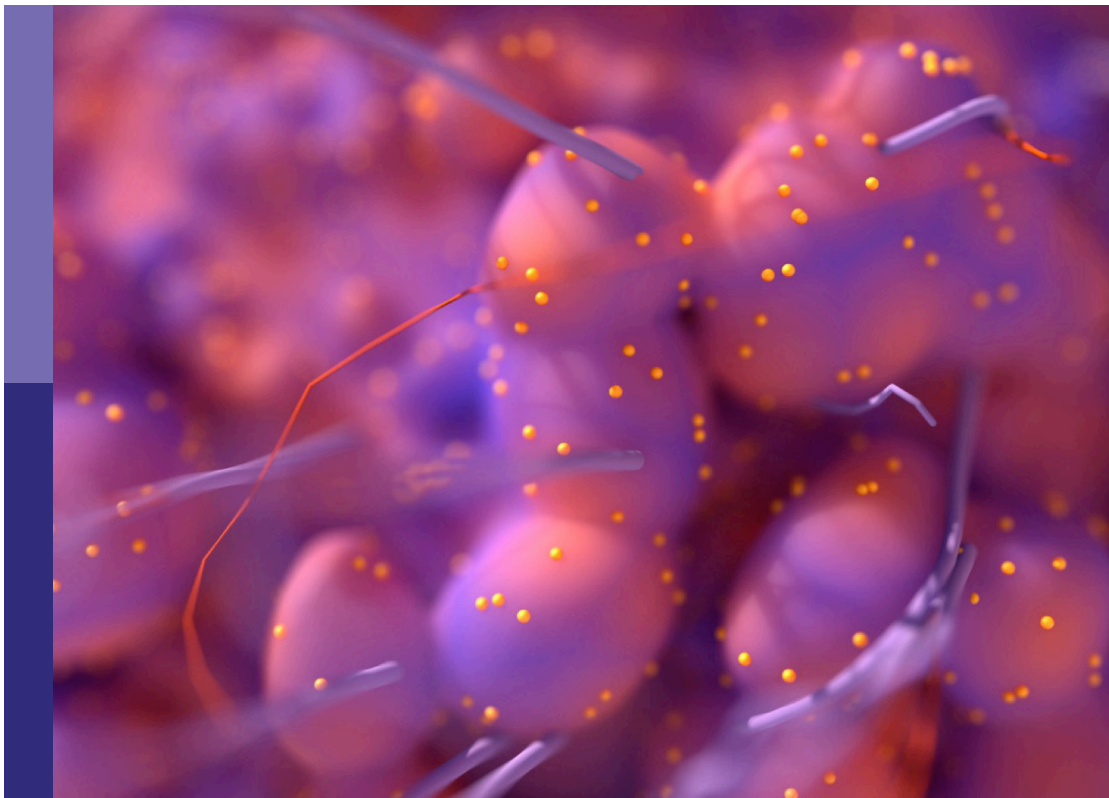

ISSN 1664-8714
ISBN 978-2-8325-3192-1
DOI 10.3389/978-2-8325-3192-1

About Frontiers

Frontiers is more than just an open access publisher of scholarly articles: it is a pioneering approach to the world of academia, radically improving the way scholarly research is managed. The grand vision of Frontiers is a world where all people have an equal opportunity to seek, share and generate knowledge. Frontiers provides immediate and permanent online open access to all its publications, but this alone is not enough to realize our grand goals.

Frontiers journal series

The Frontiers journal series is a multi-tier and interdisciplinary set of open-access, online journals, promising a paradigm shift from the current review, selection and dissemination processes in academic publishing. All Frontiers journals are driven by researchers for researchers; therefore, they constitute a service to the scholarly community. At the same time, the *Frontiers journal series* operates on a revolutionary invention, the tiered publishing system, initially addressing specific communities of scholars, and gradually climbing up to broader public understanding, thus serving the interests of the lay society, too.

Dedication to quality

Each Frontiers article is a landmark of the highest quality, thanks to genuinely collaborative interactions between authors and review editors, who include some of the world's best academicians. Research must be certified by peers before entering a stream of knowledge that may eventually reach the public - and shape society; therefore, Frontiers only applies the most rigorous and unbiased reviews. Frontiers revolutionizes research publishing by freely delivering the most outstanding research, evaluated with no bias from both the academic and social point of view. By applying the most advanced information technologies, Frontiers is catapulting scholarly publishing into a new generation.

What are Frontiers Research Topics?

Frontiers Research Topics are very popular trademarks of the *Frontiers journals series*: they are collections of at least ten articles, all centered on a particular subject. With their unique mix of varied contributions from Original Research to Review Articles, Frontiers Research Topics unify the most influential researchers, the latest key findings and historical advances in a hot research area.

Find out more on how to host your own Frontiers Research Topic or contribute to one as an author by contacting the Frontiers editorial office: frontiersin.org/about/contact

Circulating molecular biomarkers: Next-generation tools for monitoring minimal residual disease in cancer patients

Topic editors

Rana Jahanban-Esfahlan — Tabriz University of Medical Sciences, Iran

Zohreh Amoozgar — Massachusetts General Hospital, Harvard Medical School, United States

Mehdi - Jaymand — Kermanshah University of Medical Sciences, Iran

Citation

Jahanban-Esfahlan, R., Amoozgar, Z., Jaymand, M., eds. (2023). *Circulating molecular biomarkers: Next-generation tools for monitoring minimal residual disease in cancer patients*. Lausanne: Frontiers Media SA. doi: 10.3389/978-2-8325-3192-1

Table of contents

frontiers | Frontiers in Oncology

TYPE Editorial
PUBLISHED 24 July 2023
DOI 10.3389/fonc.2023.1226974

OPEN ACCESS

EDITED AND REVIEWED BY
Tao Liu,
University of New South Wales, Australia

*CORRESPONDENCE
Rana Jahanban-Esfahlan
jahanbanr@tbzmed.ac.ir

RECEIVED 22 May 2023
ACCEPTED 14 July 2023
PUBLISHED 24 July 2023

CITATION
Amoozgar Z, Jaymand M and Jahanban-Esfahlan R (2023) Editorial: Circulating molecular biomarkers: next-generation tools for monitoring minimal residual disease in cancer patients.
Front. Oncol. 13:1226974.
doi: 10.3389/fonc.2023.1226974

Editorial: Circulating molecular biomarkers: next-generation tools for monitoring minimal residual disease in cancer patients

Zohreh Amoozgar[1], Mehdi Jaymand[2] and Rana Jahanban-Esfahlan[3]*

[1]Edwin L. Steele Laboratories, Department of Radiation Oncology, Massachusetts General Hospital and Harvard Medical School, Boston, MA, United States, [2]Nano Drug Delivery Research Center, Health Technology Institute, Kermanshah University of Medical Sciences, Kermanshah, Iran, [3]Department of Medical Biotechnology, Faculty of Advanced Medical Sciences, Tabriz University of Medical Sciences, Tabriz, Iran

KEYWORDS

tumor biomarkers, circulating tumor cells (CTCs), exosomes, cell-free DNA, liquid biopsy, cancer metastasis

Editorial on the Research Topic
Circulating molecular biomarkers: next-generation tools for monitoring minimal residual disease in cancer patients

Traditional cancer diagnosis relies on tissue biopsy, blood testing, and medical imaging, in which by the detection time, tumor size has reached several millimeters in size, and metastatic spread may have already begun. Plus, there is no accurate and timely way to monitor treatment response following surgery or drug treatment. Taking these shortcomings into account, new reliable tumor-specific biomarkers/tools that allow non-invasive early cancer detection, patient stratification for therapy, and monitoring of anti-cancer therapeutic regimens are highly demanded. The discovery of circulatory materials, including circulating tumor cells (CTCs), exosomes, cell-free DNA, and apoptotic bodies, and advances made in the fabrication of ultrasensitive biosensors that can capture and interrogate these rare yet valuable materials in different bodily fluids, plus advances in sequencing (NGS) methods and systems biology approaches have paved the path for the emergence of liquid biopsy and introduction of next-generation prognostic and diagnostic tools more powerful than traditional methods for better prediction and stratification and decision making for cancer patients at any stage from early detection to minimal residual disease monitoring (MRD) (1, 2).

In this Research Topic, several papers have reviewed the current status of circulating materials in cancer. Such that, Yi et al. shed light on the clinical use of exosomes as novel biomarkers for cancer diagnosis by focusing on exosome biogenesis, exogenous factors involved in exosome releasing from tumor cells, especially autophagy, hypoxia and

pharmacology, and exosomal molecular cargoes as potential biomarkers in liquid biopsy for cancer diagnosis. From a different point of view, Nonaka reviewed the pontifical of chemically and genetically engineered exosomes for targeted therapy purposes and as next-generation therapeutics to overcome drug resistance. As current MRD assays are based on targeting somatic mutations, Johnston et al. emphasized the current state of both genetic and epigenetic liquid biopsies for MRD detection. Compared to genetic alterations, epigenetic changes are more frequent and universal in cancer, and cfDNA is enriched with epigenetic modifications, including DNA methylation alterations and fragmentation patterns. Finally, the authors discuss the emerging paradigm of genetic and epigenetic assays for monitoring treatment response, detecting the recurrence of disease, and informing adjuvant therapy.

Circulating proteins represent a major resource of MRD and disease monitoring. However, the scope of peptide-based circulating biomarkers is limited as they only contain one-fourth of the entire proteome. To surmount this, Tanuwidjaya et al. highlighted the importance of the Soluble Human Leukocyte Antigen (HLA) that presents peptides from the entire proteome on the cell surface. The authors reviewed the currently available tools to detect and quantify sHLA circulating biomarkers and further discussed these biomarkers' challenges and future perspectives in a clinical setting.

In the sense of targeted drug delivery platforms for MRD, Mahmudi et al. highlighted the role of specific nanoparticle design formats and deciphered the role of tumor microenvironment penetrating chitosan nanoparticles to eliminate cancer relapse and MRD. This review focuses on the many advantages of chitosan as a suitable drug delivery system when combined with other biomaterials, to form hybrid and multitasking chitosan-based systems for numerous applications, in particular post-surgery implants (immunovaccines) and biosensors of tumor-derived circulating materials, as well as multimodal systems, to eliminate bulk tumors as well as lingering tumor cells to treat MRD and recurrent cancer.

In a research article, Sampathi et al. reported NanoporeMinION sequencing of clonal B cell-specific rearrangement of the (IGH) locus in cfDNA in 5 pediatric B-ALL patient samples as a biomarker for acute lymphoblastic leukemia (ALL) and MRD and its spread into the central nervous system (CNS). As a simple, rapid, and inexpensive assay, Nanopore IGH detection could monitor cell-free DNA for clinical diagnoses of MRD and CNS disease, even when diagnostic cell-count thresholds for MRD were not physically met.

Mi et al. reported a case of post-surgery and chemoradiotherapy laryngeal carcinoma patient with a high ratio of aneuploid circulating tumor endothelial cells (CTECs) to CTCs> 5 with rapid *de novo* development into pancreatic carcinomas. SE-iFISH detected a substantial amount of 107 non-hematological aneuploid circulating rare cells, including 14 CTCs (CD31-/CD45-) and 93 CTECs (CD31+/CD45-) five months before plasma increasing of CA19-9 and ten months prior to imaging-assisted diagnosis of *de novo* pancreatic cancer. Thus co-detection of aneuploid CD31- CTCs and CD31+ CTECs and the ratio CTECs to CTCs may help in the real-time evaluation of therapeutic efficacy, longitudinal monitoring of MDR, MRD, and reliable predicting post-therapy occurrence or distant metastatic recurrence of malignancy.

As an additional biomarker, Zha et al. reported the significance of FCGR3A as a new biomarker with potential predictive value for prostate cancer (PCa) using bioinformatics analysis. PPI and KEGG, as two bioinformatics tools, revealed the target gene cluster of FCGR3A, HAVCR2, CCR7, and CD28 with a high expression of FCGR3A and HAVCR2 in PCa tissue microarray ($P<0.01$). These two genes also showed a significant difference in BCR-free survival of FCGR3A and HAVCR2 as revealed by Kaplan-Meier analysis. Finally, TCGA clinical data analysis found that the expression of FCGR3A had a striking correlation with PCa clinicopathological features and tumor stage.

Wang et al. investigated the role of folate receptor-positive CTC count, lymphocyte count (LC), and derived neutrophil-to-lymphocyte ratio (dNLR) for diagnosing lung cancer relapse. Results from the clinicopathological features, routine blood tests, and CTC counts of the 69 patients indicated that a higher FR+-CTC count predicted a worse disease-or progression-free survival (DFS/PFS) in patients with lung cancer. Likewise, a retrospective study by Zhang et al. investigated the application of postoperative ctDNA for monitoring tumor recurrence in patients with non-small cell lung cancer (NSCLC) who underwent radical surgery operation followed by adjuvant therapy. Defining a positive molecular residue disease (MRD) as having at least one true shared mutation in both plasma and tissue samples from the same patient indicated that a lower recurrence-free survival (RFS) was accompanied by positive postoperatively ctDNA and MRD presence was a strong predictor of disease recurrence. The ctDNA-based MRD was a strong prognostic of RFS higher than all other clinicopathological variables and even the traditional TNM staging.

Circulatory materials and liquid biopsy are newly emerged discoveries with multiple FDA-approved tests. As such, Clonoseq explores clonally expanded VDJ sequences in blood and bone marrow-derived gDNA samples to identify and detect as few as one leukemic blast per million cells in blood cancer patients, with a sensitivity of 6.77×10^{-7} (3, 4). Also, in 2020, FoundationOne's Liquid CDx cfDNA was introduced to detect cfDNA with specific mutations in solid tumors (5). Also, in ALL, cfDNA assays can detect bone marrow relapse 30 days earlier than the standard flow cytometry-based methods. Altogether, these data pinpoint the critical role of circulating materials in the future of diagnostic tools for cancer monitoring and control of MRD. Liquid biopsy and novel biomarker discovery are expected to become the forefront of the next-coming diagnostic toolkits and pave the way for realizing personalized medicine. However, the high cost

is the limiting factor for the broad applicability of these tests, given their high sensitivity, specificity, and diagnostic value compared to traditional sample biopsy coupled with NGS, biosensing devices, and systems biology approaches yet continue to reveal and offer new opportunities by introducing novel biomarkers to predict and win the game in the battle of cancer as well as other diseases.

Author contributions

ZA, MJ, and RJ-E have equally written and edited the editorial. All authors contributed to the article and approved the submitted version.

Conflict of interest

The authors declare that the research was conducted in the absence of any commercial or financial relationships that could be construed as a potential conflict of interest.

Publisher's note

References

1. Baghban R, Roshangar L, Jahanban-Esfahlan R, Seidi K, Ebrahimi-Kalan A, Jaymand M, et al. Tumor microenvironment complexity and therapeutic implications at a glance. *Cell Commun Signaling* (2020) 18(1):59. doi: 10.1186/s12964-020-0530-4

2. Lone SN, Nisar S, Masoodi T, Singh M, Rizwan A, Hashem S, et al. Liquid biopsy: a step closer to transform diagnosis, prognosis and future of cancer treatments. *Mol Cancer* (2022) 21(1):79. doi: 10.1186/s12943-022-01543-7

3. Ching T, Duncan ME, Newman-Eerkes T, McWhorter MME, Tracy JM, Steen MS, et al. Analytical evaluation of the clonoSEQ Assay for establishing measurable (minimal) residual disease in acute lymphoblastic leukemia, chronic lymphocytic leukemia, and multiple myeloma. *BMC Cancer* (2020) 20(1):612. doi: 10.1186/s12885-020-07077-9

4. Oliva S, Genuardi E, Belotti A, Frascione PMM, Galli M, Capra A, et al. Minimal residual disease evaluation by multiparameter flow cytometry and next generation sequencing in the forte trial for newly diagnosed multiple myeloma patients. *Blood* (2019) 134:4322. doi: 10.1182/blood-2019-124645

5. Woodhouse R, Li M, Hughes J, Delfosse D, Skoletsky J, Ma P, et al. Clinical and analytical validation of FoundationOne Liquid CDx, a novel 324-Gene cfDNA-based comprehensive genomic profiling assay for cancers of solid tumor origin. *PloS One* (2020) 15(9):e0237802. doi: 10.1371/journal.pone.0237802

frontiers | Frontiers in Oncology

TYPE Review
PUBLISHED 31 August 2022
DOI 10.3389/fonc.2022.966981

OPEN ACCESS

EDITED BY
Mehdi Jaymand,
Kermanshah University of Medical Sciences, Iran

REVIEWED BY
Saravanakumar Marimuthu,
University of Nebraska Medical Center, United States
Vincenzo Lionetti,
Sant'Anna School of Advanced Studies, Italy

*CORRESPONDENCE
Tianyu Zhong
zhongtianyu@gmail.com

SPECIALTY SECTION
This article was submitted to Molecular and Cellular Oncology, a section of the journal Frontiers in Oncology

RECEIVED 12 June 2022
ACCEPTED 01 August 2022
PUBLISHED 31 August 2022

CITATION
Yi X, Chen J, Huang D, Feng S, Yang T, Li Z, Wang X, Zhao M, Wu J and Zhong T (2022) Current perspectives on clinical use of exosomes as novel biomarkers for cancer diagnosis. *Front. Oncol.* 12:966981. doi: 10.3389/fonc.2022.966981

Current perspectives on clinical use of exosomes as novel biomarkers for cancer diagnosis

Xiaomei Yi[1,2], Jie Chen[1,2], Defa Huang[1,2], Shuo Feng[3], Tong Yang[1,2], Zhengzhe Li[1,2], Xiaoxing Wang[1,2], Minghong Zhao[1,2], Jiyang Wu[1,2] and Tianyu Zhong[1,2]*

[1]The First School of Clinical Medicine, Gannan Medical University, Ganzhou, China, [2]Laboratory Medicine, First Affiliated Hospital of Gannan Medical University, Ganzhou, China, [3]English Teaching and Research Section, Gannan Healthcare Vocational College, Ganzhou, China

Exosomes are a heterogeneous subset of extracellular vesicles (EVs) that biogenesis from endosomes. Besides, exosomes contain a variety of molecular cargoes including proteins, lipids and nucleic acids, which play a key role in the mechanism of exosome formation. Meanwhile, exosomes are involved with physiological and pathological conditions. The molecular profile of exosomes reflects the type and pathophysiological status of the originating cells so could potentially be exploited for diagnostic of cancer. This review aims to describe important molecular cargoes involved in exosome biogenesis. In addition, we highlight exogenous factors, especially autophagy, hypoxia and pharmacology, that regulate the release of exosomes and their corresponding cargoes. Particularly, we also emphasize exosome molecular cargoes as potential biomarkers in liquid biopsy for diagnosis of cancer.

KEYWORDS

exosomes, extracellular vesicles (EVs), biogenesis, exogenous factors, release, molecular cargoes, diagnostics, biomarkers

Introduction

Extracellular vesicles (EVs) are secreted from almost all cell types (1), and widely distributed in various body fluids, such as urine (2), blood (3), milk (4), saliva (5), cerebrospinal fluid (6), amniotic fluid (7) and semen (8), can transmit information between cells and participate in many physiological and pathological processes. It is known that the extraction and isolation of exosomes from different body fluids are mainly achieved by ultracentrifugation, ultrafiltration, sedimentation, density gradient centrifugation, immune-capture, precipitation and commercial reagents(Table 1). Exosomes are bi-layered lipid vesicles produced by the endosomal pathway, a subset of EVs with a diameter of 30-150nm (36, 37). However, due to the limitations of the isolation method, we usually define the particles less than 200nm in diameter are

TABLE 1 Methods for isolation of exosomes from different biological sample types.

Sample types	Isolation methods	Types of cargo	References
Urine	UC,UF,DGC,SEC,PC,PEG,IC,MF,CRG	Proteins, MiRNAs, Lipids	(9–12)
Blood	UC,UF,DGC,SEC,PC,PEG,IC,MF,CRG	Proteins, MiRNAs, Lipids	(13–17)
Milk	UC,UF, DGC,SEC,PC,CRG	Proteins,RNAs,MiRNAs,Lipids	(18–21)
Saliva	UC, UF, DGC,SEC,PC,CRG	Proteins, MiRNAs	(22–25)
Cerebrospinal fluid	UC,UF,SEC, PC,CRG	Proteins, MiRNAs	(26–30)
Amniotic fluid	UC,UF,CRG	Proteins, MiRNAs,	(31, 32)
Semen	UC, UF,PC,PEG,CRG	Proteins, MiRNAs	(33–35)

UC, ultracentrifugation; UF, ultrafiltration; DGC, density gradient centrifugation; PC, precipitation PEG, polyethylene glycol precipitation; IC, immuno-capture; MF, microfluidics; SEC, size-exclusion chromatography; CRG, Commercial reagents.

exosomes. Therefore, the International Society of Extracellular Vesicle (ISEV) statement in the Minimum Information on Extracellular Vesicle Research 2018 (MISEV2018) recommends the use of "EVs" as a general term (36). In this review, EVs mainly refer to exosomes without special instructions.

Exosomes are present in biological fluids as a form of intercellular communication to transport proteins, lipids, nucleic acids, and metabolites to the pericellular environment (38, 39). Exosome biogenesis are tightly regulated, possibly by interactions with different effectors (40, 41), which mainly involved with ESCRT-dependent and ESCRT-independent mechanisms (42). Exosome biogenesis begins in the endocytic pathway, where the plasma membrane invagination packages cell membrane proteins and some extracellular components together to form the early endosomes (EEs) (43, 44). After that, EEs exchange substances with other organelles, or further mature into late endosomes (LEs), and the late endosomal membrane invaginate to form multiple vesicles (MVBs) containing luminal vesicles (ILVs). Next, MVBs bind to lysosomes or autophagosomes for degradation, or they are transported to the plasma membrane through the cytoskeleton and microtubule network, which then efflux to form exosomes (Figure 1A) (45–47). Interestingly, exosomal cargo molecules

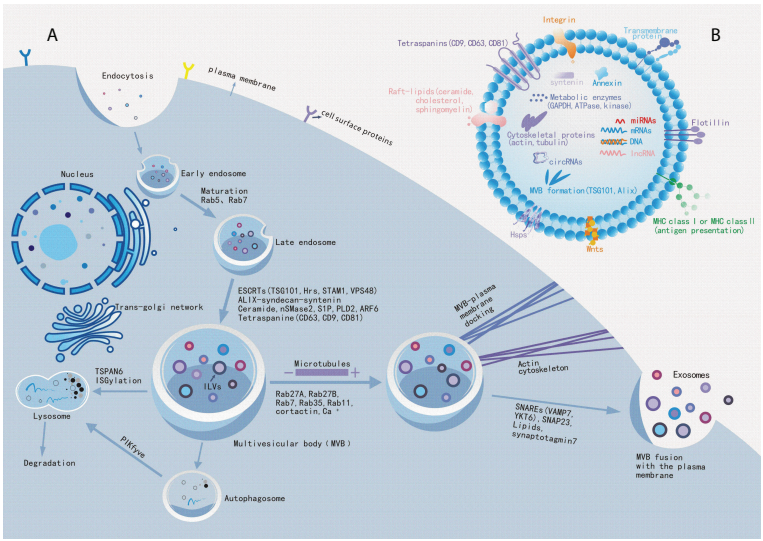

FIGURE 1
Exosome biogenesis. **(A)**: Schematic diagram of the molecular mechanisms of exosome biogenesis. Extracellular components, such as proteins, lipids, nucleic acids and small molecules, can enter cells with cell surface proteins through endocytosis and plasma membrane invagination. Under endocytosis, it leads to the formation of early endosomes and late endosomes, which bud out into multiple vesicles (MVBs) containing luminal vesicles (ILVs). Some molecules, such as ESCRT proteins (ALIX, TSG101, etc.), lipids and tetraspanin proteins mediate this process. Subsequently, MVBs will fuse to lysosomes or autophagosomes to accelerate their degradation to inhibit exosome release, or MVBs transported along the cytoskeleton and microtubule network to the plasma membrane after maturation, where it can fuse with the plasma membrane and release exosomes into extracellular space. Among these, Rabs, Actin and SNARE proteins are involved in exosome release.**(B)**: Exosome biomarkers. Exosomal luminal cargoes are mainly composed of proteins, lipids, nucleic acids, and other metabolites that can function in the recipient cells. Among these, CD9, CD63, CD81, flotillin, and Annexin can be used as exosome biomarkers.

(Figure 1B) (proteins, lipids, and nucleic acids) regulate the whole process (42, 45, 48, 49). For example, tetraspanin proteins (e. g.: CD9, CD63, CD81, CD82), major histocompatibility complex (MHC) molecules, heat shock proteins (HSPs), endosomal sorting complex (ESCRT) proteins (e. g. Alix, TSG101), Rab proteins, actin, soluble N-acetamide sensitive factor attachment proteins (SNAREs) are the major participating proteins (50–53). Similarly, lipid components such as ceramide, cholesterol, phosphatidic acid, phosphatidylinositol 3-phosphate, phosphatidylinositol-3, 5-diphosphate, and sphingosine 1-phosphate are also involved in the process (54–57). A summary of the molecular cargoes associated with exosome biogenesis process is presented in Table 2.

Initial studies suggested that exosomes were some waste materials excreted by cells in order to maintain homeostasis (138). Recent reports suggest that exosomes are capable of material transport and information transfer between cells, thereby mediating many physiological and pathological processes (51, 72, 139, 140). Furthermore, these small vesicles are involved in immunomodulation and intercellular communication (141), and mediate the disease progression of cancer (142), cardiovascular disease (143–145), metabolic disease (146), degenerative change (147) and autoimmunity (148). It is currently believed that the key to exosomes biological functions lies in their molecular cargoes, including proteins, lipids, and nucleic acids. For example, phosphatidylinositol glycan-1 (GPC1) is a cell surface proteoglycan rich in cancer cell-derived exosomes, and Melo et al. (120) identified that GPC1 has the potential for early detection of pancreatic cancer lesions to promote the possibility of curative surgical treatment (120) found that CRC cell-derived exosomal HSPC111 protein promotes pre-metastatic niche formation and CRC liver metastases (CRLM) *via* reprogramming lipid metabolism in cancer-associated fibroblasts (CAFs), which implicate HSPC111 may be a potential therapeutic target for preventing CRLM (149). In addition, phosphatidylserine, cholesterol and ceramide are also play key roles in exosome formation, which affect cargo sorting, signaling and exosomes structure (150, 151). MicroRNAs (miRNAs) are one of the most abundant RNA species in exosomes, and miRNAs play roles in various biological

TABLE 2 The Role of Related Molecular Cargoes in Exosome Formation.

Molecular Cargo Types	Process Involved	The Role Played in Exosome Formation	References
Proteins			
Tetraspanin proteins (e. g., CD9, CD63, CD81, CD82)	Exosome biogenesis, the targeting and release of exosomes cargo	Mediating the budding of ILVs and interacting with cholesterol to induce membrane curvature and the fusion of MVBs with the plasma membrane	(58–61)
Major histocompatibility composite (MHC) molecules (e. g., class MHC I and class MHC II)	Exosome biogenesis and antigen presentation	Mediating the budding of the ILVs	(62, 63)
Heat shock proteins (Hsps) (e. g. HSP90 and HSP70)	Exosome release and signaling	Induced membrane deformation and the fusion of MVBs with the plasma membrane	(64, 65)
ESCRT proteins (e. g., Alix, TSG101)	Exosome biogenesis	Interaction with the s yndecans-syntenin-Alix complex promotes the budding of ILVs	(66–68)
Rab proteins (e. g., Rab11, Rab35, Rab27A, and Rab27B)	Exosome biogenesis and release	Involved in vesicle budding, transport, and fusion	(69–71)
actin	Exosome release	Participating in the transport process of MVBs	(72, 73)
SNARE proteins	Exosome release	Induced fusion of MVBs with the plasma membrane	(74, 75)
Lipids			
ceramide	Exosome biogenesis and cargo sorting	Negative curvature of the induced membrane	(76, 77)
cholesterol	Exosome biogenesis, transport, and release	MVBs are induced to fuse with the plasma membrane, interact with ORP1L and control endosome movement along microtubules	(78–80)
sphingomyelin	Exosome biogenesis and signaling	Negative curvature of the induced membrane	(77, 81)
PA	Exosome biogenesis	Induced the negative curvature of the membrane, interacting with syntenin to recruit syndecan, CD63, and ALIX at the budding site	(82, 83)
Phosphatidylinositol 3-phosphate	Cargo sorting	Interaction with HRS proteins sorted cargo into endosomes and binding with ESCRT-0 in the membrane to recruit ESCRT-I, -II and-III	(84, 85)
Phosphatidylinositol-3, 5-diphosphate	Exosome release	Fusion with lysosomes regulates MVBs with lysosomal degradation	(86)
1-Sphingosine phosphate	Cargo sorting	Interactions with the inhibitory G protein-coupled S1P receptors in the MVBs membrane	(87)

processes such as exocytosis and exosome-mediated cellular communication (73, 152). For example, Fu et al. (153) found that exosomes content miR-98-5p inhibits the progression of pancreatic ductal adenocarcinoma(PDAC) by targeting MAPK signaling (153). In addition, microarray profiles identified that miR-106a-5p and miR-19b-3p were remarkably overexpressed in the serum exosomes of patients with gastric cancer(GC). Notably, integrating the two miRNAs could identify GC patients among healthy volunteers with a 0.814 area under the curve (AUC) value, which was higher than that obtained using CEA or AFP (154). *Of note*, the parental information of these exosomes may differ significantly between healthy people and patients, making some molecular cargoes in exosomes potentially as specific biomarkers of cancer. Importantly, the ability to selectively control the release of exosomes in pathological situations without compromising their role as essential components in physiological situations would make exosomes have promising clinical applications in disease diagnosis, treatment and prognosis. In this review, we conclude the role of exosomes molecular cargoes in their biogenesis. We also underline the potential mechanisms by which autophagy, hypoxia and pharmacology exogenous factors affect exosome release. And summarize the key roles of exosome molecular cargoes play in cancer diagnosis. Furthermore, we discuss the challenges and potential applications of exosomes research.

Exogenous factors modulate exosome release

The biogenesis of exosomes is influenced by a variety of extrinsic factors in addition to the molecular correlation of the above-mentioned cargoes. A greater understanding of the underlying mechanisms that influence exosome release factors could provide new targets for disease diagnosis and treatment. The potential mechanisms by which autophagy, hypoxia, and pharmacological factors affect exosome release are presented below.

Autophagy modulates exosome release

Autophagy is a process that causes the degradation of cellular material at the lysosome. Autophagosomes can fuse with MVBs or directly with lysosomes to degrade cargoes (155). It was found that autophagy-related proteins, such as ATG5 and ATG16L1, affects exosome release process. For example, Abdulrahma et al. reported that when the autophagy protein ATG5 was knocked down, it greatly promoted the release of prion protein (PRNP) exosomes (156). Recently, Zheng et al. demonstrated that sulforaphane inhibits autophagy and induces exosome release *via* regulating mTOR/TEF3 (157). In addition, Guo et al. showed that ATG16L1 and ATG5 autophagy proteins protected MVBs from lysosomal degradation and thus facilitated the fusion of MVBs with the plasma membrane to facilitate exosome release. Conversely, silencing of ATG16L1 and ATG5 decreased exosome release, probably due to the ability of ATG5 to separate ATP6V1E1 from V1V0-ATPase, thereby inhibiting MVBs acidification and facilitating exosome release (158). Crucially, Keller et al. identified that ATG proteins promoted exosome release through a lysosomal non-dependent pathway, i.e. secretory autophagy, which in turn excreted bacterial toxin receptors from the membrane surface in the form of exosomes, assisting host cells to resist toxin damage and enhancing the antimicrobial response of the organism (159). These studies all suggest that autophagy may play a specific role to affect exosome release.

Hypoxia modulates exosome release

Hypoxia may affect exosome release through hypoxia-inducible factors (HIF), Rab-GTPases, NF-κB and four transmembrane protein signaling pathways, but the specific mechanisms involved remains unclear (160). Hypoxia-inducible factor (HIF) is a major component of the hypoxia-related signaling pathway that directly or indirectly regulates the process of exosome release. Recently, it has been reported that HIF mediates endocytosis mainly by increasing the expression of glucose transporter protein (GLUT-1), transferrin receptor and epidermal growth factor receptor (EGFR), which in turn induces exosome release (161). It was found that the increased release of exosomes from rat proximal renal tubular cells (RPTC) (162) and breast cancer cells (163) in hypoxic environment was mainly mediated by HIF-1α. In particular, hypoxia can cause glycolysis and lactate accumulation. Ban et al. demonstrated that exosome markers such as CD9, CD63, and HSP70 expression increased under acidic conditions and were more conducive to exosome release, whereas exosomal proteins and exosomal RNA were not detected in alkaline environments and exosome release was reduced (164). Wang et al. demonstrated that hypoxia increased the number of exosomes released from colorectal cancer cells compared to hyperoxic conditions (165). On the other hand, hypoxia not only alters exosome size, sorting mechanisms and exosome uptake and binding capacity in the tumor microenvironment, but also impacts exosome-mediated tumor biological functions (166). Interestingly, different hypoxic conditions, such as duration and severity of hypoxia, can have dramatically variable impacts on the amount and content of exosomes released by different cell types (167)

Pharmacology modulates exosome release

Nowadays, utilizing exosome as nanomaterials for drug delivery is of great interest to researchers. Notably, drugs may have a dramatic impact on drug repositioning and as potential novel anticancer agents by affecting certain molecules in the exosome release process. However, there are no drugs available to control the production of harmful exosomes in tumor cells (168). PH and Ca2+ are required for exosome release. Amiloride is a drug that inhibits Na +/H + exchange pump and Na +/Ca 2+ channels, and Savina et al. demonstrated that it reduced exosome release (169). Importantly, amiloride inhibits ceramide formation by indirectly inhibiting acid sphingomyelinase (aSMase), which in turn inhibits exosome release (170). Similarly, promethazine, a tricyclic antidepressant, has been found to reduce exosome release through inhibition of aSMase activity in the prostate cancer cell line PC3 by Kosgodage et al. (171). Metformin is the first-line drug for the treatment of type 2 diabetes, which increases insulin sensitivity and reduces fat synthesis (172). Recently, Liao et al. have demonstrated that metformin promotes the fusion of MVBs with the plasma membrane through autophagy and thus increased exosome release from mesenchymal stem cells (MSCs), which improved their therapeutic effect on senescent cells (173). In addition, metformin may promote exosome release to regulate stress by increasing the production of reactive oxygen species in tumor cells (174). Gao al.demonstrated that all-trans retinoic acid suppressed GES-1 cell proliferation induced by exosomes from patients with precancerous lesions by arresting the cell cycle in S-phase (175). Therefore, these drugs may act by acting on certain molecules released from exosomes, promoting exosome release may be a protective method against drug stress conditions to eliminate cellular damage.

Ticagrelor is a purinergic drug, it has been widely used in patients with acute coronary syndrome (ACS) and myocardial infarction (176). Existing studies have reported that ticagrelor enhanced the release of cell-derived exosomes from the anti-hypoxic cardiac group by increasing cell proliferation *in vitro* (177). In addition, extracellular vesicles derived from cardiomyocytes pretreated with ticagrelor have a protective effect on hyperglycemic cardiomyocytes by attenuating oxidative and endoplasmic reticulum stress (178). Recently, Kulshreshtha et al. confirmed that simvastatin, a HMG CoA inhibitor, mediates exosome release by altering MVBs transport and that its mediated reduction in monocyte-derived exosome secretion is protective *in vitro* model of atherosclerosis (179). Likewise, exosomes derived from mesenchymal stem cells (MSCs) pretreated with atorvastatin (ATV) dramatically enhanced the efficacy of treatment of acute myocardial infarction (AMI), possibly by enhancing endothelial cell function through paracrine mechanisms (180). It was also found that extracellular vesicles of cannabis with high cannabidiol (CBD) content induce anticancer signaling in human hepatocellular carcinoma (181).

Notably, Zhang et al. reported that neutral sphingomyelinase inhibitor (Manumycin A) and ketoconazole had no effect on exosomes released from normal cells, but affected exosomes released from tumor cells, which is crucial for disease treatment (182). It remains to be further investigated whether this can be mediated by the influence of proto-oncogenes and/or oncogenes in the tumor cells or by other factors. Considering that most of the experiments were performed on tumors, it remains to be further explored how these drugs affect the cancer phenotype by influencing the exosome release process and thus the cancer phenotype. Furthermore, we need to be aware that drugs have certain side effects. In the future, there is also need to focus on what doses of these drugs should be used to reach specific sites of cancer in a particular way to inhibit or promote exosome release as a form of cancer treatment.

In addition, other factors such as food compounds (183, 184), temperature (185, 186), radiotherapy (187) and chemotherapy (188, 189)affect intercellular communication mechanisms by mediating exosome release process, which allows exosomes to perform different functions and then contributes to the diagnosis and treatment of diseases.

Exosome molecular cargoes are used as disease diagnostic biomarkers

Exosome components indicate the biological state of the initiating cells and reflect the health status of the organs. Recently, more and more studies have shown that EVs contents can be applied in the diagnosis of various diseases (13, 190–193). This section summarizes the biomarkers that may become clinically common diseases in several major classes of molecular cargoes.

Exosomal nucleic acids

Exosomal mRNAs

Messenger RNA (mRNA) is a single-stranded ribonucleic acid that carries genetic information and can guide protein synthesis. mRNA is not only an important exosome cargo, but also acts as a functional modulator in cancer cell-derived exosome processes (194). In order to study the diagnostic performance of circulating exosomal messenger RNA (emRNA) and tissue mRNA in prostate cancer (PCa) patients, Ji et al. (195) demonstrated circulating emRNA is more advantageous as a diagnostic biomarker in PCa patients. Recipient operating characteristic curve (ROC) analysis indicated that the AUC value of circulating emRNA in PCa

screening and diagnosis was 0.948 and 0.851 respectively. Furthermore, the six molecules in emRNA including CDC42, IL32, MAX, NCF2, PDGFA and SRSF2 were upregulated in the screening and diagnosis of PCa patients compared to healthy controls (195). Similarly, Shephard et al. (88) said that serum-derived EV-mRNA has great potential for the differential diagnosis of prostate cancer. Among these, increased serum-derived EV-mRNA CTGF molecule or decreased EV-mRNA CAV1 molecule were closely associated with the rate of disease progression, and the AUC values of CTGF and CAV1 were 0.8600 and 0.8100 respectively. However, serum PSA could not predict disease progression, suggesting that EV-mRNA CTGF and CAV1 are superior to PSA in predicting disease progression (88). Another study proved that mRNA index of membrane matrix type 1 metalloproteinase (MT1-MMP) was significantly up-regulated in gastric cancer (GC) patients, with an AUC of 0.788, sensitivity of 63.9% and specificity of 87.1%, while the AUC value of serum CEA was only 0.655. Meanwhile, the combined exosomes diagnosis of mRNA(MT1-MMP) and CEA (AUC=0.821) was significantly better than the detection of mRNA (MT1-MMP) or CEA separately in identifying GC patients. In addition, it has been shown that exosomal epithelial growth factor receptor (EGFR) mRNA may be a potential predictor of glioblastoma (196). Serum exosome mRNA(MT1-MMP) was significantly associated with tumor differentiation, depth of invasion, lymphatic metastasis, distal metastasis and TNM stage (89). In brief, these studies show that exosomal mRNAs may have the potential to act as cancer biomarkers, but their specificity for the disease should be further investigated.

Exosomal miRNAs

MiRNA is a class of small endogenous noncoding RNA composed of 18-24 nucleotides, and the miRNA that delivered to the recipient cells can regulate various gene expression by preventing translation and inducing mRNA degradation (197). In addition, Exosomal miRNAs are more stable than free miRNAs as they are protected from degradation owing to RNase activity in biofluids (198). Recent studies have revealed that exosomal miRNAs may serve as potential biomarkers in certain cancers. For example, Yang et al. (104) found that exosomal miR-423-5p level was highly expressed in gastric cancer (GC) patients serum, and the AUC values of exosomal miR-423-5p, serum CEA and CA-199 were 0.763, 0.596 and 0.607 respectively (104). Notably, the combined detection of miRNAs can improve diagnostic accuracy. Huang et al. (199) found that six miRNAs were significantly higher expressed in serum exosomes of GC patients, whose AUC values were 0.627 (miR-10b-5p), 0.652 (miR-132-3p), 0.637 (miR-185-5p), 0.683 (miR-195-5p), 0.637 (miR-20a-3p) and 0.652 (miR-296-5p). At the same time, the AUC of the combined detection of the six miRNAs was 0.703, significantly improved the diagnostic accuracy of GC patients (199). Another study showed that the AUC values of serum exosomal miR-19b-3p and miR-106a-5p were 0.813 and 0.806 respectively. The AUC of their combined diagnosis was 0.826 (154). Similarly, in urinary exosomes from patients with renal clear cell carcinoma (ccRCC), different combinations of miRNAs, including miR-126-3p + miR-449a, miR-126-3p + miR-34b-5p, miR-126-3p + miR-486-5p, miR-25-3p + miR-34b-5p, miR-34b-5p, miR-2 b-5p-34 b-5p and miR-150-5 p + miR-126-3p have been reported to be potential diagnostic biomarkers in ccRCC patients. The sensitivities of these six combinations were 60.6%, 67.3%, 52.9%, 73.1%, 74%, and 61.5% respectively. Accordingly, specificities were 100%, 82.8%, 95.8%, 79.3%, 72.4%, and 82.8%, respectively. Furthermore, the targets of these miRNAs may be related to cell cycle regulation, tumorigenesis and angiogenesis (200). Muramatsu-Maekawa et al. (201) stated that miRNA-4525 in serum EVs is significantly higher expression in patients with advanced renal cell carcinoma (RCC) (201). Initially, serum exosomal miR-17-5p and miR-21 levels were considered as potential biomarkers for the differentiation of primary adenocarcinoma (PC). The mean levels of miR-17-5p and miR-21 were significantly higher in PC patients than in healthy controls (HPs) and non-PC groups, and the AUC values for miR-17-5p and miR-21 were 0.887 and 0.897 respectively, and the sensitivity and specificity of miR-17-5p were 72.7% and 92.6%, and 95.5% and 81.5% for miR-21 respectively (93). Subsequently, serum exosomal miRNAs (including miR-1246, miR-4644, miR-3976, and miR-4306) were also proposed as potential diagnostic biomarkers for pancreatic cancer (202). Notably, Manterola et al. (203) found that serum exosomal miR-320 and miR-574-3p were significantly higher expression in patients with glioblastoma multiforme (GBM) as compared with healthy controls, and ROC curve analysis indicated AUC for exosomal miR-320 and miR-574-3p of 0.720 and 0.738 respectively (203). In conclusion, exosomal miRNAs may be regarded as potential biomarkers of diseases.

Exosomal lncRNAs

In addition to miRNAs, exosomal lncRNAs are also attractive as potential diagnostic biomarkers. Long noncoding RNA (lncRNA) exists in the nucleus or cytoplasm, and they can interact with DNA, RNA, or proteins (204). Several studies have shown that exosomal lncRNAs may have the potential to act as biomarkers for cancer diagnosis. For example, plasma expression of lncUEGC1 was significantly higher in gastric cancer (GC) patients of stage I or II, and plasma exosomal lncUEGC1 (AUC =0.8760) was significantly superior to serum CEA (AUC = 0.6614). This suggests that exosomal lncUEGC1 may be a highly potential sensitive biomarker in early gastric cancer diagnosis (107). In addition, serum exosomal lncRNA HOTTIP was found to be a potential diagnostic index for gastric cancer patients. The ROC curve indicated that HOTTIP had

high diagnostic value with an AUC value of 0.827 and higher diagnostic power than CEA, CA19-9 and CA72-4 (AUC values of 0.653, 0.685 and 0.639, respectively). It's important that HOTTIP expression level was significantly correlated with the depth of invasion and TNM stage in gastric cancer (108). Another study confirmed that circulating exosomal long noncoding RNA-GC1 (lncRNA-GC1) expression could distinguish early gastric cancer patients and healthy controls, and ROC curve indicated that better exosomal lncRNA-GC1 (AUC=0.9033) compared to serum CEA, CA72-4 and CA19-9 (AUC values of 0.5987,0.6816 and 0.6482, respectively) (109). In addition, LINC00152 was also significantly elevated in the plasma exosomes of gastric cancer patients. Elevated exosomal LINC00152 was considered as a potential diagnostic indicator of gastric cancer with an AUC value of 0.657 (205). Similarly, Xiao et al. (110) demonstrated that lncRNA CCAT1 was significantly higher in serum EVs in gastric cancer patients than in healthy controls, chronic gastritis or dysplasia, with EVs lncRNA CCAT1 having an AUC of 0.890, sensitivity of 79.6%, specificity of 92.6%, while EVs lncRNA CCAT1 and embryo antibody combinations of 0.910 of 80.5% and 92.6% respectively. Moreover, EVs lncRNA CCAT1 may promote gastric cancer cells proliferation, migration and invasion through c-Myc or Bmi-1 upmodulation (110).

Exosomal circRNAs

Circular RNA (circRNA) is a class of noncoding RNA, mainly produced by pre-mRNA splicing. In contrast to miRNA, circRNA is abnormally stable, conserved and has cells or tissue-specific expression pattern (206). Exosomal circRNAs are anti-degradative, and its secretion into the extracellular environment can be used for many biological applications. Importantly, exosomal circRNAs may serve as novel diagnostic biomarkers. For example, Shao et al. (115) found that the expression of plasma exosomal hsa_circ_0065149 was significantly reduced in gastric cancer patients compared with healthy cohort, suggesting that reduced hsa_circ_0065149 is a potential diagnostic biomarker for gastric cancer (AUC=0.640) (115). Similarly, Xie et al. (116) found significant higher serum circSHKBP1 level in gastric cancer patients with a sharp decrease in exosomal circSHKBP1 after surgical resection of the tumor (116). A previous study in plasma EVs from breast cancer patients proved that nine circRNAs (including hsa_circ_0002190, hsa_circ_0007177, hsa_circ_0000642, hsa_circ_0001439, hsa_circ_0001417, hsa_circ_0005552, hsa_circ_0001073, hsa_circ_0000267 and hsa_circ_04004) combinations display maximum AUC values, and the AUC is 0.83 (207). In cholangiocarcinoma, circ-0000284 was significantly elevated in cholangiocarcinoma cell lines, its tissues and plasma exosomes, and higher expression of circ-0000284 promoted the migration, invasion and proliferation capacity of cholangiocarcinoma cells *in vitro* and *in vivo* (208). Therefore, the exosomal circ-0000284 could be used as a potential metastatic diagnostic biomarker. Circulating exosomal hsa-circ-0004771 was significantly upregulated in colorectal cancer (CRC) patients and AUC values of hsa-circ-0004771 were 0.59, 0.86 and 0.88 in differentiating between intercancer, stage I/II and CRC patients and healthy controls respectively, suggesting that hsa-circ-0004771 could serve as a new potential diagnostic biomarker for CRC patients (209). Moreover, exosomal circRNAs in serum and urine have the potential to act as diagnostic biomarker for idiopathic membranous nephropathy (IMN) (210). In short, these studies suggest that exosomal circRNAs have the possibility of act as biomarkers for disease diagnosis. However, whether its expression levels are specific for different disease and tumor subtypes remains to be further investigated.

Exosomal proteins

In addition to nucleic acids, exosomal proteins have been found to act as potential biomarkers for diseases. Because exosomes contain multiple protein molecules that reflect the characteristics of its parental cells (211). Exosomal proteins have been found in different body fluids (including serum, plasma, urine, saliva and cerebrospinal fluid) and may have the potential to serve as biomarkers for cancer diagnosis. For example, the cell surface proteoglycan Glypican-1 (GPC1), a member of the heparan sulfate proteoglycan family, is a widespread cell surface protein (212). It has been suggested that GPC1-positive exosomal was highly expressed in the serum of pancreatic cancer patients, and the diagnostic power of the exosomal protein GPC1 (AUC = 1.0) was significantly better than CA19-9 (AUC =0.739) in distinguishing pancreatic cancer patients from healthy controls. CA19-9 serum levels cannot distinguish patients with intraductal papillary mucinous tumors (PCPL) from healthy controls, while GPC1-positive serum exosomal had 100% sensitivity and specificity in all stages of pancreatic cancer (e. g.: cancer in situ, stage I, and stage II-IV) (120). Similarly, the exosomal protein GPC1 expression was significantly increased in both plasma and tissue samples of colorectal cancer (CRC) patients, and both normalized after surgical treatment (213). Another study indicated that the downregulation of serum exosomal Gastrokine 1 (GKN1) protein may be a valid diagnostic biomarker in gastric cancer patients (129).

Recently, the proteomic analysis of extracellular vesicles and granules (EVP) from 426 human samples derived from tissue explants (TE), plasma and other body fluids by Hoshino et al. (214). They confirmed that CD63 and flotillins were heterogeneous in plasma and tissue EVP. And Leucine-rich repeat protein 26 (LRRC26), ATP-dependent translocase ABCB1 (ABCB1), Bile salt export pump (ABCB11), Adhesion G protein-coupled receptor G6 (ADGRG6), Desmosomes-1

(DSC1), Desmoglein-1 (DSG1), Keratin and Plasminogen-like protein B (PLGLB1) were present only in plasma-derived EVP in patients with pancreatic cancer (PaCa), absent or extremely low expression in tumor tissue (TT) and adjacent normal tissue (AT) -derived EVP. This suggests that these proteins have the potential to act as characteristic tumor-associated EVP proteins. In addition, they said that EVP proteins can distinguish between cancer in the early stages of pancreatic cancer (PaCa) and lung adenocarcinoma (Luca) patients (214). It is interesting that, by proteomic analysis of Sun et al. (215), Annexin family members (Annexin A1, A2, A3, A5, A6, A11), Nitrogen permease regulator 2-like protein(NPRL2), Carcinoembryonic antigen-related cell adhesion molecule 1 (CEACAM1), Mucin 1(MUC1), Prominin-1 (PROM1), Histone H4 (HIST1H4A) and Tumor necrosis factor alpha-induced protein 3 (TNFAIP3) were associated with lung cancer, which is helpful in lung cancer diagnosis (215). The expression levels of plasma exosomal Tim-3 and Galectin-9 protein molecules were significantly increased in non-small-cell lung cancer (NSCLC) patients, as compared with healthy controls. It's important that exosomal Tim-3 and Galectin-9 expression levels were positively correlated with clinicopathological features such as patient age, tumor size, distant metastasis and cancer stage. Moreover, exosomal Tim-3 is also associated with lymph node metastasis. Therefore, exosomal Tim-3 and Galectin-9 may serve as potential biomarkers for the clinical application of NSCLC (216). All of these findings suggest that exosomal proteins have the potential to serve as biomarkers for disease diagnosis. In the future, we still need to focus on the expression levels of specific proteins in a certain disease.

Exosomal lipids

Lipid molecules in exosomes are mainly used to maintain their external morphology. It has been reported that lipid molecules in EVs can not only protect nucleic acids and protein contents from harmful stimuli in the extracellular environment, but also exert bioactive functions to participate in tumor biological processes as signaling molecules (217, 218). It has been shown that lipid molecules in exosomes can also be used as potential biomarkers in cancer patients (136, 219–222). Among them, the expression levels of phosphatidylcholine(PC), phosphatidylethanolamine (PE),phosphatidylinositol(PI), sphingomyelin(SM),ceramide(Cer) and cholesterol are various in difference diseases (150, 223–225).

Previously, Skotland et al. (223) pointed out that urinary exosomal lipid molecules (such as phosphoresterdylserine and lactoceramide) have potential as biomarkers in prostate cancer (134). Subsequently, Brzozowski et al. (226) performed lipid analysis in exosomes released from non-tumorigenic (RWPE1), tumorigenic (NB26) and metastatic (PC-3) prostate cell lines, and they found significant differences in lipid species abundance in cells of these three different prostate species. The abundance of Diacylglycerol (DG) and Triacylglycerol (TG) species were reduced in both the NB26 and PC-3 cell lines EVs as compared to the EVs in the RWPE1 cell line. However, in contrast to EVs in the RWPE1 cell line, EVs in the NB2 and PC-3 cell lines were rich in glycerophospholipids, while Cer and SM species do not differ much among the three cell lines (226). In addition, Exosomal lipid components have been detected in Hepatocellular Carcinoma (HepG2/C3a and Huh7 cells) (227), Melanoma (B16-F10 cells) (228), Glioblastoma (U87 cells) (229)and Pancreatic cancer (AsPC-1 cells) (230). Recently, Glover et al. (135) stated that the content of exosomal lipid molecules such as glycerophospholipids, glycerolips, and sterols is reduced in the urine of patients with hereditary-trypsinaemia (135). Overexpression of exosomal lipid molecules such as acid sphingolipase in the cerebrospinal fluid of multiple sclerosis(MS) patients is strongly associated with disease severity, creating new opportunities for the diagnosis and treatment of the disease (137). Furthermore, sphingomyelin, derived from EVs in tumor cells, promotes endothelial cell migration and angiogenesis during tumor growth and metastasis (231). To sum up, this suggests that the great potential of EVs lipid molecules for cancer diagnostic biomarkers.

Summarizing the role of exosomal molecular cargoes in cancer diagnosis

In conclusion, exosomal nucleic acids, proteins and lipid molecular cargoes in different body fluids have broad application prospects as cancer diagnostic biomarkers (Table 3). Previous researches have shown that exosomal molecular cargoes are differentially expressed in body fluids, and exosomal molecular cargoes with higher AUC values may effectively distinguish cancer patients from healthy individuals (232–234). It is worth noting that the combined detection of multiple potential exosome molecular cargoes may provide a rapid, reliable and non-invasive aid to the diagnosis of diseases. In addition, that exosomes used as diagnostic biomarkers also requires consideration of all preanalytical variables associated with sample collection, such as whole blood (or other biofluid) treatment, hemolysis interference, and other contaminant interference (235). In the future, we should also focus on large-scale preparation and standardized protocols for exosomes analysis, and need advanced techniques to minimize contaminants in the samples as well.

Conclusion

In this review, we illustrate that exosomal molecular cargoes participate in exosome biogenesis, which is a complex process

TABLE 3 Exosomal molecular cargoes are used as biomarkers for disease diagnosis.

Potential Molecular Cargoes	Expression	Diseases	Source	Isolation	AUC	Clinical Significance	References
mRNAs							
CTGF	↑	Prostate cancer	Serum	UC	0.8600	Early diagnosis & Prognostic monitoring	(88)
CAV1	↓	Prostate cancer	Serum	UC	0.8100	Early diagnosis & Prognostic monitoring	(88)
THBS1	↓	Prostate cancer	Serum	UC	0.8200	Early diagnosis	(88)
TIMP2	↓	Prostate cancer	Serum	UC	0.8000	Early diagnosis	(88)
MT1-MMP	↑	Gastric cancer	Serum	CRG	0.7880	Diagnosis, Treatment, and Prognosis	(89)
hnRNPH1	↑	Hepatocellular carcinoma	Serum	CRG	0.8650	Early diagnosis & Prognostic monitoring	(90)
miRNAs							
miR-141	↑	Prostate cancer	Serum	PC	0.8694	Early diagnosis	(91)
miR-196a-5p	↓	Prostate cancer	Urine	UC	0.7300	Early diagnosis	(92)
miR-501-3p	↓	Prostate cancer	Urine	UC	0.6900	Early diagnosis	(92)
miR-196a	↓	Prostate cancer	Urine	UC	0.9200	Early diagnosis	(92)
miR-17-5p	↑	Pancreatic cancer	Serum	UC	0.8870	Early diagnosis & Prognostic monitoring	(93)
miR-196a	↑	Pancreatic cancer	Plasma	UC	0.8100	Early diagnosis & Prognostic monitoring	(94)
miR-1246	↑	Pancreatic cancer	Saliva	CRG	0.8140	Early diagnosis	(95)
miR-4644	↑	Pancreatic cancer	Saliva	CRG	0.7630	Early diagnosis	(95)
miR-101	↓	Ovarian cancer	Serum	PC	—	Early diagnosis & Treatment assessment	(96)
miR-224	↑	Hepatocellular carcinoma	Serum	PC	0.9100	Early diagnosis & Prognostic monitoring	(97)
miR-92b	↑	Hepatocellular carcinoma	Serum	PC	0.9250	Early diagnosis of recurrence after living donor liver transplantation (LD LT)	(98)
miR-122	↑	Hepatocellular carcinoma	Serum	PC	0.9900	Early diagnosis	(99)
miR-92b	↑	Colorectal cancer	Plasma	UC	0.7930	Early diagnosis	(100)
miR-122	↑	Colorectal cancer	Serum	PC	0.8900	Early diagnosis & Prognostic monitoring	(101)
miR-520c-3p	↑	Nonsmall-cell lung cancer	Serum	UC 、PC	0.8190	Early diagnosis	(102)
miR-1274b	↑	Nonsmall-cell lung cancer	Serum	UC 、PC	0.7880	Early diagnosis	(102)
miR-15a-5p	↑	Endometrial carcinoma	Plasma	PC	0.8130	Early diagnosis	(103)
miR-423-5p	↑	Gastric cancer	Serum	PC	0.7630	Early diagnosis & Prognostic monitoring	(104)
miR-15b-3p	↑	Gastric cancer	Serum	UC	0.8200	Early diagnosis & Prognostic monitoring	(105)
miR-4732-5p	↑	Epithelial Ovarian cancer	Plasma	CRG	0.8890	Early diagnosis	(106)
lncRNAs							
lncRNA-UEGC1	↑	Gastric cancer	Plasma	UC	0.8760	Early diagnosis	(107)
lncRNA-HOTTIP	↑	Gastric cancer	Serum	UC	0.8270	Early diagnosis & Prognostic monitoring	(108)

(Continued)

TABLE 3 Continued

Potential Molecular Cargoes	Expression	Diseases	Source	Isolation	AUC	Clinical Significance	References
lncRNA-GC1	↑	Gastric cancer	Serum	UC	0.9033	Early diagnosis	(109)
lncRNA-CCAT 1	↑	Gastric cancer	Serum	UC, CRG	0.8900	Early diagnosis	(110)
lncRNA-UCA1	↑	Bladder cancer	Serum	CRG	0.7530	Early diagnosis	(111)
lncRNA - PTENP1	↓	Bladder cancer	Plasma	CRG	0.7430	Early diagnosis & Prognostic monitoring	(112)
lncRNA - TERC	↑	Bladder cancer	Urine	UC	0.8360	Early diagnosis & Prognostic monitoring	(112)
lncRNA -LINC00635	↑	Hepatocellular carcinoma	Serum	CRG	0.7500	Early diagnosis & Prognostic monitoring	(113)
lncRNA -HOTAIR	↑	Glioblastoma	Serum	CRG	0.9130	Early diagnosis & Prognostic monitoring	(114)
circRNAs							
hsa_circ_0065149	↓	Gastric cancer	Plasma	CRG	0.6400	Early diagnosis & Prognostic monitoring	(115)
circSHKBP1	↑	Gastric cancer	Serum	PC	—	Early diagnosis & Prognostic monitoring	(116)
circ-KIAA1244	↓	Gastric cancer	Plasma	CRG	0.7481	Early diagnosis	(117)
circSATB2	↑	Lung cancer	Serum	UC	0.6600	Early diagnosis	(118)
circLPAR1	↓	Colorectal cancer	Plasma	CRG	0.8580	Early diagnosis	(119)
Proteins							
glypican-1	↑	Pancreatic cancer	Serum	UC	1.0000	Early diagnosis	(120)
Survivin	↑	Prostate cancer	Plasma	UC	—	Early diagnosis & Prognostic monitoring	(121)
EphrinA2	↑	Prostate cancer	Serum	UC	0.7666	Early diagnosis	(122)
MAGE 3/6	↑	Ovarian cancer	Plasma	UC	—	Early diagnosis & Treatment assessment	(123)
Epcam-CD63	↑	Colorectal cancer	Plasma	UC	0.9600	Early diagnosis & Prognostic monitoring	(124)
TRIM3	↓	Gastric cancer	Serum	PC	—	Early diagnosis	(125)
MUC1	↑	Nonsmall-cell lung cancer	Plasma	CRG	0.6850	Early diagnosis	(126)
Del-1	↑	Breast cancer	Plasma	ELISA (CD63* capture)	0.9610	Early diagnosis	(127)
Fibronectin	↑	Breast cancer	Plasma	ELISA (CD63* capture)	0.7700	Early diagnosis	(128)
GKN1	↓	Gastric cancer	Serum	UC	1.0000	Early diagnosis & Treatment assessment	(129)
CP	↑	Renal cell carcinoma	Urine	UC	1.0000	Early diagnosis	(130)
PODXL	↑	Renal cell carcinoma	Urine	UC	1.0000	Early diagnosis	(130)
EpCAM	↑	Metastatic breast cancer	Plasma	UC	0.9709	Early diagnosis	(131)
PD-L1	↑	Nonsmall-cell lung cancer	Serum	UC	0.9700	Early diagnosis	(132)
CD24	↑	Ovarian cancer	Plasma	UC	1.0000	Early diagnosis	(133)
EpCAM	↑	Ovarian cancer	Plasma	UC	1.0000	Early diagnosis	(133)
FRα	↓	Ovarian cancer	Plasma	UC	0.9950	Early diagnosis	(133)

(Continued)

TABLE 3 Continued

Potential Molecular Cargoes	Expression	Diseases	Source	Isolation	AUC	Clinical Significance	References
Lipids							
Phosphatidylserine (PS) 18:1/18:1 and lactose ceramide (d18:1/16:0)	↑	Prostate cancer	Urine	UC	0.9890 (In combination)	Early diagnosis	(134)
Glycerophospholipids, glycerolips and sterols	↓	Hereditary alpha-tryptophanemia	Urine	UC	–	Early diagnosis	(135)
PC (P-14:0/22:2)	↑	Pancreatic cancer	Serum	PC	–	Early diagnosis & Prognostic monitoring	(136)
Acid sphingomyelinase	↑	Multiple sclerosis	Cerebrospinal fluid	UC	0.7700	Early diagnosis & Treatment assessment	(137)

↑, increased; ↓, decreased; –, unrevealed; UC, ultracentrifugation; PC, precipitation; CRG, Commercial reagents.

that may vary in cargoes or cellular origin. In addition, the regulation of exosome biogenesis processes involves the coordination of many different molecular cargoes and signaling mechanisms, mainly dominated by ESCRT-dependent, lipid raft and tetraspanin protein mechanisms, and Rab proteins further assists cargo sorting and exosome release. Notably, this cargo molecules interact with each other to mainly mediate exosome biogenesis by regulating the negative curvature of the cell membrane (236). So far, ESCRT and ceramide pathways are established for exosome biogenesis.

Furthermore, exosomes and their molecular cargoes are elaborated as effective tools for the diagnosis of cancer. Although tissue biopsy is still the gold standard for tumor diagnosis, but it is invasive. An ideal diagnostic approach for cancer should accurately detect tumor-specific biomarkers using non-invasive techniques at the pre-metastatic stage (237). Most of the current molecules used as tumor diagnostic biomarkers are based on detecting the higher expression molecules above the threshold in healthy individuals. For instance, PSA and CEA serve as diagnostic biomarkers for prostate cancer and gastrointestinal cancer respectively, and these biomarkers are significantly elevated only at tumor progression state (238). Since exosomes are present in most body fluids and their stability properties, and the molecular cargoes carried by exosomes reflects the genetic or signaling changes in the cancer cells of origin. If it would be detected earlier as biomarkers, so as to achieve a means of treating the disease, it would make exosomes potentially replace invasive biopsies as cancer diagnostic biomarkers of important clinical significance (239, 240).

Understanding the process of exosome biogenesis is an important part of the research and physiological significance of exosomes function, especially for disease diagnosis, treatment, and prognosis. Controlling exosome generation in pathological states may serve as a therapeutic opportunity to reduce tumorigenesis. However, it is still challenging to investigate the whole mechanism of exosome biogenesis. Because the exosome formation pathway may be different according to different cell types, some specific molecules will participate in multiple processes, leading to the exact mechanism of action of many molecules is not clear, for which their heterogeneity may be a disadvantage of their use as biomarkers. It is worth noting that most studies in the field of exosomes are conducted *in vitro*, and the laboratory culture conditions or technical methods also affect the biological characteristics of exosomes (241). Therefore, special attention should also be paid to the methods of exosomes extraction used in each study. How to promote the yield and purity of exosomes is a top priority, which has been a bottleneck limiting their translational applications. Recent studies have shown that appropriate combinations of several methods for extracting and purifying exosomes can effectively improve the above problems, and how to integrate them for optimum results remains to be further investigated. More work needs to be done in the future to elucidate the role of exosomes in diseases progression, with particular attention to the precise mechanisms by which exosome biogenesis pathways influence cellular function. The questions will be raised such as, will different biogenesis pathways produce vesicles with different or similar functions? Will there be any correlation between vesicles produced by this biogenesis pathways? This will be useful for treatments involving the pathological mechanisms of exosomes. Understanding the physiological effects and how they can be induced into pathological factors is crucial when developing new therapeutic strategies.

Author contributions

XY searched for literature and wrote the first draft of this article,JC revised the manuscript and developed the main content of this manuscript. SF provided great help for polishing the manuscript. DH, TY, ZL, XW, MZ, and JW were involved in edited the manuscript. TZ supervised the project and

contributed to the revision of the final manuscript. All authors contributed to the article and approved the submitted version.

Funding

This work was supported by the Key R&D Planning Project of Jiangxi Science and Technology Commission, China (No. 20203BBGL73126).

Acknowledgments

We thank Yaojiang Que edited the figure, Zhigang Li reviewed the manuscript and polished the grammar.

Conflict of interest

The authors declare that the research was conducted in the absence of any commercial or financial relationships that could be construed as a potential conflict of interest.

Publisher's note

References

1. Gandham S, Su X, Wood J, Nocera AL, Alli SC, Milane L, et al. Technologies and standardization in research on extracellular vesicles. *Trends Biotechnol* (2020) 38:1066–98. doi: 10.1016/j.tibtech.2020.05.012

2. Barreiro K, Dwivedi OP, Valkonen S, Groop PH, Tuomi T, Holthofer H, et al. Urinary extracellular vesicles: Assessment of pre-analytical variables and development of a quality control with focus on transcriptomic biomarker research. *J extracellular vesicles* (2021) 10:e12158. doi: 10.1002/jev2.12158

3. Dutta S, Hornung S, Kruayatidee A, Maina KN, Del Rosario I, Paul KC, et al. α-synuclein in blood exosomes immunoprecipitated using neuronal and oligodendroglial markers distinguishes parkinson's disease from multiple system atrophy. *Acta neuropathologica* (2021) 142:495–511. doi: 10.1007/s00401-021-02324-0

4. Yan C, Chen J, Wang C, Yuan M, Kang Y, Wu Z, et al. Milk exosomes-mediated miR-31-5p delivery accelerates diabetic wound healing through promoting angiogenesis. *Drug delivery* (2022) 29:214–28. doi: 10.1080/10717544.2021.2023699

5. Li K, Lin Y, Luo Y, Xiong X, Wang L, Durante K, et al. A signature of saliva-derived exosomal small RNAs as predicting biomarker for esophageal carcinoma: a multicenter prospective study. *Mol Cancer* (2022) 21:21. doi: 10.1186/s12943-022-01499-8

6. Li Y, Gu J, Mao Y, Wang X, Li Z, Xu X, et al. Cerebrospinal fluid extracellular vesicles with distinct properties in autoimmune encephalitis and herpes simplex encephalitis. *Mol Neurobiol* (2022) 59:2441–55. doi: 10.1007/s12035-021-02705-2

7. Li P, Lu X, Hu J, Dai M, Yan J, Tan H, et al. Human amniotic fluid derived-exosomes alleviate hypoxic encephalopathy by enhancing angiogenesis in neonatal mice after hypoxia. *Neurosci Lett* (2022) 768:136361. doi: 10.1016/j.neulet.2021.136361

8. Su Q, Zhang Y, Cui Z, Chang S, Zhao P. Semen-derived exosomes mediate immune escape and transmission of reticuloendotheliosis virus. *Front Immunol* (2021) 12:735280. doi: 10.3389/fimmu.2021.735280

9. Sadik N, Cruz L, Gurtner A, Rodosthenous RS, Dusoswa SA, Ziegler O, et al. Extracellular RNAs: A new awareness of old perspectives. *Methods Mol Biol (Clifton N.J.)* (2018) 1740:1–15. doi: 10.1007/978-1-4939-7652-2_1

10. Markowska A, Pendergrast RS, Pendergrast JS, Pendergrast PS. A novel method for the isolation of extracellular vesicles and RNA from urine. *J circulating Biomarkers* (2017) 6:1849454417712666. doi: 10.1177/1849454417712666

11. Merchant ML, Rood IM, Deegens JKJ, Klein JB. Isolation and characterization of urinary extracellular vesicles: implications for biomarker discovery. *Nat Rev Nephrol* (2017) 13:731–49. doi: 10.1038/nrneph.2017.148

12. Vitorino R, Ferreira R, Guedes S, Amado F, Thongboonkerd V. What can urinary exosomes tell us? *Cell Mol Life Sci CMLS* (2021) 78:3265–83. doi: 10.1007/s00018-020-03739-w

13. Yu D, Li Y, Wang M, Gu J, Xu W, Cai H, et al. Exosomes as a new frontier of cancer liquid biopsy. *Mol Cancer* (2022) 21:56. doi: 10.1186/s12943-022-01509-9

14. Burkova EE, Sedykh SE, Nevinsky GA. Human placenta exosomes: Biogenesis, isolation, composition, and prospects for use in diagnostics. *Int J Mol Sci* (2021) 22. doi: 10.3390/ijms22042158

15. Yamashita T, Takahashi Y, Nishikawa M, Takakura Y. Effect of exosome isolation methods on physicochemical properties of exosomes and clearance of exosomes from the blood circulation. *Eur J pharmaceutics biopharmaceutics Off J Arbeitsgemeinschaft fur Pharmazeutische Verfahrenstechnik e.V* (2016) 98:1–8. doi: 10.1016/j.ejpb.2015.10.017

16. Li S, Yi M, Dong B, Tan X, Luo S, Wu K. The role of exosomes in liquid biopsy for cancer diagnosis and prognosis prediction. *Int J Cancer* (2021) 148:2640–51. doi: 10.1002/ijc.33386

17. Wang YT, Shi T, Srivastava S, Kagan J, Liu T, Rodland KD. Proteomic analysis of exosomes for discovery of protein biomarkers for prostate and bladder cancer. *Cancers* (2020) 12. doi: 10.3390/cancers12092335

18. Wijenayake S, Eisha S, Tawhidi Z, Pitino MA, Steele MA, Fleming AS, et al. Comparison of methods for pre-processing, exosome isolation, and RNA extraction in unpasteurized bovine and human milk. *PLoS One* (2021) 16:e0257633. doi: 10.1371/journal.pone.0257633

19. Sidhom K, Obi PO, Saleem A. A review of exosomal isolation methods: Is size exclusion chromatography the best option? *Int J Mol Sci* (2020) 21. doi: 10.3390/ijms21186466

20. Sedykh S, Kuleshova A, Nevinsky G. Milk exosomes: Perspective agents for anticancer drug delivery. *Int J Mol Sci* (2020) 21. doi: 10.3390/ijms21186646

21. Vaswani K, Koh YQ, Almughlliq FB, Peiris HN, Mitchell MD. A method for the isolation and enrichment of purified bovine milk exosomes. *Reprod Biol* (2017) 17:341–8. doi: 10.1016/j.repbio.2017.09.007

22. Cheshmi B, Cheshomi H. Salivary exosomes: properties, medical applications, and isolation methods. *Mol Biol Rep* (2020) 47:6295–307. doi: 10.1007/s11033-020-05659-1

23. Han Y, Jia L, Zheng Y, Li W. Salivary exosomes: Emerging roles in systemic disease. *Int J Biol Sci* (2018) 14:633–43. doi: 10.7150/ijbs.25018

24. Cheng J, Nonaka T, Wong DTW. Salivary exosomes as nanocarriers for cancer biomarker delivery. *Materials (Basel Switzerland)* (2019) 12. doi: 10.3390/ma12040654

25. Zlotogorski-Hurvitz A, Dayan D, Chaushu G, Korvala J, Salo T, Sormunen R, et al. Human saliva-derived exosomes: comparing methods of isolation. *J Histochem Cytochem Off J Histochem Soc* (2015) 63:181–9. doi: 10.1369/0022155414564219

26. Tan YJ, Wong BYX, Vaidyanathan R, Sreejith S, Chia SY, Kandiah N, et al. Altered cerebrospinal fluid exosomal microRNA levels in young-onset alzheimer's disease and frontotemporal dementia. *J Alzheimer's Dis Rep* (2021) 5:805–13. doi: 10.3233/adr-210311

27. Thompson AG, Gray E, Mager I, Fischer R, Thézénas ML, Charles PD, et al. UFLC-derived CSF extracellular vesicle origin and proteome. *Proteomics* (2018) 18:e1800257. doi: 10.1002/pmic.201800257

28. Yao YF, Qu MW, Li GC, Zhang FB, Rui HC. Circulating exosomal miRNAs as diagnostic biomarkers in parkinson's disease. *Eur Rev Med Pharmacol Sci* (2018) 22:5278–83. doi: 10.26355/eurrev_201808_15727

29. Hou X, Gong X, Zhang L, Li T, Yuan H, Xie Y, et al. Identification of a potential exosomal biomarker in spinocerebellar ataxia type 3/Machado-Joseph disease. *Epigenomics* (2019) 11:1037–56. doi: 10.2217/epi-2019-0081

30. Thompson AG, Gray E, Mäger I, Thézénas ML, Charles PD, Talbot K, et al. CSF extracellular vesicle proteomics demonstrates altered protein homeostasis in amyotrophic lateral sclerosis. *Clin Proteomics* (2020) 17:31. doi: 10.1186/s12014-020-09294-7

31. Ding K, Yu L, Huang Z, Zheng H, Yang X, Tian T, et al. [Differential expression profile of miRNAs in amniotic fluid exosomes from fetuses with down syndrome]. *Nan fang yi ke da xue xue bao = J South Med Univ* (2022) 42:293–9. doi: 10.12122/j.issn.1673-4254.2022.02.18

32. Tang GY, Yu P, Zhang C, Deng HY, Lu MX, Le JH. The neuropeptide-related HERC5/TAC1 interactions may be associated with the dysregulation of lncRNA GAS5 expression in gestational diabetes mellitus exosomes. *Dis Markers* (2022) 2022:8075285. doi: 10.1155/2022/8075285

33. Baskaran S, Panner Selvam MK, Agarwal A. Exosomes of male reproduction. *Adv Clin Chem* (2020) 95:149–63. doi: 10.1016/bs.acc.2019.08.004

34. Yang C, Guo WB, Zhang WS, Bian J, Yang JK, Qi T, et al. [Extraction and identification of semen-derived exosomes using PEG6000]. *Nan fang yi ke da xue xue bao = J South Med Univ* (2016) 36:1531–5.

35. Mercadal M, Herrero C, López-Rodrigo O, Castells M, de la Fuente A, Vigués F, et al. Impact of extracellular vesicle isolation methods on downstream mirna analysis in semen: A comparative study. *Int J Mol Sci* (2020) 21. doi: 10.3390/ijms21175949

36. Théry C, Witwer KW, Aikawa E, Alcaraz MJ, Anderson JD, Andriantsitohaina R, et al. Minimal information for studies of extracellular vesicles 2018 (MISEV2018): a position statement of the international society for extracellular vesicles and update of the MISEV2014 guidelines. *J extracellular vesicles* (2018) 7:1535750. doi: 10.1080/20013078.2018.1535750

37. Sasaki R, Kanda T, Yokosuka O, Kato N, Matsuoka S, Moriyama M. Exosomes and hepatocellular carcinoma: From bench to bedside. *Int J Mol Sci* (2019) 20. doi: 10.3390/ijms20061406

38. Gurunathan S, Kang MH, Qasim M, Khan K, Kim JH. Biogenesis, membrane trafficking, functions, and next generation nanotherapeutics medicine of extracellular vesicles. *Int J nanomedicine* (2021) 16:3357–83. doi: 10.2147/ijn.S310357

39. Modani S, Tomar D, Tangirala S, Sriram A, Mehra NK, Kumar R, et al. An updated review on exosomes: biosynthesis to clinical applications. *J Drug Targeting* (2021) 29:925–40. doi: 10.1080/1061186x.2021.1894436

40. Lo Cicero A, Stahl PD, Raposo G. Extracellular vesicles shuffling intercellular messages: for good or for bad. *Curr Opin Cell Biol* (2015) 35:69–77. doi: 10.1016/j.ceb.2015.04.013

41. Huang D, Chen J, Hu D, Xie F, Yang T, Li Z, et al. Advances in biological function and clinical application of small extracellular vesicle membrane proteins. *Front Oncol* (2021) 11:675940. doi: 10.3389/fonc.2021.675940

42. Hessvik NP, Llorente A. Current knowledge on exosome biogenesis and release. *Cell Mol Life Sci CMLS* (2018) 75:193–208. doi: 10.1007/s00018-017-2595-9

43. Kalluri R, LeBleu VS. The biology, function, and biomedical applications of exosomes. *Sci (New York N.Y.)* (2020) 367. doi: 10.1126/science.aau6977

44. Huotari J, Helenius A. Endosome maturation. *EMBO J* (2011) 30:3481–500. doi: 10.1038/emboj.2011.286

45. Pegtel DM, Gould SJ. Exosomes. *Annu Rev Biochem* (2019) 88:487–514. doi: 10.1146/annurev-biochem-013118-111902

46. Shao H, Im H, Castro CM, Breakefield X, Weissleder R, Lee H. New technologies for analysis of extracellular vesicles. *Chem Rev* (2018) 118:1917–50. doi: 10.1021/acs.chemrev.7b00534

47. Preethi KA, Selvakumar SC, Ross K, Jayaraman S, Tusubira D, Sekar D. Liquid biopsy: Exosomal microRNAs as novel diagnostic and prognostic biomarkers in cancer. *Mol Cancer* (2022) 21:54. doi: 10.1186/s12943-022-01525-9

48. Bebelman MP, Smit MJ, Pegtel DM, Baglio SR. Biogenesis and function of extracellular vesicles in cancer. *Pharmacol Ther* (2018) 188:1–11. doi: 10.1016/j.pharmthera.2018.02.013

49. Bestard-Escalas J, Maimó-Barceló A, Lopez DH, Reigada R, Guardiola-Serrano F, Ramos-Vivas J, et al. Common and differential traits of the membrane lipidome of colon cancer cell lines and their secreted vesicles: Impact on studies using cell lines. *Cancers* (2020) 12. doi: 10.3390/cancers12051293

50. Andreu Z, Yáñez-Mó M. Tetraspanins in extracellular vesicle formation and function. *Front Immunol* (2014) 5:442. doi: 10.3389/fimmu.2014.00442

51. Mathivanan S, Ji H, Simpson RJ. Exosomes: extracellular organelles important in intercellular communication. *J Proteomics* (2010) 73:1907–20. doi: 10.1016/j.jprot.2010.06.006

52. van Niel G, Porto-Carreiro I, Simoes S, Raposo G. Exosomes: a common pathway for a specialized function. *J Biochem* (2006) 140:13–21. doi: 10.1093/jb/mvj128

53. Michael A, Bajracharya SD, Yuen PS, Zhou H, Star RA, Illei GG, et al. Exosomes from human saliva as a source of microRNA biomarkers. *Oral Dis* (2010) 16:34–8. doi: 10.1111/j.1601-0825.2009.01604.x

54. Zhang C, Ji Q, Yang Y, Li Q, Wang Z. Exosome: Function and role in cancer metastasis and drug resistance. *Technol Cancer Res Treat* (2018) 17:1533033818763450. doi: 10.1177/1533033818763450

55. Bestard-Escalas J, Reigada R, Reyes J, de la Torre P, Liebisch G, Barceló-Coblijn G. Fatty acid unsaturation degree of plasma exosomes in colorectal cancer patients: A promising biomarker. *Int J Mol Sci* (2021) 22. doi: 10.3390/ijms22105060

56. Melero-Fernandez de Mera RM, Villaseñor A, Rojo D, Carrión-Navarro J, Gradillas A, Ayuso-Sacido A, et al. Ceramide composition in exosomes for characterization of glioblastoma stem-like cell phenotypes. *Front Oncol* (2021) 11:788100. doi: 10.3389/fonc.2021.788100

57. Lin M, Liao W, Dong M, Zhu R, Xiao J, Sun T, et al. Exosomal neutral sphingomyelinase 1 suppresses hepatocellular carcinoma *via* decreasing the ratio of sphingomyelin/ceramide. *FEBS J* (2018) 285:3835–48. doi: 10.1111/febs.14635

58. Zhao L, Gu C, Gan Y, Shao L, Chen H, Zhu H. Exosome-mediated siRNA delivery to suppress postoperative breast cancer metastasis. *J Controlled release Off J Controlled Release Soc* (2020) 318:1–15. doi: 10.1016/j.jconrel.2019.12.005

59. Rana S, Yue S, Stadel D, Zöller M. Toward tailored exosomes: the exosomal tetraspanin web contributes to target cell selection. *Int J Biochem Cell Biol* (2012) 44:1574–84. doi: 10.1016/j.biocel.2012.06.018

60. Hemler ME. Tetraspanin proteins mediate cellular penetration, invasion, and fusion events and define a novel type of membrane microdomain. *Annu Rev Cell Dev Biol* (2003) 19:397–422. doi: 10.1146/annurev.cellbio.19.111301.153609

61. Perez-Hernandez D, Gutiérrez-Vázquez C, Jorge I, López-Martín S, Ursa A, Sánchez-Madrid F, et al. The intracellular interactome of tetraspanin-enriched microdomains reveals their function as sorting machineries toward exosomes. *J Biol Chem* (2013) 288:11649–61. doi: 10.1074/jbc.M112.445304

62. Lynch S, Santos SG, Campbell EC, Nimmo AM, Botting C, Prescott A, et al. Novel MHC class I structures on exosomes. *J Immunol (Baltimore Md. 1950)* (2009) 183:1884–91. doi: 10.4049/jimmunol.0900798

63. Gauvreau ME, Côté MH, Bourgeois-Daigneault MC, Rivard LD, Xiu F, Brunet A, et al. Sorting of MHC class II molecules into exosomes through a ubiquitin-independent pathway. *Traffic (Copenhagen Denmark)* (2009) 10:1518–27. doi: 10.1111/j.1600-0854.2009.00948.x

64. Caruso Bavisotto C, Cappello F, Macario AJL, Conway de Macario E, Logozzi M, Fais S, et al. Exosomal HSP60: a potentially useful biomarker for diagnosis, assessing prognosis, and monitoring response to treatment. *Expert Rev Mol diagnostics* (2017) 17:815–22. doi: 10.1080/14737159.2017.1356230

65. Lauwers E, Wang YC, Gallardo R, Van der Kant R, Michiels E, Swerts J, et al. Hsp90 mediates membrane deformation and exosome release. *Mol Cell* (2018) 71:689–702.e689. doi: 10.1016/j.molcel.2018.07.016

66. Larios J, Mercier V, Roux A, Gruenberg J. ALIX- and ESCRT-III-dependent sorting of tetraspanins to exosomes. *J Cell Biol* (2020) 219. doi: 10.1083/jcb.201904113

67. Buschow SI, Liefhebber JM, Wubbolts R, Stoorvogel W. Exosomes contain ubiquitinated proteins. *Blood cells molecules Dis* (2005) 35:398–403. doi: 10.1016/j.bcmd.2005.08.005

68. Théry C, Boussac M, Véron P, Ricciardi-Castagnoli P, Raposo G, Garin J, et al. Proteomic analysis of dendritic cell-derived exosomes: a secreted subcellular compartment distinct from apoptotic vesicles. *J Immunol (Baltimore Md. 1950)* (2001) 166:7309–18. doi: 10.4049/jimmunol.166.12.7309

69. Ostrowski M, Carmo NB, Krumeich S, Fanget I, Raposo G, Savina A, et al. Rab27a and Rab27b control different steps of the exosome secretion pathway. *Nat Cell Biol* (2010) 12:19–30; sup pp 11-13. doi: 10.1038/ncb2000

70. Auger C, Brunel A, Darbas T, Akil H, Perraud A, Bégaud G, et al. Extracellular vesicle measurements with nanoparticle tracking analysis: A different appreciation of up and down secretion. *Int J Mol Sci* (2022) 23. doi: 10.3390/ijms23042310

71. Fukuda M. Regulation of secretory vesicle traffic by rab small GTPases. *Cell Mol Life Sci CMLS* (2008) 65:2801–13. doi: 10.1007/s00018-008-8351-4

72. Mathieu M, Martin-Jaular L, Lavieu G, Théry C. Specificities of secretion and uptake of exosomes and other extracellular vesicles for cell-to-cell communication. *Nat Cell Biol* (2019) 21:9–17. doi: 10.1038/s41556-018-0250-9

73. Zhang Y, Liu Y, Liu H, Tang WH. Exosomes: biogenesis, biologic function and clinical potential. *Cell bioscience* (2019) 9:19. doi: 10.1186/s13578-019-0282-2

74. Verweij FJ, Bebelman MP, Jimenez CR, Garcia-Vallejo JJ, Janssen H, Neefjes J, et al. Quantifying exosome secretion from single cells reveals a modulatory role for GPCR signaling. *J Cell Biol* (2018) 217:1129–42. doi: 10.1083/jcb.201703206

75. Wei Y, Wang D, Jin F, Bian Z, Li L, Liang H, et al. Pyruvate kinase type M2 promotes tumour cell exosome release *via* phosphorylating synaptosome-associated protein 23. *Nat Commun* (2017) 8:14041. doi: 10.1038/ncomms14041

76. Trajkovic K, Hsu C, Chiantia S, Rajendran L, Wenzel D, Wieland F, et al. Ceramide triggers budding of exosome vesicles into multivesicular endosomes. *Sci (New York N.Y.)* (2008) 319:1244–7. doi: 10.1126/science.1153124

77. Menck K, Sönmezer C, Worst TS, Schulz M, Dihazi GH, Streit F, et al. Neutral sphingomyelinases control extracellular vesicles budding from the plasma membrane. *J extracellular vesicles* (2017) 6:1378056. doi: 10.1080/20013078.2017.1378056

78. Inuzuka T, Inokawa A, Chen C, Kizu K, Narita H, Shibata H, et al. ALG-2-interacting tubby-like protein superfamily member PLSCR3 is secreted by an exosomal pathway and taken up by recipient cultured cells. *Bioscience Rep* (2013) 33:e00026. doi: 10.1042/bsr20120123

79. Subra C, Laulagnier K, Perret B, Record M. Exosome lipidomics unravels lipid sorting at the level of multivesicular bodies. *Biochimie* (2007) 89:205–12. doi: 10.1016/j.biochi.2006.10.014

80. Rocha N, Kuijl C, van der Kant R, Janssen L, Houben D, Janssen H, et al. Cholesterol sensor ORP1L contacts the ER protein VAP to control Rab7-RILP-p150 glued and late endosome positioning. *J Cell Biol* (2009) 185:1209–25. doi: 10.1083/jcb.200811005

81. Parolini I, Federici C, Raggi C, Lugini L, Palleschi S, De Milito A, et al. Microenvironmental pH is a key factor for exosome traffic in tumor cells. *J Biol Chem* (2009) 284:34211–22. doi: 10.1074/jbc.M109.041152

82. Kooijman EE, Chupin V, Fuller NL, Kozlov MM, de Kruijff B, Burger KN, et al. Spontaneous curvature of phosphatidic acid and lysophosphatidic acid. *Biochemistry* (2005) 44:2097–102. doi: 10.1021/bi0478502

83. Kooijman EE, Chupin V, de Kruijff B, Burger KN. Modulation of membrane curvature by phosphatidic acid and lysophosphatidic acid. *Traffic (Copenhagen Denmark)* (2003) 4:162–74. doi: 10.1034/j.1600-0854.2003.00086.x

84. Morel E, Chamoun Z, Lasiecka ZM, Chan RB, Williamson RL, Vetanovetz C, et al. Phosphatidylinositol-3-phosphate regulates sorting and processing of amyloid precursor protein through the endosomal system. *Nat Commun* (2013) 4:2250. doi: 10.1038/ncomms3250

85. Raiborg C, Schink KO, Stenmark H. Class III phosphatidylinositol 3-kinase and its catalytic product PtdIns3P in regulation of endocytic membrane traffic. *FEBS J* (2013) 280:2730–42. doi: 10.1111/febs.12116

86. Hessvik NP, Øverbye A, Brech A, Torgersen ML, Jakobsen IS, Sandvig K, et al. PIKfyve inhibition increases exosome release and induces secretory autophagy. *Cell Mol Life Sci CMLS* (2016) 73:4717–37. doi: 10.1007/s00018-016-2309-8

87. Kajimoto T, Okada T, Miya S, Zhang L, Nakamura S. Ongoing activation of sphingosine 1-phosphate receptors mediates maturation of exosomal multivesicular endosomes. *Nat Commun* (2013) 4:2712. doi: 10.1038/ncomms3712

88. Shephard AP, Giles P, Mbengue M, Alraies A, Spary LK, Kynaston H, et al. Stroma-derived extracellular vesicle mRNA signatures inform histological nature of prostate cancer. *J extracellular vesicles* (2021) 10:e12150. doi: 10.1002/jev2.12150

89. Dong Z, Sun X, Xu J, Han X, Xing Z, Wang D, et al. Serum membrane type 1-matrix metalloproteinase (MT1-MMP) mRNA protected by exosomes as a potential biomarker for gastric cancer. *Med Sci monitor Int Med J Exp Clin Res* (2019) 25:7770–83. doi: 10.12659/msm.918486

90. Xu H, Dong X, Chen Y, Wang X. Serum exosomal hnRNPH1 mRNA as a novel marker for hepatocellular carcinoma. *Clin Chem Lab Med* (2018) 56:479–84. doi: 10.1515/cclm-2017-0327

91. Li Z, Ma YY, Wang J, Zeng XF, Li R, Kang W, et al. Exosomal microRNA-141 is upregulated in the serum of prostate cancer patients. *OncoTargets Ther* (2016) 9:139–48. doi: 10.2147/ott.S95565

92. Rodríguez M, Bajo-Santos C, Hessvik NP, Lorenz S, Fromm B, Berge V, et al. Identification of non-invasive miRNAs biomarkers for prostate cancer by deep sequencing analysis of urinary exosomes. *Mol Cancer* (2017) 16:156. doi: 10.1186/s12943-017-0726-4

93. Que R, Ding G, Chen J, Cao L. Analysis of serum exosomal microRNAs and clinicopathologic features of patients with pancreatic adenocarcinoma. *World J Surg Oncol* (2013) 11:219. doi: 10.1186/1477-7819-11-219

94. Xu YF, Hannafon BN, Zhao YD, Postier RG, Ding WQ. Plasma exosome miR-196a and miR-1246 are potential indicators of localized pancreatic cancer. *Oncotarget* (2017) 8:77028–40. doi: 10.18632/oncotarget.20332

95. Machida T, Tomofuji T, Maruyama T, Yoneda T, Ekuni D, Azuma T, et al. miR–1246 and miR–4644 in salivary exosome as potential biomarkers for pancreatobiliary tract cancer. *Oncol Rep* (2016) 36:2375–81. doi: 10.3892/or.2016.5021

96. Xu Y, Xu L, Zheng J, Geng L, Zhao S. MiR-101 inhibits ovarian carcinogenesis by repressing the expression of brain-derived neurotrophic factor. *FEBS Open Bio* (2017) 7:1258–66. doi: 10.1002/2211-5463.12257

97. Cui Y, Xu HF, Liu MY, Xu YJ, He JC, Zhou Y, et al. Mechanism of exosomal microRNA-224 in development of hepatocellular carcinoma and its diagnostic and prognostic value. *World J Gastroenterol* (2019) 25:1890–8. doi: 10.3748/wjg.v25.i15.1890

98. Nakano T, Chen IH, Wang CC, Chen PJ, Tseng HP, Huang KT, et al. Circulating exosomal miR-92b: Its role for cancer immunoediting and clinical value for prediction of posttransplant hepatocellular carcinoma recurrence. *Am J Transplant Off J Am Soc Transplant Am Soc Transplant Surgeons* (2019) 19:3250–62. doi: 10.1111/ajt.15490

99. Wang Y, Zhang C, Zhang P, Guo G, Jiang T, Zhao X, et al. Serum exosomal microRNAs combined with alpha-fetoprotein as diagnostic markers of hepatocellular carcinoma. *Cancer Med* (2018) 7:1670–9. doi: 10.1002/cam4.1390

100. Min L, Chen L, Liu S, Yu Y, Guo Q, Li P, et al. Loss of circulating exosomal miR-92b is a novel biomarker of colorectal cancer at early stage. *Int J Med Sci* (2019) 16:1231–7. doi: 10.7150/ijms.34540

101. Sun L, Liu X, Pan B, Hu X, Zhu Y, Su Y, et al. Serum exosomal miR-122 as a potential diagnostic and prognostic biomarker of colorectal cancer with liver metastasis. *J Cancer* (2020) 11:630–7. doi: 10.7150/jca.33022

102. Zhong Y, Ding X, Bian Y, Wang J, Zhou W, Wang X, et al. Discovery and validation of extracellular vesicle-associated miRNAs as noninvasive detection biomarkers for early-stage non-small-cell lung cancer. *Mol Oncol* (2021) 15:2439–52. doi: 10.1002/1878-0261.12889

103. Zhou L, Wang W, Wang F, Yang S, Hu J, Lu B, et al. Plasma-derived exosomal miR-15a-5p as a promising diagnostic biomarker for early detection of endometrial carcinoma. *Mol Cancer* (2021) 20:57. doi: 10.1186/s12943-021-01352-4

104. Yang H, Fu H, Wang B, Zhang X, Mao J, Li X, et al. Exosomal miR-423-5p targets SUFU to promote cancer growth and metastasis and serves as a novel marker for gastric cancer. *Mol carcinogenesis* (2018) 57:1223–36. doi: 10.1002/mc.22838

105. Wei S, Peng L, Yang J, Sang H, Jin D, Li X, et al. Exosomal transfer of miR-15b-3p enhances tumorigenesis and malignant transformation through the DYNLT1/Caspase-3/Caspase-9 signaling pathway in gastric cancer. *J Exp Clin Cancer Res CR* (2020) 39:32. doi: 10.1186/s13046-019-1511-6

106. Liu J, Yoo J, Ho JY, Jung Y, Lee S, Hur SY, et al. Plasma-derived exosomal miR-4732-5p is a promising noninvasive diagnostic biomarker for epithelial ovarian cancer. *J Ovarian Res* (2021) 14:59. doi: 10.1186/s13048-021-00814-z

107. Lin LY, Yang L, Zeng Q, Wang L, Chen ML, Zhao ZH, et al. Tumor-originated exosomal lncUEGC1 as a circulating biomarker for early-stage gastric cancer. *Mol Cancer* (2018) 17:84. doi: 10.1186/s12943-018-0834-9

108. Zhao R, Zhang Y, Zhang X, Yang Y, Zheng X, Li X, et al. Exosomal long noncoding RNA HOTTIP as potential novel diagnostic and prognostic biomarker test for gastric cancer. *Mol Cancer* (2018) 17:68. doi: 10.1186/s12943-018-0817-x

109. Guo X, Lv X, Ru Y, Zhou F, Wang N, Xi H, et al. Circulating exosomal gastric cancer-associated long noncoding RNA1 as a biomarker for early detection and monitoring progression of gastric cancer: A multiphase study. *JAMA Surg* (2020) 155:572–9. doi: 10.1001/jamasurg.2020.1133

110. Xiao K, Dong Z, Wang D, Liu M, Ding J, Chen W, et al. Clinical value of lncRNA CCAT1 in serum extracellular vesicles as a potential biomarker for gastric cancer. *Oncol Lett* (2021) 21:447. doi: 10.3892/ol.2021.12708

111. Xue M, Chen W, Xiang A, Wang R, Chen H, Pan J, et al. Hypoxic exosomes facilitate bladder tumor growth and development through transferring long non-coding RNA-UCA1. *Mol Cancer* (2017) 16:143. doi: 10.1186/s12943-017-0714-8

112. Zheng R, Du M, Wang X, Xu W, Liang J, Wang W, et al. Exosome-transmitted long non-coding RNA PTENP1 suppresses bladder cancer progression. *Mol Cancer* (2018) 17:143. doi: 10.1186/s12943-018-0880-3

113. Xu H, Chen Y, Dong X, Wang X. Serum exosomal long noncoding RNAs ENSG00000258332.1 and LINC00635 for the diagnosis and prognosis of hepatocellular carcinoma. *Cancer epidemiology Biomarkers Prev Publ Am Assoc Cancer Research cosponsored by Am Soc Prev Oncol* (2018) 27:710–6. doi: 10.1158/1055-9965.Epi-17-0770

114. Tan SK, Pastori C, Penas C, Komotar RJ, Ivan ME, Wahlestedt C, et al. Serum long noncoding RNA HOTAIR as a novel diagnostic and prognostic biomarker in glioblastoma multiforme. *Mol Cancer* (2018) 17:74. doi: 10.1186/s12943-018-0822-0

115. Shao Y, Tao X, Lu R, Zhang H, Ge J, Xiao B, et al. Hsa_circ_0065149 is an indicator for early gastric cancer screening and prognosis prediction. *Pathol Oncol Res POR* (2020) 26:1475–82. doi: 10.1007/s12253-019-00716-y

116. Xie M, Yu T, Jing X, Ma L, Fan Y, Yang F, et al. Exosomal circSHKBP1 promotes gastric cancer progression *via* regulating the miR-582-3p/HUR/VEGF axis and suppressing HSP90 degradation. *Mol Cancer* (2020) 19:112. doi: 10.1186/s12943-020-01208-3

117. Tang W, Fu K, Sun H, Rong D, Wang H, Cao H. CircRNA microarray profiling identifies a novel circulating biomarker for detection of gastric cancer. *Mol Cancer* (2018) 17:137. doi: 10.1186/s12943-018-0888-8

118. Zhang N, Nan A, Chen L, Li X, Jia Y, Qiu M, et al. Circular RNA circSATB2 promotes progression of non-small cell lung cancer cells. *Mol Cancer* (2020) 19:101. doi: 10.1186/s12943-020-01221-6

119. Zheng R, Zhang K, Tan S, Gao F, Zhang Y, Xu W, et al. Exosomal circLPAR1 functions in colorectal cancer diagnosis and tumorigenesis through suppressing BRD4 *via* METTL3-eIF3h interaction. *Mol Cancer* (2022) 21:49. doi: 10.1186/s12943-021-01471-y

120. Melo SA, Luecke LB, Kahlert C, Fernandez AF, Gammon ST, Kaye J, et al. Glypican-1 identifies cancer exosomes and detects early pancreatic cancer. *Nature* (2015) 523:177–82. doi: 10.1038/nature14581

121. Khan S, Jutzy JM, Valenzuela MM, Turay D, Aspe JR, Ashok A, et al. Plasma-derived exosomal survivin, a plausible biomarker for early detection of prostate cancer. *PLoS One* (2012) 7:e46737. doi: 10.1371/journal.pone.0046737

122. Li S, Zhao Y, Chen W, Yin L, Zhu J, Zhang H, et al. Exosomal ephrinA2 derived from serum as a potential biomarker for prostate cancer. *J Cancer* (2018) 9:2659–65. doi: 10.7150/jca.25201

123. Szajnik M, Derbis M, Lach M, Patalas P, Michalak M, Drzewiecka H, et al. Exosomes in plasma of patients with ovarian carcinoma: Potential biomarkers of tumor progression and response to therapy. *Gynecol obstetrics (Sunnyvale Calif.)* (2013) (Suppl 4):3. doi: 10.4172/2161-0932.S4-003

124. Wei P, Wu F, Kang B, Sun X, Heskia F, Pachot A, et al. Plasma extracellular vesicles detected by single molecule array technology as a liquid biopsy for colorectal cancer. *J extracellular vesicles* (2020) 9:1809765. doi: 10.1080/20013078.2020.1809765

125. Fu H, Yang H, Zhang X, Wang B, Mao J, Li X, et al. Exosomal TRIM3 is a novel marker and therapy target for gastric cancer. *J Exp Clin Cancer Res CR* (2018) 37:162. doi: 10.1186/s13046-018-0825-0

126. Pan D, Chen J, Feng C, Wu W, Wang Y, Tong J, et al. Preferential localization of MUC1 glycoprotein in exosomes secreted by non-small cell lung carcinoma cells. *Int J Mol Sci* (2019) 20. doi: 10.3390/ijms20020323

127. Moon PG, Lee JE, Cho YE, Lee SJ, Jung JH, Chae YS, et al. Identification of developmental endothelial locus-1 on circulating extracellular vesicles as a novel biomarker for early breast cancer detection. *Clin Cancer Res an Off J Am Assoc Cancer Res* (2016) 22:1757–66. doi: 10.1158/1078-0432.Ccr-15-0654

128. Moon PG, Lee JE, Cho YE, Lee SJ, Chae YS, Jung JH, et al. Fibronectin on circulating extracellular vesicles as a liquid biopsy to detect breast cancer. *Oncotarget* (2016) 7:40189–99. doi: 10.18632/oncotarget.9561

129. Yoon JH, Ham IH, Kim O, Ashktorab H, Smoot DT, Nam SW, et al. Gastrokine 1 protein is a potential theragnostic target for gastric cancer. *Gastric Cancer Off J Int Gastric Cancer Assoc Japanese Gastric Cancer Assoc* (2018) 21:956–67. doi: 10.1007/s10120-018-0828-8

130. Raimondo F, Morosi L, Corbetta S, Chinello C, Brambilla P, Della Mina P, et al. Differential protein profiling of renal cell carcinoma urinary exosomes. *Mol Biosyst* (2013) 9:1220–33. doi: 10.1039/c3mb25582d

131. Tian F, Zhang S, Liu C, Han Z, Liu Y, Deng J, et al. Protein analysis of extracellular vesicles to monitor and predict therapeutic response in metastatic breast cancer. *Nat Commun* (2021) 12:2536. doi: 10.1038/s41467-021-22913-7

132. Pang Y, Shi J, Yang X, Wang C, Sun Z, Xiao R. Personalized detection of circling exosomal PD-L1 based on Fe(3)O(4)@TiO(2) isolation and SERS immunoassay. *Biosensors bioelectronics* (2020) 148:111800. doi: 10.1016/j.bios.2019.111800

133. Zhang P, Zhou X, He M, Shang Y, Tetlow AL, Godwin AK, et al. Ultrasensitive detection of circulating exosomes with a 3D-nanopatterned microfluidic chip. *Nat Biomed Eng* (2019) 3:438–51. doi: 10.1038/s41551-019-0356-9

134. Skotland T, Ekroos K, Kauhanen D, Simolin H, Seierstad T, Berge V, et al. Molecular lipid species in urinary exosomes as potential prostate cancer biomarkers. *Eur J Cancer (Oxford Engl 1990)* (2017) 70:122–32. doi: 10.1016/j.ejca.2016.10.011

135. Glover SC, Nouri MZ, Tuna KM, Mendoza Alvarez LB, Ryan LK, Shirley JF, et al. Lipidomic analysis of urinary exosomes from hereditary α-tryptasemia patients and healthy volunteers. *FASEB bioAdvances* (2019) 1:624–38. doi: 10.1096/fba.2019-00030

136. Tao L, Zhou J, Yuan C, Zhang L, Li D, Si D, et al. Metabolomics identifies serum and exosomes metabolite markers of pancreatic cancer. *Metabolomics Off J Metabolomic Soc* (2019) 15:86. doi: 10.1007/s11306-019-1550-1

137. Pieragostino D, Cicalini I, Lanuti P, Ercolino E, di Ioia M, Zucchelli M, et al. Enhanced release of acid sphingomyelinase-enriched exosomes generates a lipidomics signature in CSF of multiple sclerosis patients. *Sci Rep* (2018) 8:3071. doi: 10.1038/s41598-018-21497-5

138. Gurunathan S, Kang MH, Jeyaraj M, Qasim M, Kim JH. Review of the isolation, characterization, biological function, and multifarious therapeutic approaches of exosomes. *Cells* (2019) 8. doi: 10.3390/cells8040307

139. Record M, Carayon K, Poirot M, Silvente-Poirot S. Exosomes as new vesicular lipid transporters involved in cell-cell communication and various pathophysiologies. *Biochim Biophys Acta* (2014) 1841:108–20. doi: 10.1016/j.bbalip.2013.10.004

140. Xiao Y, Zhong J, Zhong B, Huang J, Jiang L, Jiang Y, et al. Exosomes as potential sources of biomarkers in colorectal cancer. *Cancer Lett* (2020) 476:13–22. doi: 10.1016/j.canlet.2020.01.033

141. Yáñez-Mó M, Siljander PR, Andreu Z, Zavec AB, Borràs FE, Buzas EI, et al. Biological properties of extracellular vesicles and their physiological functions. *J extracellular vesicles* (2015) 4:27066. doi: 10.3402/jev.v4.27066

142. Rajagopal C, Harikumar KB. The origin and functions of exosomes in cancer. *Front Oncol* (2018) 8:66. doi: 10.3389/fonc.2018.00066

143. Barile L, Cervio E, Lionetti V, Milano G, Ciullo A, Biemmi V, et al. Cardioprotection by cardiac progenitor cell-secreted exosomes: role of pregnancy-associated plasma protein-a. *Cardiovasc Res* (2018) 114:992–1005. doi: 10.1093/cvr/cvy055

144. Terrasini N, Lionetti V. Exosomes in critical illness. *Crit Care Med* (2017) 45:1054–60. doi: 10.1097/ccm.0000000000002328

145. Carrozzo A, Casieri V, Di Silvestre D, Brambilla F, De Nitto E, Sardaro N, et al. Plasma exosomes characterization reveals a perioperative protein signature in older patients undergoing different types of on-pump cardiac surgery. *GeroScience* (2021) 43:773–89. doi: 10.1007/s11357-020-00223-y

146. Chang W, Wang J. Exosomes and their noncoding RNA cargo are emerging as new modulators for diabetes mellitus. *Cells* (2019) 8. doi: 10.3390/cells8080853

147. Elashiry M, Elashiry MM, Elsayed R, Rajendran M, Auersvald C, Zeitoun R, et al. Dendritic cell derived exosomes loaded with immunoregulatory cargo reprogram local immune responses and inhibit degenerative bone disease *in vivo*. *J extracellular vesicles* (2020) 9:1795362. doi: 10.1080/20013078.2020.1795362

148. Riazifar M, Mohammadi MR, Pone EJ, Yeri A, Lässer C, Segaliny AI, et al. Stem cell-derived exosomes as nanotherapeutics for autoimmune and neurodegenerative disorders. *ACS nano* (2019) 13:6670–88. doi: 10.1021/acsnano.9b01004

149. Zhang C, Wang XY, Zhang P, He TC, Han JH, Zhang R, et al. Cancer-derived exosomal HSPC111 promotes colorectal cancer liver metastasis by reprogramming lipid metabolism in cancer-associated fibroblasts. *Cell Death Dis* (2022) 13:57. doi: 10.1038/s41419-022-04506-4

150. Skotland T, Hessvik NP, Sandvig K, Llorente A. Exosomal lipid composition and the role of ether lipids and phosphoinositides in exosome biology. *J Lipid Res* (2019) 60:9–18. doi: 10.1194/jlr.R084343

151. Skryabin GO, Komelkov AV, Savelyeva EE, Tchevkina EM. Lipid rafts in exosome biogenesis. *Biochem Biokhimiia* (2020) 85:177–91. doi: 10.1134/s0006297920020054

152. Huang X, Yuan T, Tschannen M, Sun Z, Jacob H, Du M, et al. Characterization of human plasma-derived exosomal RNAs by deep sequencing. *BMC Genomics* (2013) 14:319. doi: 10.1186/1471-2164-14-319

153. Fu Y, Liu X, Chen Q, Liu T, Lu C, Yu J, et al. Downregulated miR-98-5p promotes PDAC proliferation and metastasis by reversely regulating MAP4K4. *J Exp Clin Cancer Res CR* (2018) 37:130. doi: 10.1186/s13046-018-0807-2

154. Wang N, Wang L, Yang Y, Gong L, Xiao B, Liu X. A serum exosomal microRNA panel as a potential biomarker test for gastric cancer. *Biochem Biophys Res Commun* (2017) 493:1322–8. doi: 10.1016/j.bbrc.2017.10.003

155. Buratta S, Tancini B, Sagini K, Delo F, Chiaradia E, Urbanelli L, et al. Lysosomal exocytosis, exosome release and secretory autophagy: The autophagic- and endo-lysosomal systems go extracellular. *Int J Mol Sci* (2020) 21. doi: 10.3390/ijms21072576

156. Abdulrahman BA, Abdelaziz DH, Schatzl HM. Autophagy regulates exosomal release of prions in neuronal cells. *J Biol Chem* (2018) 293:8956–68. doi: 10.1074/jbc.RA117.000713

157. Zheng K, Ma J, Wang Y, He Z, Deng K. Sulforaphane inhibits autophagy and induces exosome-mediated paracrine senescence *via* regulating mTOR/TFE3. *Mol Nutr Food Res* (2020) 64:e1901231. doi: 10.1002/mnfr.201901231

158. Guo H, Chitiprolu M, Roncevic L, Javalet C, Hemming FJ, Trung MT, et al. Atg5 disassociates the V(1)V(0)-ATPase to promote exosome production and tumor metastasis independent of canonical macroautophagy. *Dev Cell* (2017) 43:716–30.e717. doi: 10.1016/j.devcel.2017.11.018

159. Keller MD, Ching KL, Liang FX, Dhabaria A, Tam K, Ueberheide BM, et al. Decoy exosomes provide protection against bacterial toxins. *Nature* (2020) 579:260–4. doi: 10.1038/s41586-020-2066-6

160. Jafari R, Rahbarghazi R, Ahmadi M, Hassanpour M, Rezaie J. Hypoxic exosomes orchestrate tumorigenesis: molecular mechanisms and therapeutic implications. *J Trans Med* (2020) 18:474. doi: 10.1186/s12967-020-02662-9

161. Choudhry H, Harris AL. Advances in hypoxia-inducible factor biology. *Cell Metab* (2018) 27:281–98. doi: 10.1016/j.cmet.2017.10.005

162. Zhang W, Zhou X, Yao Q, Liu Y, Zhang H, Dong Z. HIF-1-mediated production of exosomes during hypoxia is protective in renal tubular cells. *American journal of physiology. Renal Physiol* (2017) 313:F906–f913. doi: 10.1152/ajprenal.00178.2017

163. King HW, Michael MZ, Gleadle JM. Hypoxic enhancement of exosome release by breast cancer cells. *BMC Cancer* (2012) 12:421. doi: 10.1186/1471-2407-12-421

164. Ban JJ, Lee M, Im W, Kim M. Low pH increases the yield of exosome isolation. *Biochem Biophys Res Commun* (2015) 461:76–9. doi: 10.1016/j.bbrc.2015.03.172

165. Wang Y, Yin K, Tian J, Xia X, Ma J, Tang X, et al. Granulocytic myeloid-derived suppressor cells promote the stemness of colorectal cancer cells through exosomal S100A9. *Advanced Sci (Weinheim Baden-Wurttemberg Germany)* (2019) 6:1901278. doi: 10.1002/advs.201901278

166. He G, Peng X, Wei S, Yang S, Li X, Huang M, et al. Exosomes in the hypoxic TME: from release, uptake and biofunctions to clinical applications. *Mol Cancer* (2022) 21:19. doi: 10.1186/s12943-021-01440-5

167. Duan P, Tan J, Miao Y, Zhang Q. Potential role of exosomes in the pathophysiology, diagnosis, and treatment of hypoxic diseases. *Am J Trans Res* (2019) 11:1184–201.

168. Datta A, Kim H, McGee L, Johnson AE, Talwar S, Marugan J, et al. High-throughput screening identified selective inhibitors of exosome biogenesis and secretion: A drug repurposing strategy for advanced cancer. *Sci Rep* (2018) 8:8161. doi: 10.1038/s41598-018-26411-7

169. Savina A, Furlán M, Vidal M, Colombo MI. Exosome release is regulated by a calcium-dependent mechanism in K562 cells. *J Biol Chem* (2003) 278:20083–90. doi: 10.1074/jbc.M301642200

170. Serrano D, Bhowmick T, Chadha R, Garnacho C, Muro S. Intercellular adhesion molecule 1 engagement modulates sphingomyelinase and ceramide, supporting uptake of drug carriers by the vascular endothelium. *Arteriosclerosis thrombosis Vasc Biol* (2012) 32:1178–85. doi: 10.1161/atvbaha.111.244186

171. Kosgodage US, Trindade RP, Thompson PR, Inal JM, Lange S. Chloramidine/Bisindolylmaleimide-I-Mediated inhibition of exosome and microvesicle release and enhanced efficacy of cancer chemotherapy. *Int J Mol Sci* (2017) 18. doi: 10.3390/ijms18051007

172. Flory J, Lipska K. Metformin in 2019. *JAMA* (2019) 321:1926–7. doi: 10.1001/jama.2019.3805

173. Liao Z, Li S, Lu S, Liu H, Li G, Ma L, et al. Metformin facilitates mesenchymal stem cell-derived extracellular nanovesicles release and optimizes therapeutic efficacy in intervertebral disc degeneration. *Biomaterials* (2021) 274:120850. doi: 10.1016/j.biomaterials.2021.120850

174. Mogavero A, Maiorana MV, Zanutto S, Varinelli L, Bozzi F, Belfiore A, et al. Metformin transiently inhibits colorectal cancer cell proliferation as a result of either AMPK activation or increased ROS production. *Sci Rep* (2017) 7:15992. doi: 10.1038/s41598-017-16149-z

175. Gao L, He Y, Wang K, Wang C, Wu H, Hu A, et al. All-trans retinoic acid suppressed GES-1 cell proliferation induced by exosomes from patients with precancerous lesions by arresting the cell cycle in s-phase. *Eur J Cancer Prev Off J Eur Cancer Prev Organisation (ECP)* (2021) 30:113–9. doi: 10.1097/cej.0000000000000571

176. Wernly B, Erlinge D, Pernow J, Zhou Z. Ticagrelor: a cardiometabolic drug targeting erythrocyte-mediated purinergic signaling? *American journal of physiology. Heart Circulatory Physiol* (2021) 320:H90–h94. doi: 10.1152/ajpheart.00570.2020

177. Casieri V, Matteucci M, Pasanisi EM, Papa A, Barile L, Fritsche-Danielson R, et al. Ticagrelor enhances release of anti-hypoxic cardiac progenitor cell-derived exosomes through increasing cell proliferation *In vitro*. *Sci Rep* (2020) 10:2494. doi: 10.1038/s41598-020-59225-7

178. Bitirim CV, Ozer ZB, Aydos D, Genc K, Demirsoy S, Akcali KC, et al. Cardioprotective effect of extracellular vesicles derived from ticagrelor-pretreated cardiomyocyte on hyperglycemic cardiomyocytes through alleviation of oxidative and endoplasmic reticulum stress. *Sci Rep* (2022) 12:5651. doi: 10.1038/s41598-022-09627-6

179. Kulshreshtha A, Singh S, Ahmad M, Khanna K, Ahmad T, Agrawal A, et al. Simvastatin mediates inhibition of exosome synthesis, localization and secretion *via* multicomponent interventions. *Sci Rep* (2019) 9:16373. doi: 10.1038/s41598-019-52765-7

180. Huang P, Wang L, Li Q, Tian X, Xu J, Xu J, et al. Atorvastatin enhances the therapeutic efficacy of mesenchymal stem cells-derived exosomes in acute myocardial infarction *via* up-regulating long non-coding RNA H19. *Cardiovasc Res* (2020) 116:353–67. doi: 10.1093/cvr/cvz139

181. Tajik T, Baghaei K, Moghadam VE, Farrokhi N, Salami SA. Extracellular vesicles of cannabis with high CBD content induce anticancer signaling in human hepatocellular carcinoma. *Biomedicine pharmacotherapy = Biomedecine pharmacotherapie* (2022) 152:113209. doi: 10.1016/j.biopha.2022.113209

182. Zhang H, Lu J, Liu J, Zhang G, Lu A. Advances in the discovery of exosome inhibitors in cancer. *J Enzyme inhibition medicinal Chem* (2020) 35:1322–30. doi: 10.1080/14756366.2020.1754814

183. Lionetti V, Tuana BS, Casieri V, Parikh M, Pierce GN. Importance of functional food compounds in cardioprotection through action on the epigenome. *Eur Heart J* (2019) 40:575–82. doi: 10.1093/eurheartj/ehy597

184. Mantilla-Escalante DC, López de Las Hazas MC, Crespo MC, Martín-Hernández R, Tomé-Carneiro J, Del Pozo-Acebo L, et al. Mediterranean Diet enriched in extra-virgin olive oil or nuts modulates circulating exosomal non-coding RNAs. *Eur J Nutr* (2021) 60:4279–93. doi: 10.1007/s00394-021-02594-0

185. Otsuka K, Yamamoto Y, Ochiya T. Uncovering temperature-dependent extracellular vesicle secretion in breast cancer. *J extracellular vesicles* (2020) 10:e12049. doi: 10.1002/jev2.12049

186. Cheng Y, Zeng Q, Han Q, Xia W. Effect of pH, temperature and freezing-thawing on quantity changes and cellular uptake of exosomes. *Protein Cell* (2019) 10:295–9. doi: 10.1007/s13238-018-0529-4

187. Mutschelknaus L, Peters C, Winkler K, Yentrapalli R, Heider T, Atkinson MJ, et al. Exosomes derived from squamous head and neck cancer promote cell survival after ionizing radiation. *PLoS One* (2016) 11:e0152213. doi: 10.1371/journal.pone.0152213

188. Ab Razak NS, Ab Mutalib NS, Mohtar MA, Abu N. Impact of chemotherapy on extracellular vesicles: Understanding the chemo-EVs. *Front Oncol* (2019) 9:1113. doi: 10.3389/fonc.2019.01113

189. Avisar A, Cohen M, Brenner B, Bronshtein T, Machluf M, Bar-Sela G, et al. Extracellular vesicles reflect the efficacy of wheatgrass juice supplement in colon cancer patients during adjuvant chemotherapy. *Front Oncol* (2020) 10:1659. doi: 10.3389/fonc.2020.01659

190. Yu W, Hurley J, Roberts D, Chakrabortty SK, Enderle D, Noerholm M, et al. Exosome-based liquid biopsies in cancer: opportunities and challenges. *Ann Oncol Off J Eur Soc Med Oncol* (2021) 32:466–77. doi: 10.1016/j.annonc.2021.01.074

191. Sahoo S, Adamiak M, Mathiyalagan P, Kenneweg F, Kafert-Kasting S, Thum T. Therapeutic and diagnostic translation of extracellular vesicles in cardiovascular diseases: Roadmap to the clinic. *Circulation* (2021) 143:1426–49. doi: 10.1161/circulationaha.120.049254

192. Kugeratski FG, Hodge K, Lilla S, McAndrews KM, Zhou X, Hwang RF, et al. Quantitative proteomics identifies the core proteome of exosomes with syntenin-1 as the highest abundant protein and a putative universal biomarker. *Nat Cell Biol* (2021) 23:631–41. doi: 10.1038/s41556-021-00693-y

193. Tang XH, Guo T, Gao XY, Wu XL, Xing XF, Ji JF, et al. Exosome-derived noncoding RNAs in gastric cancer: functions and clinical applications. *Mol Cancer* (2021) 20:99. doi: 10.1186/s12943-021-01396-6

194. Zhou R, Chen KK, Zhang J, Xiao B, Huang Z, Ju C, et al. The decade of exosomal long RNA species: an emerging cancer antagonist. *Mol Cancer* (2018) 17:75. doi: 10.1186/s12943-018-0823-z

195. Ji J, Chen R, Zhao L, Xu Y, Cao Z, Xu H, et al. Circulating exosomal mRNA profiling identifies novel signatures for the detection of prostate cancer. *Mol Cancer* (2021) 20:58. doi: 10.1186/s12943-021-01349-z

196. Skog J, Würdinger T, van Rijn S, Meijer DH, Gainche L, Sena-Esteves M, et al. Glioblastoma microvesicles transport RNA and proteins that promote tumour growth and provide diagnostic biomarkers. *Nat Cell Biol* (2008) 10:1470–6. doi: 10.1038/ncb1800

197. Esquela-Kerscher A, Slack FJ. Oncomirs - microRNAs with a role in cancer. *Nat Rev Cancer* (2006) 6:259–69. doi: 10.1038/nrc1840

198. Mitchell PS, Parkin RK, Kroh EM, Fritz BR, Wyman SK, Pogosova-Agadjanyan EL, et al. Circulating microRNAs as stable blood-based markers for cancer detection. *Proc Natl Acad Sci United States America* (2008) 105:10513–8. doi: 10.1073/pnas.0804549105

199. Huang Z, Zhu D, Wu L, He M, Zhou X, Zhang L, et al. Six serum-based miRNAs as potential diagnostic biomarkers for gastric cancer. *Cancer epidemiology Biomarkers Prev Publ Am Assoc Cancer Research cosponsored by Am Soc Prev Oncol* (2017) 26:188–96. doi: 10.1158/1055-9965.Epi-16-0607

200. Butz H, Nofech-Mozes R, Ding Q, Khella HWZ, Szabó PM, Jewett M, et al. Exosomal MicroRNAs are diagnostic biomarkers and can mediate cell-cell communication in renal cell carcinoma. *Eur Urol Focus* (2016) 2:210–8. doi: 10.1016/j.euf.2015.11.006

201. Muramatsu-Maekawa Y, Kawakami K, Fujita Y, Takai M, Kato D, Nakane K, et al. Profiling of serum extracellular vesicles reveals miRNA-4525 as a potential biomarker for advanced renal cell carcinoma. *Cancer Genomics Proteomics* (2021) 18:253–9. doi: 10.21873/cgp.20256

202. Madhavan B, Yue S, Galli U, Rana S, Gross W, Müller M, et al. Combined evaluation of a panel of protein and miRNA serum-exosome biomarkers for pancreatic cancer diagnosis increases sensitivity and specificity. *Int J Cancer* (2015) 136:2616–27. doi: 10.1002/ijc.29324

203. Manterola L, Guruceaga E, Gállego Pérez-Larraya J, González-Huarriz M, Jauregui P, Tejada S, et al. A small noncoding RNA signature found in exosomes of GBM patient serum as a diagnostic tool. *Neuro-oncology* (2014) 16:520–7. doi: 10.1093/neuonc/not218

204. Rinn JL, Chang HY. Genome regulation by long noncoding RNAs. *Annu Rev Biochem* (2012) 81:145–66. doi: 10.1146/annurev-biochem-051410-092902

205. Li Q, Shao Y, Zhang X, Zheng T, Miao M, Qin L, et al. Plasma long noncoding RNA protected by exosomes as a potential stable biomarker for gastric cancer. *Tumour Biol J Int Soc Oncodevelopmental Biol Med* (2015) 36:2007–12. doi: 10.1007/s13277-014-2807-y

206. Wang Y, Liu J, Ma J, Sun T, Zhou Q, Wang W, et al. Exosomal circRNAs: biogenesis, effect and application in human diseases. *Mol Cancer* (2019) 18:116. doi: 10.1186/s12943-019-1041-z

207. Lin L, Cai GX, Zhai XM, Yang XX, Li M, Li K, et al. Plasma-derived extracellular vesicles circular RNAs serve as biomarkers for breast cancer diagnosis. *Front Oncol* (2021) 11:752651. doi: 10.3389/fonc.2021.752651

208. Wang S, Hu Y, Lv X, Li B, Gu D, Li Y, et al. Circ-0000284 arouses malignant phenotype of cholangiocarcinoma cells and regulates the biological functions of peripheral cells through cellular communication. *Clin Sci (London Engl 1979)* (2019) 133:1935–53. doi: 10.1042/cs20190589

209. Pan B, Qin J, Liu X, He B, Wang X, Pan Y, et al. Identification of serum exosomal hsa-circ-0004771 as a novel diagnostic biomarker of colorectal cancer. *Front Genet* (2019) 10:1096. doi: 10.3389/fgene.2019.01096

210. Ma H, Xu Y, Zhang R, Guo B, Zhang S, Zhang X. Differential expression study of circular RNAs in exosomes from serum and urine in patients with idiopathic membranous nephropathy. *Arch Med Sci AMS* (2019) 15:738–53. doi: 10.5114/aoms.2019.84690

211. Mirzaei H, Sahebkar A, Jaafari MR, Goodarzi M, Mirzaei HR. Diagnostic and therapeutic potential of exosomes in cancer: The beginning of a new tale? *J Cell Physiol* (2017) 232:3251–60. doi: 10.1002/jcp.25739

212. Wang S, Qiu Y, Bai B. The expression, regulation, and biomarker potential of glypican-1 in cancer. *Front Oncol* (2019) 9:614. doi: 10.3389/fonc.2019.00614

213. Li J, Chen Y, Guo X, Zhou L, Jia Z, Peng Z, et al. GPC1 exosome and its regulatory miRNAs are specific markers for the detection and target therapy of colorectal cancer. *J Cell Mol Med* (2017) 21:838–47. doi: 10.1111/jcmm.12941

214. Hoshino A, Kim HS, Bojmar L, Gyan KE, Cioffi M, Hernandez J, et al. Extracellular vesicle and particle biomarkers define multiple human cancers. *Cell* (2020) 182:1044–61.e1018. doi: 10.1016/j.cell.2020.07.009

215. Sun Y, Xia Z, Shang Z, Sun K, Niu X, Qian L, et al. Facile preparation of salivary extracellular vesicles for cancer proteomics. *Sci Rep* (2016) 6:24669. doi: 10.1038/srep24669

216. Gao J, Qiu X, Li X, Fan H, Zhang F, Lv T, et al. Expression profiles and clinical value of plasma exosomal Tim-3 and galectin-9 in non-small cell lung cancer. *Biochem Biophys Res Commun* (2018) 498:409–15. doi: 10.1016/j.bbrc.2018.02.114

217. Simbari F, McCaskill J, Coakley G, Millar M, Maizels RM, Fabriás G, et al. Plasmalogen enrichment in exosomes secreted by a nematode parasite versus those derived from its mouse host: implications for exosome stability and biology. *J extracellular vesicles* (2016) 5:30741. doi: 10.3402/jev.v5.30741

218. Vlassov AV, Magdaleno S, Setterquist R, Conrad R. Exosomes: current knowledge of their composition, biological functions, and diagnostic and therapeutic potentials. *Biochim Biophys Acta* (2012) 1820:940–8. doi: 10.1016/j.bbagen.2012.03.017

219. Beloribi S, Ristorcelli E, Breuzard G, Silvy F, Bertrand-Michel J, Beraud E, et al. Exosomal lipids impact notch signaling and induce death of human pancreatic tumoral SOJ-6 cells. *PLoS One* (2012) 7:e47480. doi: 10.1371/journal.pone.0047480

220. Beloribi-Djefaflia S, Siret C, Lombardo D. Exosomal lipids induce human pancreatic tumoral MiaPaCa-2 cells resistance through the CXCR4-SDF-1α signaling axis. *Oncoscience* (2015) 2:15–30. doi: 10.18632/oncoscience.96

221. Wu Q, Ishikawa T, Sirianni R, Tang H, McDonald JG, Yuhanna IS, et al. 27-hydroxycholesterol promotes cell-autonomous, ER-positive breast cancer growth. *Cell Rep* (2013) 5:637–45. doi: 10.1016/j.celrep.2013.10.006

222. Roberg-Larsen H, Lund K, Seterdal KE, Solheim S, Vehus T, Solberg N, et al. Mass spectrometric detection of 27-hydroxycholesterol in breast cancer exosomes. *J Steroid Biochem Mol Biol* (2017) 169:22–8. doi: 10.1016/j.jsbmb.2016.02.006

223. Skotland T, Sandvig K, Llorente A. Lipids in exosomes: Current knowledge and the way forward. *Prog Lipid Res* (2017) 66:30–41. doi: 10.1016/j.plipres.2017.03.001

224. Donoso-Quezada J, Ayala-Mar S, González-Valdez J. The role of lipids in exosome biology and intercellular communication: Function, analytics and applications. *Traffic (Copenhagen Denmark)* (2021) 22:204–20. doi: 10.1111/tra.12803

225. Gurung S, Perocheau D, Touramanidou L, Baruteau J. The exosome journey: from biogenesis to uptake and intracellular signalling. *Cell communication Signaling CCS* (2021) 19:47. doi: 10.1186/s12964-021-00730-1

226. Brzozowski JS, Jankowski H, Bond DR, McCague SB, Munro BR, Predebon MJ, et al. Lipidomic profiling of extracellular vesicles derived from prostate and prostate cancer cell lines. *Lipids Health Dis* (2018) 17:211. doi: 10.1186/s12944-018-0854-x

227. Chapuy-Regaud S, Dubois M, Plisson-Chastang C, Bonnefois T, Lhomme S, Bertrand-Michel J, et al. Characterization of the lipid envelope of exosome encapsulated HEV particles protected from the immune response. *Biochimie* (2017) 141:70–9. doi: 10.1016/j.biochi.2017.05.003

228. Sancho-Albero M, Jarne C, Savirón M, Martín-Duque P, Membrado L, Cebolla VL, et al. High-performance thin-layer chromatography-Densitometry-Tandem ESI-MS to evaluate phospholipid content in exosomes of cancer cells. *Int J Mol Sci* (2022) 23. doi: 10.3390/ijms23031150

229. Haraszti RA, Didiot MC, Sapp E, Leszyk J, Shaffer SA, Rockwell HE, et al. High-resolution proteomic and lipidomic analysis of exosomes and microvesicles from different cell sources. *J extracellular vesicles* (2016) 5:32570. doi: 10.3402/jev.v5.32570

230. Linton SS, Abraham T, Liao J, Clawson GA, Butler PJ, Fox T, et al. Tumor-promoting effects of pancreatic cancer cell exosomes on THP-1-derived macrophages. *PLoS One* (2018) 13:e0206759. doi: 10.1371/journal.pone.0206759

231. Kim CW, Lee HM, Lee TH, Kang C, Kleinman HK, Gho YS. Extracellular membrane vesicles from tumor cells promote angiogenesis *via* sphingomyelin. *Cancer Res* (2002) 62:6312–7.

232. Jiang C, Hopfner F, Berg D, Hu MT, Pilotto A, Borroni B, et al. Validation of α-synuclein in L1CAM-immunocaptured exosomes as a biomarker for the stratification of parkinsonian syndromes. *Movement Disord Off J Movement Disord Soc* (2021) 36:2663–9. doi: 10.1002/mds.28591

233. Huang C, Pan L, Shen X, Tian H, Guo L, Zhang Z, et al. Hsp16.3 of mycobacterium tuberculosis in exosomes as a biomarker of tuberculosis. *Eur J Clin Microbiol Infect Dis Off Publ Eur Soc Clin Microbiol* (2021) 40:2427–30. doi: 10.1007/s10096-021-04246-x

234. Liu Y, Li Y, Zang J, Zhang T, Li Y, Tan Z, et al. CircOGDH is a penumbra biomarker and therapeutic target in acute ischemic stroke. *Circ Res* (2022) 130:907–24. doi: 10.1161/circresaha.121.319412

235. Sharma R, Huang X, Brekken RA, Schroit AJ. Detection of phosphatidylserine-positive exosomes for the diagnosis of early-stage malignancies. *Br J Cancer* (2017) 117:545–52. doi: 10.1038/bjc.2017.183

236. Cesselli D, Parisse P, Aleksova A, Veneziano C, Cervellin C, Zanello A, et al. Extracellular vesicles: How drug and pathology interfere with their biogenesis and function. *Front Physiol* (2018) 9:1394. doi: 10.3389/fphys.2018.01394

237. Drabovich AP, Martínez-Morillo E, Diamandis EP. Toward an integrated pipeline for protein biomarker development. *Biochim Biophys Acta* (2015) 1854:677–86. doi: 10.1016/j.bbapap.2014.09.006

238. Špilak A, Brachner A, Kegler U, Neuhaus W, Noehammer C. Implications and pitfalls for cancer diagnostics exploiting extracellular vesicles. *Advanced Drug delivery Rev* (2021) 175:113819. doi: 10.1016/j.addr.2021.05.029

239. Boukouris S, Mathivanan S. Exosomes in bodily fluids are a highly stable resource of disease biomarkers. *Proteomics. Clin Appl* (2015) 9:358–67. doi: 10.1002/prca.201400114

240. Rak J. Extracellular vesicles - biomarkers and effectors of the cellular interactome in cancer. *Front Pharmacol* (2013) 4:21. doi: 10.3389/fphar.2013.00021

241. Margolis L, Sadovsky Y. The biology of extracellular vesicles: The known unknowns. *PLoS Biol* (2019) 17:e3000363. doi: 10.1371/journal.pbio.3000363

frontiers | Frontiers in Oncology

TYPE Case Report
PUBLISHED 12 September 2022
DOI 10.3389/fonc.2022.981907

OPEN ACCESS

,
Jaymand,
Kermanshah University of Medical Sciences, Iran

REVIEWED BY
Xiaojie Wang,
Fujian Medical University Union Hospital, China
Leila Arabi,
Mashhad University of Medical Sciences, Iran

*CORRESPONDENCE
Qi Zeng
zengqi37@mail.sysu.edu.cn
Peter Ping Lin
plin@cytelligen.com

†These authors have contributed equally to this work

SPECIALTY SECTION
This article was submitted to Molecular and Cellular Oncology, a section of the journal Frontiers in Oncology

RECEIVED 29 June 2022
ACCEPTED 22 August 2022
PUBLISHED 12 September 2022

CITATION
Mi J, Yang F, Liu J, Liu M, Lin AY, Wang DD, Lin PP and Zeng Q (2022) Case report: Post-therapeutic laryngeal carcinoma patient possessing a high ratio of aneuploid CTECs to CTCs rapidly developed *de novo* malignancy in pancreas. *Front. Oncol.* 12:981907. doi: 10.3389/fonc.2022.981907

Case report: Post-therapeutic laryngeal carcinoma patient possessing a high ratio of aneuploid CTECs to CTCs rapidly developed *de novo* malignancy in pancreas

Jiaoping Mi[1†], Fang Yang[2†], Jiani Liu[2], Mingyang Liu[3], Alexander Y. Lin[4], Daisy Dandan Wang[4], Peter Ping Lin[4*] and Qi Zeng[2*]

[1]Department of Otolaryngology-Head and Neck Surgery, The Fifth Affiliated Hospital of Sun Yat-Sen University, Zhuhai, China, [2]Cancer Center, The Fifth Affiliated Hospital of Sun Yat-Sen University, Zhuhai, China, [3]State Key Laboratory of Molecular Oncology, National Cancer Center/National Clinical Research Center for Cancer/Cancer Hospital, Chinese Academy of Medical Sciences and Peking Union Medical College, Beijing, China, [4]Department of Oncology, Cytelligen, San Diego, CA, United States

Effectively evaluating therapeutic efficacy, detecting minimal residual disease (MRD) after therapy completion, and predicting early occurrence of malignancy in cancer patients remain as unmet imperative clinical demands. This article presents a case of a laryngeal carcinoma patient who had a surgical resection and complete post-operative chemoradiotherapy in combination with the targeted therapy, then rapidly developed pancreatic adenocarcinoma. Detected by SE-iFISH, the patient had a substantial amount of 107 non-hematological aneuploid circulating rare cells including 14 circulating tumor cells (CTCs, $CD31^-/CD45^-$) and 93 circulating tumor endothelial cells (CTECs, $CD31^+/CD45^-$) with a high ratio of CTECs/CTCs > 5 upon finishing post-surgical combination regimens. Positive detection of those aneuploid non-hematological circulating rare cells was five months prior to subsequent plasma CA19-9 increasing and ten months before the *de novo* pancreatic cancer was diagnosed by medical imaging modalities. Besides previously reported clinical utilities of co-detection of aneuploid $CD31^-$ CTCs and $CD31^+$ CTECs in real-time evaluation of therapeutic efficacy, longitudinal monitoring of emerging treatment resistance and adequate detection of MRD, a large cohort study is necessary to further investigate whether, and how, a high ratio of MRD CTECs to CTCs may function as an appropriate index forecasting either occurrence or metastatic distant recurrence of malignancy in post-therapeutic cancer patients.

KEYWORDS

MRD, prediction of cancer occurrence, liquid biopsy, aneuploid CTCs and CTECs, SE-iFISH

Introduction

Effectively evaluating therapeutic efficacy and predicting cancer patients possessing a high risk of malignancy remain highly challenging. Current clinical strategies to detect cancer occurrence mainly rely on medical imaging modalities, including computed tomography (CT) to show the location, anatomic shape, and size of a lesion; magnetic resonance imaging (MRI) that uses strong magnets to create cross-section images inside the body; and positron emission tomography (PET) to identify an increased glucose consumption spot of neoplasm. However, the hurdle of conventional clinical imaging is its limitation to detect only visible-sized tumors. Medical imaging detection of invisible minimal residual disease (MRD), which are a small number of cancer cells remaining in the body after treatment (1), has not yet been achieved.

The association of quantified circulating tumor cells (CTCs) with cancer occurrence has been reported elsewhere (2–5). Recent CTC studies have indicated that phenotypic and karyotypic variations in highly heterogeneous CTCs constantly occur throughout tumor progression and therapy (6). Conventional EpCAM and cytokeratin-dependent CTC enumeration alone is no longer sufficient to corelate the full spectrum of CTC characteristics with distinct clinical utilities (7).

Neoangiogenesis, a hallmark of cancers, is essential for tumorigenesis, progression, and cancer metastasis (8). A majority of endothelial cells (ECs) in tumor vasculatures are tumor endothelial cells (TECs), showing aneuploidy of chromosomes and phenotypic expression of CD31 (platelet endothelial cell adhesion molecule-1, PECAM-1) (9). TECs are predominately derived from the endothelialization of cancer cells and cancerization of ECs in the hypoxic tumor microenvironment (TME) (10). Contribution of diverse subpopulations of TECs to tumor progression (11), patients' survival, VEGF blockade, and regulating immune surveillance has recently been described (12). Similar to CTCs, TECs also shed from tumor vasculatures into peripheral blood and turn into $CD31^+$ aneuploid circulating TECs, known as CTECs (10, 13, 14). The clinical significance of CTECs, particularly PD-$L1^+$ (15), the stemness marker $CD44^+$ (16), and $EpCAM^+$/$Vimentin^+$ CTECs (17), in multiple types of cancers has been recently addressed (18–20). CTCs and CTECs are a unique pair of cellular circulating tumor biomarkers and have cross-talk and functional interplay in cancer patients (6, 10).

A novel strategy integrating subtraction enrichment (SE) and immunostaining-fluorescence *in situ* hybridization (SE-iFISH) has recently been reported to effectively co-detect and molecularly characterize aneuploid CTCs and CTECs (6, 13, 21). In contrast to conventional CTC detection methods, the EpCAM-independent subtraction enrichment (SE) strategy is able to enrich heterogeneously sized non-hematologic circulating rare cells, regardless of cell surface protein expression, followed by a comprehensive *in situ* phenotypic and karyotypic molecular characterization as well as categorization of enriched circulating rare cells (13, 21–23).

In this report, we present a case showing that a post-surgical laryngocarcinoma patient, after receiving a complete chemoradiotherapy, still showed a large quantity of CTCs and CTECs with a substantially high ratio of CTECs/CTCs > 5. Positive detection of CTCs and CTECs occurred ten months prior to the diagnosed pancreatic cancer. This case highlights potential unique clinical utilities of the co-detection of aneuploid $CD31^-$ CTCs and $CD31^+$ CTECs for adequate evaluation of treatment outcome, detection of MRD, as well as prediction of early occurrence of new primary lesion in post-therapeutic cancer patients.

Case presentation

As depicted in Figures 1A, B, a 57-year-old male was diagnosed with a primary hypolarynx squamous cell carcinoma (T2N1M0, stage III with a microinvasion) in July 2018 (t1). The patient was immediately subjected to a surgical resection to remove the malignant lesion. No abnormality was observed by abdominal color Doppler ultrasonography. From August 2018 (t2), the subject started receiving the intensity-modulated radiation therapy (IMRT, 60Gy/28F), concurrently in combination with three cycles of nedaplatin chemotherapy (140 mg) and six cycles of nimotuzumab targeted therapy.

Instead of longitudinal detection along with therapy process (15, 17, 22), co-detection of MRD aneuploid $CD31^-$ CTCs and $CD31^+$ CTECs was performed according to the protocol (13) at the end of combination regimens (t3, September 2018) in this case to evaluate surgery outcome and the therapeutic efficacy of the complete combination regimens. Comprehensive quantification and molecular characterization of aneuploid CTCs and CTECs were revealed in Figure 2A. A large quantity of 107 non-hematological circulating aneuploid rare cells including 14 CTCs and 93 CTECs were detected, with a high ratio of CTECs/CTCs > 5. Among 14 $CD31^-$ CTCs, four were small sized cells (4/14 = 28.6%). A majority of CTCs were multiploid in chr8 (≥ pentasomy 8, 57.1%). Out of 93 $CD31^+$ CTECs, most were large cells (89/93 = 95.7%). The predominant karyotype of CTECs was multiploidy. Large multiploid cells constitute the main population of detected CTECs ($_{L}CTECs^{multi}$, 80/93 = 86%). Representative images of CTCs and CTECs detected in this patient are demonstrated in Figure 2B.

In February 2019 (t4), as depicted in Figures 1Ca, b, the follow-up examination showed an increased cancer antigen 19-9 (CA19-9) (161.42 U/ml, reference range: 0-37 U/ml) and carcinoembryonic antigen (CEA) (6.71 ng/ml, reference range:

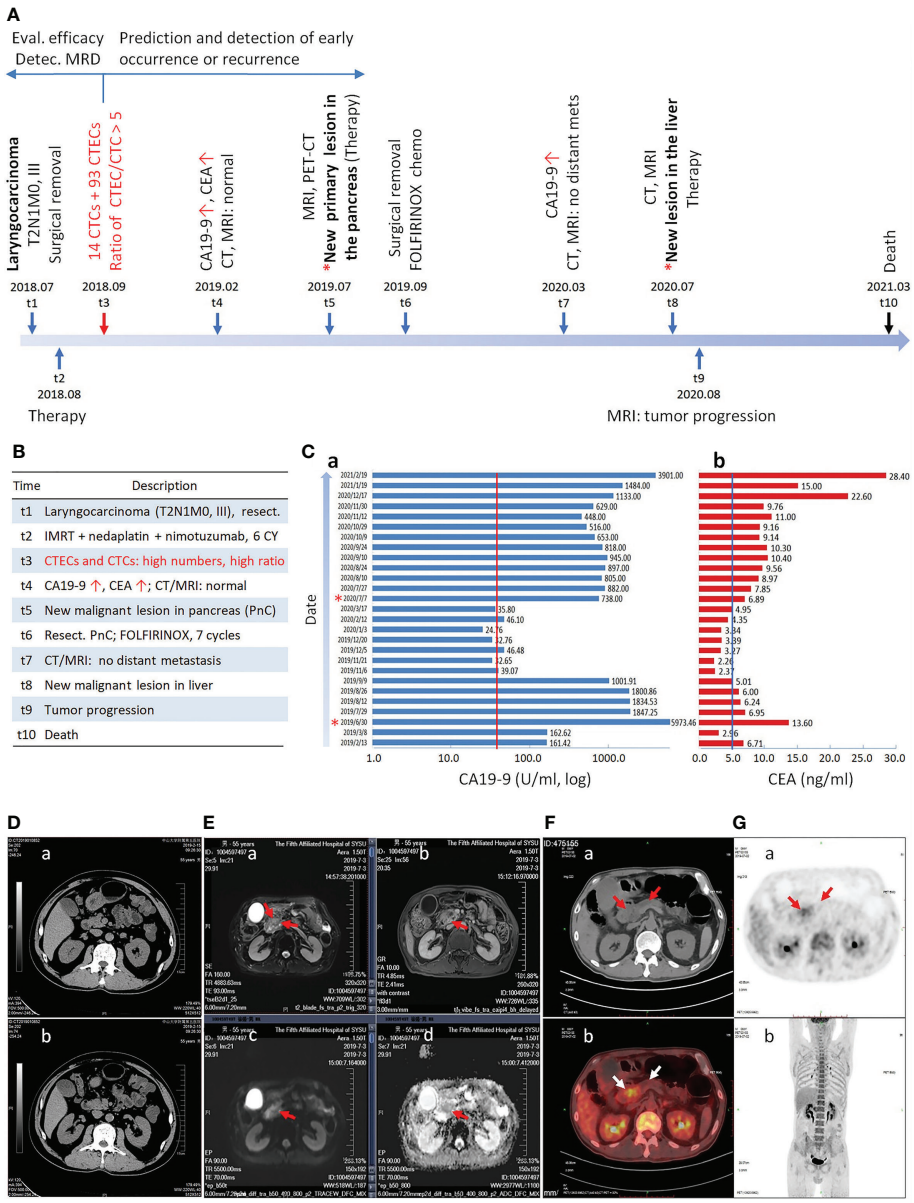

FIGURE 1
Longitudinal progression of the cancer patient. **(A)** Timeline of diagnosis and treatment of the patient at different time intervals is illustrated. The primary laryngocarcinoma is diagnosed at t1, followed by detection of CTCs and CTECs at t3. A new malignant lesion in the pancreas is confirmed at t5. Detection of CTCs and CTECs at the end of therapy could effectively evaluate therapeutic efficacy, detect MRD, and predict early occurrence of malignancy. **(B)** Description of each time point from t1 to t10. **(C)** Continuous monitoring of CA19-9 and CEA. The patient has the highest concentration of CA19-9 at t5. The cut-off values of CA19-9 (37 U/ml) and CEA (5 ng/ml) are indicated by red and blue line, respectively. **(D–G)** Medical imaging. **(Da, b)** Abdominal CT scan shows no abnormality in pancreas. **(Ea–d)** Epigastric MRI, CE-MRI, MRCP and DWI indicate the metastatic pancreatic head carcinoma. **(Ea)** A space-occupying lesion in pancreas T2WI (red arrows). **(Eb)** An increase contrast signal in a space-occupying lesion in pancreas T1WI (red arrow). **(Ec)** A strong signal in a space-occupying lesion in pancreas T1WI by DWI (red arrow). **(Ed)** ADC imaging shows decrease signal in a space-occupying lesion in pancreas T1WI (red arrow). **(F, G)** A pancreatic space-occupying lesion with enhanced glycometabolism shown by PET-CT (red and white arrows).

0-5 ng/ml) for the first time. However, the cervical MRI scan showed no laryngeal cancer recurrence. Additional abdominal color Doppler ultrasonography, abdominal CT scan (Figures 1Da, b), epigastric contrast enhanced (CE) MRI, and magnetic resonance cholangiopancreatography (MRCP) all showed no abnormality in pancreas and other visceral organs. The patient was diagnosed with a *de novo* pancreatic adenocarcinoma in July 2019 (t5). As illustrated in

A Comprehensive quantification and molecular characterization of aneuploid CTCs and CTECs

Categorization		haploid	diploid	triploid	tetraploid	multiploid	Sum1	% (Sum1/Total)	Total
CD31⁻ CTC	Large	0	n/c	2	0	8	10	71.4%	14
	Small	0	n/c	3	1	0	4	28.6%	
	Sum2	0	n/c	5	1	8			
	% (Sum2/Total)	0	n/c	35.7%	7.1%	57.1%			
CD31⁺ CTEC	Large	0	n/c	6	3	80	89	95.7%	93
	Small	0	n/c	3	1	0	4	4.3%	
	Sum2	0	n/c	9	4	80			
	% (Sum2/Total)	0	n/c	9.7%	4.3%	86.0%			

B Representative images of aneuploid CD31⁻ CTCs and CD31⁺ CTECs detected by SE-iFISH

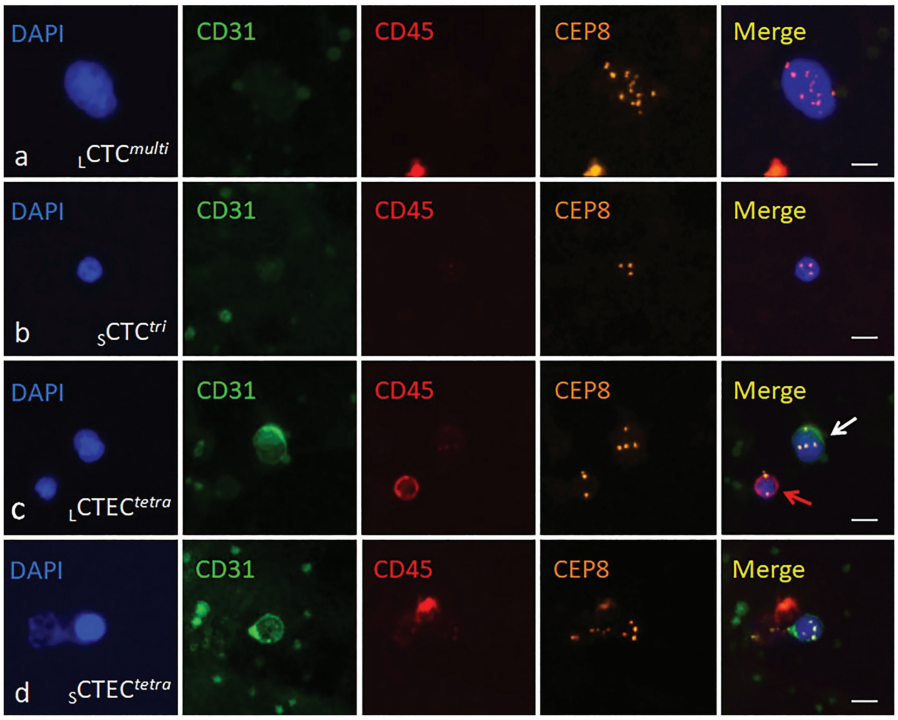

FIGURE 2
Detection and molecular characterization of aneuploid CD31⁻ CTCs and CD31⁺ CTECs performed by SE-iFISH. **(A)** Quantitative analysis of the detected CTCs and CTECs. Among 14 CTCs, 10 of them are large cells (10/14 = 71.4%), remaining 4 CTCs are in small cell size (28.6%). Different degrees of aneuploidy harbored by CTCs are trisomy 8 (35.7%), tetrasomy 8 (7.1%), and multisomy 8 (≥pentasomy 8, 57.1%), respectively. Most of detected 93 CTECs are large cells (89/93 = 95.7%), and the rest are small CTECs (4/93 = 4.3%). Degrees of aneuploidy in CTECs are 9.7% for triploidy, 4.3% for tetraploidy and 86% for multiploidy. n/c, not counted. **(B)** Representative images of the detected CTCs and CTECs. Ba, a large CTC with multiploid chr8 (CD31⁻/CD45⁻, >5 mm WBC size, $_{L}CTC^{multi}$). Bb, a small CTC with trisomy 8 (≤5 mm WBC, $_{S}CTC^{tri}$). Bc, a large tetraploid CTEC (CD31⁺/CD45⁻, $_{L}CTEC^{tetra}$) is indicated by a white arrow; a diploid CD45⁺ WBC is indicated by a red arrow. Bd, a small tetraploid CTEC ($_{S}CTEC^{tetra}$). Bars=5 μm.

Figures 1Ea–d, epigastric MRI scan, CE-MRI, MRCP, and diffusion-weighted imaging (DWI) indicated the pancreatic head carcinoma. PET-CT in Figures 1F, G showed a pancreatic space-occupying lesion with enhanced glycometabolism.

The patient was subjected to four cycles of FOLFIRINOX chemotherapy in July, followed by palliative resection of the pancreatic lesion in September 2019 (t6) (Histopathology: moderately-to-poorly differentiated adenocarcinoma, 3*2*1 cm). The subject afterwards received seven cycles of FOLFIRINOX adjuvant chemotherapy. A follow-up examination of abdominal CT and MRI scan in March 2020 (t7) showed no additional tumor metastasis. The hepatic metastasis was diagnosed in July 2020 (t8). Following three cycles of Gem plus Taxotere (GT) chemotherapy, tumor progression was observed by abdominal MRI scan in August 2020 (t9). The patient was subjected to four cycles of

FOLFIRINOX chemotherapy and subsequent combination therapy, whereas no progress was made on progression of the pancreatic cancer. The patient died in March 2021 (t10).

Discussion

Liquid biopsy detection of circulating tumor biomarkers, including circulating tumor DNA (ctDNA) and CTCs, has served as a non-invasive approach applied in diagnosis and treatment of cancers, as well as detection of therapy-resistant MRD (24). ctDNA is composed of small DNA fragments secreted from tumor cells or the breakdown product of necrotic carcinoma cells including CTCs (25). Compared to the non-negligible drawbacks of the non-specificity of small fragment ctDNA due to its very low amount in blood (26), detection of viable and bioactive CTCs which possess aneuploidy (6, 27), cancer stemness (28), and epithelial-to-mesenchymal transition (EMT) (29) allows for real-time providing valuable clinical information more relevant to metastasis and therapeutic efficacy alongside the cancer treatment.

Aneuploidy is the hallmark of malignant neoplastic cells (6, 10, 27). The degree of aneuploidy is proportional to the grade of malignancy of carcinoma cells: the higher the degree of aneuploidy, the higher the malignancy grade, and the poorer the prognosis in cancer patients (30, 31). Moreover, aneuploidy was also reported to correlate with chemo- and targeted therapy resistance (22, 32). In addition to aneuploidy, recent studies on CTC morphology indicated that CTCs in small cell size (≤5 μm white blood cell) were relevant to gastric and lung cancer patients' hepatic metastasis (33, 34), adverse prognosis (35), and post-surgical occurrence in hepatocellular carcinoma (HCC) patients (36). Unlike large cell CTCs, single cell DNA sequencing (scDNA-seq) analyses revealed that small cell sized CTCs exhibited a different therapy-resistance mechanism (33). Contrary to conventional CTC enumeration methods biased towards only EpCAM and CK-double positive neoplastic cells, which may bring a nonnegligible false negative detection due to intrinsic highly heterogeneities of cancer cells, SE-iFISH applied in this case allows to effectively co-detect, comprehensively characterize and subcategorize CTCs and CTECs into diverse subtypes based upon the degree of aneuploidy, tumor marker expression and cell morphology (cell size and cluster) (13, 21). Each subtype of CTCs and CTECs possess distinct clinical significance in terms of cancer metastasis, risk stratification, guiding targeted therapy, susceptibility or resistance to therapeutic agents, etc. (15, 17, 22, 23).

The present case showed that, after resection of the primary lesion and receiving a complete six cycles of chemoradiotherapy plus nimotuzumab, the patient still had a substantial amount of 107 $CD45^-$ aneuploid circulating rare cells including 14 CTCs and 93 CTECs. Among those cells, 28.6% CTCs were in small cell size and 86% of CTECs as well as 57.1% CTCs had a high degree of chr8 aneuploidy (≥pentasomy 8). Comparing to an average of less than 2.8 ± 3.6 CTECs (Mean ± SD) per 6.5 ml blood in healthy donors (13), a large quantity of CTECs and CTCs detected in this patient after receiving a complete post-surgical chemoradiotherapy retrospectively suggested that the efficacy of the applied combination regimens was not as effective as expected.

It has been reported that CTCs do not exhibit the same chemosensitivity as the primary tumor cells in breast cancer patients (37). During a selective multistep metastasizing process, metastatic CTCs might be derived from only a few subclones of neoplastic cells in the primary lesion consisting of multiclonal carcinoma cells, followed by further hematogenous spreading selection in peripheral circulation. Eventually, survived CTCs and CTECs, which may have profound differences compared to primary tumor cells, participate in the formation of distant metastatic lesion(s). This may explain why CTCs and CTECs exhibit a different pattern of chemosensitivity to that of the primary tumor (38), indicating the necessity of active monitoring and characterization of CTCs and CTECs alongside and after treatment as for an adequate assessment of therapy effectiveness.

In addition to evaluation of therapeutic efficacy, the impact of CTCs on occurrence of malignancy was reported by others (2–5). In the current report, because squamous cell laryngeal carcinoma and the subsequent pancreatic adenocarcinoma histopathologically differ from each other, the pancreatic cancer was most likely the *de novo* malignancy following therapy. Post-therapeutically detected 107 aneuploid CTCs and CTECs were likely a mixture of laryngocarcinoma's MRD (24), neoplastic cells from the subsequent *de novo* pancreatic cancer at the very early stage, and the new clones of dormant tumor cells awakened by the stress (39), all were resistant or insensitive to the applied combination regimens. CTCs were found as an effective indicator able to, despite invisible malignant lesions (40), independently predict early occurrence of pancreatic cancer (41) and melanoma in cancer patients (4). In non-small cell lung cancer (NSCLC) patients, CTCs positively detected one month after radial resection significantly correlated with an inferior prognosis and a high risk of early malignancy occurrence (7). As described in this report, two months after surgery, the patient showed the existence of abundant CTCs and CTECs upon finishing complete post-surgical combination therapy and, at the time, no abnormal blood test result or abnormal medical image scanning was observed. As depicted in Figure 1, positive detection of CTCs and CTECs (t3, August 2019) occurred five months prior to increasement of CA19-9 and CEA (t4, February 2019), and ten months prior to the diagnosed pancreatic cancer (t5, July 2019). Currently, most studies were performed to enumerate CTCs alone either at baseline or after surgery with regards to predicting cancer occurrence or recurrence, whereas the detection time point reported in this article is critical, indicating that detection of aneuploid CTCs and CTECs in a patient following receiving complete therapeutic regimens warrants an adequate evaluation of the finished

treatments' efficacy and an effective stratification of patient's occurrence risk.

CTECs, harboring dual properties of both cancerous malignancy and endothelial vascularization ability, are predominately derived from the endothelialization of cancer cells either *in vivo* or *in vitro* (10, 42, 43), the process that enables carcinoma cells to express CD31 on their surface. CTECs, the $CD31^+$ cancer cells in essence and referred to as a "wolf in sheep's clothing" (10, 44), integrate multiple properties of epithelium, endothelium, mesenchyme, aneuploidy, malignancy, and motility. Thus, they are expected to play a vital role in tumorigenesis, neovascularization, disease progression, and cancer metastasis (10). We realized a large quantity and a high ratio of CTECs to CTCs > 5 in this case, and proposed for the first time that the large numbers and high ratio of CTECs/CTCs may associate with or impact cancers' rapid occurrence.

Following recent progress in the innovation and clinical validation of tumor marker-iFISH, such as CA19-9/CEA/PD-L1/HER2-iFISH (10, 20), and the novel iFISH (NC) to distinguish and co-detect viable and necrotic aneuploid $CD31^-$ CTCs as well as $CD31^+$ CTECs (45), longitudinal monitoring of CTCs and CTECs with the updated six-channel multi-tumor marker-iFISH throughout combination regimens will help illustrate whether and how CTCs and CTECs expressing tumor markers have a mutual effect on tumor progression alongside treatment (15, 17, 22), thus allowing for a better assessment of therapy outcome and a more effective forecasting strategy of cancer relapse.

Conclusions

Co-detection of aneuploid $CD31^-$ CTCs and $CD31^+$ CTECs in patients at the end of complete therapy cycles may provide a unique dual cellular evaluation and prediction approach, in terms of effectively evaluating therapeutic efficacy in post-therapeutic cancer patients, stratifying malignancy risk, and appropriately guiding systemic adjuvant therapy to target adequate subjects. A large amount and a high ratio of aneuploid CTECs to CTCs following a complete treatment indicate both the existence of therapy-resistant MRD and higher risk of cancer occurrence or metastatic distant recurrence. An effective therapeutic regimen, therefore, should be able to eradicate the targeted non-hematological aneuploid circulating rare cells in an effort to reduce the risk of post-therapeutic cancer occurrence or relapse (37).

Data availability statement

The raw data supporting the conclusions of this article will be made available by the authors, without undue reservation.

Ethics statement

The study was conducted according to the Declaration of Helsinki Principles. Informed consent form, approved by the Ethics Review Committees (ERC) of the Fifth Affiliated Hospital of Sun Yat-Sen University, Zhuhai, Guangdong, China, was signed and obtained from the patient.

Author contributions

JM, FY, JL, and QZ participated in patient treatment and analysis of results. ML contributed writing original draft. AL contributed methodology and writing original draft. AL and DW contributed methodology and validation. QZ and PL contributed conceptualization, writing – original draft, review, and editing. All authors contributed to the article and approved the submitted version.

Funding

This study was supported by the Science and Technology Planning Project for Health Care of Zhuhai City (General Project) Grant ZH22036201210051PWC to QZ.

Acknowledgments

Authors thank staffs at the Fifth Affiliated Hospital of Sun Yat-Sen University, Cytointelligen (China Medical City, Taizhou, Jiangsu, China) and Cytelligen (San Diego, CA, USA) for providing support to this study.

Conflict of interest

i•FISH® is the registered trademarks of Cytelligen. PL is the president at Cytelligen. None of authors owns Cytelligen's stock shares.

The remaining authors declare that the research was conducted in the absence of any commercial or financial relationships that could be construed as a potential conflict of interest.

Publisher's note

References

1. Meads MB, Gatenby RA, Dalton WS. Environment-mediated drug resistance: a major contributor to minimal residual disease. *Nat Rev Cancer* (2009) 9(9):665–74. doi: 10.1038/nrc2714

2. Chemi F, Rothwell DG, McGranahan N, Gulati S, Abbosh C, Pearce SP, et al. Pulmonary venous circulating tumor cell dissemination before tumor resection and disease relapse. *Nat Med* (2019) 25(10):1534–9. doi: 10.1038/s41591-019-0593-1

3. Franken B, de Groot MR, Mastboom WJ, Vermes I, van der Palen J, Tibbe AG, et al. Circulating tumor cells, disease recurrence and survival in newly diagnosed breast cancer. *Breast Cancer Res* (2012) 14(5):R133. doi: 10.1186/bcr3333

4. Lucci A, Hall CS, Patel SP, Narendran B, Bauldry JB, Royal RE, et al. Circulating tumor cells and early relapse in node-positive melanoma. *Clin Cancer Res* (2020) 26(8):1886–95. doi: 10.1158/1078-0432.CCR-19-2670

5. Sparano J, O'Neill A, Alpaugh K, Wolff AC, Northfelt DW, Dang CT, et al. Association of circulating tumor cells with late recurrence of estrogen receptor-positive breast cancer: A secondary analysis of a randomized clinical trial. *JAMA Oncol* (2018) 4(12):1700–6. doi: 10.1001/jamaoncol.2018.2574

6. Lin PP. Aneuploid CTC and CEC. *Diagnostics (Basel)* (2018) 8(2):26. doi: 10.3390/diagnostics8020026

7. Bayarri-Lara C, Ortega FG, Cueto Ladron de Guevara A, Puche JL, Ruiz Zafra J, de Miguel-Perez D, et al. Et al: Circulating tumor cells identify early recurrence in patients with non-small cell lung cancer undergoing radical resection. *PloS One* (2016) 11(2):e0148659. doi: 10.1371/journal.pone.0148659

8. Hanahan D, Weinberg RA. Hallmarks of cancer: The next generation. *Cell* (2011) 144(5):646–74. doi: 10.1016/j.cell.2011.02.013

9. Hida K, Klagsbrun M. A new perspective on tumor endothelial cells: unexpected chromosome and centrosome abnormalities. *Cancer Res* (2005) 65 (7):2507–10. doi: 10.1158/0008-5472.CAN-05-0002

10. Lin PP. Aneuploid circulating tumor-derived endothelial cell (CTEC): A novel versatile player in tumor neovascularization and cancer metastasis. *Cells* (2020) 9(6):1539. doi: 10.3390/cells9061539

11. Hida K, Maishi N, Annan DA, Hida Y. Contribution of tumor endothelial cells in cancer progression. *Int J Mol Sci* (2018) 19(5):1272. doi: 10.3390/ijms19051272

12. Goveia J, Rohlenova K, Taverna F, Treps L, Conradi LC, Pircher A, et al. An integrated gene expression landscape profiling approach to identify lung tumor endothelial cell heterogeneity and angiogenic candidates. *Cancer Cell* (2020) 37 (1):21–36. doi: 10.1016/j.ccell.2019.12.001

13. Lin PP, Gires O, Wang DD, Li L, Wang H. Comprehensive in situ co-detection of aneuploid circulating endothelial and tumor cells. *Sci Rep* (2017) 7 (1):9789. doi: 10.1038/s41598-017-10763-7

14. Mehran R, Nilsson M, Khajavi M, Du Z, Cascone T, Wu HK, et al. Tumor endothelial markers define novel subsets of cancer-specific circulating endothelial cells associated with antitumor efficacy. *Cancer Res* (2014) 74(10):2731–41. doi: 10.1158/0008-5472.CAN-13-2044

15. Zhang L, Zhang X, Liu Y, Zhang T, Wang Z, Gu M, et al. PD-L1$^+$ aneuploid circulating tumor endothelial cells (CTECs) exhibit resistance to the checkpoint blockade immunotherapy in advanced NSCLC patients. *Cancer Lett* (2020) 469:355–66. doi: 10.1016/j.canlet.2019.10.041

16. Xing C, Li Y, Wang S, Zhang H, Li P, Dai M. CD44$^+$ circulating tumor endothelial cells indicate poor prognosis in pancreatic ductal adenocarcinoma after radical surgery: A pilot study. *Cancer Manag Res* (2021) 13:4417–31. doi: 10.2147/CMAR.S309115

17. Zhang T, Zhang L, Gao Y, Wang Y, Liu Y, Zhang H, et al. Role of aneuploid circulating tumor cells and CD31$^+$ circulating tumor endothelial cells in predicting and monitoring anti-angiogenic therapy efficacy in advanced NSCLC. *Mol Oncol* (2021) 15(11):2891–909. doi: 10.1002/1878-0261.13092

18. Lei Y, Sun N, Zhang G, Liu C, Lu Z, Huang J, et al. Combined detection of aneuploid circulating tumor-derived endothelial cells and circulating tumor cells may improve diagnosis of early stage non-small-cell lung cancer. *Clin Transl Med* (2020) 10:e128. doi: 10.1002/ctm2.128

19. Ma G, Jiang Y, Liang M, Li J, Mao X, Veeramootoo JS, et al. Dynamic monitoring of CD45-/CD31+/DAPI+ circulating endothelial cells aneuploid for chromosome 8 during neoadjuvant chemotherapy in locally advanced breast cancer. *Ther Adv Med Oncol* (2020) 12:1758835920918470. doi: 10.1177/1758835920918470

20. Zhao Y, Li J, Li D, Wang Z, Zhao J, Wu X, et al. Tumor biology and multidisciplinary strategies of oligometastasis in gastrointestinal cancers. *Semin Cancer Biol* (2020) 60:334–43. doi: 10.1016/j.semcancer.2019.08.026

21. Lin PP. Integrated EpCAM-independent subtraction enrichment and iFISH strategies to detect and classify disseminated and circulating tumors cells. *Clin Transl Med* (2015) 4(1):38. doi: 10.1186/s40169-015-0081-2

22. Li Y, Zhang X, Liu D, Gong J, Wang DD, Li S, et al. Evolutionary expression of HER2 conferred by chromosome aneuploidy on circulating gastric cancer cells contributes to developing targeted and chemotherapeutic resistance. *Clin Cancer Res* (2018) 24(21):5261–71. doi: 10.1158/1078-0432.CCR-18-1205

23. Liu X, Li J, Cadilha BL, Markota A, Voigt C, Huang Z, et al. Epithelial-type systemic breast carcinoma cells with a restricted mesenchymal transition are a major source of metastasis. *Sci Adv* (2019) 5(6):eaav4275. doi: 10.1126/sciadv.aav4275

24. Pantel K, Alix-Panabieres C. Liquid biopsy and minimal residual disease - latest advances and implications for cure. *Nat Rev Clin Oncol* (2019) 16(7):409–24. doi: 10.1038/s41571-019-0187-3

25. Jahr S, Hentze H, Englisch S, Hardt D, Fackelmayer FO, Hesch RD, et al. DNA Fragments in the blood plasma of cancer patients: quantitations and evidence for their origin from apoptotic and necrotic cells. *Cancer Res* (2001) 61 (4):1659–65.

26. Merker JD, Oxnard GR, Compton C, Diehn M, Hurley P, Lazar AJ, et al. Circulating tumor DNA analysis in patients with cancer: American society of clinical oncology and college of American pathologists joint review. *J Clin Oncol* (2018) 36:1631–41. doi: 10.1200/JCO.2017.76.8671

27. Gordon DJ, Resio B, Pellman D. Causes and consequences of aneuploidy in cancer. *Nat Rev Genet* (2012) 13(3):189–203. doi: 10.1038/nrg3123

28. Papadaki MA, Stoupis G, Theodoropoulos PA, Mavroudis D, Georgoulias V, Agelaki S. Circulating tumor cells with stemness and epithelial-to-Mesenchymal transition features are chemoresistant and predictive of poor outcome in metastatic breast cancer. *Mol Cancer Ther* (2019) 18(2):437–47. doi: 10.1158/1535-7163.MCT-18-0584

29. Wang H, Stoecklein NH, Lin PP, Gires O. Circulating and disseminated tumor cells: diagnostic tools and therapeutic targets in motion. *Oncotarget* (2017) 8 (1):1884–912. doi: 10.18632/oncotarget.12242

30. Danielsen HE, Pradhan M, Novelli M. Revisiting tumour aneuploidy - the place of ploidy assessment in the molecular era. *Nat Rev Clin Oncol* (2016) 13 (5):291–304. doi: 10.1038/nrclinonc.2015.208

31. Stopsack KH, Whittaker CA, Gerke TA, Loda M, Kantoff PW, Mucci LA, et al. Aneuploidy drives lethal progression in prostate cancer. *Proc Natl Acad Sci USA* (2019) 116:11390–5. doi: 10.1073/pnas.1902645116

32. Li YL, Zhang XT, Ge S, Gao J, Gong JF, Lu M, et al. Clinical significance of phenotyping and karyotyping of circulating tumor cells in patients with advanced gastric cancer. *Oncotarget* (2014) 5(16):6594–602. doi: 10.18632/oncotarget.2175

33. Chen Y, Li Y, Qi C, Zhang C, Liu D, Deng Y, et al. Dysregulated KRAS gene-signaling axis and abnormal chromatin remodeling drive therapeutic resistance in heterogeneous-sized circulating tumor cells in gastric cancer patients. *Cancer Lett* (2021) 517:78–87. doi: 10.1016/j.canlet.2021.06.002

34. Wang Y, Liu Y, Zhang L, Tong L, Gao Y, Hu F, et al. Vimentin expression in circulating tumor cells (CTCs) associated with liver metastases predicts poor progression-free survival in patients with advanced lung cancer. *J Cancer Res Clin Oncol* (2019) 145(12):2911–20. doi: 10.1007/s00432-019-03040-9

35. Hong Y, Si J, Zhang J, Xiong Y, Zhang J, Lin PP, et al. Small cell size circulating aneuploid cells as a biomarker of prognosis in resectable non-small cell lung cancer. *Front Oncol* (2021) 11:590952. doi: 10.3389/fonc.2021.590952

36. Wang L, Li Y, Xu J, Zhang A, Wang X, Tang R, et al. Quantified postsurgical small cell size CTCs and EpCAM$^+$ circulating tumor stem cells with cytogenetic abnormalities in hepatocellular carcinoma patients determine cancer relapse. *Cancer Lett* (2018) 412:99–107. doi: 10.1016/j.canlet.2017.10.004

37. Pierga JY, Bidard FC, Mathiot C, Brain E, Delaloge S, Giachetti S, et al. Circulating tumor cell detection predicts early metastatic relapse after neoadjuvant chemotherapy in large operable and locally advanced breast cancer in a phase II randomized trial. *Clin Cancer Res* (2008) 14(21):7004–10. doi: 10.1158/1078-0432.CCR-08-0030

38. Pantel K, Brakenhoff RH. Dissecting the metastatic cascade. *Nat Rev Cancer* (2004) 4(6):448–56. doi: 10.1038/nrc1370

39. Perego M, Tyurin VA, Tyurina YY, Yellets J, Nacarelli T, Lin C, et al. Reactivation of dormant tumor cells by modified lipids derived from stress-activated neutrophils. *Sci Transl Med* (2020) 12(572):eabb5817. doi: 10.1126/scitranslmed.abb5817

40. Kiss I, Kolostova K, Pawlak I, Bobek V. Circulating tumor cells in gynaecological malignancies. *J BUON* (2020) 25(1):40–50.

41. Park Y, Jun HR, Choi HW, Hwang DW, Lee JH, Song KB, et al. Circulating tumour cells as an indicator of early and systemic recurrence after surgical resection in pancreatic ductal adenocarcinoma. *Sci Rep* (2021) 11(1):1644. doi: 10.1038/s41598-020-80383-1

42. Lapis K, Paku S, Liotta LA. Endothelialization of embolized tumor cells during metastasis formation. *Clin Exp Metastasis* (1988) 6(1):73–89. doi: 10.1007/BF01580408

43. Liu Z, Qi L, Li Y, Zhao X, Sun B. VEGFR2 regulates endothelial differentiation of colon cancer cells. *BMC Cancer* (2017) 17(1):593. doi: 10.1186/s12885-017-3578-9

44. Duelli D, Lazebnik Y. Cell fusion: a hidden enemy? *Cancer Cell* (2003) 3 (5):445–8. doi: 10.1016/S1535-6108(03)00114-4

45. Lin AY, Wang DD, Li L, Lin PP. Identification and comprehensive Co-detection of necrotic and viable aneuploid cancer cells in peripheral blood. *Cancers* (2021) 13:5108. doi: 10.3390/cancers13205108

frontiers | Frontiers in Oncology

TYPE Original Research
PUBLISHED 24 November 2022
DOI 10.3389/fonc.2022.1014888

OPEN ACCESS

EDITED BY
Rana Jahanban-Esfahlan,
Tabriz University of Medical Sciences, Iran

REVIEWED BY
Abedalrhman Alkhateeb,
University of Windsor, Canada
Hassan Seradj,
Shiraz University of Medical Sciences, Iran

*CORRESPONDENCE
Weide Zhong
zhongwd2009@live.cn

†These authors have contributed equally to this work

SPECIALTY SECTION
This article was submitted to Molecular and Cellular Oncology, a section of the journal Frontiers in Oncology

RECEIVED 09 August 2022
ACCEPTED 26 September 2022
PUBLISHED 24 November 2022

CITATION
Zha Z, Hong Y, Tang Z, Du Q, Wang Y, Yang S, Wu Y, Tan H, Jiang F and Zhong W (2022) FCGR3A: A new biomarker with potential prognostic value for prostate cancer. *Front. Oncol.* 12:1014888. doi: 10.3389/fonc.2022.1014888

FCGR3A: A new biomarker with potential prognostic value for prostate cancer

Zeyu Zha[1,2,3†], Yuan Hong[3,4†], ZhenFeng Tang[3], Qiuling Du[3], Yan Wang[3], Shengbang Yang[3,5], Yongding Wu[3], Huijing Tan[3], Funneng Jiang[3] and Weide Zhong[1,3*]

[1]School of Medicine, Jinan University, Guangzhou, China, [2]The Second Affiliated Hospital of Bengbu Medical College, Bengbu, China, [3]Department of Urology, Guangdong Key Laboratory of Clinical Molecular Medicine and Diagnostics, Guangzhou First People's Hospital, School of Medicine, South China University of Technology, Guangzhou, China, [4]College of The First Clinical Medicine, Guangzhou University of Chinese Medicine, Guangzhou, China, [5]School of Medicine, Guizhou University, Guiyang, China

To screen target gene cluster by bioinformatics analysis and verify them by *in vitro* experiment and clinicopathological correlation analysis. We try to find a new biomarker with prognostic value for prostate cancer (PCa). 42 candidate marker genes were constructed by protein protein interaction (PPI) network and enriched by KEGG pathway to find out the gene cluster we are interested in. Prognostic model was established to preliminarily analyze the prognostic value of this gene cluster in PCa, and Cox risk regression was used for comparative analysis. Immunohistochemistry was used to detect the expression of each gene in clinical tissue microarray. Finally, we analyzed the correlation between each gene and their clinicopathological features of PCa combined with TCGA clinical data. Based on the analysis of PPI and KEGG, we found the target gene cluster (FCGR3A, HAVCR2, CCR7 and CD28). Prognostic model analysis showed that this gene cluster had the ability to predict biochemical recurrence, and the survival rate and ROC analysis showed favorable prediction effect. Univariate Cox regression analysis showed that the risk scores of Gleason score (GS), T stage, N stage and PSA were significantly different ($P<0.05$), and the risk ratio of high expression was 2.30 times that of low expression ($P=0.004$). However, it was not statistically significant in multivariate Cox regression analysis ($P>0.05$). The results of tissue microarray showed that FCGR3A and HAVCR2 were highly expressed in PCa ($P<0.01$), while the expression of CCR7 and CD28 had no significant difference ($P>0.05$). Kaplan-Meier analysis showed that there was significant difference in BCR free survival of FCGR3A and HAVCR2 (FCGR3A, $P=0.010$; HAVCR2, $P=0.018$), while the expression of CCR7 and CD28 had no significant difference on the survival and prognosis of PCa patients ($P>0.05$). TCGA clinical data analysis found that the expression of FCGR3A had a unique correlation

with the clinicopathological features of PCa, which was closely related to the tumor stage. The expression of FCGR3A is related to BCR free survival of PCa patients. Therefore, FCGR3A is a new biomarker with potential prognostic value of PCa.

KEYWORDS

prostate cancer, prognosis, FCGR3A, tumor microenvironment, bioinformatics analysis

Introduction

Prostate cancer (PCa) is a malignant tumor and is the second most fatal cancer for men (1). Due to an aging population, the morbidity of PCa is increasing (2). As the early symptoms of PCa are not obvious, most PCa patients are in the terminal stage when they are examined and then with short survival period (3, 4). Although the current clinical treatment, including enzalutamide and abiraterone therapy, can significantly improve the overall survival rate of PCa patients, is not ideal for PCa patients with terminal stage (5–7). Prostate specific antigen (PSA) is a biomarker of PCa, but its detection results are easily affected by drugs, inflammation and benign prostate lesions, especially lack of specificity and sensitivity in the early diagnosis and prediction of recurrence of PCa (8, 9). Therefore, it is necessary to study the progression of PCa and identify the operative prognosis biomarkers.

Tumor microenvironment (TME) is composed of different cell subsets, including tumor cells, blood vessels, immune cells, stromal cells and other ingredients (10). PCa is highly heterogeneous in TME, so the morbidity of terminal or metastatic PCa (especially bone metastasis) has increased over the last years (11–13). However, whether the changes of cell subsets in TME are related to tumor prognosis has aroused our intense concern. In a recent study (14), Researchers obtained 36424 cells from 13 prostate tumor tissues and performed single cell transcriptome sequencing on these cells and found that multiple progression-related transcriptome programs were activated in TME and 42 marker genes (ACTA2, PECAM1, VWF, ENG, CMA1, MS4A2, TPSAB1, TPSB2, AR, KRT19, KRT18, KRT8, TP63, KRT14, KRT5, LYZ, FCGR3A, CSF1R, CD68, CD163, CD14, UCHL1, HAVCR2, PDCD1, CTLA4, CD8A, SELL, PTPRC, CD4, BTLA, IL2RA, IL7R, CCR7, CD28, CD27, SLAMF1, DPP4, CD7, CD2, CD3G, CD3E and CD3D) were identified in multiple cell subpopulations including T cells, monocytes, endothelial cells and fibroblasts. We concluded that these genes are mainly related to cell communication, antigen presentation process and immune cell receptor signaling pathway. And some of them have been predicted to have favorable prognostic value in PCa, such as VWF, AR and CSF1R (15–18). The above 42 marker genes are selected as candidate genes for bioinformatics analysis and we attempt to discover a new biomarker with potential prognostic value of PCa.

FCGR3A (Fc fragment of IgG receptor IIIa), a transmembrane glycoprotein, is expressed on natural killer cells and inhibits the growth of liver tumor cells. FCGR3A gene is associated with the risk of lesions in several oncological diseases, for example, FCGR3A gene polymorphisms are positively associated with the risk of lesions in colorectal cancer, and genetic variants of FCGR3A are associated with drug resistance in rheumatoid arthritis (19, 20). FCGR3A has been shown to be involved in multiple immune cell infiltration and DNA mismatch repair genes, while drug sensitivity analysis showed that higher FCGR3A expression predicted lower IC50 (half maximal inhibitory concentration) values for the majority of drugs (21), however, the prognostic value of FCGR3A expression in prostate tumors and its correlation with immune infiltration are unclear.

In recent decades, the advancement of bioinformatics has enabled researchers to more comprehensively investigate its biological mechanisms and more effectively identify key therapeutic and prognostic molecules. In this study, we performed a series of comprehensive bioinformatics analyses of tumor-associated genes. Our study aims to provide new therapeutic targets for prostate cancer and help to understand the underlying immune mechanism of prostate cancer. At the same time, through the analysis of various cancer-related genes, we can understand the development correlation of various diseases and provide a basis for combined treatment.

Materials and methods

PPI network construction

Protein-protein interaction database, String (https://cn.string-db.org/), was used to calculate and analyze the interaction relationship between 42 candidate genes. Cytoscape software (V3.8.2) was used to visualize the gene interaction network.

KEGG pathway enrichment analysis

KEGG rest API (https://www.kegg.jp/kegg/rest/keggapi.html) was used for the latest gene annotation as background. Then, 42 candidate genes were mapped into the background set, and R software package, clusterProfiler (Version 3.14.3), was used for enrichment analysis to obtain gene enrichment results. Set the minimum gene set as 5 and the maximum gene set as 5,000, $P<0.05$ and $FDR<0.1$ was considered statistically significant.

Prognostic model construction

PCa data used in this study downloaded from the public database TCGA (https://xenabrowser.net/). The downloaded data type is count, and Deseq2 is used to standardize the data. The clinical information of PCa sample downloaded from cBioPortal (http://www.cbioportal.org/). We constructed prognostic models for the target gene cluster (FCGR3A, HAVCR2, CCR7 and CD28). Prognostic model predicts the prognosis of patients according to the level of risk score by calculating it in each sample. The expression data used in this analysis downloaded from TCGA's PRAD dataset (PRAD had 427 samples with both RNA SEQ data and BCR data).

The samples of PRAD were divided into training set (214 samples) and test set (213 samples) according to 1:1. First, the risk score of the training set samples was sorted from small to large, and the samples were divided into low-risk group (n=107) and high-risk group (n=107) according to the median of 2.5734. Then, the risk score of the test set samples was sorted from small to large, and the samples were divided into low-risk group (n=117) and high-risk group (n=96) according to the same threshold value as the training set. Finally, integrated the training set and test set samples. The GGlpot2 package of R language was used to make the risk score, survival state and characteristic gene expression diagram. The survminer package was used to make survival curve. The survival ROC package was used to make time-dependent curve. The survival package was used to do univariate Cox regression analysis. The glmnet package was used to do Lasso regression analysis.

Patients and tissue samples

Tissue microarray (Cat No: DC-PRO01026; TMA, n=80) was purchased from Avilabio Biotechnology Company (Shaanxi Province, China), including 10 prostate samples from healthy individuals and 70 prostate samples from patients with primary PCa, and with information on pathological grade, Gleason grade, Gleason score, TNM and clinical stage. Patients treated with chemotherapy or radiotherapy before the surgery were excluded from this study. In order to quantify the mRNA expression of FCGR3A, havcr2, CCR7 and CD28, clinical information and gene expression data of 427 PCa patients were collected from TCGA database.

Immunohistochemistry analysis

Paraffin sections were dewaxed by xylene, soaked in 100%, 95%, 70% ethanol and distilled water for 5 min successively, and then washed with PBS solution. Sections were added with EDTA buffer for microwave antigen repair. Endogenous peroxidase was blocked by incubation in 3% hydrogen peroxide solution at 24°C for 10 min. Antigen was blocked with 5%BSA and incubated at 24°C for 20 min. After sealing, the sections were incubated at 4° C overnight with anti-FCGR3A (rabbit monoclonal antibody, 1:50, ET7109-97, HuaBio), anti-HAVCR2 (mouse monoclonal antibody, 1:800, EM1701-18, HuaBio), anti-CCR7 (rabbit monoclonal antibody, 1:200, ab253187, Abcam) and anti-CD28 (rabbit polyclonal antibody, bs-1297R, Bioss) antibodies. Then, 150 μl secondary antibody was added for incubation, followed by DAB color rendering and hematoxylin redyeing. The positive cell rate and the degree of staining were scored by scanning imaging. Positive cell rate score: 0%-10%, 1 point; 10%-50%, 2 points; 50%-75%, 3 points; 75%-100%, 4 points. Staining degree score: no positive staining, 0 point; canary yellow, 1 point; brownish yellow, 2 points; tan, 3 points. The immune risk score (IRS) is the product of the above two scores.

Statistical analysis

Statistical analyzes were performed using SPSS 22.0 software. Continuous variables were expressed as mean ± SD. Kaplan-meier method was used to analyze the relationship between the expression of FCGR3A, HAVCR2, CCR7 and CD28 and the survival period of PCa patients. Pearson's chi-squared tests and Fisher's exact test were used to analyze the association of FCGR3A, HAVCR2, CCR7 and CD28 mRNA expression with clinico-pathological features. Student's T-tests were used to analyze the association of FCGR3A, HAVCR2, CCR7 and CD28 protein expression with clinico-pathological features. Univariate analysis comparisons and multivariate survival comparisons were performed using Cox proportional hazard regression models. Differences were statistically significant when $P<0.05$.

Results

Identify target gene cluster: FCGR3A, HAVCR2, CCR7 and CD28

We constructed PPI networks for 42 candidate genes, and found that FCGR3A, HAVCR2, CCR7 and CD28 interacted

with each other (Figure 1A), which aroused our curiosity. KEGG pathway enrichment analysis of this gene cluster showed that FCGR3A was mainly enriched in Staphylococcus aureus infection process; CCR7 was mainly enriched in cytokine-cytokine receptor interaction; CD28 was mainly enriched in Hematopoietic cell lineage, T cell receptor signaling pathway, cell adhesion molecules and primary immunodeficiency process (Figure 1B). Therefore, we speculate that this gene cluster may be involved in the occurrence and development of PCa. Then, whether this gene cluster can be used as an independent prognostic factor for PCa patients, we will verify our suppose through bioinformatics and *in vitro* experiments.

Target gene cluster is an independent prognostic factor for the survival of PCa patients

We analyzed the relationship between the expression of target gene cluster and the survival of PCa patients by using the TCGA database. After constructing the 4-gene model, we calculated the risk score according to the model of each patient in the cohort and drawn the distribution map. The results showed that the risk of death of high-risk patients (n=96) was significantly higher than that of patients with low risk scores (n=117), and our model could better distinguish the distribution

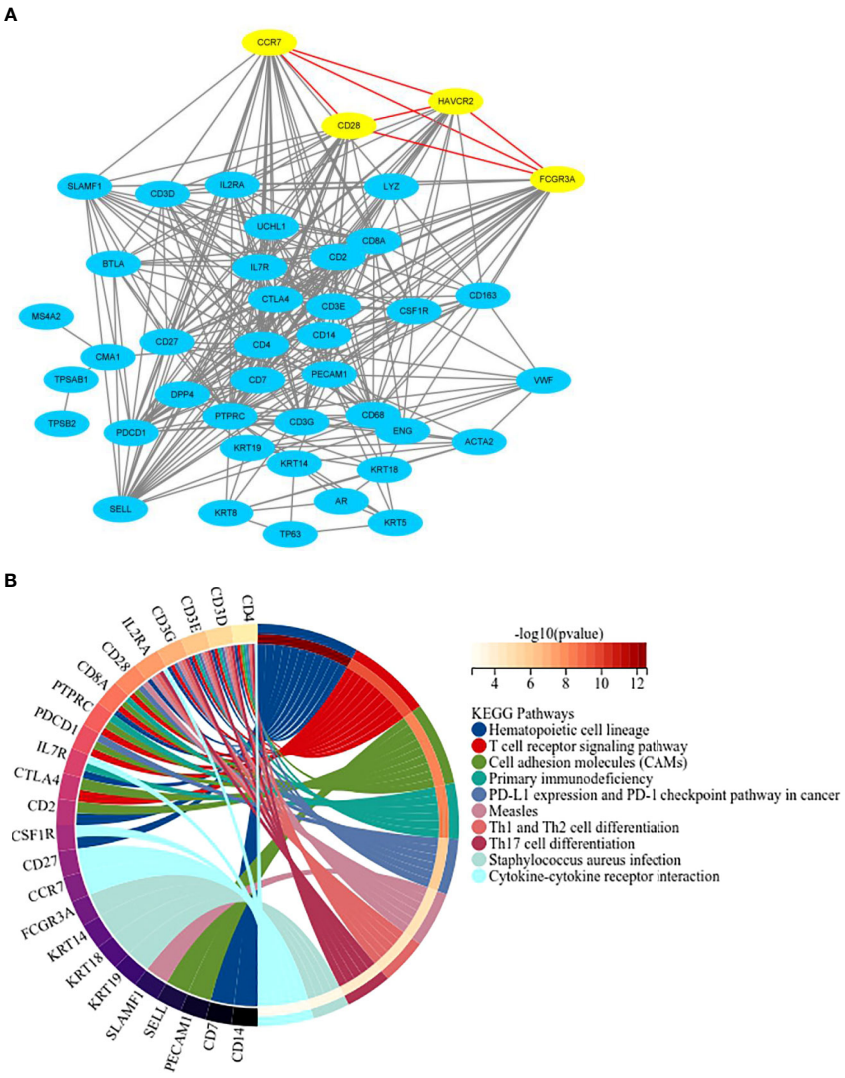

FIGURE 1
PPI network construction and KEGG pathway enrichment analysis. **(A)** Protein-protein interaction network for 42 candidate marker genes in String database. **(B)** The top 10 pathways of KEGG pathway enrichment analysis.

10.3389/fonc.2022.1014888

of 4 genes expression in the cohort of low-risk and high-risk PCa patients, among which FCGR3A was the best and CCR7 and CD28 were the worst (Figure 2A). Kaplan-meier analysis of survival rate showed that patients with high score had a worse prognosis than those with low score (P=0.0012) (Figure 2B). ROC analysis showed that the model could effectively predict 5-year survival of PCa patients, and AUC values at 1, 2, 3, 4 and 5 years were 0.677, 0.6024, 0.6516, 0.6887 and 0.7048 respectively (Figure 2C). Therefore, the target gene cluster have the ability to predict biochemical recurrence of patients and can be used as independent prognostic factors for the survival of PCa patients.

To further identify whether the expression of target gene cluster can be an independent prognostic factor for PCa patients, we investigated the association between clinical characteristics and risk score. Univariate Cox regression analysis showed that there were significant differences in risk score between tumor and Gleason Score, T stage, N stage and PSA (P<0.05), and the risk ratio of high expression was 2.30 times higher than low expression (P=0.004) (Table 1). Multivariate analysis showed that although there were significant differences in risk score between tumor, T stage and PSA (P<0.05), there was no statistical significance in the difference of risk ratio between high expression and low expression (P>0.05) (Table 1). We hypothesized that this might be caused by the poor distribution of CCR7 and CD28 in the cohort of low-risk and high-risk PCa patients. Subsequently, we verified our suppose by survival analysis of each gene and clinical tissue microarray testing.

TABLE 1 Prognostic value of 4 target genes expression for BCR free survival by Cox proportional hazards model.

Variable	BCR free survival	
	HR (95%CI)	*P*
Univariate analysis		
Age (≤60 or >60)	1.10 (0.64-1.90)	0.720
Gleason score (≤8 or >8)	2.70 (1.50-4.60)	<0.001***
Tumor Stage (T1-T2 or T3-T4)	5.20 (2.00-13.00)	<0.001***
Lymph node stage (N0 or N1)	2.00 (1.10-3.50)	0.025*
Distant metastasis (M0 or M1)	0.00 (0.00-2.00)	1.000
PSA (<2 or ≥2)	9.00 (5.00-16.00)	<0.001***
Risk score (Low risk or High risk)	2.30 (1.30-4.20)	0.004**
Multivariate analysis		
Gleason score (≤8 or >8)	1.19 (0.66-2.13)	0.568
Tumor Stage (T1-T2 or T3-T4)	3.52 (1.31-9.46)	0.013*
Lymph node stage (N0 or N1)	1.25 (0.68-2.29)	0.474
PSA (<2 or ≥2)	7.19 (3.96-13.04)	<0.001***
Risk score (Low risk or High risk)	1.63 (0.90-2.92)	0.105

*means the difference is significant at the 0.05 level ,** means the difference is significant at the 0.01 level , *** means the difference is significant at the 0.01 level.

High expression of FCGR3A and HAVCR2 has a poor prognosis for PCa patients

We used TCGA database to analyze the relationship between the expression of 4 target genes and the survival of PCa patients.

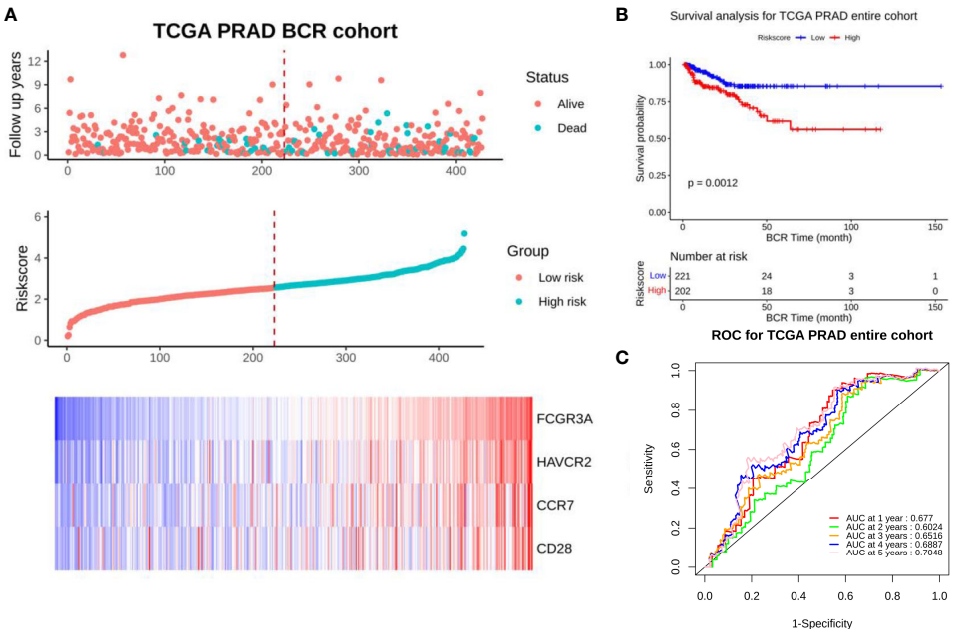

FIGURE 2
Prognostic model analysis of entire set. **(A)** Distribution of 4 target genes in low-risk and high-risk groups in TCGA-PRAD dataset. **(B)** BCR free survival curve of 4 target genes in TCGA-PRAD dataset (P=0.0012). **(C)** 5-year ROC curve of 4 target genes in TCGA-PRAD dataset (AUC>0.6).

The genes expression was divided into high-expression group and low-expression group with median as the boundary. The blue curve (n=211) and the orange curve (n=212) represent the survival of PCa patients with low and high gene expression respectively. Kaplan-meier analysis showed that the BCR free survival of FCGR3A and HAVCR2 was significantly different (FCGR3A, P=0.010; HAVCR2, P=0.018) (Figures 3A, B), indicating that the high expression of FCGR3A and HAVCR2 had a poor prognosis for PCa patients. In addition, the expression of CCR7 and CD28 had no significance for the survival and prognosis of PCa patients (P>0.05) (Figures 3C, D), indicating that CCR7 and CD28 had no prognostic value.

High expression of FCGR3A and HAVCR2 in PCa tissues

We further verified the role of the expression of 4 target genes in the prostate of PCa patients by immunohistochemistry. Immunostaining results showed that FCGR3A, CCR7 and CD28 proteins were all expressed in the cytoplasm and membrane, while HAVCR2 protein was mainly expressed in the cytoplasm and membrane and a small amount in the nucleus (Figure 4A). Based on immune response score (IRS=0-4, low expression; IRS=4-12, high expression), we found that FCGR3A and HAVCR2 proteins were up-regulated in prostate tissues of PCa patients compared with normal tissues (P<0.01), while the expression of CCR7 and CD28 proteins were not significantly different between them (P>0.05) (Figure 4B). In addition, we found that the expression of FCGR3A and HAVCR2 proteins was gradually up-regulated with the increase of Gleason score (GS) grade in tissue samples of different tumor development stages (GS=4+4, high; GS=3+4, medium; GS=2+2, low), among which the expression of FCGR3A was most significantly up-regulated, while the expression of CCR7 and CD28 proteins showed no significant difference (Figure 4C).

Expression of FCGR3A is uniquely correlated with the clinicopathological features of PCa

Tables 2–5 summarizes the correlation between the expression of 4 target genes and the different clinicopathological features of PCa patients. In TMA, IRS<4 was considered as low expression, and IR≥4 was considered as high expression. In

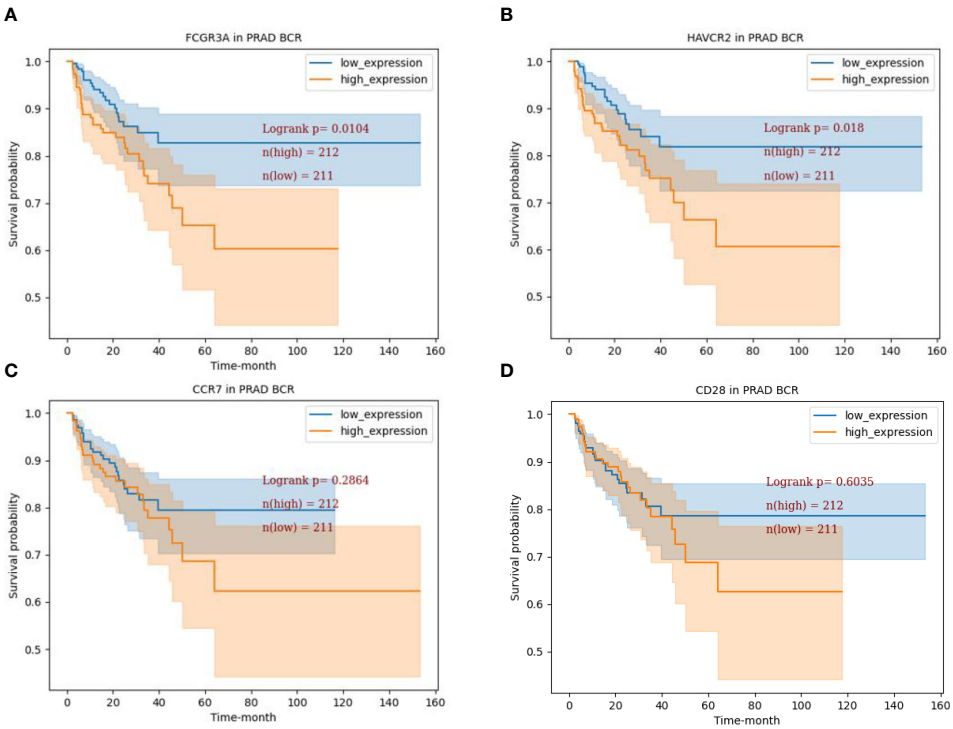

FIGURE 3
BCR free survival analysis of 4 target genes. **(A)** BCR free survival curve of FCGR3A in TCGA-PRAD dataset (P=0.0104). **(B)** BCR free survival curve of HAVCR2 in TCGA-PRAD dataset (P=0.0180). **(C)** BCR free survival curve of CCR7 in TCGA-PRAD dataset (P=0.2864) **(D)**. BCR free survival curve of CCR7 in TCGA-PRAD dataset (P=0.6035).

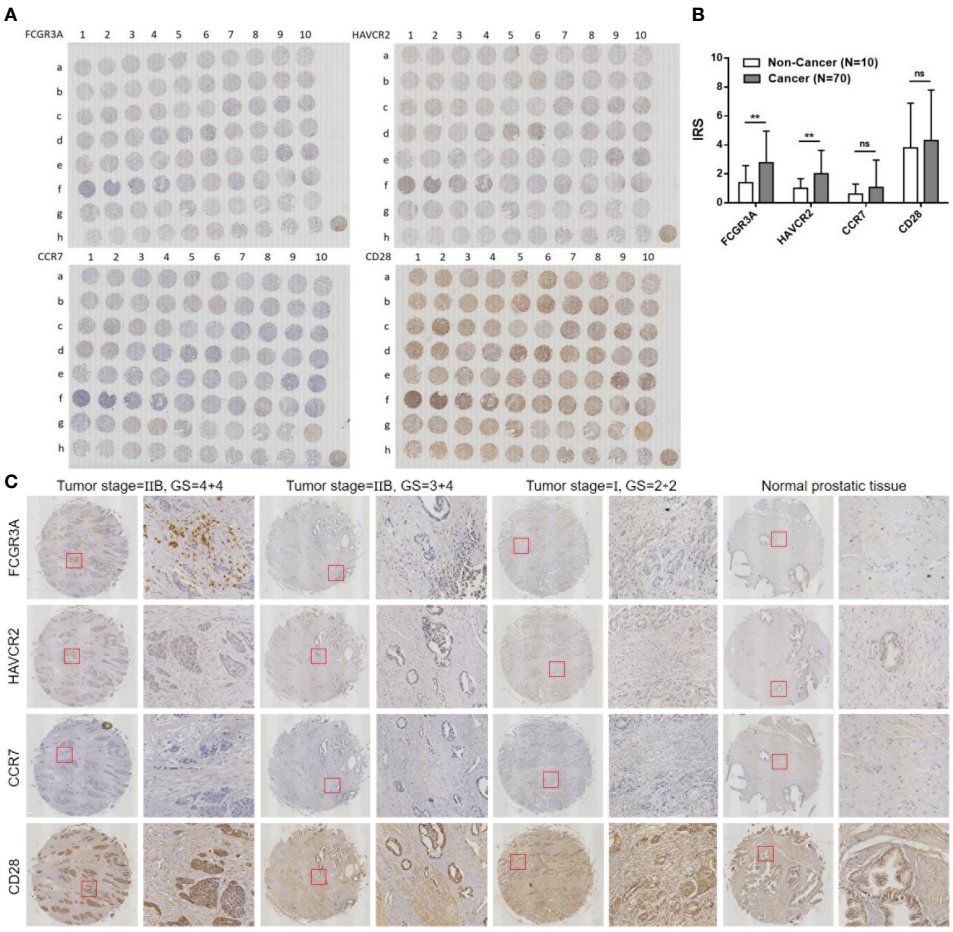

FIGURE 4
Immunohistochemical staining for 4 target genes expression in PCa and normal prostate tissue samples. **(A)** Full view of the immunohistochemistry staining for 4 target genes expression. **(B)** (no significance, ns P>0.05) Immune risk score (IRS) of 4 target genes in PCa and normal prostate tissue samples (Cancer vs. Non-Cancer, ***P*<0.01). **(C)** 4 target genes expression in PCa tissue samples with different tumor stages and Gleason score (GS).

TCGA, 427 PCa samples were divided into low-expression group (n=213, 49.88%) and high-expression group (n=213, 50.12%). We were surprised to find that FCGR3A expression was inconsistent with clinicopathological features in age and GS, while consistent with clinicopathological features in tumor stage (TMA, *P*=0.030; TCGA, *P*=0.006). TMA and TCGA results showed that FCGR3A was highly expressed in tumor T2 stage (which was consistent with the result of tissue microarray), but showed the opposite result in tumor T3 stage. And the expression of HAVCR2, CCR7 and CD28 had poor correlation with the clinicopathological features of PCa in age, GS and tumor stage.

Discussion

PCa is considered to be a multi-stage progressive disease, which generally develops from prostatic intraepithelial tumor to hormone dependent invasive adenocarcinoma in situ, and finally to hormone independent metastatic tumor. Radical treatments, such as radical prostatectomy, radiotherapy and cryotherapy, are always adopted for the early PCa. And for the advanced PCa, androgen deprivation therapy (ADT) is the main treatment for it, but most patients will gradually develop castration resistant PCa (CRPC). When the tumor infiltrates out of the prostate capsule, the treatment effect and prognosis become worse. At this time, the standard treatment is radiotherapy, followed by chemotherapy and enzalutamide, but some patients are prone to drug resistance (22). Docetaxel is the first drug approved by FDA to treat CRPC after ADT failure, which can significantly improve the survival rate of advanced PCa (23). Although enzalutamide and chemotherapeutic drugs can prolong the survival time of PCa patients, they will produce side effects such as drug resistance, and ultimately cannot curb tumor growth and metastasis. TME is filled with a large number of cancerous cells and stromal cells. The

10.3389/fonc.2022.1014888

TABLE 2 Correlation of FCGR3A expression with clinicopathological features in PCa patients.

Clinical features	TMA				TCGA			
	Case	Low, n (%)	High, n (%)	*P*	Case	Low, n (%)	High, n (%)	*P*
Tissue								
Cancer	70	32 (45.71)	38 (54.29)	0.397	427	213 (49.88)	214 (50.12)	–
Non-cancer	10	6 (60.00)	4 (40.00)	–	0	–	–	–
Age (years)								
≤60	14	7 (50.00)	7 (50.00)	0.837	190	105 (55.26)	85 (44.74)	0.047*
>60	66	31 (46.97)	35 (53.03)	–	237	108 (45.57)	129 (54.43)	–
Gleason score								
≤8	46	22 (47.83)	24 (52.17)	0.623	300	171 (57.00)	129 (43.00)	<0.001***
>8	24	10 (41.67)	14 (58.33)	–	127	42 (33.07)	85 (66.93)	–
Serum PSA levels (ng/ml)								
≤2	–	–	–	–	378	196 (51.85)	182 (48.15)	0.003**
>2	–	–	–	–	35	9 (25.71)	26 (74.29)	–
Pathological grade								
pT1-pT2	4	3 (75.00)	1 (25.00)	0.213	–	–	–	–
pT3	65	28 (43.08)	37 (56.92)	–	–	–	–	–
Tumor stage								
T1	0	–	–	-	153	92 (60.13)	61 (39.87)	0.006**
T2	42	16 (38.10)	26 (61.90)	0.030*	155	75 (48.39)	80 (51.61)	–
T3	14	10 (71.43)	4 (28.57)	–	48	16 (33.33)	32 (66.67)	–
T4	0	–	–	–	1	0 (0.00)	1 (100.00)	–
Lymph nodemetastasis								
N0	56	26 (46.43)	30 (53.57)	–	303	155 (51.16)	148 (48.84)	<0.001***
N1	0	–	–	–	69	20 (28.99)	49 (71.01)	–
Distant metastasis								
M0	56	26 (46.43)	30 (53.57)	–	401	200 (49.88)	201 (50.12)	0.568
M1	0	–	–	–	3	1 (33.33)	2 (66.67)	–

∗means the difference is significant at the 0.05 level ,** means the difference is significant at the 0.01 level, *** means the difference is significant at the 0.01 level.

TABLE 3 Correlation of HAVCR2 expression with clinicopathological features in PCa patients.

Clinical features	TMA				TCGA			
	Case	Low, n (%)	High, n (%)	*P*	Case	Low, n (%)	High, n (%)	*P*
Tissue								
Cancer	70	6 (8.57)	64 (91.43)	0.260	427	213 (49.88)	214 (50.12)	–
Non-cancer	10	2 (20.00)	8 (80.00)	–	0	–	–	–
Age (years)								
≤60	14	2 (14.29)	12 (85.71)	0.556	190	107 (56.32)	83 (43.68)	0.017*
>60	66	6 (9.09)	60 (90.91)	–	237	106 (44.73)	131 (55.27)	–
Gleason score								
≤8	46	3 (6.52)	43 (93.48)	0.396	300	172 (57.33)	128 (42.67)	<0.001***
>8	24	3 (12.50)	21 (87.50)	–	127	41 (32.28)	86 (67.72)	–
Serum PSA levels (ng/ml)								
≤2	–	–	–	–	378	194 (51.32)	184 (48.68)	0.010**
>2	–	–	–	–	35	10 (28.57)	25 (71.43)	–
Pathological grade								

(Continued)

10.3389/fonc.2022.1014888

TABLE 3 Continued

Clinical features	TMA				TCGA			
	Case	Low, n (%)	High, n (%)	*P*	Case	Low, n (%)	High, n (%)	*P*
pT1-pT2	4	0 (0.00)	4 (100.00)	0.525	–	–	–	–
pT3	65	6 (9.23)	59 (90.77)	–	–	–	–	–
Tumor stage								
T1	0	–	–	-	153	88 (57.52)	61 (42.48)	0.053
T2	42	4 (9.52)	38 (90.48)	0.787	155	74 (47.74)	80 (52.26)	–
T3	14	1 (7.14)	13 (92.86)	–	48	22 (45.83)	32 (54.17)	–
T4	0	–	–	–	1	0 (0.00)	1 (100.00)	–
Lymph nodemetastasis								
N0	56	5 (8.93)	51 (91.07)	–	303	154 (50.83)	149 (49.17)	0.002**
N1	0	–	–	–	69	21 (30.43)	48 (69.57)	–
Distant metastasis								
M0	56	5 (8.93)	51 (91.07)	–	401	199 (49.63)	202 (50.37)	0.574
M1	0	–	–	–	3	1 (33.33)	2 (66.67)	–

∗means the difference is significant at the 0.05 level ,** means the difference is significant at the 0.01 level, *** means the difference is significant at the 0.01 level.

TABLE 4 Correlation of CCR7 expression with clinicopathological features in PCa patients.

Clinical features	TMA				TCGA			
	Case	Low, n (%)	High, n (%)	*P*	Case	Low, n (%)	High, n (%)	*P*
Tissue								
Cancer	70	31 (44.29)	39 (55.71)	0.734	427	213 (49.88)	214 (50.12)	–
Non-cancer	10	5 (50.00)	5 (50.00)	–	0	–	–	–
Age (years)								
≤60	14	7 (50.00)	7 (50.00)	0.679	190	84 (44.21)	106 (55.79)	0.036*
>60	66	29 (43.94)	37 (56.06)	–	237	129 (54.43)	108 (45.57)	–
Gleason score								
≤8	46	21 (45.65)	25 (54.35)	0.750	300	150 (50.00)	150 (50.00)	0.941
>8	24	10 (41.67)	14 (58.33)	–	127	63 (49.61)	64 (50.39)	–
Serum PSA levels (ng/ml)								
≤2	–	–	–	–	378	190 (50.26)	188 (49.74)	0.245
>2	–	–	–	–	35	14 (40.00)	21 (60.00)	–
Pathological grade								
pT1-pT2	4	2 (50.00)	2 (50.00)	0.834	–	–	–	–
pT3	65	29 (44.62)	36 (55.38)	–	–	–	–	–
Tumor stage								
T1	0	–	–	-	153	81 (52.94)	72 (47.06)	0.249
T2	42	17 (40.48)	25 (59.52)	0.277	155	69 (44.52)	86 (55.48)	–
T3	14	8 (57.14)	6 (42.86)	–	48	27 (56.25)	21 (43.75)	–
T4	0	–	–	–	1	0 (0.00)	1 (100.00)	–
Lymph nodemetastasis								
N0	56	25 (44.64)	31 (55.36)	–	303	147 (48.51)	156 (51.49)	0.450
N1	0	–	–	–	69	30 (43.48)	39 (56.52)	–
Distant metastasis								
M0	56	25 (44.64)	31 (55.36)	–	401	196 (48.88)	205 (51.12)	0.539
M1	0	–	–	–	3	2 (66.67)	1 (33.33)	–

*means the difference is significant at the 0.05 level.

10.3389/fonc.2022.1014888

TABLE 5 Correlation of CD28 expression with clinicopathological features in PCa patients.

Clinical features	TMA				TCGA			
	Case	Low, n (%)	High, n (%)	*P*	Case	Low, n (%)	High, n (%)	*P*
Tissue								
Cancer	70	35 (50.00)	35 (50.00)	0.554	427	213 (49.88)	214 (50.12)	–
Non-cancer	10	4 (40.00)	6 (60.00)	–	0	–	–	–
Age (years)								
≤60	14	9 (64.29)	5 (35.71)	0.200	190	98 (51.58)	92 (48.42)	0.530
>60	66	30 (45.45)	36 (54.55)	–	237	115 (48.52)	122 (51.48)	–
Gleason score								
≤8	46	25 (54.35)	21 (45.65)	0.314	300	156 (52.00)	144 (48.00)	0.179
>8	24	10 (41.67)	14 (58.33)	–	127	57 (44.88)	70 (55.12)	–
Serum PSA levels (ng/ml)								
≤2	–	–	–	–	378	193 (51.06)	185 (48.94)	0.026*
>2	–	–	–	–	35	11 (31.43)	24 (68.57)	–
Pathological grade								
pT1-pT2	4	1 (25.00)	3 (75.00)	0.317	–	–	–	–
pT3	65	33 (50.77)	32 (49.23)	–	–	–	–	–
Tumor stage								
T1	0	–	–	–	153	88 (57.52)	65 (42.48)	0.138
T2	42	23 (54.76)	19 (45.24)	0.272	155	76 (49.03)	79 (50.97)	–
T3	14	10 (71.43)	4 (28.57)	–	48	20 (41.67)	28 (58.33)	–
T4	0	–	–	–	1	0 (0.00)	1 (100.00)	–
Lymph nodemetastasis								
N0	56	33 (58.93)	23 (41.07)	–	303	148 (48.84)	155 (51.16)	0.215
N1	0	–	–	–	69	28 (40.58)	41 (59.42)	–
Distant metastasis								
M0	56	33 (58.93)	23 (41.07)	–	401	199 (49.63)	202 (50.37)	0.574
M1	0	–	–	–	3	1 (33.33)	2 (66.67)	–

*means the difference is significant at the 0.05 level.

latter are usually composed of inflammatory cells, smooth muscle cells, adipocytes, fibroblasts, neuroendocrine cells, endothelial cells and microvessels, with cytokines, growth factors, low pH, hypoxia and various extracellular matrices (24). Many studies have found that (25–27), TME played an important role in the physiological regulation of inducing tumor acquired drug resistance and resisting apoptosis.

FCGRs is the receptor for the Fc segment of immunoglobulin (IgG), which can be divided into three types: FCGRI (CD64), FCGRII (CD32) and FCGRIII (CD16). The gene encoding FCGRs has polymorphism and is involved in the stimulation of many biological functions, such as phagocytosis, cell lysis and inflammatory cascade reactions (28–30). FCGR3A (CD16), a member of FCGRs family, is mainly expressed on the surface of natural killer (NK) cell membrane and is a transmembrane receptor, which plays a role of bridge for immune cells to directly kill target cells (31). HAVCR2 (Tim3), a member of Tim3 family, is expressed on the membrane of various immune cells as a transmembrane protein (32). HAVCR2 not only acts on differentiated and mature T lymphocytes, but also plays an immunomodulatory role in a variety of innate immune cells (33). Studies had found that HAVCR2 was highly expressed in NK cells in TME, and hepatocellular carcinoma cells could lead to dysfunction of NK cell population by inhibiting PI3K/Akt/mTORC1 signaling pathway mediated by HAVCR2 (34). Therefore, FCGR3A and HAVCR2 are highly expressed in various cancer models and are likely to participate in the immune process of NK cells. However, the roles of FCGR3A and HAVCR2 in PCa are rarely reported. We first analyzed the PPI network construction of 42 candidate genes, and found that FCGR3A and HAVCR2 interacted with each other, and they were closely related to CCR7 and CD28. As we konw, B7/CD28 is a classic costimulatory signaling pathway, and activation of this pathway can lead to activation of $CD8^+$ and $CD28^+$ T cells (35). However, most tumor cells can inhibit the activation of T cells by down-regulating which the expression of CD28 to achieve immune escape in TME (36). TME is also filled with a large number of inflammatory and chemotactic factors, which can activate tumor cells and promote their metastasis. It was found that TNF-α in TME could promote PCa metastasis and diffusion

from lymph nodes by activating the CCL21/CCR7 signaling axis (37). Therefore, CCR7 and CD28 also play an important roles of immune regulation in TME.

During the occurrence and development of PCa, the relationship between FCGR3A, HAVCR2, CCR7 and CD28 was still unclear, which requires preliminary research. After incorporating this gene cluster into the prognostic model, we found that this gene cluster had the ability to predict the biochemical recurrence of PCa patients. Cox regression analysis showed that the risk ratio of high expression of these genes was 2.30 times higher than that of low expression in single-factor analysis, but there was no statistical significance in the multivariate analysis. We hypothesized that this might be due to the uneven expression of individual genes in the tissues of PCa patients. Subsequently, proof of our hypothesis by survival analysis and clinical tissue microarray assays. The results showed that the survival rate and prognosis of PCa patients were lower, and the high expression of FCGR3A and HAVCR2 proteins in PCa tissues increased gradually with the increase of GS when FCGR3A and HAVCR2 were overexpressed. These results were consistent with the findings of FCGR3A and HAVCR2 in other immunological or cancer diseases (38–41). These results suggest that the expression of FCGR3A and HAVCR2 is correlated with the degree of malignancy in PCa patients, and the high expression of FCGR3A and HAVCR2 has a poor prognosis for PCa patients. Finally, we compared the correlation between the expression of 4 target genes and different clinicopathological features of PCa patients. The results showed that the expression of FCGR3A had a unique correlation with the clinicopathological features of PCa. This is similar to FCGR3A in other tumor models, for example, the level of natural killing activity in peripheral blood mononuclear cells of patients with bladder cancer is correlated with the clinical evolution and pathological stage of the disease (42).

FCGR3A is the target of many drugs such as rituximab and its expression in prostate cancer cells is positively correlated with other markers (43). Long-term use of some common drugs leads to mutations in FCGR3A and related genes, which produces resistance to the disease, such as non-small cell lung cancer (44, 45). Different new disease targets, FCGR3A as an important marker gene for a variety of diseases, on the one hand, can promote the development of new uses of old drugs faster, on the other hand, through the analysis of the interaction between FCGR3A and other cancer markers, find out the dominant gene, which is conducive to the combined treatment of a variety of diseases. FCGR3A has developed resistance to some drugs, so it will be more difficult to develop new drugs.

In conclusion, FCGR3A is a biomarker with potential prognostic value for PCa, which can predict the survival of PCa patients and provide a new basis for rational administration in clinical of PCa patients.With the development of new technologies, FCGR3A is expected to become a new breakthrough point for potent drugs.

Data availability statement

The original contributions presented in the study are included in the article/Supplementary Material. Further inquiries can be directed to the corresponding author.

Ethics statement

Written informed consent was obtained from the individual(s) for the publication of any potentially identifiable images or data included in this article.

Author contributions

ZZ and W-DZ contributed to conception and design of the study. YH organized the database. ZT performed the statistical analysis. Q-LD wrote the first draft of the manuscript. YW, S-BY, Y-DW, H-JT, and F-NJ wrote sections of the manuscript. All authors contributed to manuscript revision, read, and approved the submitted version.

Funding

This work was supported by grants from National Natural Science Foundation of China (Grant No. 82072813, Grant No. 81571427), Scientific research start-up project of Guangzhou First People's Hospital (Grant No. KYQD0004), Guangzhou General Science and Technology Project of Health and Family Planning (Grant No. 20201A011012), Guangzhou Planned Project of Science and Technology (Grant No. 202102010038, Grant No. 202102080029).

Conflict of interest

The authors declare that the research was conducted in the absence of any commercial or financial relationships that could be construed as a potential conflict of interest.

Publisher's note

All claims expressed in this article are solely those of the authors and do not necessarily represent those of their affiliated organizations, or those of the publisher, the editors and the reviewers. Any product that may be evaluated in this article, or claim that may be made by its manufacturer, is not guaranteed or endorsed by the publisher.

Supplementary material

The Supplementary Material for this article can be found online at: https://www.frontiersin.org/articles/10.3389/fonc.2022.1014888/full#supplementary-material

References

1. Bray F, Ferlay J, Soerjomataram I, Siegel RL, Torre LA, Jemal A. Global cancer statistics 2018: GLOBOCAN estimates of incidence and mortality worldwide for 36 cancers in 185 countries. *CA Cancer J Clin* (2018) 68(6):394–424. doi: 10.3322/caac.21492

2. Bellamri M, Turesky RJ. Dietary carcinogens and DNA adducts in prostate cancer. *Adv Exp Med Biol* (2019) 1210:29–55. doi: 10.1007/978-3-030-32656-2_2

3. Fernandes RC, Toubia J, Townley S, Hanson AR, Dredge BK, Pillman KA, et al. Post-transcriptional gene regulation by MicroRNA-194 promotes neuroendocrine transdifferentiation in prostate cancer. *Cell Rep* (2021) 34 (1):108585. doi: 10.1016/j.celrep.2020.108585

4. Andrews JR, Hebert KJ, Boswell TC, Avant RA, Boonipatt T, Kreutz-Rodrigues L, et al. Pubectomy and urinary reconstruction provides definitive treatment of urosymphyseal fistula following prostate cancer treatment. *BJU Int* (2021) 128(4):460–7. doi: 10.1111/bju.15333

5. Rescigno P, Dolling D, Conteduca V, Rediti M, Bianchini D, Lolli C, et al. Early post-treatment prostate-specific antigen at 4 weeks and abiraterone and enzalutamide treatment for advanced prostate cancer: An international collaborative analysis. *Eur Urol. Oncol* (2020) 3(2):176–82. doi: 10.1016/j.euo.2019.06.008

6. Taneja SS. Re: Enzalutamide with standard first-line therapy in metastatic prostate cancer. *J Urol.* (2020) 203(1):32–3. doi: 10.1097/01.JU.0000611504.41578.ee

7. Kweldam CF, van Leenders GJ, van der Kwast T. Grading of prostate cancer: a work in progress. *Histopathology* (2019) 74(1):146–60. doi: 10.1111/his.13767

8. Llop E, Ferrer-Batallé M, Barrabés S, Guerrero PE, Ramírez M, Saldova R, et al. Erratum: Improvement of prostate cancer diagnosis by detecting PSA glycosylation-specific changes: Erratum. *Theranostics* (2018) 8(3):746–8. doi: 10.7150/thno.23906

9. Liu Y, Liu Y, Yuan B, Yin L, Peng Y, Yu X. FOXM1 promotes the progression of prostate cancer by regulating PSA gene transcription. *Oncotarget* (2017) 8 (10):17027–37. doi: 10.18632/oncotarget.15224

10. Kuninty PR, Schnittert J, Storm G, Prakash J. MicroRNA targeting to modulate tumor microenvironment. *Front Oncol* (2016) 6:3. doi: 10.3389/fonc.2016.00003

11. Riquelme MA, Cardenas ER, Jiang JX. Osteocytes and bone metastasis. *Front Endocrinol* (2020) 11:567844. doi: 10.3389/fendo.2020.567844

12. Zhu BP, Guo ZQ, Lin L, Serum BSP. PSADT, and spondin-2 levels in prostate cancer and the diagnostic significance of their ROC curves in bone metastasis. *Eur Rev Med Pharmacol Sci* (2017) 21(1):61–7.

13. Weiner AB, Matulewicz RS, Eggener SE, Schaeffer EM. Increasing incidence of metastatic prostate cancer in the united states (2004-2013). *Prostate. Cancer Prostatic Dis* (2016) 19(4):395–7. doi: 10.1038/pcan.2016.30

14. Chen S, Zhu G, Yang Y, Wang F, Xiao Y, Zhang N, et al. Single-cell analysis reveals transcriptomic remodellings in distinct cell types that contribute to human prostate cancer progression. *Nat Cell Biol* (2021) 23(1):87–98. doi: 10.1038/s41556-020-00613-6

15. Miyata Y, Sakai H. Reconsideration of the clinical and histopathological significance of angiogenesis in prostate cancer: Usefulness and limitations of microvessel density measurement. *Int J Urol.* (2015) 22(9):806–15. doi: 10.1111/iju.12840

16. Sperger JM, Emamekhoo H, McKay RR, Stahlfeld CN, Singh AC, Chen XE, et al. Prospective evaluation of clinical outcomes using a multiplex liquid biopsy targeting diverse resistance mechanisms in metastatic prostate cancer. *J Clin Oncol* (2021) 39(26):2926–37. doi: 10.1200/JCO.21.00169

17. Conteduca V, Wetterskog D, Gonzalez-Billalabeitia E, Brighi N, Giorgia UD, Attard G. Circulating androgen receptor for prognosis and treatment selection in prostate cancer. *Eur Urol. Oncol* (2021) 4(5):740–4. doi: 10.1016/j.euo.2020.12.009

18. Richardsen E, Uglehus RD, Due J, Busch C, Busund R. The prognostic impact of m-CSF, CSF-1 receptor, CD68 and CD3 in prostatic carcinoma. *Histopathology* (2008) 53(1):30–8. doi: 10.1111/j.1365-2559.2008.03058.x

19. Sun K, Fei X, Xu R, Xu M. FCGR3A is a prognostic biomarker and correlated with immune infiltrates in lower-grade glioma. *J Oncol* (2022) 11:317–33. doi: 10.1155/2022/9499317

20. Noelia M, María M, Cristina P, Fernando MM, Juan EM, Abdelali D, et al. Influence of the FCGR2A rs1801274 and FCGR3A rs396991 polymorphisms on response to abatacept in patients with rheumatoid arthritis. (2021) 11:573–89. doi: 10.3390/jpm11060573

21. Yu H, Liu Y, Li C, Wang JH, Yu B, Wu Q, et al. Bioinformatic analysis of neuroimmune mechanism of neuropathic pain. *BioMed Res Int* (2020) 11:349–59. doi: 10.1155/2020/4516349

22. Ganju A, Yallapu MM, Khan S, Behrman SW, Chauhan SC, Jaggi M, et al. Nanoways to overcome docetaxel resistance in prostate cancer. *Drug Resist Updat.* (2014) 17(1-2):13–23. doi: 10.1016/j.drup.2014.04.001

23. Petrylak DP, Tangen CM, Hussain MH , Lara PN, Jones JA, Taplin ME, et al. Docetaxel and estramustine compared with mitoxantrone and prednisone for advanced refractory prostate cancer. *N Engl J Med* (2004) 351(15):1513–20. doi: 10.1056/NEJMoa041318

24. Martínez-Reyes I, Chandel NS. Cancer metabolism: looking forward. *Nat Rev Cancer* (2021) 21(10):669–80. doi: 10.1038/s41568-021-00378-6

25. Gil V, Miranda S, Riisnaes R, Gurel B, D'Ambrosio MA, Vasciaveo A, et al. HER3 is an actionable target in advanced prostate cancer. *Cancer Res* (2021) 81 (24):6207–18. doi: 10.1158/0008-5472.CAN-21-3360

26. Sun BL. Immunotherapy in treatment of metastatic prostate cancer: An approach to circumvent immunosuppressive tumor microenvironment. *Prostate* (2021) 81(15):1125–34. doi: 10.1002/pros.24213

27. Wang C, Zhang Y, Gao WQ. The evolving role of immune cells in prostate cancer. *Cancer Lett* (2022) 525:9–21. doi: 10.1016/j.canlet.2021.10.027

28. Bruhns P, Jönsson F. Mouse and human FcR effector functions. *Immunol Rev* (2015) 268(1):25–51. doi: 10.1111/imr.12350

29. Nimmerjahn F, Ravetch JV. Fcgamma receptors as regulators of immune responses. *Nat Rev Immunol* (2008) 8(1):34–47. doi: 10.1038/nri2206

30. Bruhns P. Properties of mouse and human IgG receptors and their contribution to disease models. *Blood* (2012) 119(24):5640–9. doi: 10.1182/blood-2012-01-380121

31. Ravetch JV, Bolland S. IgG fc receptors. *Annu Rev Immunol* (2001) 19:275–90. doi: 10.1146/annurev.immunol.19.1.275

32. Du W, Yang M, Turner A , Xu C, Ferris RL, Huang JN, et al. TIM-3 as a target for cancer immunotherapy and mechanisms of action. *Int J Mol Sci* (2017) 18 (3):645. doi: 10.3390/ijms18030645

33. Gandhi AK, Kim WM, Sun ZJ, Huang YH, Bonsor DA, Sundberg EJ, et al. High resolution X-ray and NMR structural study of human T-cell immunoglobulin and mucin domain containing protein-3. *Sci Rep* (2018) 30;8(1):17512. doi: 10.1038/s41598-018-35754-0

34. Tan S, Xu Y, Wang Z, Wang TX, Du XH, Song XJ, et al. Tim-3 hampers tumor surveillance of liver-resident and conventional NK cells by disrupting PI3K signaling. *Cancer Res* (2020) 80(5):1130–42. doi: 10.1158/0008-5472.CAN-19-2332

35. Janakiram M, Shah UA, Liu W, Zhao AM, Schoenberg MP, Zang XX. The third group of the B7-CD28 immune checkpoint family: HHLA2, TMIGD2, B7x, and B7-H3. *Immunol Rev* (2017) 276(1):26–39. doi: 10.1111/imr.12521

36. Zhao X, Yuan C, Wangmo D, Subramanian S. Tumor-secreted extracellular vesicles regulate T-cell costimulation and can be manipulated to induce tumor-specific T-cell responses. *Gastroenterology* (2021) 161(2):560–74. doi: 10.1053/j.gastro.2021.04.036

37. Maolake A, Izumi K, Natsagdorj A, Iwamoto H, Kadomoto S, Makino T, et al. Tumor necrosis factor-α induces prostate cancer cell migration in lymphatic metastasis through CCR7 upregulation. *Cancer Sci* (2018) 109(5):1524–31. doi: 10.1111/cas.13586

38. Lykowska-Szuber L, Walczak M, Skrzypczak-Zielinska M, Suszynska-Zajczyk J, Stawczyk-Eder K, Waszak K, et al. Effect of anti-TNF therapy on mucosal apoptosis genes expression in crohn's disease. *Front Immunol* (2021) 12:615539. doi: 10.3389/fimmu.2021.615539

39. Jiménez Morales A, Maldonado-Montoro M, Martínez de la Plata JE, Martínez de la Plata JE, Pérez R, Daddaoua A, et al. FCGR2A/FCGR3A gene polymorphisms and clinical variables as predictors of response to tocilizumab and rituximab in patients with rheumatoid arthritis. *J Clin Pharmacol* (2019) 59 (4):517–31. doi: 10.1002/jcph.1341

40. Kandel S, Adhikary P, Li G, Chen K. The TIM3/Gal9 signaling pathway: An emerging target for cancer immunotherapy. *Cancer Lett* (2021) 10:510:67–78. doi: 10.1016/j.canlet.2021.04.011

41. Chen K, Gu Y, Cao Y, Fang H, Lv KP, Liu X, et al. TIM3$^+$ cells in gastric cancer: clinical correlates and association with immune context. *Br J Cancer* (2022) 126(1):100–8. doi: 10.1038/s41416-021-01607-3

42. Bi T, Jin F, Wu W, Long J, Li Y, Gong X, et al. Phase II clinical trial of two different modes of administration of the induction chemotherapy for locally advanced nasopharyngeal carcinoma. *Clin Trial.* (2015) 37(9):676–81.

43. Tavakolpour S, Alesaeidi S, Darvishi M, GhasemiAdl M, Darabi-Monadi S, Akhlaghdoust Mc , et al. A comprehensive review of rituximab therapy in rheumatoid arthritis patients. *Clin Rheumatol* (2019) 38:2977–94. doi: 10.1007/s10067-019-04699-8

44. Wang H, Yang J, Xie D, Liang ZG, Wang Y, Fu RY, et al. Single-cell RNA sequencing infers the role of malignant cells in drug-resistant multiple myeloma. *Clin Trans Med* (2021) 11:653–64. doi: 10.1002/ctm2.653

45. Luo R, Ge C, Xiao X, Song J, Miao SQ, Tang YY, et al. Identification of genetic variations associated with drug resistance in non-small cell lung cancer patients undergoing systemic treatment. *Briefings Bioinf* (2019) 22:187–205. doi: 10.1093/bib/bbab187

frontiers | Frontiers in Oncology

TYPE Review
PUBLISHED 30 November 2022
DOI 10.3389/fonc.2022.1054029

OPEN ACCESS

EDITED BY
Erik Arnold Bey,
Wood Hudson Cancer Research Laboratory, United States

REVIEWED BY
Zehra Edis,
Ajman University, United Arab Emirates
Yang Bo,
University of Illinois at Urbana-Champaign, United States

*CORRESPONDENCE
Zohreh Amoozgar
zamoozgar@mgh.harvard.edu
Rana Jahanban-Esfahlan
jahanbanr@tbzmed.ac.ir

SPECIALTY SECTION
This article was submitted to Molecular and Cellular Oncology, a section of the journal Frontiers in Oncology

RECEIVED 26 September 2022
ACCEPTED 09 November 2022
PUBLISHED 30 November 2022

CITATION
Mahmudi H, Adili-Aghdam MA, Shahpouri M, Jaymand M, Amoozgar Z and Jahanban-Esfahlan R (2022) Tumor microenvironment penetrating chitosan nanoparticles for elimination of cancer relapse and minimal residual disease.
Front. Oncol. 12:1054029.
doi: 10.3389/fonc.2022.1054029

Tumor microenvironment penetrating chitosan nanoparticles for elimination of cancer relapse and minimal residual disease

Hossein Mahmudi[1,2], Mohammad Amin Adili-Aghdam[3], Mohammad Shahpouri[1], Mehdi Jaymand[4], Zohreh Amoozgar[5]* and Rana Jahanban-Esfahlan[1,6]*

[1]Department of Medical Biotechnology, Faculty of Advanced Medical Sciences, Tabriz University of Medical Sciences, Tabriz, Iran, [2]Student Research Committee, Tabriz University of Medical Sciences, Tabriz, Iran, [3]Research Center for Pharmaceutical Nanotechnology, Biomedicine Institute, Tabriz University of Medical Sciences, Tabriz, Iran, [4]Nano Drug Delivery Research Center, Health Technology Institute, Kermanshah University of Medical Sciences, Kermanshah, Iran, [5]Edwin L. Steele Laboratories, Department of Radiation Oncology, Massachusetts General Hospital and Harvard Medical School, Boston, MA, United States, [6]Stem Cell Research Center, Tabriz University of Medical Sciences, Tabriz, Iran

Chitosan and its derivatives are among biomaterials with numerous medical applications, especially in cancer. Chitosan is amenable to forming innumerable shapes such as micelles, niosomes, hydrogels, nanoparticles, and scaffolds, among others. Chitosan derivatives can also bring unprecedented potential to cross numerous biological barriers. Combined with other biomaterials, hybrid and multitasking chitosan-based systems can be realized for many applications. These include controlled drug release, targeted drug delivery, post-surgery implants (immunovaccines), theranostics, biosensing of tumor-derived circulating materials, multimodal systems, and combination therapy platforms with the potential to eliminate bulk tumors as well as lingering tumor cells to treat minimal residual disease (MRD) and recurrent cancer. We first introduce different formats, derivatives, and properties of chitosan. Next, given the barriers to therapeutic efficacy in solid tumors, we review advanced formulations of chitosan modules as efficient drug delivery systems to overcome tumor heterogeneity, multi-drug resistance, MRD, and metastasis. Finally, we discuss chitosan NPs for clinical translation and treatment of recurrent cancer and their future perspective.

KEYWORDS

chitosan, tumor heterogeneity, tumor microenvironment, recurrent cancer, drug delivery, minimal residual disease

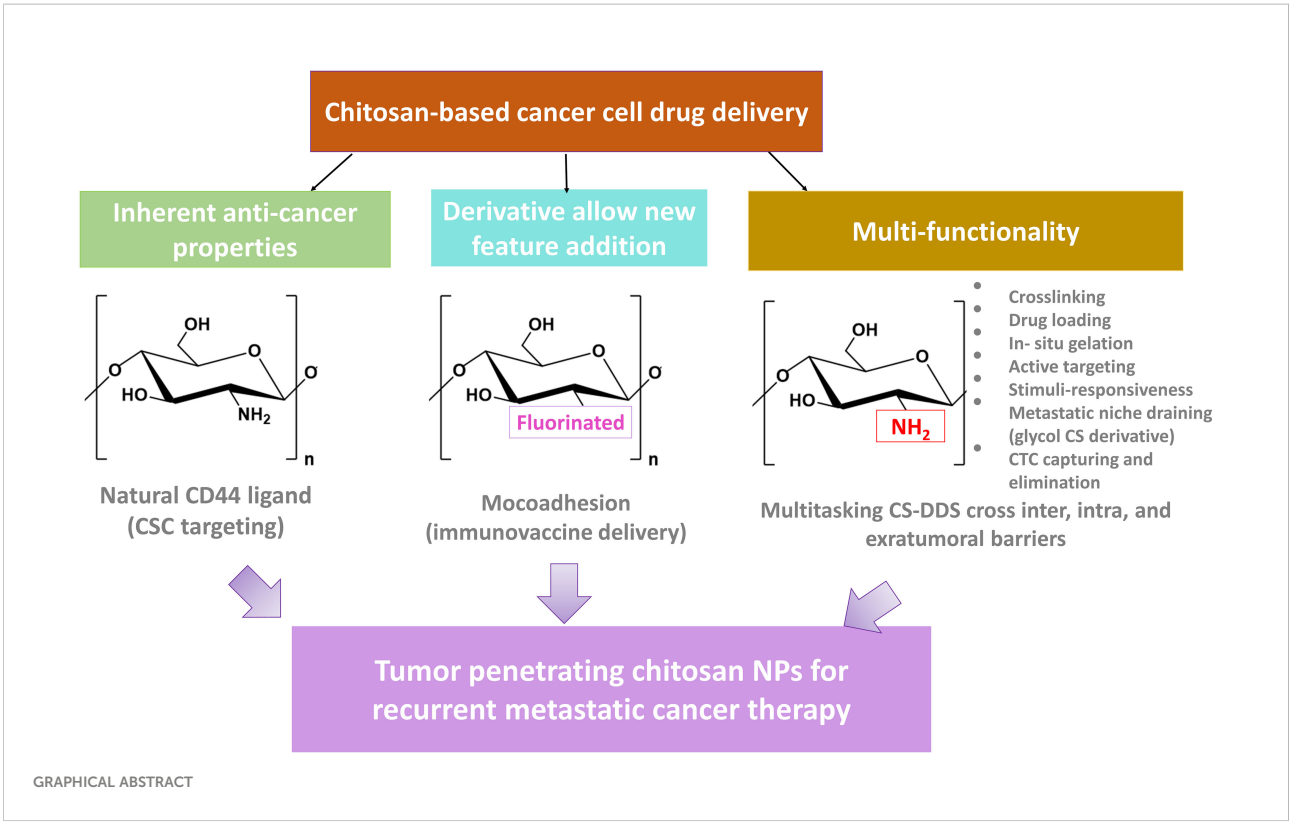

1 Introduction

Despite all advancements in drug delivery strategies developed for targeting solid tumors, efficacy is still suboptimal due to numerous biological barriers, including endothelial, cell membrane, organelle membrane, and the nanoparticle's ability for on-target/off-target recognition, penetration, localization, concentration, and homogenous distribution. Most of these bottlenecks for successful NP delivery originate from the nature of the solid tumor microenvironment (TME), including the ability of immune editing, hypoxia, cancer stem cells (CSCs), extracellular matrix (ECM) components, and heterogeneity, among others (1, 2). TME leverages inherent resistance mechanisms such as hypoxia and pH gradients and acquired resistance mechanisms such as clonal evolution and heterogeneity after surgery or chemotherapy. These mechanisms promote a rare population of resistant tumor cells with properties of cancer stem-like cells (CSLS), which survive therapy and promote tumorigenesis, relapse, and metastasis (3, 4).

We often use natural products to develop drugs, scaffolds, and nanodrug delivery systems (NDDS) for biomedical applications and human clinical trials. Chitosan (CS) is the second most abundant polysaccharide after cellulose. CS is a biocompatible and biodegradable long copolymer of glucosamine and *N*-acetyl glucosamine as it breaks down into harmless and readily absorbed amino sugars (5). Alkaline deacetylation of chitin polysaccharides—ranging from 70% to 85%—produces CS with an average molecular weight of 3.8 to 500 kDa, and can be digested by lysozyme. CS is the only polysaccharide with a positive charge due to amine groups (5).

CS is widely studied for NDDS because of its biocompatibility, low cost, nontoxicity, low immunogenicity, and biodegradability. An added advantage of CS is functionalizability with multiple moieties and other polymers. Therefore, we can build multitasking platforms, including hybrid, theranostics, and multimodal systems for efficient cancer treatment (6, 7). Also, CS's poor solubility in aqueous solutions above pH 6 promoted the development of various CS derivatives with improved solubility over a broad pH range. As each derivative is functionalized with a specific moiety such as carboxyl, fluorinated, quaternized, glycosylated, methyl, and others, this modification has far broadened the many applications. The broad application has made a CS the biomaterial of choice for numerous purposes, especially for efficient drug delivery by crossing a variety of biological barriers and on-demand drug release to overcome the heterogeneous nature of solid tumors, with the capability to avoid cancer relapse by targeting residual tumor cells lingering after therapy/surgery (8).

In this review, we aim to highlight the potential of CS and its derivatives as a promising biomaterial to meet numerous biomedical demands, with a particular emphasis on its capability to build advanced enabling NDDS platforms to

cross multiple biological barriers, including blood, membrane, and TME-related obstacles and for the treatment of minimal residual disease (MRD) and recurrent cancer. To this end, we first looked into chitosan's inherent properties and its different derivatives. Then, we discussed other formats and implications of CS-derived NDDS for targeting and eliminating recurrence. Finally, we included an overview of the clinical translation of CS NPs for the treatment of recurrent cancer.

2 Chitosan: Inherent properties

Chitosan is a linear polysaccharide derived by the deacetylation of the *N*-acetyl glucosamine units of chitin, a natural polymer from crustacean shells, through hydrolysis at high temperatures under alkaline conditions. Chitosan is abundant in nature and possesses inherent properties that render it appealing to use as a drug delivery system. We will highlight the critical features of chitosan in the following section.

2.1 Antibacterial

Chitosan-based biomaterials possess superior antimicrobial and antifungal activity against clinically important antibiotic-resistant pathogens, such as *E. coli* and MERS. As a cationic agent, chitosan binds to negatively charged bacteria membrane and increases membrane permeability, resulting in leakage of intracellular components and, finally, cell death (9, 10). Notably, unlike tested antibiotics used in human and veterinary medicine, there was no observation for developing resistant mutants in serial passage assays over a long period of more than 15 days (11).

2.2 Biocompatibility, biodegradability, and pH responsiveness

pH changes can degrade chitosan NPs. Meanwhile, functionalization can increase CS stability. In this line, the pH responsiveness of CS allows for the formulation of biodegradable yet controlled and sustained release of cargoes. Thus, biodegradable static forms are synthesized through physical ionic gelation of CS using a polyanionic agent such as TPP (12). Meanwhile, a dynamic or non-biodegradable form of CS generated through chemical cross-linking allows for repeated and regenerative potential with controlled swelling and shrinkage performance of hydrogel in response to biochemical changes in their environment. The latter feature can be highly appreciated for tissue regeneration and treatment of chronic disease and can be formulated for systemic or local (drug depot) purposes (9).

2.3 Drug reservoir and controlled release/local treatment

Chitosan can be used as an efficient drug reservoir for the codelivery of various hydrophilic and hydrophobic cargoes. Complexation with nucleic acids such as miRNA, siRNA, plasmid DNA, and CpG ODN can be achieved by simple electrostatic adsorption (10). CS DDSs can accommodate different types of cargoes loaded, including natural, synthetic, and semi-synthetic vesicular particles such as niosomes, liposomes, and different cell types (CAR T cells, stem cells, dendrimers, gold NPs, photosensitizer agents, chemotherapeutic drugs, small-molecule drugs, and therapeutic antibodies/vaccines, among others) (13). Chitosan-based NPs are shown to offer controlled drug release upon the inherent pH responsiveness of CS or in response to internal (expression of specific marker) or external stimulators (NIR) (14, 15).

2.4 Multifunctionalization capability

Due to the presence of functional groups, including hydroxyl and amine, Cs modification is possible through chemical cross-linking with other hydrophilic/hydrophobic polymers, such as polyethylene glycol (PEG), polysaccharides, sugars, short peptides, antibodies, and other functional groups (16). The purpose of functionalization varies from PEGylation to improve CS NP stability, ligand moiety for targeted drug delivery (17), labeling with imaging agents (18), synthesis of self-assembled vesicular NPS (19), affording stimuli-responsive sol-gel transition (20), generating different derivatives of CS (21), to advanced hybrid and composite versions. At the same time, CS can be modified with different functional moieties to afford theranostics (imaging and therapy) (8).

2.5 Targeted therapy

A specific derivative of chitosan named oligosaccharide chitosan (OCS) can act as an analog of hyaluronic acid (HA), with binding specificity to CD44 ligands. Accordingly, as a targeting moiety, NP decorated with OCS is developed for $CD44^{+}$-overexpressing cells (22). Also, chitosan is shown to have an affinity for the MUC1 mucin adhesion molecule (CD227), a cell membrane glycoprotein, which is overexpressed in cancer cells such as glioma (23).

2.6 Transfecting agent: Gene delivery and endosomal escape

As the only positively charged polysaccharide due to the presence of amine groups in its structure, Cs DDSs possess several main advantages for gene therapy: (i) as to be complexed with negatively charged nucleic acids such as siRNA, shRNA, CRISPR-Cas9 mediated gene therapy, miRNA, CpG oligonucleotide adjuvants, and avoid their nuclease degradation; (ii) it acts as a transfecting agent, enabling cell-membrane adsorption and internalization of nucleic acid payloads; and (iii) it can withstand the proton sponge effect to escape the lysosome inside the target cells (tumor cells). Many advanced CS-based gene therapy approaches are designed to target and modulate a specific gene expression, silence oncogene gene expression, or upregulate a tumor suppressor gene expression (Figure 1). A review on chitosan-based gene delivery can be found in Ref (10).

Furthermore, transfecting ability and stability can be enhanced by the fabrication of CS-gold nanoparticles (AuNPs), as AuNPs are shown to be selectively internalized by tumor cells. Not to forget the effect of size and zeta potential in NP cellular uptake, the degree of PEGylation as a common NP stabilization and functionalization method to avoid "protein corona" formation can affect both size and charge of CS-based formulation as a transfecting agent. In this line, 5% PEG2000 Cs–AuNP displayed comparable transfecting potential to Lipofectamine 3000 with 75% gene knockdown. Using ELISA, the highest degree of protein c-MYC expression was achieved for Cs–AuNP with 2% PEG400 (~147 nm, −44.5 mV, 95%), >5% PEG400 (~154 nm, −33 mV, 90.5%), Cs–AuNP (~144 nm, −35 mV, 86.5%), 2% PEG2000 (~164 nm, −25.8 mV, 79.7%), and 5% PEG2000 (~171 nm, −25.5 mV, 75%) in a breast cancer cell model. This observation that PEGylation positively improved uptake of gold-CS nano complexes was irrespective of NP size and enabled efficient siRNA delivery compared to non-pegylated control (27). Among CS derivatives, N-acylated chitosan and chitosan oligosaccharide (CSO) are tested as plasmid DNA carriers complexed with AuNPs in cell culture (HEK-293). The transfection efficacy was validated by measurement of β-galactosidase activity and green fluorescence protein expression recorded at 27%, 33%, and 60% for chitosan, acylated chitosan, and CSO, with a TEM size of ~3.4, 4.6, and 7.3–15.6 nm, respectively, and positively charged zeta between 40 and 55 mV before complexation with plasmid DNA (28).

Other factors impacting siRNA delivery and its biodistribution involve chitosan molecular weight (~10 kDa for stability and knockdown), deacetylation degree and amine-to-phosphate (N:P) ratio, and increased surface charge (29). Taking advantage of pH-activated endolysosomal escape and drug release potential of chitosan, precise targeting of POLR2A using RNA interference (RNAi) is adopted as a therapeutic strategy for augmented cytosolic delivery of POLR2A siRNA for the treatment of human triple-negative breast cancer (TNBC) (30).

In a dual delivery system, folate-Cs-PEG nanoparticles were employed to encapsulate pRNA dimers, which simultaneously carry siRNA and aptamer, to selectively deliver it near or into target cells *via* aptamer-mediated endocytosis or proper particle size. Higher accumulation of siRNA in the tumor site, stronger tumor inhibition, and longer circulating time were also observed with CNPPs compared to other formulations *in vitro* and *in vivo*. Furthermore, pRNA hexamers can be designed to simultaneously carry six different substances (31).

The oral route is ideal for drug delivery as it is simple and allows multiple dosing if its bioavailability is not affected by gastrointestinal (GI) environments and nonspecific biological trafficking. Inspired by the enterohepatic recycling of bile acids, taurocholic acid (TCA) was coated on the surface of oral NPs to quarantine siRNA protection from GI degradation and facilitate colorectal liver metastases (CLM) targeting through the enterohepatic recycling process. An orally redox-responsive AuNP-thiolated siRNA-glycol Cs-taurocholic acid nanoparticle (AR-GT NPs) was developed in which Akt2 siRNA composed of dual padlocked nonviral vectors is conjugated with AuNPs and then covered by bifunctional glycol Cs-taurocholic acid through a charge-to-charge interaction. Three NPs were produced with different 50 and 100 AR : GT ratio complexation as AR-chitosan, AR-GT50, and AR-GT100 with mean diameters of 59 ± 10, 100 ± 3, and 115 ± 2 nm, respectively, with zeta potential values of AR-GT50 and ARGT100 of 29 ± 1 and 4 ± 1 mV. Among these, AR-GT100 was the most promising platform. It could selectively deliver siRNA to suppress AKT signaling, facilitate active transport through enterocytes, and enhance selective accumulation and inhibition of colorectal liver metastases (Figure 1A) (24). Another interesting study targeted 17q23 amplicon using a systemically delivered RNA-laden chitosan-based NPs capable of codelivery of GSK2830371 (WIP1 inhibitor), and antagomiR21 is reported to overcome the resistance to anti-HER2 therapy in the HER2+ breast cancer model. The core–shell NP with a diameter of 115 ± 9.7 nm was synthesized by a double-emulsion water-in-oil-in-water method, in which anti-miR21 inhibitor and pluronic F127 (PF127)-CG-CO2 were encapsulated in the inner water phase making an NP core. The shell structure contained hydrophobic GSK2830371 together with poly(d,l-lactide-co-glycolide) (PLGA) and 1,2-dipalmitoyl-sn-glycerol-3-phosphocholine (DPPC) dissolved in the oil phase. CS modification with the guanidine group (CG-CO_2) formed chitosan-guanidine (CG) that reversibly reacts with carbon to produce carbon dioxide gas affording the nanobomb effect. More specifically, endocytosis-mediated uptake of the nanoparticles could generate CO_2 to break open endo/lysosomes. This formulation protected antagomiR21 serum nuclease degradation up to 36 h and resulted in more than 95% tumor growth inhibition with significant efficacy on Her-resistant primary and metastatic tumors (Figure 1B) (25).

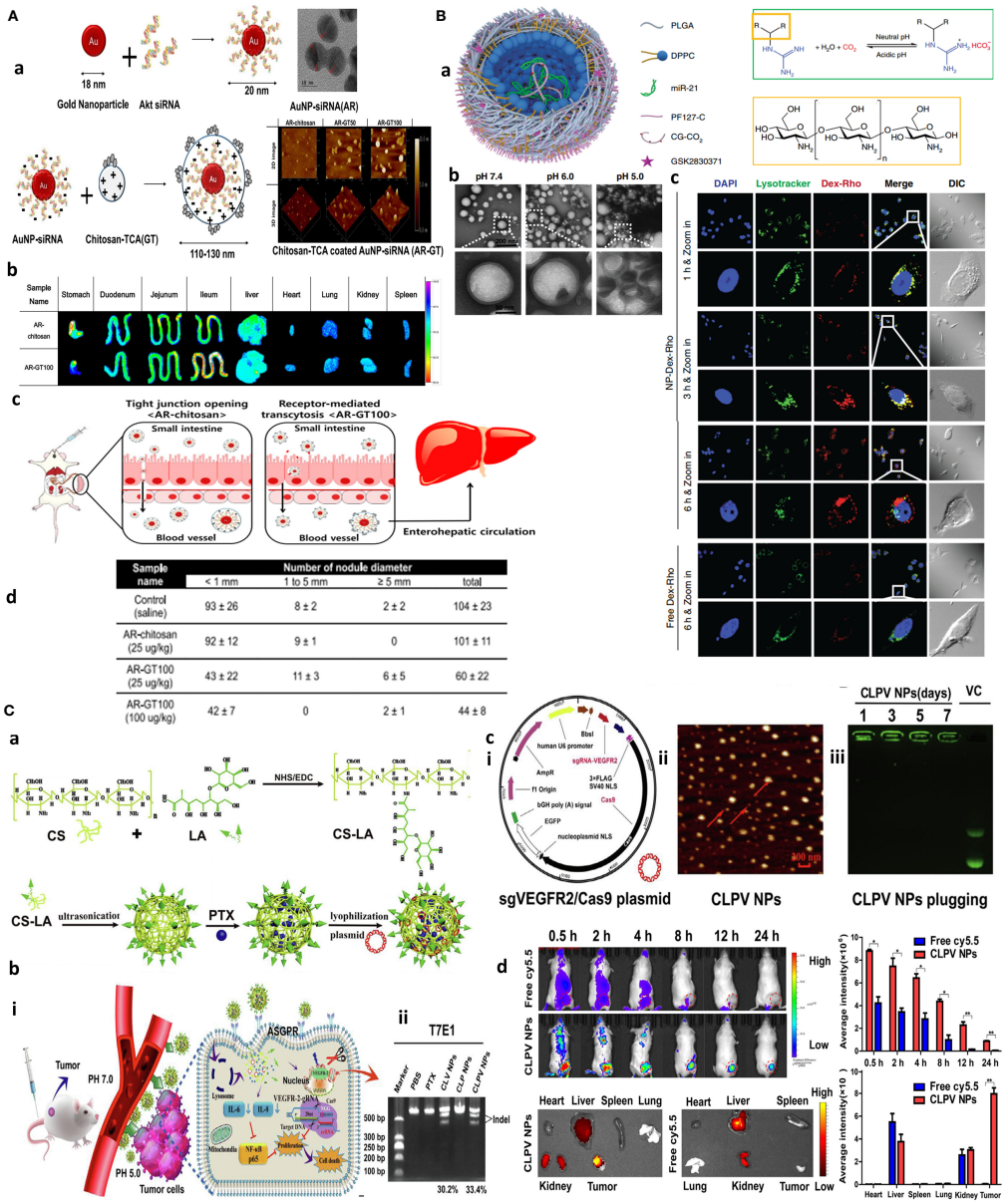

FIGURE 1
Chitosan NPs afford effective gene therapy and endo/lysosomal escape. **(A)** Bioinspired glycol chitosan NPs for GI passing and endosomal escape delivery of oral siRNA for successful treatment of CLM. **(a)** Synthesis and characterization of AR-GT NPs. **(b)** Ex *vivo* fluorescence images of major organs of the AR-coated chitosan and glycol chitosan (GC)-coated NPs in treated animals for 30 min. **(c)** In vivo mechanism of AR-GT100 transport, which is designed to occur through transcytosis, inspired from enterocytic-mediated recycling of amphipathic fatty acid bilirubin, with specific accumulation in the ileum. For chitosan, this occurs through tight junctions. **(d)** Therapeutic efficacy in a CLM cancer mouse model after oral delivery of AR-chitosan and AR-GT100 (25 or 100 μg/kg) and CLM lung antimetastatic potential. Reprinted with permission from (24), Copyright (2017), American Chemical Society. **(B)** Chitosan NPs for precisely targeting POLR2A as a therapeutic strategy for human triple-negative breast cancer. **(a)** Scheme for NP synthesis. **(b)** TEM images showing pH-responsive NPs and nanobomb effect that occur under low pH 5.0–6.0 endolysosomes, leading to NP enlargement and cracking. At the same time, spherical core–shell NPs are intact under pH 7.4. **(c)** Endosomal escape of Dextran-Rhodamine (Dex-Rho) NPs. In early hours, the red color largely overlapped with LysoTracker green fluorescence. After 6 h, this overlap is minimum, indicating successful endosomal escape of core–shell chitosan-loaded anti-Mir21 due to the nanobomb effect. Reprinted from (25) Under Creative commons Attribution License 4.0, Copyright (2018) Springer Nature. **(C)** pH-responsive chitosan-based nanocomplex for efficient CRISPR/Cas9 gene-chemo synergistic HCC therapy. **(a)** Schematics of preparation and characterizations of CLPV NPs. **(b)** (i) Working principle of CLPV NPs for precise targeting of VEGFR2 and downstream tumorigenic pathways IL-6/IL-8-NF-κB p65; (ii) T7E1 analysis of the VEGFR2 sgRNA sites on tumor tissues. **(c)** (i) Plasmid profile of recombinant sgVEGFR2/Cas9 (VC); (ii) AFM image of 238.2-nm CLPV NPs; (iii) agarose gel electrophoresis analysis for VC stability on NPs. **(d)** *In vivo* biodistribution studies using injected free cy5.5 and cy5.5-loaded CLPV NPs recorded at different time points from the major organs and tumor tissues. Reprinted with permission from (26), Copyright (2018) Elsevier.

The clustered regularly interspaced short palindromic repeat (CRISPR)-associated Cas9 nuclease system (CRISPR/Cas9) has become a powerful tool for genome editing and gene knockout with better targeting effect than siRNA; however, its targeted delivery is challenging. To this, a β-galactose-carrying lactobionic acid (LA) functionalized pH-responsive chitosan-based nanocomplex is designed for combined gene chemotherapy by codelivery of sgVEGFR2/Cas9 plasmid and paclitaxel for hepatocellular carcinoma (HCC) therapy. LA was used to specifically deliver spherical CLPV NPs to asialoglycoprotein receptors (ASGPR) overexpressing HepG2 cells. Genome editing efficiency was 38.6% and 33.4% in difficult-to-transfect HepG2 cells *in vitro* and in tumor tissues *in vivo*, respectively, with more than 60% reduction in VEGFR2 protein expression and 70% tumor growth suppression in mice (Figure 1C) (26).

2.7 Immune-adjuvant

Chitosan deacetylation (DAc) of ≤17% and its high molecular weight and specific derivatives (*N*,*N*,*N*-trimethyl chitosan) are shown to elicit better immune-activating potential (32, 33).

Immune-adjuvants can increase vaccine efficacy by modeling the quality (type of immune response) and the host immune response quantity (rate and magnitude). Conventional adjuvants such as cytokines, toll-like receptor (TLR) agonist (CpG ODN), and aluminum salt stimulate the immune system. A good adjuvant, though, should be applicable for both systemic and local administration, safe, effective, low-cost, and capable of crossing physiological (mucosal/blood) barriers and immune targeting, all of which can be provided by chitosan (33). For example, a catalytic mucosal adjuvant strategy for an influenza WIV nasal vaccine based on CS functionalized iron oxide nanozyme (CS-IONzyme) is developed. CS modification not only increases antigen adhesion to nasal mucosa by 30-fold compared to H1N1 WIV alone; it also increased catalase-like activity of iron NPs for reactive oxygen species (ROS)-dependent dendritic cell (DC) maturation. This enhanced H1N1 WIV-loaded DCs migration into the draining lymph nodes for antigen presentation, resulting in 8.9-fold increase of IgA-mucosal adaptive immunity in mice and a 100% protection against influenza, compared to 30% protection by H1N1 WIV alone (34).

2.8 Mucoadhesion

Chitosan is shown to possess mucoadhesive properties, as it shows an affinity for the MUC1 adhesion molecule (CD227), a cell membrane glycoprotein, overexpressed by tumor cells. This property of chitosan is used for targeted oral delivery, as well as packaging and guiding of other small NPs, such as niosome-encapsulated paclitaxel conjugated with BODIPY 564/570. Accordingly, thermo-sensitive cross-linked chitosan hydrogel as a double package nanodelivery system was adopted for local, sustained, and timely burst release of niosomes upon targeting MUC1 mucin surface antigen overexpressing tumor cells (Figure 2C) (23). Also, chitosan-encapsulated niosomes are used for enhanced oral delivery of atorvastatin to hyperlipidemic mice. Chitosan encapsulation resulted in lower NP size, with 96.9 nm compared with 143.2 nm for unencapsulated niosomes (35).

2.9 Multitasking performance: Multimodal systems, theranostics, and combination therapy

Besides surface functionalization, chitosan NPs can afford simultaneous delivery of various payloads to form multifunctional NPs including theranostics (therapeutic and imaging agent) and multimodal or combination therapy employing more than one drug/strategy for a synergistic effect to overcome multidrug resistance (MDR).

2.9.1 Multimodal/combination systems for reversing MDR

As an example of multimodal system, CS NPs are used for encapsulating both photothermal (IR780) and photodynamic [5-aminolevulinic acid (5-ALA)] reagents for photothermally enhanced photodynamic therapy (5-ALA&IR780@CS NPs) for oral delivery and local treatment of CT-26 colon tumors in mice (Figure 3A) (36). Moreover, as a local delivery platform (tumor skin-inserted), microneedle (MN) array is attempted for cancer chemo- and photothermal combination therapy, in which micromolding and electrospraying techniques were used to produce layer-by-layer MN patches with polyvinylpyrrolidone (PVP) as the base of the needle. CS-DOX as an internal layer and polyvinyl alcohol (PVA) gold-silica nanorods (AuMSS) as external layers were deposited on the surface of the PVP MNs through the electrospraying procedure. MNs promoted the sequential delivery of doxorubicin and AuMSS in response to pH (chitosan) and photothermal stimuli (Figure 3B) (37).

Moreover, multifunctional chitosan NPs involving DOX-loaded chitosan-capped gold nanoparticles (CS-GNPs) are used for chemo-radiotherapy of MCF-7 breast cancer cells (39). Likewise, targeted cetuximab chitosan nanoparticles (Cet-CTS NPs) are used to deliver Quercetin (QUE) and paclitaxel (PTX) using an ionic cross-linking method. This formulation significantly decreased tumor growth in PTX-resistant xenografts (40). Given the highly promising results achieved with glycol chitosan (GC) for resistant cancer therapy, one study reported GC NP encapsulation of both chemotherapeutics (DOX) and siRNA (BCL-2) to achieve maximal efficacy to

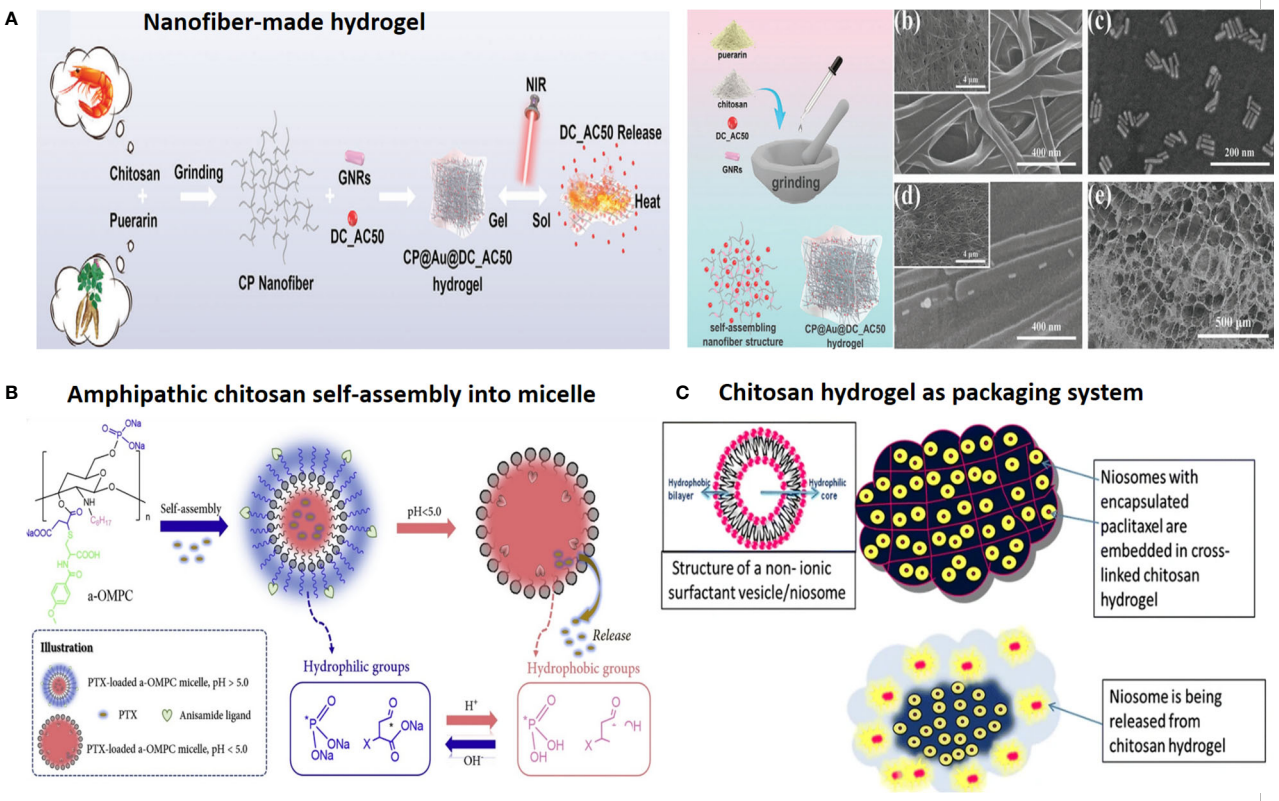

FIGURE 2
Chitosan-based drug delivery systems for cancer targeting. **(A)** Nanofiber-based chitosan hydrogel as injectable drug depot. Reprinted from (65) under Creative Commons Attribution License 4.0, Copyright (2021) Wiley-VCH GmbH. **(B)** Amphipathic chitosan can self-assemble into vesicular core–shell particles. Reprinted with permission from (66), Copyright (2021) Elsevier. **(C)** Chitosan hydrogel as a packaging system for other NPs (niosome in hydrogel). Reprinted from (23) under Creative Commons Attribution License 4.0, Copyright (2020) Springer Nature.

overcome MDR (41). Likewise, self-assembly of chitosan/vitamin E conjugate into micelle is used to entrap oxaliplatin (OXPt) to overcome conventional OXPt-mediated drug resistance/nephrotoxicity in breast cancer (42). Also, folic acid-functionalized chitosan nanocarrier is developed for codelivery of DOX and oleanolic acid (OA), to form a copolymer with self-assembly into 180-nm NPs in water. These pH-responsive FA-CS-g-OA@DOX NPs exhibit apoptosis-enhancing and antiproliferative capacities on MDR breast tumors *in vivo*, by sensitizing MDA-MB-231 cancer cells to DOX and mitigating DOX toxicity to healthy tissues (43). Furthermore, chemosensitizing NPs based on amphiphilic oligosaccharide CS-DOX–indomethacin conjugate are used for surmounting the efflux of cellular uptaken DOX *via* MDR-associated protein (MRP) in a lung tumor-xenografted mouse model (44).

2.9.2 Theranostics (imaging-guided therapy)

Palladium, as a near-infrared plasmonic material alternative to gold NPs, was used for photo-based imaging and therapy owing to its near-infrared (NIR) heat generation potential for photothermal therapy (PTT) and generation of satisfactory photoacoustic signals for ultrasound imaging (45). The RGD peptide-functionalized oligosaccharide chitosan was coated on the surface of palladium nanoparticles (Pd@COS-RGD) to make biocompatible NPs acting as theranostics. Similar work adopted DOX-loaded hollow mesoporous silica nanoparticles (HMSNs) coated with chitosan-copper sulfide nanodots (HMSNs-CS-DOX@CuS), a theranostic, multimodal, and combination platform by merging chemotherapy and PTT into a single formulation. CuS dots are used to plug HMSN pores to avoid burst release of DOX into the systemic circulation, unless S–S bonds connecting the CuS dots to the HMSNs are selectively cleaved under the reducing microenvironment of the tumor, permitting targeted drug release. This system was capable of combinatorial chemotherapy and PTT, and multimodal thermal/photoacoustic imaging due to the incorporation of CuS nanodots for efficiently targeted tumor imaging and therapy (Figure 3C) (38). Also, self-assembly of amphipathic photosensitizer tetraphenyl chlorin (TPC)-chitosan (PS-CS)

conjugate polymers into micellar nanoparticles in aqueous buffers are used for delivery of lipophilic drugs mertansine (MRT) or cabazitaxel (CBZ) for chemotherapy and PDT therapy of ferroptosis-resistant MCF-7 cells, with potential to be utilized as contrast agents (46).

3 Chitosan derivatives: Synthesis procedure

Despite the superior physicochemical as well as biological features of chitosan, the most significant drawback of this semi-synthetic biopolymer is the lack of solubility at pH values above its pKa (pH ~5.5–6.5), owing to the formation of interchain and intrachain hydrogen bonding between the hydroxyl and amine functionalities (16). The most important strategy for circumvention of this problem is chemical modification of chitosan through its hydroxyl or amine side groups. In this context, the popular methods used are *N*-substitution, *O*-substitution, *N*,*O*-substitution, chelation of metals, dendrimer attaching, fluorination, oxidation (e.g., with 2,2,6,6-tetramethyl-1-piperidinyloxy; TEMPO), depolymerization of chitosan to afford chitooligosaccharides (COS) *via* acid chitosanolysis, sulfonation, and polymer grafting (5). These modifications significantly improve its mechanical and thermal stability, acidic pH tolerance, and hydrophilicity, and can be used for controlling the interactions between chitosan and other elements, including drugs, metal ions, and organic compounds. The *N*- and *O*-substitution approaches are the most commonly used strategies toward chitosan derivatives (47).

In *N*-substitution, the amino group (-NH_2) of chitosan reacts with various reactive reagents to afford chitosan derivatives. The most important approaches for the *N*-substitution of chitosan are quaternization, *N*-alkylation, and *N*-arylation with aldehydes through "Schiff-Base" reaction followed by the reduction of the formed imine group to the more stable amine group, epoxy, and reactive halide derivatives, and *N*-acylation with anhydride and acid halides (Figure 4) (45, 48).

O-substitution of chitosan is another efficient approach for improving the physicochemical properties of chitosan that regularly requires the protection/deprotection of its amino groups owing to the higher reactivity of amino groups than those of the hydroxyl groups. The most commonly used approaches toward *O*-substituted chitosan are illustrated in Figure 5 (48, 49).

Amidation with coupling catalysts [e.g., *N*-(3-dimethylaminopropyl-*N*-ethylcar-bodiimide) hydrochloride (EDC)/*N*-hydroxysuccinimide (NHS)] is another important approach for functionalization of chitosan using its amino group. This approach can be used for fluorination as well as conjugation of bioactive small molecules or macromolecules (e.g., folic acid and RGD peptide) (50). Finally, polymer grafting can be considered an efficient strategy for modified chitosan with tunable physicochemical and biological properties.

This polymerization technique is one of the most exploited approaches toward chitosan graft copolymers. The grafting process can be achieved through ceric-initiated and Fenton's free radical graft copolymerization that is used for vinyl monomer grafting, cyclic monomer grafting *via* ring-opening copolymerization, post-grafting *via* various coupling agents (e.g., click chemistry, EDC/NHS, and nucleophilic reactions), and reversible deactivation radical polymerization (RDRP; also famous as controlled or "living" radical polymerization) approach (51). The RDRP technique is categorized as atom transfer radical polymerization (ATRP), nitroxide-mediated polymerization (NMP), and reversible addition-fragmentation chain transfer (RAFT) polymerization that allows the synthesis of well-defined macromolecular architectures with relatively low dispersity (52–54).

4 Chitosan derivatives: Formats and features

Herein, we aim to overview different formats and applications of most important chitosan derivatives for cancer therapy.

4.1 Glycol chitosan: Targeting tumor heterogeneity and lymph node trafficking

GC is a chitosan derivative with much better solubility as it is conjugated with hydrophilic ethylene glycol branches. This modification renders GC soluble in neutral/acidic pH, while the amine groups of GC remain unaffected for further modification/functionalization. The molecular weight of GC (20 to 250 kDa) and the degree of deacetylation (60% to 82.7%) affect GC's physicochemical and biological properties. Among Cs derivatives, GC is a well-known nanoparticle for cancer therapy, particularly for cancer heterogeneity (5). Moreover, cationic particles are known to promote trafficking and retention of therapeutic payloads in lymph nodes. For example, a dendrimer-based icluster nanobomb is shown to specifically inhibit lymph node metastasis, after size changes in the primary tumor site (~100 nm to ~5 nm) wherein resultant small NPs promoted particle intravasation into tumor lymphatics and migration into LNs, and complete tumor remission in 4 out of the 10 mice for 110 days (55). Meanwhile, GC-based theranostics, such as glycol-chitosan-coated gold nanoparticles (GC-AuNPs), are employed for a photoacoustic contrast agent imaging of lymph nodes without the need for targeting moiety/surface modification and are capable of tumor antigen delivery to macrophages to present the model ovalbumin (OVA) epitope at targeted lymph nodes for cancer immunotherapy (56).

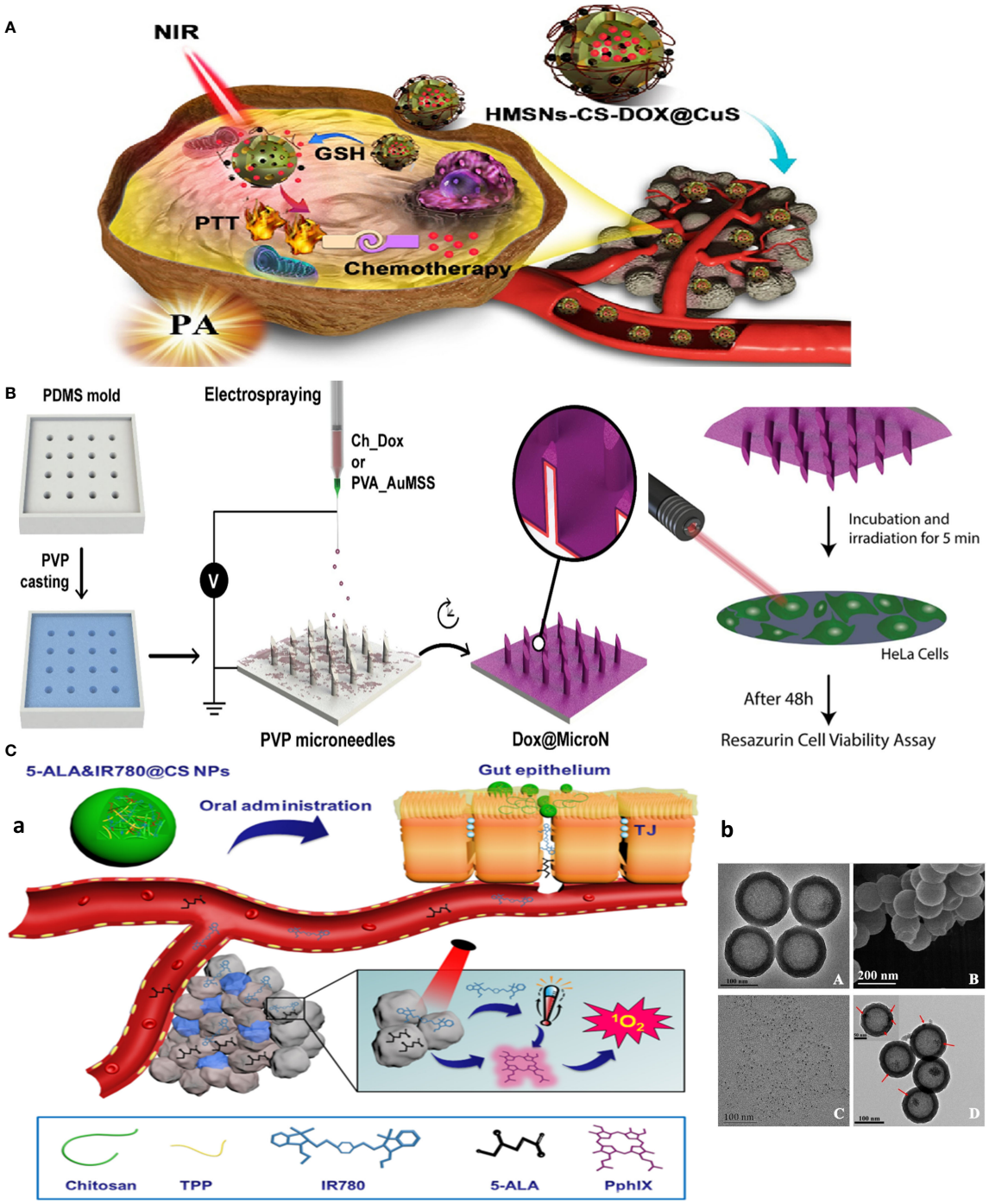

FIGURE 3
Chitosan-based multitasking drug delivery systems for treatment of MDR cancer. **(A)** Chitosan-based multimodal system for PTT-enhanced PDT therapy. Reprinted with permission from (36), Copyright (2020) Elsevier. **(B)** Chitosan MN patches for combined chemo-PTT cancer therapy. Reprinted with permission from (37), Copyright (2020) Elsevier. **(C)** Chitosan-based theranostics for thermal-photoacoustic (PA) imaging-guided tumor chemo-PTT therapy. **(a)** Schematic of NP working design. **(b)** Electron microscopy images: **(A)** TEM and **(B)** SEM images of HMSNs. TEM image of **(C)** CuS nanodots **(D)** and HMSNs-CS-DOX@CuS. Red arrows indicate the CuS nanodots on the HMSN surfaces. Reprinted with permission from (38), Copyright (2021) Elsevier.

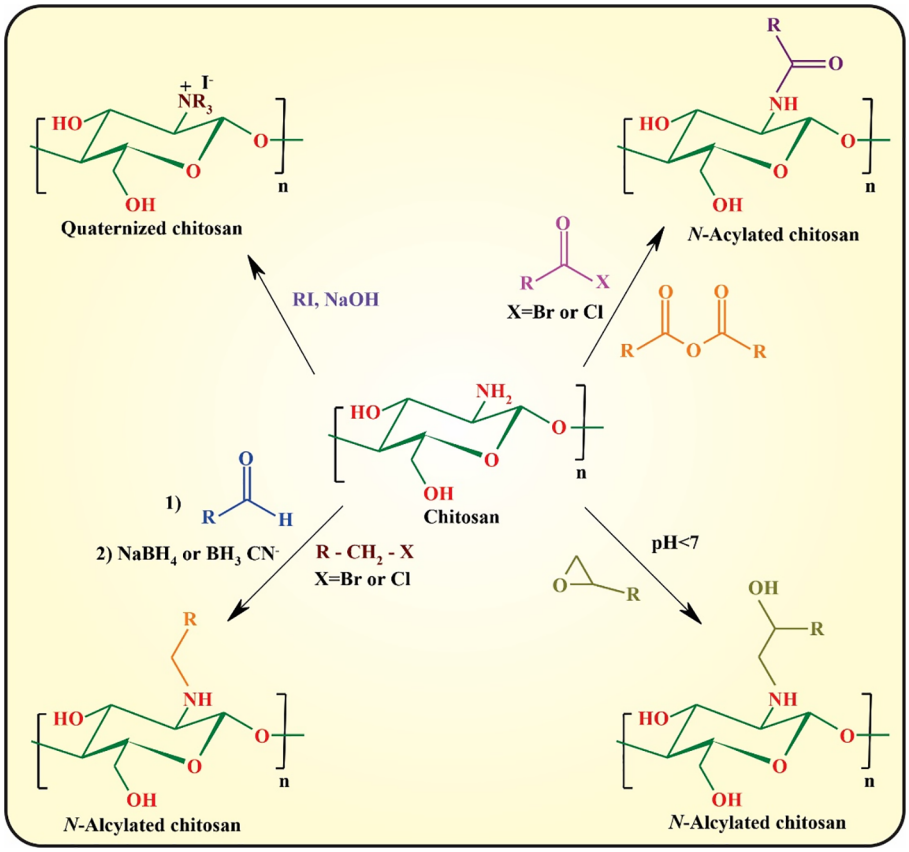

FIGURE 4
N-substitution of chitosan by different approaches.

4.2 Fluorinated chitosan: Mucoadhesion/forming stealth NPs

As an additional modification, fluorination of functional drug delivery system materials can result in satisfactory performances such as improved stability, resisting protein adsorption, and enhancing cell membrane permeability. In this regard, fluorinated chitosan is used for enhanced transmucosal delivery of different cargoes such as catalase or chemotherapy agents (57, 58). Fluorination can form stealth NPs to avoid protein corona, reduce RES capture, and improve drug accumulation in tumor sites (59).

4.3 Oligosaccharide chitosan: Anticancer and cell-specific targeting

CSOs, which are obtained from chitosan degradation, possess some interesting molecular weight-dependent biological properties, especially anticancer activity (60). CSO has a low molecular weight, is water-soluble, and acts as a specific HA analog. CSO-decorated NPs can be used for CD44-overexpressing cancer tumor cells, such as TNBC cells (22).

4.4 Carboxylated chitosan: Functionalization, pH responsiveness, drug release, and endo/lysosomal escape

Chitosan possesses a positive charge; however, sometimes a negative charge is desirable to achieve additional features. Such carboxylated chitosan is used to improve the efficacy of mesoporous silica nanoparticles for targeted drug delivery of HER2-overexpressing breast cancer. This involved chitosan-coated, DOX-loaded anti-EGFR/HER2 aptamer-mesoporous silica nanoparticle (MSN) bioconjugates. Partially carboxylated chitosan as coating imparted pH responsiveness and greater DOX release in a shorter time, endo/lysosomal escape ability to MSN delivery for cytosolic delivery of DOX, and conjugation targeting agents (aptamer) for active targeting (61). Also, genistein ($C_{15}H_{10}O_5$), a soy isoflavone and superparamagnetic

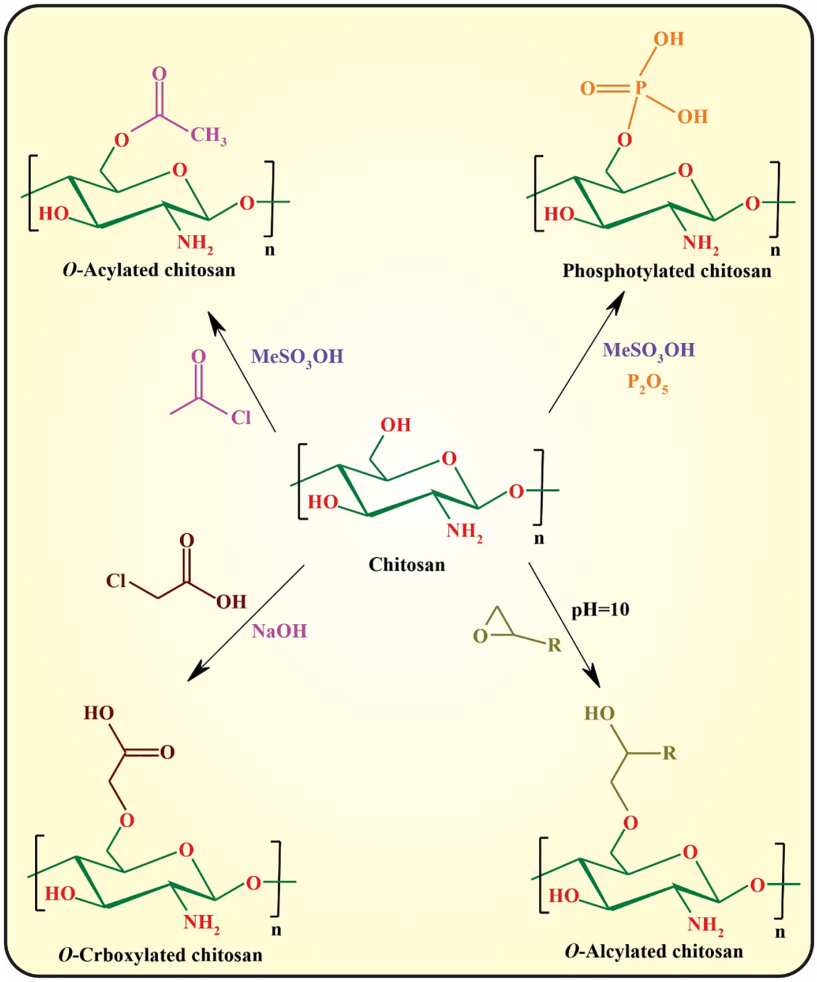

FIGURE 5
N-substitution of chitosan by different approaches.

Fe_3O_4 decorated with bio-compatible carboxymethylated chitosan, is used to target acute leukemia lymphoma (62).

4.5 Quaternized: Antimicrobial and tissue regeneration

Though the antimicrobial activity of chitosan is affected by pH, molecular weight, and the presence of interfering substances like lipids and proteins, CS modification such as succinoylated, hydrophobic, sulfonated, sulfonamidated, and in particular quaternary can enhance its antimicrobial performance (30). Quaternized chitosan (QCS), is a water-soluble chitosan derivative with good biocompatibility and enhanced antibacterial effects. Due to the presence of positively charged cations in its amino and quaternary amine groups, QCS possesses strong tissue adhesive properties and can induce tissue repair, hemostasis, and regeneration. In addition, quaternized aminated chitosan (Q-AmCs) derivative is used for the efficient encapsulation and slow release of the therapeutic drugs (21).

4.6 Cathecholic CS: Wet adhesion and hemostatic

Inspired by the super adhesion performance of mussel to rocks owing to the specific amino acid content of its adhesive proteins Mfp-3 and Mfp-5, namely, catecholic amino acid (3,4-dihy-droxyphenylalanine, DOPA) and L-lysine (63), catechol groups are used in the fabrication of Cs possessing super adhesion potential under wet conditions, such as surgical trauma and internal bleeding.

4.7 Sulfated: Angiogenesis inhibitor

Chitosan sulfate inhibits angiogenesis *via* blocking the VEGF/VEGFR2 pathway and suppresses tumor growth *in vivo*. Heparinoid chitosan sulfate inhibits neovascularization much higher than heparin control (63.8% *vs*. 30.7%) and possesses anticoagulant activity *in vivo* (64).

4.8 Amphiphilic: Self-assembled NPs

Chitosan-based drug delivery systems can be prepared using different methods such as chemical or ionic gelation, mini-emulsion, spray-drying, and coacervation/precipitation methods. An alternative to these is self-assembly, a spontaneous process for easy making of organized structures with particular functions, achieved by amphiphilic chitosan derivates (19).

For example, anisamide-conjugated *N*-octyl-*N*,*O*-maleoyl-*O*-phosphoryl chitosan (a-OMPC) amphiphilic micelles featuring pH-responsive release and high affinity to sigma-1 receptor-overexpressed tumors are developed for paclitaxel (PTX) delivery. Maleoyl functionalization of chitosan has several advantages: (i) improved chitosan solubility in organic system, (ii) endo/lysosomal pH-responsive drug release due to conversion from phosphate/carboxylate to hydrophobic phosphoric acid/carboxylic acid, (iii) and providing α,β-unsaturated ketone double bond for anisamide conjugation, to afford chitosan a high affinity to bind sigma-1 receptor overexpressed on the surface of prostate cancer (PCa) cells (Figure 2B) (66).

Pluronic is an amphiphilic tri-block copolymer composed of poly(ethylene oxide) (PEO) and poly(propylene oxide) (PPO) and can form micelles for delivery of both hydrophobic and hydrophilic drugs within the hydrophilic PEO and hydrophobic PPO blocks forming the corona and the core of the micelles, respectively. To overcome the instability of polymeric micelles made of pluronic®F127 (PF), the pluronic-chitosan copolymer is exploited. Aptamer-modified pluronic®F127 and chitosan are used to enhance PTX loading capacity and increase micelle stability (86.22 ± 1.45 nm) (67). Likewise, owing to the temperature-responsive potential of pluronic, the poloxamer 407-chitosan copolymer is used to develop thermoresponsive hydrogels as drug depots and single-shot vaccines capable of synchronous and sustained release of lactic-co-glycolic acid (PLGA) nanoparticles loaded with antigen and adjuvants. This chitosan hydrogel vaccine induced strong, long-lasting, humoral cellular responses in the murine melanoma model (68).

5 Types of chitosan nanoparticles

Chitosan and its derivatives can be formulated into different types of NDDSs; the most popular forms include hydrogel, vesicles, nanoparticles, and composite/hybrid ones (Figure 2).

Through ionic or chemical gelation, CSO can form 3D cross-linked/entangled hydrophilic networks, known as hydrogels. Under their LCST, hydrogel can adopt state transition from gelation (gel) to solution (sol) and *vice versa*. Another classification is based on the hydrogel route of administration, to be used as drug depot (injectable/sprayed hydrogel), systemic delivery (nanogel with size <200 nm), or microgel (bulk gel), which comes in different forms such as fiber, cryogel, sponge, film, patch, and glue with the application as wound dressing or scaffold. The sol-gel transition capability is important for the formulation of injectable hydrogels, upon injection into the tissue site, where gelation and local entrapping of cargo occur. Thus, it serves as a drug depot for long-lasting release. Chitosan can also be cross-linked with hydrophobic moieties, to form amphipathic copolymers that can self-assemble into vesicular particles such as micelles and liposomes. Also, CS NPs alone or complexed with other materials/NPs (e.g., chitosan-dendrimer) and polysaccharides (e.g., chitosan-alginate) form composite or hybrid NPs. This capability further extends and advances CS application into a single all-in-one robust platform with multitasking potential for imaging, therapeutic, and prevention of recurrent disease in a controlled manner.

6 Tumor-penetrating chitosan NPs cross biological and microenvironmental barriers

Considering the solid TME, various physiological barriers exist in the way CS NPs advance toward the tumor parenchyma. In this section, we aim to introduce these critical barriers and formats of CS-based drug delivery systems that take advantage of CS inherent properties to build effective therapeutics to fight recurrent cancer and MRD.

6.1 Blood barrier

The first barrier for systemically injected CS NPs is the formation of a protein corona, which results in the clearance of NP by the phagocytic system and diminished circulation time of NP. This barrier can be tackled by using protein corona repelling approaches, using dysponins such as PEGylation, BSA coating, protein corona formation, and cell-derived camouflaged membranes. Concerning CS, mucoadhesive properties and its cationic charge act as a double sword: it affords adsorption-mediated cross-linking through cell membrane; in the same way, it could also possess high fouling properties to bind with serum-abundant proteins such as albumin, complement proteins, immunoglobulins, and, thus, phagocytosis (69). Meanwhile, as discussed before, the fluorinated form of CS can possess repelling properties and act as stealth coating (59). A recent

paper detailed these strategies implemented to increase the stability of systemically administered chitosan nanoparticles. Besides PEG, different coating materials, using polysaccharides, chitosan derivatives, stealth chitosan, and zwitterionic chitosan plus their advantages and disadvantages are also discussed (69).

6.2 Membrane/stroma barriers

After the protein corona is tackled, NP must cross biological barriers to penetrate tumor cells. These include crossing the vascular wall (intravasation), then dense ECM and stroma cells (convection) and finally tumor cell membrane (internalization). The first one, vascular wall, is for systemically injected NPs, while the rest are common between locally and systemically injected NPs, as for CS-based DDSs. These barriers can be targeted using active/passive targeting, multi-stage acting NPs, nanosweepers, and Trojan systems discussed in the next section.

6.2.1 Ligand and ligand-independent delivery

Unlike what has been accepted for a long time, that enhanced permeation and retention (EPR) is the main inactive route for targeted delivery of NPs to solid tumors, recent meta-analysis data contradicted this fact as it indicated that only a mean of 1.48% of the injected dose (%ID) of NPs is delivered to cancer cells (70). Vascular permeability determines NP localization in tumor lesions. A higher NP accumulation, besides EPR, needs an active targeting by using ligand-decorated NPs to enjoy the transcytosis mechanism to promote both intravasation and internalization of NPs.

Different ligands can be used to achieve this; however, a ligand of choice is the one that is expressed abundantly by both tumor and tumor-associated endothelial cells, enabling a DDSs to tackle several barriers using a single targeting moiety, here, vascular wall and tumor cell membrane internalization (71). Examples include NGR, which targets CD13 expressed by both tumor and endothelial cells (72). Likewise, the cell-penetrating peptide iRGD containing the CendR sequence can first target integrin receptor to cross the blood–brain barrier and then provides the second moiety to bind Neuropilin-1 (NRP-1) and Neuropilin-2 (NRP-2) for crossing the brain–tumor barrier (73). Lactoferrin receptor (LfR) is another example with dual expression on tumor and endothelial cells for glioma therapy (71). Chitosan micelles incorporating Telmisartan can sequentially target overexpressed angiotensin II type I receptor (AT_1R) on CAFs and tumor cells (74). Bispecific antibodies can also provide dual-targeting ability of NPs using a single formulation (75). Other approaches employ a single receptor either for tumor cell or endothelial cells targeting combined with stimuli responsiveness behavior (multi-stage NPs), or polyplexes/cationic particles [such as chitosan, dendrimer, and polyethyleneimine (PEI)], cationic cell-penetrating peptides (CPP), and cationic lipids to afford adsorption-mediated internalization.

As both OCS and HA show affinity to selectively bind CD44-expressing cells, self-cross-linkable chitosan-HA dialdehyde nanoparticles are used for CD44-targeted siRNA delivery to target oncogene Bcl2 for bladder cancer therapy (76). Likewise, the HA-CS nanocomposite can be used for the generation of polyionic nano-complexes, which affords CD44-mediated active delivery of both positively charged (DOX) and negatively charged (mir-34-a) cargoes for the treatment of MDA-MB-231 breast cancer cells (77).

Besides affording ligand-mediated endocytosis, cyclic RGD (cRGD) can possess antiangiogenic and antimetastatic potential by inhibiting αvβ3 integrin receptors (78). For one, cRGD-decorated chitosan NPs are used for encapsulating chemotherapeutic drug raloxifene, while free amines of chitosan afforded NP stability under low pH of TME and realized active targeted delivery to selectively suppress angiogenesis and tumor growth in breast cancer (79).

In another formulation, targeted delivery is afforded using ligand-based delivery coupled with microenvironment-responsive properties. A chitosan-based cascade–responsive nanoplatform is developed for TNBC therapy involving dual pH/thermosensitive poly(N-vinylcaprolactam) (PNVCL)-CS copolymer modified with the CPP (CPP-CS-co-PNVCL NPs) and loaded with DOX. Core–shell self-assembly of amphipathic 200-nm NPs with DOX entrapped in the hydrophobic core occurs due to amphiphilic block copolymers. Upon systemic injection, NPs are intact while reaching the tumor site, and the bond between CPP and CS is degraded by matrix metalloproteinase enzymes. *In vivo* experiments employing a TNB xenograft mouse model demonstrated a significant reduction in tumor volume and life span, with no obvious systemic toxicity (Figure 6A) (15).

On the other hand, as discussed earlier, Cs, particularly its fluorinated derivative (FC), can be used for enhanced mucoadhesion of NPs and deep tumor cell penetration by coupling FC to sonosensitizer-conjugated catalase post-intravesical instillation. FC but not CS can open tight bladder epithelium junctions by reversible modulating transepithelial electrical resistance (TEER) (57). Likewise, FC is coupled to copper selenide nanoparticles for NIR-triggered (Figure 6B) (80) as well as photo-activated H2 generation using a catalyst [FeFe] TPP for hydrogen-chemotherapy (gemcitabin) of bladder cancer (58).

6.2.2 Charge/size-shifting NPs

As discussed before, chitosan and its derivatives, as a cationic biomaterial with mucoadhesive potential, afford a ligand-independent yet active delivery platform to cross and transport across cellular membranes and successive endocytosis.

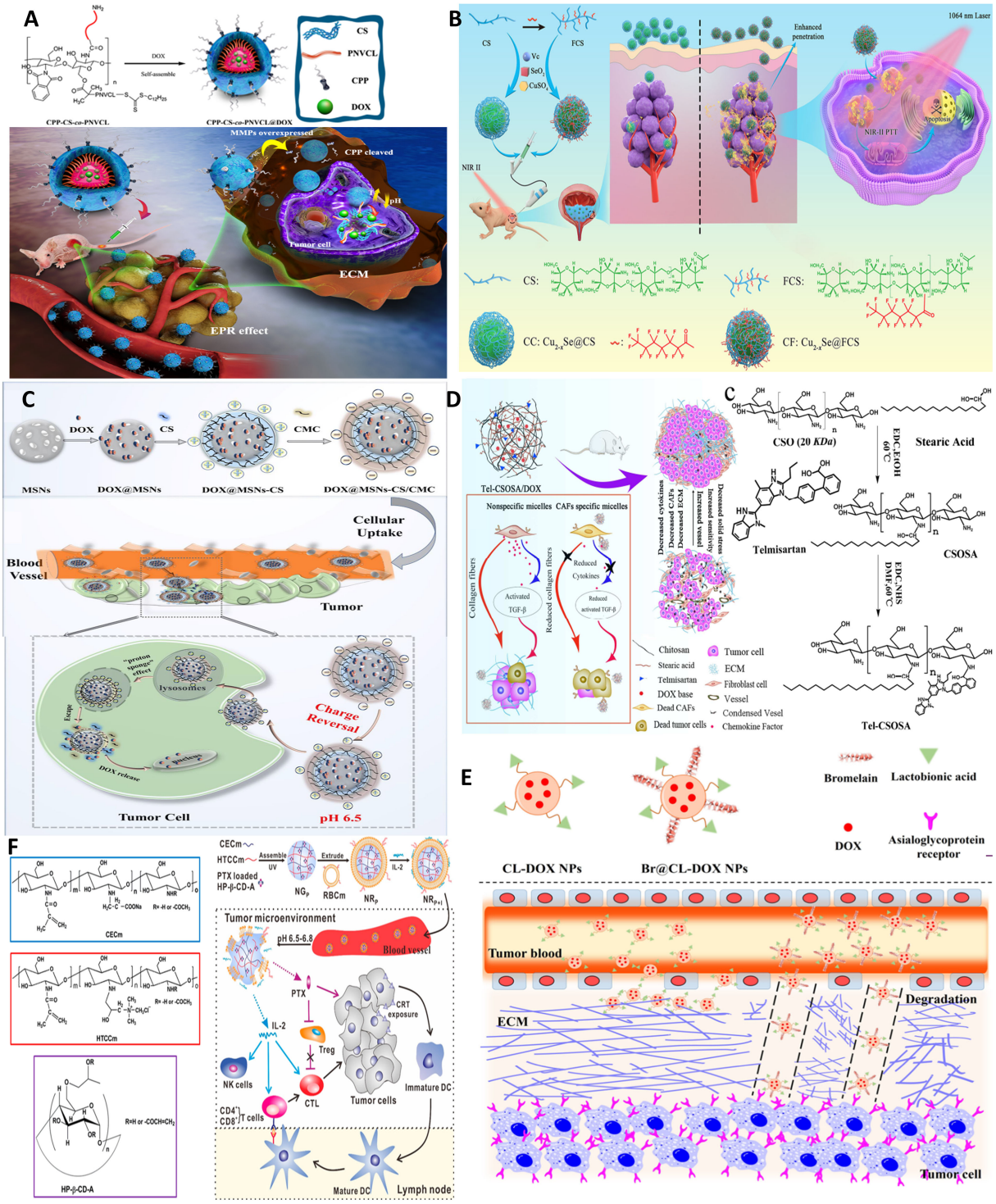

FIGURE 6
Chitosan NPs affords crossing stroma and biological membranes. **(A)** EPR and CPP-mediated active targeting. Reprinted from (15) under Creative Commons Attribution License 4.0, Copyright (2019) Springer Nature. **(B)** FC affords superior mucoadhesion potential to cross epithelial barriers of bladder cancer. Reprinted with permission from (80), Copyright (2021) Wiley-VCH GmbH. **(C)** Multi-stage acting CS NPs. Reprinted with permission from (81), Copyright (2019) American Chemical Society. **(D)** Stroma cell depletion afforded by chitosan-modified CAF inhibitor. Reprinted with permission from (74), Copyright (2018) Elsevier. **(E)** Chitosan nanosweeper for ECM drilling. Reprinted with permission from (82), Copyright (2018) Elsevier. **(F)** Chitosan-clocked NPs with RBC membrane as Trojan system. Reprinted from (83), Copyright (2017) American Chemical Society.

Nonetheless, positive charge is a problem for protein corona formation, and thus, a microenvironment-responsive multi-stage acting NPs are desirable with the capacity for charge/size-shifting. For example, surface-charge-switchable chitosan nanoclusters (CMGCC) as synergistic theranostic are fabricated for T1-weighted magnetic resonance imaging and intracellular antioxidant glutathione (GSH) depletion-enhanced PDT. CMGCC contains chlorin-e6-conjugated GC polymeric micelles incorporating catalase-stabilized MnO_2 nanoparticles. In this system, GC polymers with pH-sensitive surface charge switchability from neutral (pH 7.4) to positive (pH 6.5) could improve the PS accumulation within the tumor region. At the same time, the combined work of CAT and MnO_2 could effectively consume H_2O_2 and GSH to reoxygenate the hypoxic tumor *via* catalyzing endogenous hydrogen peroxide to O_2, and $^1O_2$, respectively; meanwhile generated Mn^{2+} serves as a contrast agent. Thus, a charge-reversal activity that only occurs under the low pH of TME restores the positive charge of GC for PS accumulation and subsequent enhanced PDT efficacy toward subcutaneous Hela tumors (84).

In another preparation, core–shell hybrid MSNs-CS/CMC NPs composed of mesoporous silica nanoparticles (MSNs) stabilized by positively charged OCS and negatively charged carboxymethyl chitosan with pH-triggered charge-reversal potential are used for effective intracellular delivery of DOX. The pH-triggered charge-reversal CS/CMC bilayer was key to NP internalization, endosomal escape, and DOX release. The surface charge of DOX@MSNs-CS/CMC was reversed from −16 (pH 7.4 in blood) to 11 mV (pH 6.5 in TME) and 15 mV (pH 5.5 in endosome). Thus, the reversible protonation–deprotonation strategy using CS derivatives provides an alternative ligand-independent platform for efficient drug delivery in breast cancer therapy (Figure 6C) (81).

Another form of multi-stage acting NPs is those that use an ECM-biodegradable coating such as gelatin to be degraded by matrix metalloprotease or hyaluronidase two abundantly expressed enzymes in TME. This strategy is specifically useful as the transport of polycationic NPs such as chitosan can be hindered due to the presence HA, which tends to form cationic/anionic complexes. Thus, HA coating protects the cationic core, and after degradation, in the second stage, the positive charge of the core element, e.g., chitosan, can be revealed to promote cellular uptake. Detailed examples of change-shifting NPs as a category of multi-stage acting NPs are reviewed in Refs (85, 86).

6.2.3 Nanosweepers

Dense stroma and ECM as seen for fibrotic/desmoplastic tumors such as breast, HCC, and pancreatic ductal adenocarcinoma (PDAC) can dramatically diminish NP convection. They may result in heterogeneous accumulation of NPs within solid tumors. Thus, strategies are required to afford deep NP penetration by ECM normalization or stroma cell targeting. The main targets are collagen, HA, and cancer-associated fibroblasts (CAFs) as the main constituents and contributors to the formation of dense ECM in desmoplastic tumors (87).

As one strategy, ECM-degrading enzymes, such as collagenase, can be decorated on the surface of NPs, acting as sweepers, as they digest ECM components along their way. Collagen I depletion is another strategy reported by inhibitors of collagen synthesis, such as lysyl oxidase or collagen-degrading enzymes, e.g., collagenase (88). Also, losartan is shown to improve oxygen distribution in tumor tissues by collagen depletion, allowing for deep percolation of paclitaxel-encapsulated liposomes (89). MSN conjugated with pineapple-derived peptidase papain family, bromelain (Br), can drill through ECM and enable the uptake of the particles by endothelial, macrophage, and cancer cell lines (90). Such lactobionic acid-modified bromelain-immobilized chitosan nanoparticles are used for enhanced active targeting and drug penetration respectively in tumor tissues (Figure 6E) (82).

ECM loosening is attempted by reprogramming stroma cells involved in collagen synthesis, particularly CAFs. Several strategies such as ultrasound (US) treatment, sonodynamic therapy (SDT) with tens of centimeters of depth penetration in soft tissue (57), hyperbaric oxygen, or PTT can also afford deep tumor penetration by modulating tumor permeability and ECM remodeling. In this line, deep tissue penetration of nanoparticles using US treatment improves EPR-based passive targeting efficiency of nanoparticles *in vitro* and *in vivo*. For one, pulsed high-intensity focused ultrasound (pHIFU) NPs are utilized to temporally improve blood perfusion, extravasation, and tissue penetration of fluorescent dye-labeled GC nanoparticles (FCNPs) in femoral tissue of mice by 5.7-, 8-, and 9.3-fold compared to that of non-treated ones (0 W pHIFU) (91). Hyperbaric oxygen therapy is also used for reversing hypoxia and elimination of CSCs by modulating depleted excessive ECM, such as collagen and fibronectin, and thus normalized tumor blood vessels both structurally and functionally and was effective in enhancing the efficacy of commercialized nanomedicines, Doxil and Abraxane, against TNBC and PDAC as stroma-rich solid tumors (92). As an example of dual-targeting ligands, chitosan micelles are formulated, which can target both tumor and most abundant stroma cells, CAFs, that localize near blood vessels within "finger-like" collagen-rich stroma, and lead to restrained drug transport. As mentioned before, biologically inspired Telmisartan grafting glycolipid micelles (Tel-CSOSA) can specifically eliminate CAFs and tumor cells. Uniform and deeper penetration of injected Tel-CSOSA/DOX NPs was achievable due to CAF apoptosis, which eliminates "finger-like" ECM, enforces subsequent tumor cell targeting, and renders tumor cells more vulnerable to chemotherapeutics (Figure 6D) (74).

6.2.4 Trojan system

An additional strategy to help transport DDSs across biological membranes and stroma is biomimetics inspired by

the ancient "Trojan horse", which aims to smuggle cargoes as close to the tumor nucleus as possible. This can be achieved using bacteria, macrophages, and stem cells that show inherent tumor homing tropism toward a hypoxic microenvironment through chemokine gradient, or using biomimetic/camouflaged NPs that adopt cell membranes of other types of cells including immune cells, tumor cells, red blood cells, platelets, exosomes (86), and MSCs. This way, NP coated or encapsulated within cells/cell membranes cannot be recognized by immune cells in the circulation; meanwhile, deep intratumor penetration can be afforded through hypoxia/chemotaxis gradients that drive trafficking of Trojan NPs towards solid tumors.

Chitosan, as a cationic polysaccharide, can bind with the glycoprotein receptors such as mannose receptors, Dectin 1 receptors, and TLR2 and TLR4 expressed in blood cells, monocytes, macrophages, and DCs. This, in turn, results in the endocytic uptake of chitosan-based DDSs by these cells. During recruitment to a diseased site, differentiation of monocytes to macrophage occurs. With this in mind, chitosan NP packaging in the blood is attempted by Ly-6C^{hi} monocytes, which took up COSA micelles. Furthermore, the micelles in macrophages can be exocytosed and subsequently taken up by cancer cells (93).

Also, in the light of antitumor activity of tumor necrosis factor α (TNF-α) and given the fact that macrophages can produce TNF-α in response to lipopolysaccharide (LPS), time-controlled expression of TNF as a transmembrane-expressed coating was induced to produce macrophage-tethered TNF-α to coat chitosan NPs. This biodegradable biomimetic module was effective against MCF-7, Hela, and MDA spheroids *in vitro* (94). Finally, RBC membrane-coated pH-responsive chitosan nanogel is used for combinatorial cancer chemoimmunotherapy. Nanogels were formulated with hydroxypropyl-β-cyclodextrin acrylate for paclitaxel loading and two opposite charged chitosan derivatives, namely, amphoteric methacrylamide N-carboxyethyl chitosan (CECm) and positively charged methacrylamide N-(2-hydroxy)propyl-3-trimethylammonium chitosan chloride (HTCCm), to precisely control the pH-responsive capability. Furthermore, biomimetic coating with erythrocyte membrane achieved "nanosponge" property and enhanced adsorption (through an IL-2-like agonist glycoprotein on RBC membrane), protection, and delivery of IL-2. Upon localization in tumor site by EPR, nanogel swelling exposed PTX-loaded HP-β-CD-A for low-dose sustained release of PTX, and induced calreticulin (CRT) exposure on tumor cells, along with DC stimulation and maturation, which finally activated immunosurveillance. After losing the inner core support, the membrane could be disintegrated to constantly release IL-2 into the TME for stimulating cytotoxic T lymphocytes (CTLs) and natural killer (NK) cells (Figure 6F) (83).

6.3 Microenvironmental barriers

6.3.1 Hypoxia (deep-seated tumor cells)

As a solid tumor grows up to a few millimeters in volume, its demand for oxygen and nutrients relies on neovascularization to provide blood supply. However, the high metabolic activity of tumor cells forces them to adopt a chaotic, unstructured, malfunctioning vascular system and anaerobic glycolysis (95). As a result, the TME is acidic, and there exists a gradient and heterogeneous concentration of oxygen levels within different parts of tumor layers, with a hypoxic/necrotic core and well-perfused proliferative cells at the tumor periphery (4). Hypoxic cells are characterized by upregulated expression of hypoxia-inducible factor (HIF-1a) residing in the deep regions within the tumor, rendering them inaccessible to therapeutic drugs. Also, heterogeneity concerning different pH values, oxygen, ATP, enzymes, tumor-specific receptor expression, etc., results in the uneven distribution of drugs/nanoparticles and, thus, their suboptimal efficacy towards cancer cells (3, 96). Among TME hallmarks, the role of hypoxia in cancer evolution and adaptation is well regarded. Hypoxia promotes ROS-induced genomic instability, alters DNA repair pathways, inhibits apoptosis, and promotes autophagy, tumor metabolism, angiogenesis, and the emergence of CSCs through promoting epithelial–mesenchymal transition (EMT) and immunosuppression. More importantly, a vicious cycle of hypoxia is responsible for the selection of new and more invasive and resistant clones that fail the efficacy of currently practicing anticancer regimes, resulting in recurrent cancer (97).

There are three general anticancer strategies based on tumor hypoxia: (i) harnessing it for the development of bioresponsive (hypoxia-responsive) nanomedicines; (ii) alleviating the hypoxia using vascular normalization agents (antiangiogenic therapy) or increasing oxygen level externally [oxygen delivery using hemoglobin (98) or perfluorocarbon] or internally [using oxygen generators called enzymes, which employ MnO_2 (99) and catalase (CAT) (100) to generate O_2 from H_2O_2 present abundantly in TME]; and, finally, (iii) oxygen depletion or starvation therapy, which aims to kill tumor cells by exacerbation of hypoxia and oxygen/nutrient depletion, as practiced by vascular infarction/disruption therapy using vascular disrupting agents or delivery of thrombosis-inducing agents such as coagulase fusion proteins (101, 102) or thrombin delivery (103) using a nanorobot to the tumor site to induce thrombosis selectively in tumor blood vessels. Oxygen depletion itself can be achieved externally by PDT and radiotherapy, which consumes intratumoral O_2 to generate ROS or endogenously by inherent oxygen-consuming materials such as magnesium silicide (Mg_2Si) (104), perfluorotributylamine (PFTBA) (105), or glucose oxidase (GO_X) (106). Mostly, for a better efficacy, the combination of these approaches together (107) or with other

approaches such as chemotherapy (99), radiotherapy, SDT (100), immunotherapy, and PDT (108) is desired. This can be well-achieved using CS as a carrier that can combine several tasks into one platform to overcome hypoxia-posed tumor drug resistance arising from deep-seated lingering tumor cells.

In one study, thermo-triggered *in situ* forming chitosan hydrogel is reported that is loaded with sonosensitizer meso-tetra(4-carboxyphenyl)porphine (TCPP) conjugated with catalase (CAT). The system is capable of body temperature-triggered gelation upon injection of CS-beta-glycerol phosphate disodium (GP) precursor solution into the tumor for entrapping TCPP-CAT. Then, ROS generation and deep tumor penetration can be achieved under ultrasonic treatment to effectively generate ROS as oxygen is sustainably supplied by catalase activity that decomposes endogenous H_2O_2 into molecular oxygen. Improving tumor oxygenation itself boosts the efficacy of repeating SDT to effectively eradicate solid tumors upon a single-dose injection (Figure 7A) (100).

What first appears as a problem later becomes part of the solution itself. As for hypoxia, the development of hypoxia-responsive DDSs can be envisioned using (i) hypoxia-trophic carriers such as anaerobic bacteria and stem cells, (ii) hypoxia/redox (nitroreductase enzymes)-responsive NPs using reducible cross-linking agents such azobenzene derivatives, and (iii) hypoxia-activated prodrugs (HAPs), which exclusively activate in response to oxygen degree (hypoxia/anoxia) in TME upon losing one or two electrons by activity of tumor nitroreductases to form the active drug. The significance of hypoxia responsiveness potential can be a blessing to targeted therapy of hard-to-treat tumors such as TNBC, where lack of a tumor-specific marker is a major concern.

Given that the outer proliferative tumor region is normoxic and that the optimal activity of several HAPs, such as TH302, is dependent on the extreme level of hypoxia, hypoxia aggravation by oxygen-depleting methods as described above can further improve HAPs activity. Concerning CS, an interesting oxygen-depleting self-activated nanovesicle is constructed by assembling a bilirubin (BR)-chitosan conjugate to form TH-302@BRCS NPS. BR-CS consumes O_2, and in the presence of intratumoral-abundant H_2O_2, it can be oxidized into hydrophilic biliverdin (BV)-CS. In this transformation, nanovesicles disassemble to release and activate the prodrug. The inherent oxygen-consuming potential of BR-CS aggravates hypoxia for greatly enhanced HAPs-based therapy; meanwhile, BV-chitosan can be used as a photothermal agent due to its wide absorbance from visible light to the NIR region (Figure 7B) (109).

Similar to HAPs, TME-responsive nanocarrier systems based on hypoxia can be developed for theranostic application and allow activation of therapeutic moiety only upon localization in hypoxic tumor regions. For one, a glycol CS NPS is conjugated through a ROS-sensitive thioketal (TK) linker to a photosensitizer (PS) pheophorbide. The amphiphilic GC–TK–PNA conjugates self-assemble into self-quenching NPs. Upon reaching the ROS-rich hypoxic core, the TK bond is reduced and allows the NPS to release the PS in a photoactive form to generate potent phototoxic effects upon NIR irradiation, causing a significant reduction in the tumor volume with desirable antitumor potential (112).

Other formulations exploited a targeting moiety to cross the outer proliferative layer and then deliver hypoxia-activated nanoparticles into deep-seated tumor cells. GC cross-linked with hypoxia linker, 4-nitrobenzyl chloroformate, and decorated with folic acid (FA) can specifically release drugs under hypoxic conditions. This formulation resulted in significant growth inhibition of A549 tumor-bearing athymic nude mice upon a single injection (20 mg/kg) (113).

Hypoxia responsiveness is also harnessed for boosted cancer immunotherapy. Hypoxia-responsive Ce6 photosensitizer/adjuvant CpG codelivery system, based on glycol CS-Azo linker [4,4, PEG mesoporous silica nanoparticle (CAGE)], is developed. Under hypoxia conditions, PEG is cleaved and promotes the release of CpG/glycol CS complexes. The combined work of PDT, which induces ROS and releases tumor-associated antigens (TAAs) with CpG adjutant, enables immunomodulation by recruiting DCs and their maturation by boosting antigen presentation. Twenty-four hours after i.v. injection of NPs to the B16.F1-bearing mouse allograft model, a significant and long-lasting tumor growth inhibition plus a 100% survival rate for 28 days was observed in the CAGE/CpG group (Figure 7C) (110).

CREKA peptide-functionalized CS NPs are employed for combined chemotherapy with tumor-infarction therapy and chemotherapy *via* the codelivery of DOX and thrombin to tumor and tumor blood vessels overexpressing fibrin-fibronectin. Systemic administration of the CS NPs into mice bearing B16-F10 melanomas resulted in 80% complete remission for more than 45.0 days after treatment cessation (Figure 7D) (111).

6.3.2 Immunosuppression

Crosstalk of tumor cells with various cells in the TME can inhibit host immune surveillance, resulting in tumor immune escape and tumor progression. Immune escape as a key feature of TME is shown to regulate the fate of infiltrating immune cells into the tumor. A typical example is tumor-associated macrophages (TAM), which are shifted from antitumor type M1 macrophages into pro-tumor M2 macrophages, which are related to tumor chemoresistance (3). Other mechanisms involve the secretion of immunosuppressive cytokines and host immune system dysfunction, such as excessive existence of regulatory T cells (Tregs), T-cell anergy, antigen deletion, and resistance to apoptosis. Thus, strategies to reshape immunosuppressive TME to immunostimulatory may hold promise (114) to improve the efficacy of anticancer regimes, especially cancer immunotherapy. However, direct administration of "bare" immunomodulators such as adjuvants, peptides, nucleic acids, antigens, or cytokines brings off-target toxicity and unsatisfactory efficacy due to

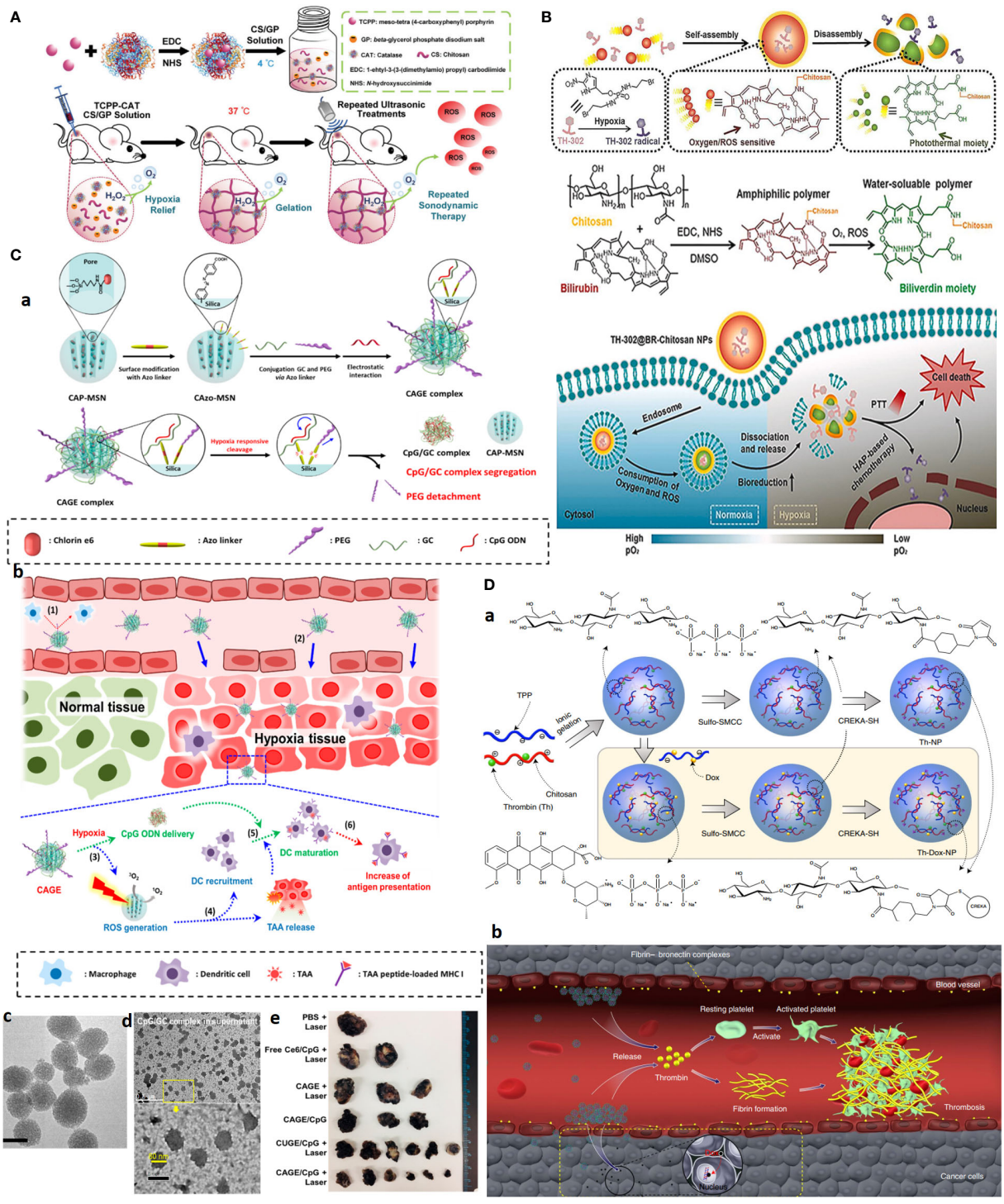

FIGURE 7
Advanced chitosan-based NPS target tumor hypoxia and result in complete tumor remission. **(A)** Hypoxia alleviation strategy. Schematics of thermo-triggered *in situ* chitosan gel formation for repeated and enhanced SDT after a single injection. Reprinted with permission from (100), Copyright (2020) Wiley-VCH GmbH. **(B)** Hypoxia depletion therapy coupled with hypoxia-activated prodrugs (HAPs). Reprinted with permission from (109), Copyright (2021) Elsevier. **(C)** Hypoxia-responsive immunomodulation of DCs for boosted PDT coupled immunotherapy. **(a)** Schematic design of NPs, **(b)** working principle. **(c, d)** TEM images of CAGE without and with CpG ODN. **(e)** The efficacy of antitumor effects *in vivo*. Reprinted with permission from (110), Copyright (2019) American Chemical Society. **(D)** Combination of tumor infarction therapy with chemotherapy for tumor starvation therapy. **(a)** Schematic design of NPs and **(b)** their working principle. Reprinted with permission from (111), Copyright (2021) Springer Nature.

suboptimal pharmacokinetics. Hopefully, chitosan-made NPs not only serve as natural immunoadjuvants, but also serve as a depot for antigen enrichment, allow for controlled as well as stepwise immumodualtion by controlled release of antigens, and carry immunotherapeutics such as DCs, cytokines, and other immuno adjunats to realize enhanced antitumor immune responses with reduced toxicity and side effects (115).

Functionalized chitosan platforms for immunotherapy involve nanogel, hydrogel, micelles, MNs (116), nanoparticles, and nanosheets with the delivery of DNA, RNA-based adjuvants as TLR agonists [e.g., CpG oligodeoxynucleotides (ODN)] (117), peptide adjuvants, as well as CAR T cell and antibody (e.g., checkpoint inhibitors) to enhance cancer immunotherapy (118). Equally, CS NPs are also used for the safe delivery and preservation of NK cells. That is, to avoid the toxic effects of cryoprotective agents, chitosan nanoparticle-mediated intracellular uptake of NK cells is replaced with dimethylsulfoxide (DMSO) to retain the potent antitumor functions of NK cells. This is the first case that delivers biocompatible nanoparticles to NK cells and shows clinical potential in manufacturing "off the shelf" safer allogeneic adoptive immunotherapies (Figure 8A) (119).

To circumvent challenges related to DC-based vaccination including multiple injections and elaborate *ex vivo* manipulation, CS NP is formed through ionic complexation as the next generation of vaccines. These NPs were used for delivery of OVA as a model antigen and polyinosinic–polycytidylic acid sodium salt (poly I:C) as an adjuvant to target TLR3 in endosomes. After injection, *in vivo* intracellular delivery of antigens to the DCs, and DC maturation, along with activation of antigen-specific cytotoxic CD8+ T cells, significantly greater antitumor efficacy in EG.7 and TC-1 tumor-bearing mice compared to the control was finally achieved (122). In another study, immunostimulatory chitosan/γ-PGA nanoparticle-based immunotherapy is harnessed as an adjuvant to radiotherapy in breast cancer to overcome the immunosuppressive nature, induce antitumor immunity, and control lung metastases in the 4T1 orthotopic breast tumor mouse model (Figure 8B) (120).

The implication of hydrogel and nanogel forms as intratumoral drug depots or post-surgery implants with immune activation potential will be discussed in the MRD section. However, an additional appealing hydrogel-based platform for immunotherapy is skin-implanted/inserted chitosan-based MN array/patches, which are capable of simultaneous sampling, injection, and sustained release of adjunct/immunostimulant agents, and given the flexibility and stretchability as wearable devices, there is no concern for their displacing or deformation upon body movement (7, 123).

For one, a needle-free injection MN array is developed with PVP on the top layer and fast-dissolving (3 min) chitosan NPs coloaded with OVA and CpG as an adjuvant to evoke systemic immune responses in mice (Figure 8C) (121). Likewise, sodium hyaluronate (SH) as tip and chitosan as needle base afforded long-term immunization using a single-shot intradermal immunization. Biodegradable chitosan base remained in the derm and afforded long-term OVA release for 4 weeks, while fast-dissolving SH acted as the promising dose by rapid releasing of encapsulated OVA, resulting in enhanced cytotoxic immunity as well as higher and more durable antibody response (124).

An additional immune-based strategy aims to reshape/reprogram immunosuppressive TME and tumor-promoting stroma into an immune-activated state, for example, by reprogramming protumor TAM-2 into antitumor TAM-1 (3), or targeting CAFs as attempted by dual targeting of CAFs and tumor cells through angiotensin II type I receptor (AT_1R) overexpressed on both CAFs and tumor cells using pathological inspired micelles (74). Additional biomaterial-based strategies that aim to reshape immunosuppressive TME in a spatiotemporal manner for enhanced cancer immunotherapy are reviewed in Ref (125).

6.3.3 Cancer stem cells

CSCs are rare subpopulations of cancer cells that are highly tumorigenic and causative of cancer relapse and metastasis owing to their high capability of initiating and/or reinitiating tumor regrowth. Hostile TME conditions such as hypoxia and external assaults such as chemotherapy treatment can promote stemness and stem cell plasticity. CSCs are hard to treat and develop drug resistance owing to their specific characteristics, including clonal evolution and heterogeneity, dormancy, enhanced DNA repair, overexpressed drug efflux pumps, and overexpression of antiapoptotic proteins (1, 126).

Up to now, CSC targeting and studying using 3D modeling systems remain an untraceable challenge as tumor cells tend to switch from EMT to MET, losing and gaining stemness behaviors. In addition, high-throughput screening of 16,000 compounds identified only ~0.2% compounds with selective toxicity for breast CSCs (127). This call for advanced strategies is effective not only against tumor bulk but also for the elimination of residual cells, including CSCs and CSLCs.

Generally, CSC targeting approaches are based on several strategies: (i) hypoxia reduction as attempted by hyperbaric oxygen therapy to improve oxygenation and enable deep penetration of commercialized nanomedicine for CSC eradication (Figure 9A) (92), (ii) CSC targeting by CSC-specific markers decorated with NPs (e.g., CD44 marker) (17), (iii) CSC "differentiation" strategy, using reprogramming factors/agents) (131) or "defanging" CSCs through nanoparticle surface engineering (Figure 9B) (128), and (iv) "cocktail" therapy (132) with the combination of multiple drugs (Figure 9D) (130), or multimodal systems combining different strategies (e.g., chemotherapy and PDT for enhanced ROS generation) (129) (Figure 9C).

Chitosan has been used for CSC targeting, and chitosan-based scaffolds (membrane) were also used as promising biomimetics for the CSC niche to study their behavior.

Cultured colon and HCC cells on chitosan membranes can develop stemness properties with increased cell motility, quiescent population, drug resistance, self-renewal capacity, and the expression levels of stemness and CSC marker genes, such as OCT4, NANOG, CD133, CD44, and EpCAM (133).

Also, single-cell mass cytometry revealed that DOX therapy of MDA-MB-231 cells increases stemness properties of their spheroids partially *via* αvβ3 integrin overexpression. An RGD-modified CS NP promoted chemotherapy efficacy against these CSCs (134). Rather than using CSC markers, CS, owing to pH responsiveness and inherent property to target $CD44^+$ CSCs, but not $CD44^+$ normal stem cells, was decorated on the surface of pluronic F127 consisting of hydrophilic PEG and the more hydrophobic polypropylene glycol (PPG). After systemic injection of developed 20-nm nanoparticles, they accumulated in the tumor through the EPR effect and afforded endolysosomal pH-dependent DOX delivery six times more efficient than DOX delivery alone to eliminate tumor-reinitiating CSLCs in 3D

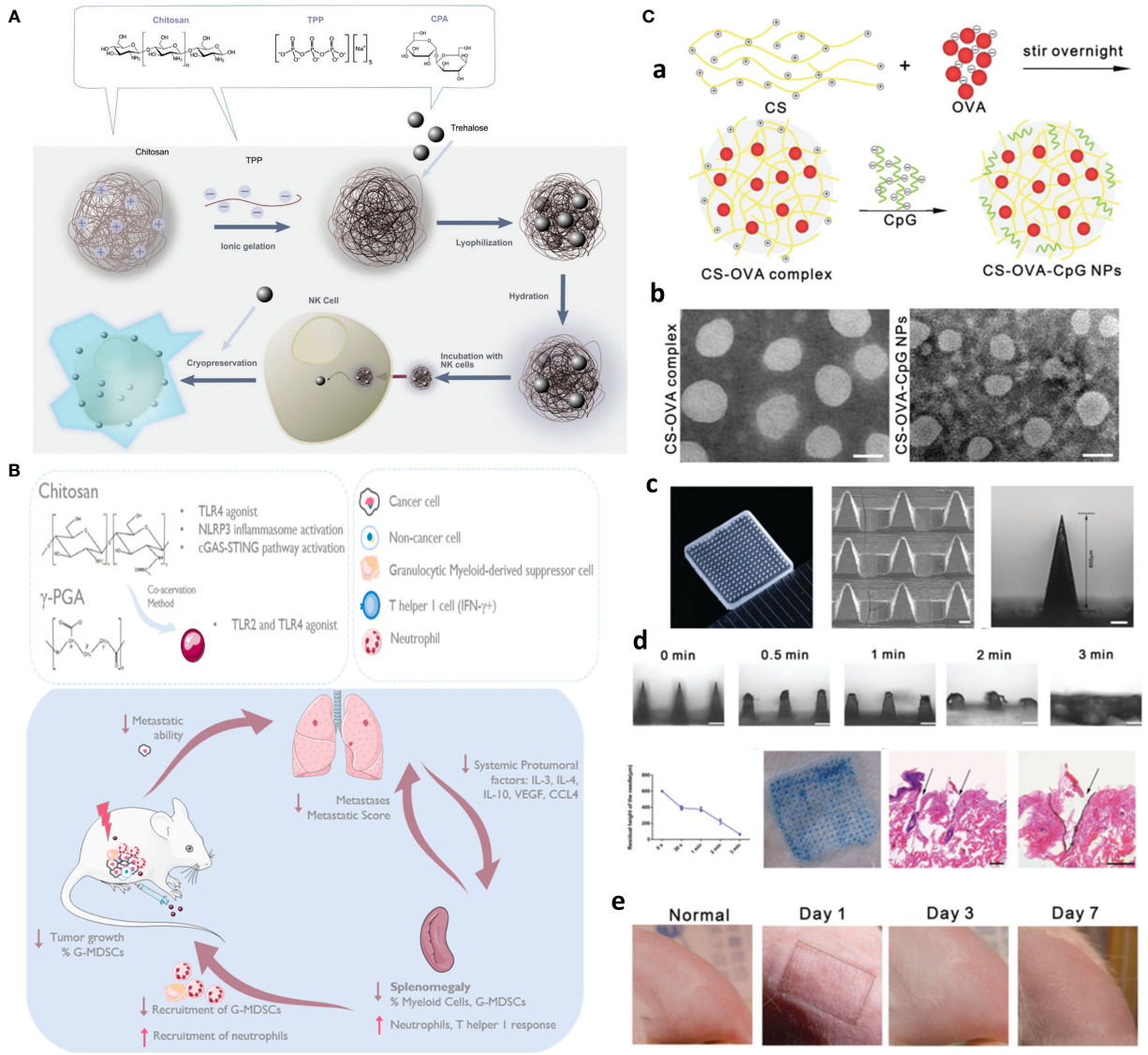

FIGURE 8
Chitosan-based platforms for active immunotherapy and metastasis inhibition. **(A)** Chitosan NPs for NK cell preservation and delivery. Reprinted from (119) under Creative Commons Attribution License 4.0, Copyright (2020) WILEY-VCH Verlag GmbH & Co. KGaA, Weinheim. **(B)** Integration of chitosan Ch/γ-PGA NPs with radiotherapy boost immune response and elicit antimetastatic potential. Reprinted with permission from (120), Copyright (2020) Elsevier. **(C)** Chitosan NP-loaded MN patch for systemic vaccination in mice. **(a)** Schematics of synthesis of CS–OVA–CpG NPs; **(b)** TEM; **(c)** macroscopic and SEM images; **(d)** dissolution kinetics, insertion, and biocompatibility in BALB/c mouse skins; and **(e)** rat skin. Reproduced with permission from (121), Copyright (2020) Royal Society of Chemistry.

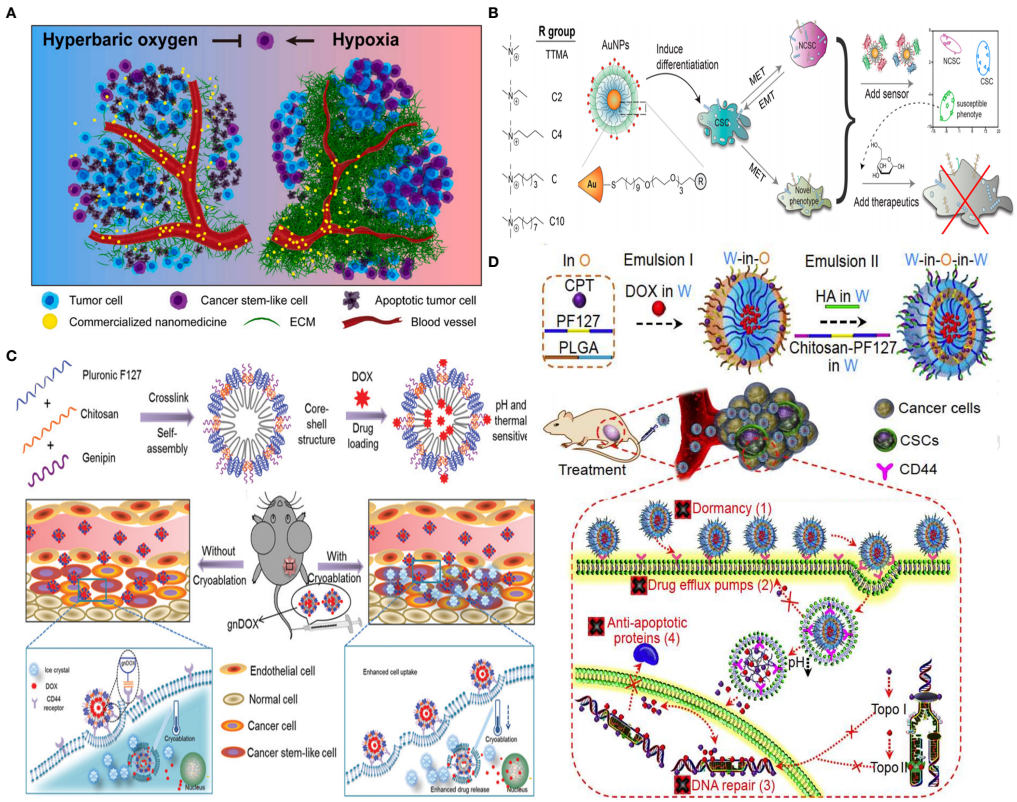

FIGURE 9
Strategies for CSC targeting and elimination. **(A)** Hyperbaric oxygen therapy. Reprinted with permission from (92), Copyright (2021) Elsevier. **(B)** NP surface modification from hydrophilic (TTMA) to highly hydrophobic (C10) tested, with C6 AuNP robustly promoted CSC differentiation by reducing stemness marker. Reprinted with permission from (128), Copyright (2020) American Chemical Society. **(C)** Multimodal system combines chemo- and cryoablation therapy. Reprinted with permission from (129), Copyright (2021) Elsevier. **(D)** Receptor-mediated dual drug combination strategy. Reprinted with permission from (130), Copyright (2021) Royal Society of Chemistry.

mammospheres and reduced the size of tumors in an orthotopic xenograft tumor model with no evident systemic toxicity (17). Likely, another formulation consisting of HA-decorated thermal and pH-responsive nanoparticles of pluronic F127, PLGA, and CS is attempted for targeted codelivery of DOX and irinotecan to eliminate CSLCs where HA is used for active targeting of CD44+ CSCs to reduce their drug resistance due to dormancy, F127 for thermal responsiveness, and chitosan for acidic pH-triggered drug release; DOX and irinotecan-loaded NPs were used to inhibit the activity of topoisomerases II (DOX) and I (irinotecan), respectively, to fight CSC drug resistance associated with their enhanced DNA repair and antiapoptosis, while minimizing drug efflux from CSCs due to drug nanoformulation. This resulted in targeting and efficient breast CSC eradication both *in vitro* and *in vivo* with up to ~500 times of enhancement compared to two drugs without nanoformulation (Figure 9C) (130). Moreover, core–shell nanoparticle formation is achieved by self-assembly of genipin cross-linked pluronic F127-chitosan nanoparticles (GNPs) and the efficient encapsulation of DOX combined with cryoablation therapy. DOX release can be triggered by thermal and pH stimuli upon deposition of a cryogenic agent at the target tumor site, allowing for synergistic effects and chitosan-mediated CSC-like targeting of chemoresistant mammary tumors (Figure 9D) (129).

6.3.4 Circulating materials: CTCs and exosomes

TME-derived circulating materials, including cell-free DNA (cf-DNA), circulating tumor cells (CTCs), and exosomes, are key contributors to MRD and occult metastasis. Though they can serve as invaluable biomarkers for early cancer detection and metastasis status, capturing (detection) and analysis of these rare and heterogeneous elements from trace biological samples in clinics are a challenge (3). Hopefully, properties of chitosan such as inherent affinity for epithelial cell adhesion and ease of functionalization with CTC-specific markers such as anti-epithelial cell adhesion molecule (anti-EpCAM) antibody inspired the devising of chitosan-based trapping systems with the capability to be integrated with microfluidic chip to bring

extraordinary potentials with simplicity, high purity, sensitivity, and viability (nondestructive release), and in a label-free fashion (135).

In one preparation, a simple and fast method for isolation of circulating exosomes is reported, which integrates chitosan electrostatic adsorption, micro-patterned substrates, and microfluidic shuttle flow control to enable the capture/release of circulating exosomes from trace clinical blood samples (10 µl) with more than 90% purity and above 84% high RNA recovery ratio within 15 min, outperforming traditional ultracentrifugation methods (Figure 10) (135). Likewise, a fibrous mat using HA-functionalized electrospun CS nanofiber (CNF) is generated and embedded in a microfluidic chip to enable the specific capture and release of CD44-overexpressing CTCs. Modification of electrospun CNFs with zwitterion carboxyl betaine acrylamide (CBAA) elicits hemocompatibility and an excellent antifouling property, and can capture A549 human lung cancer cells with an efficiency of 91% at a flow rate of 1.0 ml/h and their non-invasive efficient release (90%) upon the addition of glutathione for 40 min. In tested clinical blood samples, the presence of MRD in 5 of 5 breast cancer patients and 9 of 10 non-small-cell lung cancer patients was detected with high sensitivity down to single cell to 18 CTCs per milliliter of blood (136). Similar work is also attempted using anti-EpCAM antibody functionalized hydrogel-chitosan nanofiber with a capture yield of 79.9% in artificial blood samples (137).

7 Tumor-penetrating chitosan NPs for the treatment of minimal residual disease

Chitosan NPs afford crossing numerous biological barriers; an important application is the treatment of relapsed tumors and metastasis. The latter category involves injectable irregular wound-filing hydrogels employed for treatment of post-surgery recurrence and wound tissue reconstitution post-surgery. To achieve this, hydrogels are injected either into or in the vicinity of the tumor without the invasive procedure of tumor surgery, which triggers bleeding and metastasis.

7.1 Intratumoral injectable hydrogel

Serving as a long-lasting drug depot, direct hydrogel injection into the tumor site as preformed nanoparticles or *in situ* forming hydrogels is ideal for local treatment of chronic

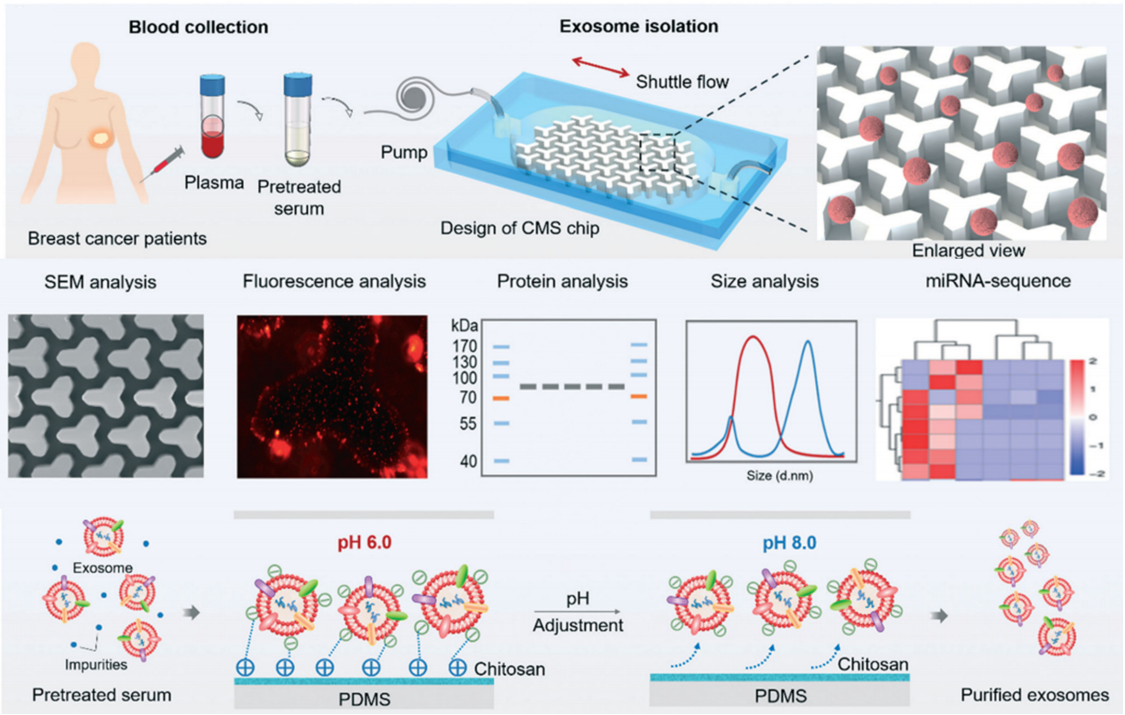

FIGURE 10
CS-based liquid biopsy for interrogation and elimination of circulating materials. Chitosan-based microfluidic platform for tumor-derived exosome isolation and analysis. Reprinted from (135), Copyright (2021) Royal Society of Chemistry.

diseases such as inflammation and cancer, with preferential, controlled, and on-demand capacity for drug release. To this, a highly efficient chimeric antigen receptor T lymphocyte (CAR T) delivery is developed for local immunotherapy of recurrent cancer. In this line, injectable thermosensitive CS-PEG hydrogel is used for loading ganglioside GD2-specific CAR T cells and their long preservation to express a recombinant immune-enhancing cytokine, interleukin-15, as a self-growth factor support for promoting T-cell proliferation, activation, and survival. CAR T cells can preserve vision as they improve antitumor effects to control retinoblastoma, with 60% complete remission and being tumor-free up to day 70 in mice (138). Also, CS hydrogel serves as a drug depot for the delivery of gold clustered liposomal DOX. CH-HG-GLDOX can be directly injected into tumor tissue without a surgical procedure and release DOX upon NIR irradiation. Furthermore, CH-HG-GL_{DOX} and poly(D,L-lactide-co-glycolic acid) nanoparticle-based vaccines increased cytotoxic CD8+ T-cell immunity, leading to enhanced synergistic chemotherapy and immunotherapy efficacy (Figure 11) (139).

In another case, an injectable and photo-responsive drug delivery antibacterial hydrogel (CP@Au@DC_AC50) is reported for uveal melanoma (UM) treatment. Mechanical strength and PTT are afforded due to the incorporation of gold nanorods and resulted in thermosensitive gel-sol transformation to release the gene-targeted drug DC_AC50 on demand in response to low-density NIR light. This multifunctional therapeutic platform affords NIR light-triggered gene-targeted therapy/PTT/antibacterial potential in the orthotopic model of UM as intraocular tumors (Figure 2A) (65). Electrospun nanofibers composed of QCS, polyvinyl alcohol (PVA), and curcumin are fabricated with excellent anticancer activity against recurrent 4T1 breast cancer cells and antimicrobial performance against *Staphylococcus aureus* and *Escherichia coli* bacteria (140).

7.2 Post-surgery injectable/implanting hydrogel

After tumor resection, chitosan-based precursors can be injected into the wound to form a hydrogel. Implants or surgical glues can also be used; however, unlike *in situ* forming gels, they cannot fill irregular wounds (141). Sol-gel transition can be triggered by internal (e.g., temperature) or external (e.g., light) triggers that allow *in situ* gelation and thus entrapping of various cargoes and their long-term retention for a sustained release. At the same time, localized yet augmented therapeutic effects with off-target systemic effects can be envisioned (9). Furthermore, controlled specific cargo release from gel in response to TME changes, such as pH, hypoxia, specific gene/protein expression changes, or externally induced by light (ultrasound waves using SDT, PTT, and PDT), can be realized,

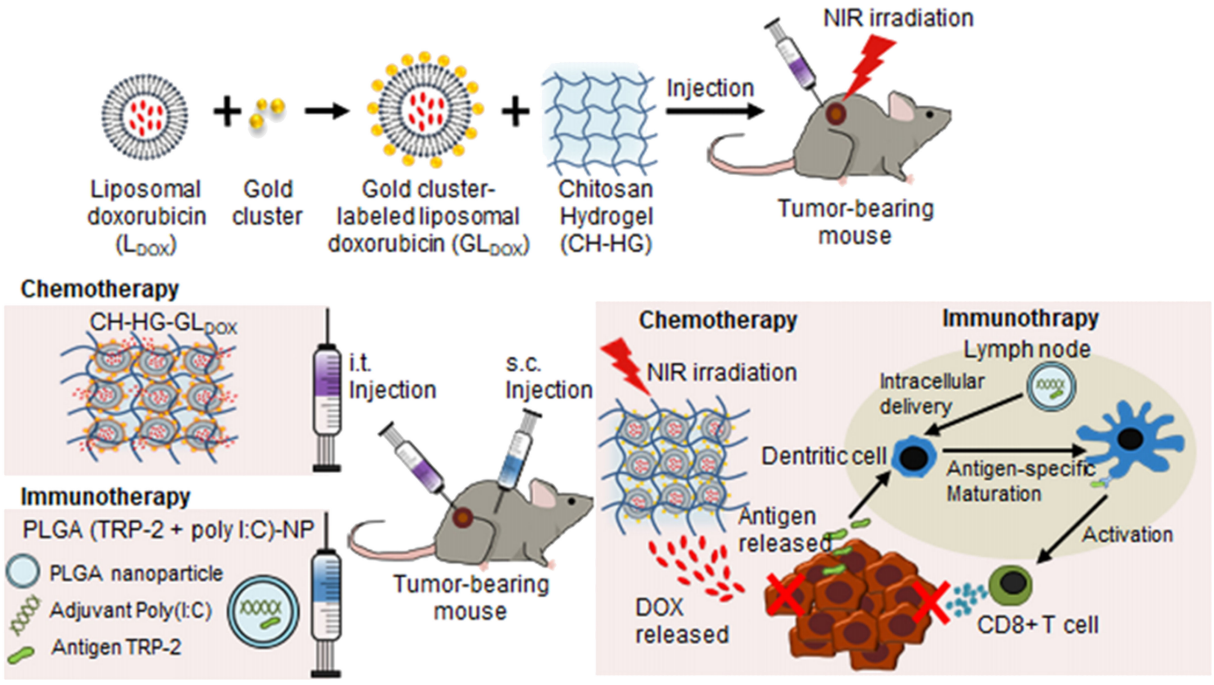

FIGURE 11
Local injectable chitosan serves as a drug depot to control tumor relapse. Intratumoral injectable chitosan nanoformulation for combined chemo- and immunotherapy of cancer. Reprinted with permission from (139), Copyright (2021) Elsevier.

which all rely on ROS generation to eliminate residual tumor cells (63, 141–143).

Nanocomposite made of CS has wound healing, antimicrobial, adhesive, and tissue regenerating potentials. The multi-functionality of advanced CS hydrogels/fibers combined with other approaches such as chemotherapy and particularly immunotherapy (e.g., anti-PDL antibody) allows for synergistic therapy to effectively detect and kill residual/regenerating tumor cells (141) (142).

Bioinspired hydrogels are another advanced and highly promising tool for clinical translation (123). In this line, inspired by catechol groups found in marine Mussel foot protein, bioinspired adhesive chitosan can be fabricated to enable additional functionality, which is capability for tight wet adhesion if it is meant to be used in surgical trauma. Another consideration is anti-inflammatory and antimicrobial potentials, as adhesive hydrogels are prone to bacterial infection while surgery wound trauma itself triggers the inflammatory condition and, thus, tumor recurrence (63, 142).

As an example of injectable CS-based hydrogels, the fabrication of a novel magnetic hydrogel is reported, which incorporates very low amounts (0.6 mg ml^{-1} compared to SPIO-magnetic hydrogels) of ferromagnetic vortex-domain iron oxide (FVIOs) grafted on the surface of GC and then mixed with DT-PEG solution, which forms coupling–uncoupling imine bonds between CS chains, affording dynamic hydrogel. FVIO-functionalized hydrogel (F-MH) possesses functional adaptability to TME as it imparts sufficient heating capacity, rapid sol (25°C)-gel (37°C) transformation (~400 s gelation time), self-conformal ability to seep into and conform to small gaps of the wounded area, self-healing, biodegradation, heating potential, and pH-responsive controlled release of DOX to effectively prevent breast cancer recurrence *in vivo* (Figure 12A) (141).

In another study, CS hydrogel composed of black phosphate nanosheets (BPNSs) and *in situ* grown copper nanoparticles (CuNPs) was developed. As an injectable gel, CS@BPNSs@CuNPs form a quick spongy-like state when the temperature is raised to 37°C and possess a 24.98% blood clotting index, a 91% antimicrobial effect against *E. coli* and *S. aureus* through ROS generation, and 10% tumor recurrence. Combined with aPD-L1-based immunotherapy, or PTT, this biodegradable injectable *in situ* forming hydrogel is promising for postoperative trauma and combating multiple primary tumors, including subcutaneous lung tumor and second primary HCC model and ectopic *in situ* glioblastoma model (Figure 12B) (142). Likewise, an injectable biocompatible thiolated chitosan (CSSH) hydrogel is fabricated, composed of DOX-loaded thiolated halloysite nanotubes (HNTs) with good mechanical properties. Further CSSH cross-linking permits gel formation of DOX@CSSH/HNTs-SH. This hydrogel allows pH responsiveness DOX release to inhibit the recurrence and repair the defected tissue after tumor resection (Figure 12C) (20). Mussel-inspired catecholic-Fe^{3+} chitosan-gallic acid (CSG) hydrogel is formulated to well-fill the tumor-resected cavity with considerable anti-inflammatory and wet-adhesion ability, surgical trauma healing, photothermal agent (catechol-Fe^{3+} moiety), and subsequent prevention of local tumor recurrence benefiting from the combined work of photothermal therapy (rising tumor Tm to ~46°C) and chemotherapy (pH and NIR-induced DOX release) in the 4T1 breast cancer model in mice (Figure 12D) (63).

Hydrogel implants are used to control MRD. Local delivery of lentinan, a stemness-depleting agent, is afforded by fabrication of a sponge-like LNT/chitosan composite to be implanted and used for sustained local drug delivery and long-term tumor relapse inhibition of postoperative breast cancer *in vitro* and *in vivo* (145). Likewise, cisplatin-loaded hyaluronate-chitosan placed as intrapleural polymeric films containing cisplatin inhibited the local recurrence of malignant pleural mesothelioma in a rat tumor model (146). Finally, 3D printed intelligent poly(lactic-co-glycolic acid), gelatin, and chitosan implant loaded with anticancer drugs 5-FU and DOX is prepared. This intelligent scaffold (IS) renders hemostatic function and accelerates the wound closure. IS allows on-demand drug release in response to pH, can adsorb residual cells (e.g., CTCs), and prevents recurrence and distal metastasis of skin-implanted MDA-MB-231 breast cancer with 80% survival rate in mice. The *in vivo* antitumor ability of the IS was observed for up to 30 days with good antitumor activity in the absence of lung metastases compared to controls (Figure 12E) (144).

8 Chitosan in the clinic: Concluding remarks and future perspective

Natural products and nature-inspired biomaterials are appealing for biomedical uses. Among the clinic's biomaterials and delivery systems are vesicular particles, mostly liposomal and polymeric (pegylated) forms as FDA-approved nanodrugs. We also recently proposed the bioinspired hydrogel-based products as next-generation biomaterials with a high chance for translation into the clinic (123). Concerning chitosan, as a natural (semi-natural) product, the many inherent properties besides its simplicity, functionality, and full addressability to be combined with other materials to make multifunctional systems can extend its potential for numerous applications for drug delivery, having different forms such as nanogels, nanofibers, hydrogels, vesicular particles for codelivery of hydrophobic and hydrophilic drugs, and multimodal and important biochips to be used for interrogation of circulating materials in plasma samples of cancer patients, enabling personalized medicine.

With tumor heterogeneity as the main hurdle for efficient nanodrug delivery and TME-derived numerous biological barriers, chitosan-based drug formulations have shown promising results. Most lycol forms of chitosan are best for

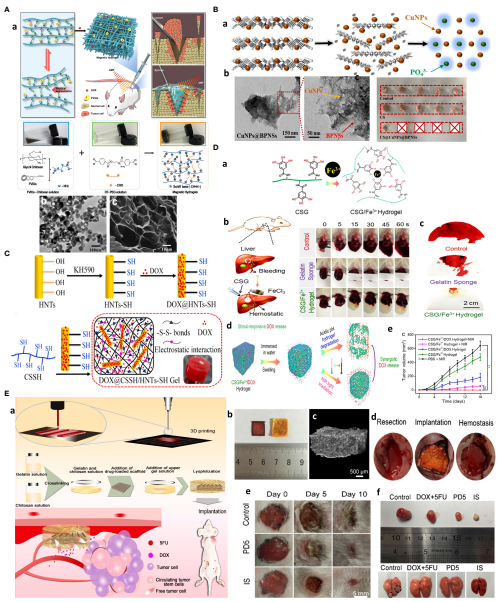

FIGURE 12
Post-surgery chitosan injectable gels/implanted scaffolds for treating recurrent cancer and MRD. **(A)** Magnetic hydrogel for the treatment of breast cancer metastasis. **(a)** Schematics of design (top) and transformation mechanism (bottom) of GC-ferrofluids to form a magnetic hydrogel. **(b)** TEM and **(c)** SEM images of porous magnetic hydrogels. Reprinted from (141) with permission, Copyright (2019) WILEY-VCH Verlag GmbH & Co. KGaA, Weinheim. **(B)** Injectable biodegradable hydrogel for multiple tumor and recurrent cancer therapy. **(a)** Schematic for the degradable process of the CS@CuNPs@BPNSs hydrogel. **(b)** TEM image **(c)** and efficacy of CuNPs@BPNSs for complete tumor remission in the lung cancer recurrence model. Reprinted from (142) with permission, Copyright (2021) Elsevier. **(C)** Thermosensitive injectable halloysite-chitosan hydrogels as drug carriers for inhibition of breast cancer recurrence and tissue reconstruction. **(a)** Synthesis procedure for thiolated halloysite nanotubes (HNT) for DOX loading and hydrogel formation by cross-linking with chitosan through SS bonds and electrostatic interactions. Reprinted from (20) with permission, Copyright (2021) Elsevier. **(D)** Anti-inflammatory and antibacterial catecholic chitosan hydrogel for rapid surgical trauma healing and subsequent prevention of breast tumor recurrence. **(a)** Synthesis route of CSG/Fe^{+3}/DOX hydrogel by Fe^{+3} chelation of chitosan (CS)–gallic acid (GA) and DOX loading. **(b)** hemostatic potential in a model of rat liver bleeding, **(c)** typical bloody filter papers. **(d)** pH/NIR-responsive DOX **(e)** Effective 4T1 tumor recurrence of the CSG/Fe3+/DOX hydrogel. Reprinted from (63) with permission. Copyright (2020) Elsevier. **(E)** 3D printed intelligent scaffold (IS) stops bleeding and adsorbs CTC after surgery to prevent recurrence and distal metastasis of breast cancer. **(a)** Electro-hydrodynamic jet 3D printing process of drug-loaded chitosan–gelatin (CG) scaffold, **(b)** macroscopic, **(c)** microscopic, **(d)** SEM images of implanted IS after 30 days, **(e)** potential of IS for wound healing and closure compared to gauze (control) and PLGA-DOX-5FU (PD5) scaffold, **(f)** potential of IS for recurrent cancer and inhibiting breast cancer lung metastatic activity. From (144), Copyright (2020) Under Creative Commons Attribution License 4.0. ivyspring.

targeting tumor heterogeneity, particularly lymph node metastasis targeting, with host immune cell evoking antimetastasis potential. Further combining different chitosan derivatives, each possessing a specific function into a single formulation, can uncouple unprecedented features to tackle tumor heterogeneity and cross several barriers at once. For example, mucoadhesion using fluorinated chitosan coating may lead to development of oral vaccines for transepithelial transport and cloak NPs for longer circulation. At the same time, oligosaccharide forms can provide stem-cell-like population targeting. Advances in chitosan platforms as implantable trapping devices for capturing and releasing CTCs through their adhesive potentials to epithelial cells are another appealing potential as a label-free diagnostic and prognostic method.

The main applications of chitosan are cosmetic, dietary supplement, teeth implant, drug excipient, wound healing dressing, and drug delivery. The FDA approves chitosan for wound dressings and drug and gene delivery in humans (13). There are a total of 117 records on clinicaltrials.gov using “chitosan”, 13 records for “chitosan” and “wound healing”, and only six clinical trials searched using “chitosan” and “cancer” as keywords (Table 1). The first two clinical trials were for chitosan used as an anticancer agent by reducing levels of AGE and as a pain killer. Concerning chitosan-based cell culture models, a recent project is recruiting lung cancer patients to evaluate the correlation of the cell detachment ratio on pH-responsive chitosan with the overall survival as a diagnostic and prognostic indicator by flow cytometry analysis of tumor (stem-like) cell-specific markers expressed by isolated cells. Acting as an adhesive barrier, Mediclore®, a mixed solid of poloxamer, gelatin, and chitosan, is undergoing tests for its safety and antiadhesive effect for post-axillary dissection surgery in breast cancer patients. The mean difference in range of motion (ROM) and pain will be compared among patients

TABLE 1 Chitosan clinical trials for advanced recurrent cancer therapy.

Title	Condition	Country	Phase	NCT number	Date
Study of chitosan for pharmacologic manipulation of AGE (advanced glycation end products) levels in prostate cancer patients	Prostate cancer	United States	Phase 1–2	NCT03712371	2019–2021
Comparison of oral morphine versus nasal ketamine spray with chitosan in cancer pain outpatients	Cancer pain	Switzerland	Phase 3	NCT02591017	2015–2018
Evaluation of the cell detachment ratio on pH-responsive chitosan as a prognostic factor in lung cancer	Lung cancer	Taiwan	Unknown	NCT04218188	2020–ongoing
Antiadhesive effect and safety of a mixed solid of poloxamer, gelatin, and chitosan (Mediclore®) after axillary dissection for breast cancer	Breast cancer	Korea	Phase 3	NCT02967146	2017–ongoing
A randomized clinical trial evaluating the use of the laser-assisted immunotherapy (LIT/inCVAX) in advanced breast cancer	Breast cancer	Peru	Phase 3	NCT03202446	2017–2018
Intratumoral injection of IP-001 following thermal ablation in patients with advanced solid tumors	Advanced solid tumors	Switzerland	Phase 1–2	NCT03993678	2019–ongoing

undergoing standard treatment for surgery and those in whom Mediclore® was injected into the surgery site and closed with a suture. In another project taking 58 weeks, local photothermal laser-based immunotherapy as a trigger for total antigen release from whole cells was combined with 1% immunostimulant glycated chitosan (GC) injection (1 ml injection in and around laser-irradiated tumor site) as an adjutant, for the activation of APCs to take up tumor antigens and activate and forward patient's tumor-specific systemic immune response, for residual/metastatic remaining tumor(s). This also involved low-dose cyclophosphamide, and the outcome was based on overall response rate and overall survival. Likewise, a similar ongoing project initiated in 2019 also aims to treat advanced solid tumors using photothermal ablation immediately followed by intratumoral injection of IP-001 (1% *N*-dihydro-galacto-chitosan, Immunophotonics Inc.) to turn "cold" into "hot" tumors by heat-mediated tumor antigen-releasing and IP-001-triggering systemic tumor-specific immune response to eliminate residual primary and metastatic tumor cells far from the treated area (also known as abscopal effect).

Together, these experiments show the potentials of chitosan for solid tumor therapy in the context of relapse and resistance. Only chitosan or its derivatives were potent; thus, there is still room to make important discoveries using various nanoformulations in the preclinical setting to be tested in the clinic. Among those, we envision that bioinspired multifunctional formulations, especially hydrogel-based formulations, are amenable as drug depots to afford long-term and pH-responsive drug release for the elimination of residual tumor cells, wound healing after tumor resection, and multimodal theranostics in an imaging-guided "hunting and killing approach" of primary and remaining tumors. Additionally, chitosan formulations can also be prepared for systemic injections and treatment of hematological cancers. Further improvement in chitosan derivatives, synthesis approaches, molecular characteristics, rational modification/functionalization, control over molecular weight and the degree of modification, and incorporation of multi-stimuli-responsive moieties enables the translation of the full potential of chitosan to clinical products.

Author contributions

HM, MJ and RJ-E have written the original draft, MAAA and MSh helped with data collection, ZA and RJ-E supervised and edited the final draft.

Acknowledgments

RJ-E is supported by NIMAD (grant number: 978679) and Tabriz University of Medical Sciences, Tabriz, Iran (grant number: 65568).

Conflict of interest

The authors declare that the research was conducted in the absence of any commercial or financial relationships that could be construed as a potential conflict of interest.

Publisher's note

References

1. Jahanban-Esfahlan R, Seidi K, Manjili MH, Jahanban-Esfahlan A, Javaheri T, Zare P. Tumor cell dormancy: Threat or opportunity in the fight against cancer. *Cancers* (2019) 11(8):1207. doi: 10.3390/cancers11081207

2. Masoumeh Sharifi–Azad MF, Cho WC, Barzegari A, Dadashi H, Dadashpour M, Jahanban–Esfahlan R. Recent advances in targeted drug delivery systems for resistant colorectal cancer. *Cancer Cell Int* (2022) 22(196):1–21. doi: 10.1186/s12935-022-02605-y

3. Baghban R, Roshangar L, Jahanban-Esfahlan R, Seidi K, Ebrahimi-Kalan A, Jaymand M, et al. Tumor microenvironment complexity and therapeutic implications at a glance. *Cell Communication Signaling* (2020) 18(1):59. doi: 10.1186/s12964-020-0530-4

4. Seidi K, Jahanban-Esfahlan R, Zarghami N. Tumor rim cells: From resistance to vascular targeting agents to complete tumor ablation. *Tumour Biol J Int Soc Oncodevelopmental Biol Med* (2017) 39(3):1010428317691001. doi: 10.1177/1010428317691001

5. Ryu JH, Yoon HY, Sun I-C, Kwon IC, Kim K. Tumor-targeting glycol chitosan nanoparticles for cancer heterogeneity. *Advanced Materials.* (2020) 32 (51):2002197. doi: 10.1002/adma.202002197

6. Moramkar N, Bhatt P. Insight into chitosan derived nanotherapeutics for anticancer drug delivery and imaging. *Eur Polymer J* (2021) 154:110540. doi: 10.1016/j.eurpolymj.2021.110540

7. Niazi M, Alizadeh E, Zarebkohan A, Seidi K, Ayoubi-Joshaghani MH, Azizi M, et al. Advanced bioresponsive multitasking hydrogels in the new era of biomedicine. *Advanced Funct Materials.* (2021) 30(45):2104123. doi: 10.1002/adfm.202104123

8. Madamsetty VS, Tavakol S, Moghassemi S, Dadashzadeh A, Schneible JD, Fatemi I, et al. Chitosan: A versatile bio-platform for breast cancer theranostics. *J Controlled Release.* (2022) 341:733–52. doi: 10.1016/j.jconrel.2021.12.012

9. Ayoubi-Joshaghani MH, Seidi K, Azizi M, Jaymand M, Javaheri T, Jahanban-Esfahlan R, et al. Potential applications of advanced Nano/Hydrogels in biomedicine: Static, dynamic, multi-stage, and bioinspired. *Adv Fun Mater* (2020) 30(n/a):2004098. doi: 10.1002/adfm.202004098

10. Chuan D, Jin T, Fan R, Zhou L, Guo G. Chitosan for gene delivery: Methods for improvement and applications. *Adv Colloid Interface Science.* (2019) 268:25–38. doi: 10.1016/j.cis.2019.03.007

11. Hoque J, Adhikary U, Yadav V, Samaddar S, Konai MM, Prakash RG, et al. Chitosan derivatives active against multidrug-resistant bacteria and pathogenic fungi: *In vivo* evaluation as topical antimicrobials. *Mol Pharmaceutics.* (2016) 13 (10):3578–89. doi: 10.1021/acs.molpharmaceut.6b00764

12. Saeed RM, Dmour I, Taha MO. Stable chitosan-based nanoparticles using polyphosphoric acid or hexametaphosphate for tandem Ionotropic/Covalent crosslinking and subsequent investigation as novel vehicles for drug delivery. *Front Bioengineering Biotechnol* (2020) 8:4. doi: 10.3389/fbioe.2020.00004

13. Lara-Velazquez M, Alkharboosh R, Norton ES, Ramirez-Loera C, Freeman WD, Guerrero-Cazares H, et al. Chitosan-based non-viral gene and drug delivery systems for brain cancer. *Front Neurol* (2020) 11:740. doi: 10.3389/fneur.2020.00740

14. Herdiana Y, Wathoni N, Shamsuddin S, Muchtaridi M. Drug release study of the chitosan-based nanoparticles. *Heliyon* (2022) 8(1):e08674. doi: 10.1016/j.heliyon.2021.e08674

15. Niu S, Williams GR, Wu J, Wu J, Zhang X, Chen X, et al. A chitosan-based cascade-responsive drug delivery system for triple-negative breast cancer therapy. *J Nanobiotechnology.* (2019) 17(1):95. doi: 10.1186/s12951-019-0529-4

16. Li J, Cai C, Li J, Li J, Li J, Sun T, et al. Chitosan-based nanomaterials for drug delivery. *Molecules* (2018) 23(10):2661. doi: 10.3390/molecules23102661

17. Rao W, Wang H, Han J, Zhao S, Dumbleton J, Agarwal P, et al. Chitosan-decorated doxorubicin-encapsulated nanoparticle targets and eliminates tumor reinitiating cancer stem-like cells. *ACS Nano.* (2015) 9(6):5725–40. doi: 10.1021/nn506928p

18. Lin F, Jia H-R, Wu F-G. Glycol chitosan: A water-soluble polymer for cell imaging and drug delivery. *Molecules* (2019) 24(23):4371. doi: 10.3390/molecules24234371

19. Yang Y, Wang S, Wang Y, Wang X, Wang Q, Chen M. Advances in self-assembled chitosan nanomaterials for drug delivery. *Biotechnol Advances.* (2014) 32(7):1301–16. doi: 10.1016/j.biotechadv.2014.07.007

20. Li R, Zhang Y, Lin Z, Lei Q, Liu Y, Li X, et al. Injectable halloysite-g-chitosan hydrogels as drug carriers to inhibit breast cancer recurrence. *Composites Part B: Engineering.* (2021) 221:109031. doi: 10.1016/j.compositesb.2021.109031

21. Omer AM, Ziora ZM, Tamer TM, Khalifa RE, Hassan MA, Mohy-Eldin MS, et al. Formulation of quaternized aminated chitosan nanoparticles for efficient encapsulation and slow release of curcumin. *Molecules* (2021) 26(2):449. doi: 10.3390/molecules26020449

22. Ding Y, Yang R, Yu W, Hu C, Zhang Z, Liu D, et al. Chitosan oligosaccharide decorated liposomes combined with TH302 for photodynamic therapy in triple negative breast cancer. *J Nanobiotechnology.* (2021) 19(1):147. doi: 10.1186/s12951-021-00891-8

23. Wiranowska M, Singh R, Falahat R, Williams E, Johnson JO, Alcantar N. Preferential drug delivery to tumor cells than normal cells using a tunable niosome–chitosan double package nanodelivery system: a novel *in vitro* model. *Cancer Nanotechnology.* (2020) 11(1):3. doi: 10.1186/s12645-020-00059-3

24. Kang SH, Revuri V, Lee S-J, Cho S, Park I-K, Cho KJ, et al. Oral siRNA delivery to treat colorectal liver metastases. *ACS Nano.* (2017) 11(10):10417–29. doi: 10.1021/acsnano.7b05547

25. Liu Y, Xu J, Choi HH, Han C, Fang Y, Li Y, et al. Targeting 17q23 amplicon to overcome the resistance to anti-HER2 therapy in HER2+ breast cancer. *Nat Commun* (2018) 9(1):4718. doi: 10.1038/s41467-018-07264-0

26. Zhang B-C, Wu P-Y, Zou J-J, Jiang J-L, Zhao R-R, Luo B-Y, et al. Efficient CRISPR/Cas9 gene-chemo synergistic cancer therapy *via* a stimuli-responsive chitosan-based nanocomplex elicits anti-tumorigenic pathway effect. *Chem Eng J* (2020) 393:124688. doi: 10.1016/j.cej.2020.124688

27. Daniels AN, Singh M. Sterically stabilized siRNA:gold nanocomplexes enhance c-MYC silencing in a breast cancer cell model. *Nanomedicine (London England).* (2019) 14(11):1387–401. doi: 10.2217/nnm-2018-0462

28. Abrica-González P, Zamora-Justo JA, Sotelo-López A, Vázquez-Martínez GR, Balderas-López JA, Muñoz-Diosdado A, et al. Gold nanoparticles with chitosan, n-acylated chitosan, and chitosan oligosaccharide as DNA carriers. *Nanoscale Res Letters.* (2019) 14(1):258. doi: 10.1186/s11671-019-3083-y

29. Alameh M, Lavertu M, Tran-Khanh N, Chang C-Y, Lesage F, Bail M, et al. siRNA delivery with chitosan: Influence of chitosan molecular weight, degree of deacetylation, and amine to phosphate ratio on in vitro silencing efficiency, hemocompatibility, biodistribution, and in vivo efficacy. *Biomacromolecules* (2018) 19(1):112–31. doi: 10.1021/acs.biomac.7b01297

30. Huang X, Xu C, Li Y, Cheng H, Wang X, Sun R. Quaternized chitosan-stabilized copper sulfide nanoparticles for cancer therapy. *Materials Sci Engineering: C.* (2019) 96:129–37. doi: 10.1016/j.msec.2018.10.062

31. Li L, Hu X, Zhang M, Ma S, Yu F, Zhao S, et al. Dual tumor-targeting nanocarrier system for siRNA delivery based on pRNA and modified chitosan. *Mol Ther - Nucleic Acids* (2017) 8:169–83. doi: 10.1016/j.omtn.2017.06.014

32. Malik A, Gupta M, Gupta V, Gogoi H, Bhatnagar R. Novel application of trimethyl chitosan as an adjuvant in vaccine delivery. *Int J Nanomedicine.* (2018) 13:7959–70. doi: 10.2147/IJN.S165876

33. Boontha S, Unginger HE, Waranuch N, Polnok A, Pitaksuteepong T. Chitosan and trimethyl chitosan particles as oral vaccine delivery systems: Comparison of the potential to initiate immune responses. *J Metals Materials Minerals* (2011) 21(1):43–7.

34. Qin T, Ma S, Miao X, Tang Y, Huangfu D, Wang J, et al. Mucosal vaccination for influenza protection enhanced by catalytic immune-adjuvant. *Advanced Science.* (2020) 7(18):2000771. doi: 10.1002/advs.202000771

35. Fayed ND, Goda AE, Essa EA, El Maghraby GM. Chitosan-encapsulated niosomes for enhanced oral delivery of atorvastatin. *J Drug Delivery Sci Technology.* (2021) 66:102866. doi: 10.1016/j.jddst.2021.102866

36. Chen G, Zhao Y, Xu Y, Zhu C, Liu T, Wang K. Chitosan nanoparticles for oral photothermally enhanced photodynamic therapy of colon cancer. *Int J Pharmaceutics.* (2020) 589:119763. doi: 10.1016/j.ijpharm.2020.119763

37. Moreira AF, Rodrigues CF, Jacinto TA, Miguel SP, Costa EC, Correia IJ. Poly (vinyl alcohol)/chitosan layer-by-layer microneedles for cancer chemo-photothermal therapy. *Int J Pharm* (2020) 576:118907. doi: 10.1016/j.ijpharm.2019.118907

38. Niu S, Zhang X, Williams GR, Wu J, Gao F, Fu Z, et al. Hollow mesoporous silica nanoparticles gated by chitosan-copper sulfide composites as theranostic agents for the treatment of breast cancer. *Acta Biomaterialia.* (2021) 126:408–20. doi: 10.1016/j.actbio.2021.03.024

39. Fathy MM, Mohamed FS, Elbialy N, Elshemey WM. Multifunctional chitosan-capped gold nanoparticles for enhanced cancer chemo-radiotherapy: An invitro study. *Physica Medica: Eur J Med Physics.* (2018) 48:76–83. doi: 10.1016/j.ejmp.2018.04.002

40. Wang Y, Yu H, Wang S, Gai C, Cui X, Xu Z, et al. Targeted delivery of quercetin by nanoparticles based on chitosan sensitizing paclitaxel-resistant lung cancer cells to paclitaxel. *Materials Sci Engineering: C.* (2021) 119:111442. doi: 10.1016/j.msec.2020.111442

41. Yoon HY, Son S, Lee SJ, You DG, Yhee JY, Park JH, et al. Glycol chitosan nanoparticles as specialized cancer therapeutic vehicles: Sequential delivery of doxorubicin and bcl-2 siRNA. *Sci Rep* (2014) 4(1):6878. doi: 10.1038/srep06878

42. Itoo AM, Paul M, Ghosh B, Biswas S. Oxaliplatin delivery *via* chitosan/vitamin e conjugate micelles for improved efficacy and MDR-reversal in breast cancer. *Carbohydr Polymers.* (2022) 282:119108. doi: 10.1016/j.carbpol.2022.119108

43. Niu S, Williams GR, Wu J, Wu J, Zhang X, Zheng H, et al. A novel chitosan-based nanomedicine for multi-drug resistant breast cancer therapy. *Chem Eng J* (2019) 369:134–49. doi: 10.1016/j.cej.2019.02.201

44. Lee J-Y, Termsarasab U, Lee MY, Kim D-H, Lee SY, Kim JS, et al. Chemosensitizing indomethacin-conjugated chitosan oligosaccharide nanoparticles for tumor-targeted drug delivery. *Acta Biomaterialia.* (2017) 57:262–73. doi: 10.1016/j.actbio.2017.05.012

45. Brasselet C, Pierre G, Dubessay P, Dols-Lafargue M, Coulon J, Maupeu J, et al. Modification of chitosan for the generation of functional derivatives. *Appl Sci* (2019) 9(7):1321. doi: 10.3390/app9071321

46. Pandya AD, Øverbye A, Sahariah P, Gaware VS, Høgset H, Masson M, et al. Drug-loaded photosensitizer-chitosan nanoparticles for combinatorial chemo- and photodynamic-therapy of cancer. *Biomacromolecules* (2020) 21(4):1489–98. doi: 10.1021/acs.biomac.0c00061

47. Wang W, Meng Q, Li Q, Liu J, Zhou M, Jin Z, et al. Chitosan derivatives and their application in biomedicine. *Int J Mol Sci* (2020) 21(2):487. doi: 10.3390/ijms21020487

48. Sahariah P, Másson M. Antimicrobial chitosan and chitosan derivatives: A review of the structure–activity relationship. *Biomacromolecules* (2017) 18 (11):3846–68. doi: 10.1021/acs.biomac.7b01058

49. Jaymand M. Chemically modified natural polymer-based theranostic nanomedicines: Are they the golden gate toward a de Novo clinical approach against cancer? *ACS Biomaterials Sci Eng* (2020) 6(1):134–66. doi: 10.1021/acsbiomaterials.9b00802

50. Cele ZED, Somboro AM, Amoako DG, Ndlandla LF, Balogun MO. Fluorinated quaternary chitosan derivatives: Synthesis, characterization, antibacterial activity, and killing kinetics. *ACS Omega.* (2020) 5(46):29657–66. doi: 10.1021/acsomega.0c01355

51. Ojeda-Hernández DD, Canales-Aguirre AA, Matias-Guiu J, Gomez-Pinedo U, Mateos-Díaz JC. Potential of chitosan and its derivatives for biomedical applications in the central nervous system. *Front Bioengineering Biotechnol* (2020) 8. doi: 10.3389/fbioe.2020.00389

52. Abbasian M, Seyyedi M, Jaymand M. Modification of thermoplastic polyurethane through the grafting of well-defined polystyrene and preparation of its polymer/clay nanocomposite. *Polymer Bulletin.* (2020) 77(3):1107–20. doi: 10.1007/s00289-019-02773-4

53. Hatamzadeh M, Jaymand M. Synthesis of conductive polyaniline-modified polymers *via* a combination of nitroxide-mediated polymerization and "click chemistry". *RSC Advances.* (2014) 4(54):28653–63. doi: 10.1039/C4RA00864B

54. Massoumi B, Mousavi-Hamamlu S-V, Ghamkhari A, Jaymand M. A novel strategy for synthesis of Polystyrene/Fe3O4 nanocomposite: RAFT polymerization, functionalization, and coordination techniques. *Polymer-Plastics Technol Engineering.* (2017) 56(8):873–82. doi: 10.1080/03602559.2016.1233270

55. Liu J, Li H-J, Luo Y-L, Xu C-F, Du X-J, Du J-Z, et al. Enhanced primary tumor penetration facilitates nanoparticle draining into lymph nodes after systemic injection for tumor metastasis inhibition. *ACS Nano.* (2019) 13(8):8648–58. doi: 10.1021/acsnano.9b03472

56. Sun I-C, Jo S, Dumani D, Yun WS, Yoon HY, Lim D-K, et al. Theragnostic glycol chitosan-conjugated gold nanoparticles for photoacoustic imaging of regional lymph nodes and delivering tumor antigen to lymph nodes. *Nanomaterials (Basel).* (2021) 11(7):1700. doi: 10.3390/nano11071700

57. Li G, Wang S, Deng D, Xiao Z, Dong Z, Wang Z, et al. Fluorinated chitosan to enhance transmucosal delivery of sonosensitizer-conjugated catalase for sonodynamic bladder cancer treatment post-intravesical instillation. *ACS Nano.* (2020) 14(2):1586–99. doi: 10.1021/acsnano.9b06689

58. Sun R, Liu X, Li G, Wang H, Luo Y, Huang G, et al. A photo-activated H2 nanogenerator for enhanced chemotherapy of bladder cancer. *ACS Nano* (2020) 14 (7):8135–48. doi: 10.1021/acsnano.0c01300

59. Cheng X, Zeng X, Zheng Y, Wang X, Tang R. Surface-fluorinated and pH-sensitive carboxymethyl chitosan nanoparticles to overcome biological barriers for improved drug delivery in vivo. *Carbohydr Polymers* (2019) 208:59–69. doi: 10.1016/j.carbpol.2018.12.063

60. Chokradjaroen C, Theeramunkong S, Yui H, Saito N, Rujiravanit R. Cytotoxicity against cancer cells of chitosan oligosaccharides prepared from chitosan powder degraded by electrical discharge plasma. *Carbohydr Polymers.* (2018) 201:20–30. doi: 10.1016/j.carbpol.2018.08.037

61. Lohiya G, Katti DS. Carboxylated chitosan-mediated improved efficacy of mesoporous silica nanoparticle-based targeted drug delivery system for breast cancer therapy. *Carbohydr Polymers.* (2022) 277:118822. doi: 10.1016/j.carbpol.2021.118822

62. Ghasemi Goorbandi R, Mohammadi MR, Malekzadeh K. Synthesizing efficacious genistein in conjugation with superparamagnetic Fe(3)O(4) decorated with bio-compatible carboxymethylated chitosan against acute leukemia lymphoma. *Biomater Res* (2020) 24:9–. doi: 10.1186/s40824-020-00187-2

63. He G, Yan X, Miao Z, Qian H, Ma Y, Xu Y, et al. Anti-inflammatory catecholic chitosan hydrogel for rapid surgical trauma healing and subsequent prevention of tumor recurrence. *Chin Chem Letters.* (2020) 31(7):1807–11. doi: 10.1016/j.cclet.2020.02.032

64. Li Y, Wang W, Zhang Y, Wang X, Gao X, Yuan Z, et al. Chitosan sulfate inhibits angiogenesis *via* blocking the VEGF/VEGFR2 pathway and suppresses tumor growth in vivo. *Biomaterials Sci* (2019) 7(4):1584–97. doi: 10.1039/C8BM01337C

65. Wang S, Chen B, Ouyang L, Wang D, Tan J, Qiao Y, et al. A novel stimuli-responsive injectable antibacterial hydrogel to achieve synergetic Photothermal/Gene-targeted therapy towards uveal melanoma. *Advanced Sci* (2021) n/a(n/a):2004721. doi: 10.1002/advs.202004721

66. Qu D, Jiao M, Lin H, Tian C, Qu G, Xue J, et al. Anisamide-functionalized pH-responsive amphiphilic chitosan-based paclitaxel micelles for sigma-1 receptor targeted prostate cancer treatment. *Carbohydr Polymers.* (2020) 229:115498. doi: 10.1016/j.carbpol.2019.115498

67. Nguyen KT, Vinh Le D, Ho Do D, Huan Le Q. Development of chitosan graft pluronic ® F127 copolymer nanoparticles containing DNA aptamer for paclitaxel delivery to treat breast cancer cells. *Adv Natural Sciences: Nanoscience Nanotechnology* (2016) 7(2):025018. doi: 10.1088/2043-6262/7/2/025018

68. Bobbala S, Gibson B, Gamble AB, McDowell A, Hook S. Poloxamer 407-chitosan grafted thermoresponsive hydrogels achieve synchronous and sustained release of antigen and adjuvant from single-shot vaccines. *Immunol Cell Biol* (2018) 96(6):656–65. doi: 10.1111/imcb.12031

69. Caprifico AE, Foot PJS, Polycarpou E, Calabrese G. Overcoming the protein corona in chitosan-based nanoparticles. *Drug Discovery Today* (2021) 26(8):1825–40. doi: 10.1016/j.drudis.2021.04.014

70. Cheng Y-H, He C, Riviere JE, Monteiro-Riviere NA, Lin Z. Meta-analysis of nanoparticle delivery to tumors using a physiologically based pharmacokinetic modeling and simulation approach. *ACS Nano.* (2020) 14(3):3075–95. doi: 10.1021/acsnano.9b08142

71. Seidi K, Neubauer HA, Moriggl R, Jahanban-Esfahlan R, Javaheri T. Tumor target amplification: Implications for nano drug delivery systems. *J Controlled release Off J Controlled Release Society.* (2018) 275:142–61. doi: 10.1016/j.jconrel.2018.02.020

72. Seidi K, Jahanban-Esfahlan R, Monhemi H, Zare P, Minofar B, Daei Farshchi Adli A, et al. NGR (Asn-Gly-Arg)-targeted delivery of coagulase to tumor vasculature arrests cancer cell growth. *Oncogene* (2018) 37:3967–80. doi: 10.1038/s41388-018-0213-4

73. Puig-Saus C, Rojas LA, Laborda E, Figueras A, Alba R, Fillat C, et al. iRGD tumor-penetrating peptide-modified oncolytic adenovirus shows enhanced tumor transduction, intratumoral dissemination and antitumor efficacy. *Gene Ther* (2014) 21(8):767–74. doi: 10.1038/gt.2014.52

74. Zhu Y, Wen L, Shao S, Tan Y, Meng T, Yang X, et al. Inhibition of tumor-promoting stroma to enforce subsequently targeting AT(1)R on tumor cells by pathological inspired micelles. *Biomaterials* (2018) 161:33–46. doi: 10.1016/j.biomaterials.2018.01.023

75. Miao D, Jiang M, Liu Z, Gu G, Hu Q, Kang T, et al. Co-Administration of dual-targeting nanoparticles with penetration enhancement peptide for antiglioblastoma therapy. *Mol Pharmaceutics.* (2014) 11(1):90–101. doi: 10.1021/mp400189j

76. Liang Y, Wang Y, Wang L, Liang Z, Li D, Xu X, et al. Self-crosslinkable chitosan-hyaluronic acid dialdehyde nanoparticles for CD44-targeted siRNA delivery to treat bladder cancer. *Bioactive Materials.* (2021) 6(2):433–46. doi: 10.1016/j.bioactmat.2020.08.019

77. Deng X, Cao M, Zhang J, Hu K, Yin Z, Zhou Z, et al. Hyaluronic acid-chitosan nanoparticles for co-delivery of MiR-34a and doxorubicin in therapy against triple negative breast cancer. *Biomaterials* (2014) 35(14):4333–44. doi: 10.1016/j.biomaterials.2014.02.006

78. Buerkle MA, Pahernik SA, Sutter A, Jonczyk A, Messmer K, Dellian M. Inhibition of the alpha-nu integrins with a cyclic RGD peptide impairs angiogenesis, growth and metastasis of solid tumours in vivo. *Br J Cancer* (2002) 86(5):788–95. doi: 10.1038/sj.bjc.6600141

79. Yadav A, Nalukurthi N, Gorain M, Bulbule A, Shetti D, Roy G, et al. RGD functionalized chitosan nanoparticle mediated targeted delivery of raloxifene selectively suppresses angiogenesis and tumor growth in breast cancer. *Nanoscale* (2020) 12(19):10664–10684. doi: 10.1039/C9NR10673A

80. Zhang S, Li G, Deng D, Dai Y, Liu Z, Wu S. Fluorinated chitosan mediated synthesis of copper selenide nanoparticles with enhanced penetration for second

near-infrared photothermal therapy of bladder cancer. *Advanced Ther* (2021) 4 (7):2100043. doi: 10.1002/adtp.202100043

81. Cui L, Liu W, Liu H, Qin Q, Wu S, He S, et al. pH-triggered charge-reversal mesoporous silica nanoparticles stabilized by chitosan Oligosaccharide/ Carboxymethyl chitosan hybrids for effective intracellular delivery of doxorubicin. *ACS Appl Bio Materials*. (2019) 2(5):1907–19. doi: 10.1021/ acsabm.8b00830

82. Wang X, He L, Wei B, Yan G, Wang J, Tang R. Bromelain-immobilized and lactobionic acid-modified chitosan nanoparticles for enhanced drug penetration in tumor tissues. *Int J Biol Macromolecules*. (2018) 115:129–42. doi: 10.1016/ j.ijbiomac.2018.04.076

83. Song Q, Yin Y, Shang L, Wu T, Zhang D, Kong M, et al. Tumor microenvironment responsive nanogel for the combinatorial antitumor effect of chemotherapy and immunotherapy. *Nano letters*. (2017) 17(10):6366–75. doi: 10.1021/acs.nanolett.7b03186

84. Zhu J, Xiao T, Zhang J, Che H, Shi Y, Shi X, et al. Surface-Charge-Switchable nanoclusters for magnetic resonance imaging-guided and glutathione depletion-enhanced photodynamic therapy. *ACS Nano*. (2020) 14(9):11225–37. doi: 10.1021/ acsnano.0c03080

85. Cheng X, Li H, Ge X, Chen L, Liu Y, Mao W, et al. Tumor-microenvironment- responsive size-shrinkable drug-delivery nanosystems for deepened penetration into tumors. *Front Mol Biosci* (2020) 7. doi: 10.3389/ fmolb.2020.576420

86. Yong T, Zhang X, Bie N, Zhang H, Zhang X, Li F, et al. Tumor exosome-based nanoparticles are efficient drug carriers for chemotherapy. *Nat Commun* (2019) 10(1):3838. doi: 10.1038/s41467-019-11718-4

87. Chen Q, Liu G, Liu S, Su H, Wang Y, Li J, et al. Remodeling the tumor microenvironment with emerging nanotherapeutics. *Trends Pharmacol Sci* (2018) 39(1):59–74. doi: 10.1016/j.tips.2017.10.009

88. Kuhn SJ, Finch SK, Hallahan DE, Giorgio TD. Proteolytic surface functionalization enhances *in vitro* magnetic nanoparticle mobility through extracellular matrix. *Nano letters*. (2006) 6(2):306–12. doi: 10.1021/nl052241g

89. Zhang L, Wang Y, Xia T, Yu Q, Zhang Q, Yang Y, et al. Suppression for lung metastasis by depletion of collagen I and lysyl oxidase *via* losartan assisted with paclitaxel-loaded pH-sensitive liposomes in breast cancer. *Drug delivery*. (2016) 23 (8):2970–9. doi: 10.3109/10717544.2015.1132798

90. Parodi A, Haddix SG, Taghipour N, Scaria S, Taraballi F, Cevenini A, et al. Bromelain surface modification increases the diffusion of silica nanoparticles in the tumor extracellular matrix. *ACS Nano*. (2014) 8(10):9874–83. doi: 10.1021/ nn502807n

91. You DG, Yoon HY, Jeon S, Um W, Son S, Park JH, et al. Deep tissue penetration of nanoparticles using pulsed-high intensity focused ultrasound. *Nano Convergence*. (2017) 4(1):30. doi: 10.1186/s40580-017-0124-z

92. Liu X, Ye N, Xiao C, Wang X, Li S, Deng Y, et al. Hyperbaric oxygen regulates tumor microenvironment and boosts commercialized nanomedicine delivery for potent eradication of cancer stem-like cells. *Nano Today* (2021) 40:101248. doi: 10.1016/j.nantod.2021.101248

93. Yang X, Lian K, Tan Y, Zhu Y, Liu X, Zeng Y, et al. Selective uptake of chitosan polymeric micelles by circulating monocytes for enhanced tumor targeting. *Carbohydr Polym*. (2020) 229:115435. doi: 10.1016/ j.carbpol.2019.115435

94. Bhattacharyya S, Ghosh SS. Transmembrane TNFα-expressed macrophage membrane-coated chitosan nanoparticles as cancer therapeutics. *ACS Omega*. (2020) 5(3):1572–80. doi: 10.1021/acsomega.9b03531

95. Jahanban-Esfahlan R, Seidi K, Banimohamad-Shotorbani B, Jahanban-Esfahlan A, Yousefi B. Combination of nanotechnology with vascular targeting agents for effective cancer therapy. *J Cell Physiol* (2017) 233(4):2982–92. doi: 10.1002/jcp.26051

96. Jahanban-Esfahlan R, de la Guardia M, Ahmadi D, Yousefi B. Modulating tumor hypoxia by nanomedicine for effective cancer therapy. *J Cell Physiol* (2017) 233(3):2019–31. doi: 10.1002/jcp.25859

97. Emami Nejad A, Najafgholian S, Rostami A, Sistani A, Shojaeifar S, Esparvarinha M, et al. The role of hypoxia in the tumor microenvironment and development of cancer stem cell: a novel approach to developing treatment. *Cancer Cell Int* (2021) 21(1):62. doi: 10.1186/s12935-020-01719-5

98. Yang J, Li W, Luo L, Jiang M, Zhu C, Qin B, et al. Hypoxic tumor therapy by hemoglobin-mediated drug delivery and reversal of hypoxia-induced chemoresistance. *Biomaterials* (2018) 182:145–56. doi: 10.1016/ j.biomaterials.2018.08.004

99. Zhou Z-h, Liang S-y, Zhao T-c, Chen X-z, Cao X-k, Qi M, et al. Overcoming chemotherapy resistance using pH-sensitive hollow MnO2 nanoshells that target the hypoxic tumor microenvironment of metastasized oral squamous cell carcinoma. *J Nanobiotechnology*. (2021) 19(1):157. doi: 10.1186/s12951-021-00901-9

100. She J, Zhou X, Zhang Y, Zhang R, Li Q, Zhu W, et al. Thermo-triggered *In situ* chitosan-based gelation system for repeated and enhanced sonodynamic therapy post a single injection. *Advanced healthcare materials*. (2021) 10(3): e2001208. doi: 10.1002/adhm.202001208

101. Jahanban-Esfahlan R, Seidi K, Monhemi H, Adli ADF, Minofar B, Zare P, et al. RGD delivery of truncated coagulase to tumor vasculature affords local thrombotic activity to induce infarction of tumors in mice. *Sci Rep* (2017) 7 (1):8126. doi: 10.1038/s41598-017-05326-9

102. Adli ADF, Jahanban-Esfahlan R, Seidi K, Farajzadeh D, Behzadi R, Zarghami N. Co-Administration of vadimezan and recombinant coagulase-NGR inhibits growth of melanoma tumor in mice. *Advanced Pharm Bull* (2020) 11 (2):385–92. doi: 10.34172/apb.2021.037

103. Li S, Jiang Q, Liu S, Zhang Y, Tian Y, Song C, et al. A DNA nanorobot functions as a cancer therapeutic in response to a molecular trigger in vivo. *Nat Biotechnol* (2018) 36(3):258–64. doi: 10.1038/nbt.4071

104. Zhang C, Ni D, Liu Y, Yao H, Bu W, Shi J. Magnesium silicide nanoparticles as a deoxygenation agent for cancer starvation therapy. *Nat Nanotechnology*. (2017) 12(4):378–86. doi: 10.1038/nnano.2016.280

105. Chen H, Fu Y, Feng K, Zhou Y, Huang H, Chen Y, et al. Polydopamine-coated UiO-66 nanoparticles loaded with perfluorotributylamine/tirapazamine for hypoxia-activated osteosarcoma therapy. *J Nanobiotechnology* (2021) 19(1):298. doi: 10.1186/s12951-021-01013-0

106. Yuan P, Dou G, Liu T, Guo X, Bai Y, Chu D, et al. On-demand manipulation of tumorigenic microenvironments by nano-modulator for synergistic tumor therapy. *Biomaterials* (2021) 275:120956. doi: 10.1016/ j.biomaterials.2021.120956

107. Chang C-C, Dinh TK, Lee Y-A, Wang F-N, Sung Y-C, Yu P-L, et al. Nanoparticle delivery of MnO2 and antiangiogenic therapy to overcome hypoxia-driven tumor escape and suppress hepatocellular carcinoma. *ACS Appl Materials Interfaces*. (2020) 12(40):44407–19. doi: 10.1021/acsami.0c08473

108. Lin T, Zhao X, Zhao S, Yu H, Cao W, Chen W, et al. O2 generating MnO2 nanoparticles for enhanced photodynamic therapy of bladder cancer by ameliorating hypoxia. *Theranostics* (2018) 8(4):990–1004. doi: 10.7150/thno.22465

109. Chen SX, Xue F, Kuang Y, Chen S, Sheng D, Chen H. A self-activating nanovesicle with oxygen-depleting capability for efficient hypoxia-responsive chemo-thermo cancer therapy. *Biomaterials* (2021) 269:120533. doi: 10.1016/ j.biomaterials.2020.120533

110. Im S, Lee J, Park D, Park A, Kim Y-M, Kim WJ. Hypoxia-triggered transforming immunomodulator for cancer immunotherapy *via* photodynamically enhanced antigen presentation of dendritic cell. *ACS Nano*. (2019) 13(1):476–88. doi: 10.1021/acsnano.8b07045

111. Li S, Zhang Y, Ho SH, Li B, Wang M, Deng X, et al. Combination of tumour-infarction therapy and chemotherapy *via* the co-delivery of doxorubicin and thrombin encapsulated in tumour-targeted nanoparticles. *Nat Biomed engineering*. (2020) 4(7):732–42. doi: 10.1038/s41551-020-0573-2

112. Uthaman S, Kim Y, Lee JY, Pillarisetti S, Huh KM, Park I-K. Self-quenched polysaccharide nanoparticles with a reactive oxygen species-sensitive cascade for enhanced photodynamic therapy. *ACS Appl Materials Interfaces*. (2020) 12 (25):28004–13. doi: 10.1021/acsami.0c06311

113. Jang EH, Shim MK, Kim GL, Kim S, Kang H, Kim J-H. Hypoxia-responsive folic acid conjugated glycol chitosan nanoparticle for enhanced tumor targeting treatment. *Int J pharmaceutics*. (2020) 580:119237. doi: 10.1016/ j.ijpharm.2020.119237

114. Qiu Y, Chen T, Hu R, Zhu R, Li C, Ruan Y, et al. Next frontier in tumor immunotherapy: macrophage-mediated immune evasion. *biomark Res* (2021) 9 (1):72. doi: 10.1186/s40364-021-00327-3

115. Zeng Y, Xiang Y, Sheng R, Tomás H, Rodrigues J, Gu Z, et al. Polysaccharide-based nanomedicines for cancer immunotherapy: A review. *Bioact Mater* (2021) 6(10):3358–82. doi: 10.1016/j.bioactmat.2021.03.008

116. Singh B, Maharjan S, Sindurakar P, Cho K-H, Choi Y-J, Cho C-S. Needle-free immunization with chitosan-based systems. *Int J Mol Sci* (2018) 19(11):3639. doi: 10.3390/ijms19113639

117. Choi JJ, Le Q-V, Kim D, Kim YB, Shim G, Oh Y-K. High molecular weight chitosan-complexed RNA nanoadjuvant for effective cancer immunotherapy. *Pharmaceutics* (2019) 11(12):680. doi: 10.3390/pharmaceutics11120680

118. Liang X, Mu M, Fan R, Zou B, Guo G. Functionalized chitosan as a promising platform for cancer immunotherapy: A review. *Carbohydr Polymers*. (2022) 290:119452. doi: 10.1016/j.carbpol.2022.119452

119. Yao X, Jovevski JJ, Todd MF, Xu R, Li Y, Wang J, et al. Nanoparticle-mediated intracellular protection of natural killer cells avoids cryoinjury and retains potent antitumor functions. *Advanced Science*. (2020) 7(9):1902938. doi: 10.1002/advs.201902938

120. Castro F, Pinto ML, Pereira CL, Serre K, Barbosa MA, Vermaelen K, et al. Chitosan/γ-PGA nanoparticles-based immunotherapy as adjuvant to radiotherapy

in breast cancer. *Biomaterials* (2020) 257:120218. doi: 10.1016/j.biomaterials.2020.120218

121. Li Z, He Y, Deng L, Zhang Z-R, Lin Y. A fast-dissolving microneedle array loaded with chitosan nanoparticles to evoke systemic immune responses in mice. *J Materials Chem B* (2020) 8(2):216–25. doi: 10.1039/C9TB02061F

122. Han HD, Byeon Y, Jang J-H, Jeon HN, Kim GH, Kim MG, et al. *In vivo* stepwise immunomodulation using chitosan nanoparticles as a platform nanotechnology for cancer immunotherapy. *Sci Rep* (2016) 6(1):38348. doi: 10.1038/srep38348

123. Seidi K, Ayoubi-Joshaghani MH, Azizi M, Javaheri T, Jaymand M, Alizadeh E, et al. Bioinspired hydrogels build a bridge from bench to bedside. *Nano Today* (2021) 39:101157. doi: 10.1016/j.nantod.2021.101157

124. Chiu YH, Chen MC, Wan SW. Sodium Hyaluronate/Chitosan composite microneedles as a single-dose intradermal immunization system. *Biomacromolecules* (2018) 19(6):2278–85. doi: 10.1021/acs.biomac.8b00441

125. Phuengkham H, Ren L, Shin IW, Lim YT. Nanoengineered immune niches for reprogramming the immunosuppressive tumor microenvironment and enhancing cancer immunotherapy. *Advanced Materials.* (2019) 31(34):1803322. doi: 10.1002/adma.201803322

126. Dianat-Moghadam H, Heydarifard M, Jahanban-Esfahlan R, Panahi Y, Hamishehkar H, Pouremamali F, et al. Cancer stem cells-emanated therapy resistance: Implications for liposomal drug delivery systems. *J Controlled release Off J Controlled Release Society*. (2018) 288:62–83. doi: 10.1016/j.jconrel.2018.08.043

127. Gupta PB, Onder TT, Jiang G, Tao K, Kuperwasser C, Weinberg RA, et al. Identification of selective inhibitors of cancer stem cells by high-throughput screening. *Cell* (2009) 138(4):645–59. doi: 10.1016/j.cell.2009.06.034

128. Geng Y, Amante JJ, Goel HL, Zhang X, Walker MR, Luther DC, et al. Differentiation of cancer stem cells through nanoparticle surface engineering. *ACS Nano*. (2020) 14(11):15276–85. doi: 10.1021/acsnano.0c05589

129. Hou Y, Sun X, Yao S, Rao W, He X. Cryoablation-activated enhanced nanodoxorubicin release for the therapy of chemoresistant mammary cancer stem-like cells. *J Mater Chem B* (2020) 8(5):908–18. doi: 10.1039/C9TB01922G

130. Wang H, Agarwal P, Zhao S, Xu RX, Yu J, Lu X, et al. Hyaluronic acid-decorated dual responsive nanoparticles of pluronic F127, PLGA, and chitosan for targeted co-delivery of doxorubicin and irinotecan to eliminate cancer stem-like cells. *Biomaterials* (2015) 72:74–89. doi: 10.1016/j.biomaterials.2015.08.048

131. Nishi M, Sakai Y, Akutsu H, Nagashima Y, Quinn G, Masui S, et al. Induction of cells with cancer stem cell properties from nontumorigenic human mammary epithelial cells by defined reprogramming factors. *Oncogene* (2014) 33 (5):643–52. doi: 10.1038/onc.2012.614

132. Gao Y, Tang M, Leung E, Svirskis D, Shelling A, Wu Z. Dual or multiple drug loaded nanoparticles to target breast cancer stem cells. *RSC Advances*. (2020) 10(32):19089–105. doi: 10.1039/D0RA02801K

133. Chang P-H, Sekine K, Chao H-M, S-h H, Chern E. Chitosan promotes cancer progression and stem cell properties in association with wnt signaling in colon and hepatocellular carcinoma cells. *Sci Rep* (2017) 7(1):45751. doi: 10.1038/srep45751

134. Wang W, Lei B, Li L, Liu J, Li Z, Pang Y, et al. Single-cell proteomic profiling identifies nanoparticle enhanced therapy for triple negative breast cancer stem cells. *Cells* (2021) 10(11):2842. doi: 10.3390/cells10112842

135. Chen W, Cao R, Su W, Zhang X, Xu Y, Wang P, et al. Simple and fast isolation of circulating exosomes with a chitosan modified shuttle flow microchip for breast cancer diagnosis. *Lab Chip.* (2021) 21(9):1759–70. doi: 10.1039/D0LC01311K

136. Wang M, Xiao Y, Lin L, Zhu X, Du L, Shi X. A microfluidic chip integrated with hyaluronic acid-functionalized electrospun chitosan nanofibers for specific capture and nondestructive release of CD44-overexpressing circulating tumor cells. *Bioconjugate Chem* (2018) 29(4):1081–90. doi: 10.1021/acs.bioconjchem.7b00747

137. Wang Z-L, Ding P, Gao T, Chen C-C, Cao Y, Sun N, et al. Capture of circulating tumor cells by hydrogel-nanofiber substrate. *Chin J Analytical Chem* (2019) 47(8):1162–9. doi: 10.1016/S1872-2040(19)61180-1

138. Wang K, Chen Y, Ahn S, Zheng M, Landoni E, Dotti G, et al. GD2-specific CAR T cells encapsulated in an injectable hydrogel control retinoblastoma and preserve vision. *Nat Cancer*. (2020) 1(10):990–7. doi: 10.1038/s43018-020-00119-y

139. Won JE, Wi TI, Lee CM, Lee JH, Kang TH, Lee J-W, et al. NIR irradiation-controlled drug release utilizing injectable hydrogels containing gold-labeled liposomes for the treatment of melanoma cancer. *Acta Biomaterialia.* (2021) 136:508–18. doi: 10.1016/j.actbio.2021.09.062

140. Sedghi R, Gholami M, Shaabani A, Saber M, Niknejad H. Preparation of novel chitosan derivative nanofibers for prevention of breast cancer recurrence. *Eur Polymer J* (2020) 123:109421. doi: 10.1016/j.eurpolymj.2019.109421

141. Gao F, Xie W, Miao Y, Wang D, Guo Z, Ghosal A, et al. Magnetic hydrogel with optimally adaptive functions for breast cancer recurrence prevention. *Advanced healthcare materials*. (2019) 8(14):e1900203. doi: 10.1002/adhm.201900203

142. Wang W, Zhang Q, Zhang M, Lv X, Li Z, Mohammadniaei M, et al. A novel biodegradable injectable chitosan hydrogel for overcoming postoperative trauma and combating multiple tumors. *Carbohydr Polymers.* (2021) 265:118065. doi: 10.1016/j.carbpol.2021.118065

143. Yang X, Gao L, Wei Y, Tan B, Wu Y, Yi C, et al. Photothermal hydrogel platform for prevention of post-surgical tumor recurrence and improving breast reconstruction. *J Nanobiotechnology.* (2021) 19(1):307. doi: 10.1186/s12951-021-01041-w

144. Shi X, Cheng Y, Wang J, Chen H, Wang X, Li X, et al. 3D printed intelligent scaffold prevents recurrence and distal metastasis of breast cancer. *Theranostics* (2020) 10(23):10652–64. doi: 10.7150/thno.47933

145. Gu S, Xu J, Teng W, Huang X, Mei H, Chen X, et al. Local delivery of biocompatible lentinan/chitosan composite for prolonged inhibition of postoperative breast cancer recurrence. *Int J Biol Macromol.* (2022) 194:233–45. doi: 10.1016/j.ijbiomac.2021.11.186

146. Ampollini L, Sonvico F, Barocelli E, Cavazzoni A, Bilancia R, Mucchino C, et al. Intrapleural polymeric films containing cisplatin for malignant pleural mesothelioma in a rat tumour model: a preliminary study☆. *Eur J Cardio-Thoracic Surgery.* (2010) 37(3):557–65. doi: 10.1016/j.ejcts.2009.08.012

frontiers | Frontiers in Oncology

TYPE Original Research
PUBLISHED 14 December 2022
DOI 10.3389/fonc.2022.958673

OPEN ACCESS

EDITED BY
Zohreh Amoozgar,
Massachusetts General Hospital and Harvard Medical School, United States

REVIEWED BY
Rana Jahanban-Esfahlan,
Tabriz University of Medical Sciences, Iran
Tejaswi Koganti,
Mayo Clinic, United States

*CORRESPONDENCE
Jessica S. Blackburn
jsblackburn@uky.edu

†These authors have contributed equally to this work

SPECIALTY SECTION
This article was submitted to Cancer Genetics, a section of the journal Frontiers in Oncology

RECEIVED 31 May 2022
ACCEPTED 28 November 2022
PUBLISHED 14 December 2022

CITATION
Sampathi S, Chernyavskaya Y, Haney MG, Moore LH, Snyder IA, Cox AH, Fuller BL, Taylor TJ, Yan D, Badgett TC and Blackburn JS (2022) Nanopore sequencing of clonal IGH rearrangements in cell-free DNA as a biomarker for acute lymphoblastic leukemia. *Front. Oncol.* 12:958673. doi: 10.3389/fonc.2022.958673

Nanopore sequencing of clonal IGH rearrangements in cell-free DNA as a biomarker for acute lymphoblastic leukemia

Shilpa Sampathi[1†], Yelena Chernyavskaya[1†], Meghan G. Haney[1,2,3], L. Henry Moore[1,3], Isabel A. Snyder[1], Anna H. Cox[1,3], Brittany L. Fuller[4], Tamara J. Taylor[4], Donglin Yan[2,5], Tom C. Badgett[4] and Jessica S. Blackburn[1,2*]

[1]Department of Molecular and Cellular Biochemistry, University of Kentucky, Lexington, KY, United States, [2]Markey Cancer Center, University of Kentucky, Lexington, KY, United States, [3]College of Medicine, University of Kentucky, Lexington, KY, United States, [4]Department of Pediatric Oncology, University of Kentucky, Lexington, KY, United States, [5]Department of Biostatistics, University of Kentucky, Lexington, KY, United States

Background: Acute Lymphoblastic Leukemia (ALL) is the most common pediatric cancer, and patients with relapsed ALL have a poor prognosis. Detection of ALL blasts remaining at the end of treatment, or minimal residual disease (MRD), and spread of ALL into the central nervous system (CNS) have prognostic importance in ALL. Current methods to detect MRD and CNS disease in ALL rely on the presence of ALL blasts in patient samples. Cell-free DNA, or small fragments of DNA released by cancer cells into patient biofluids, has emerged as a robust and sensitive biomarker to assess cancer burden, although cfDNA analysis has not previously been applied to ALL.

Methods: We present a simple and rapid workflow based on NanoporeMinION sequencing of PCR amplified B cell-specific rearrangement of the (IGH) locus in cfDNA from B-ALL patient samples. A cohort of 5 pediatric B-ALL patient samples was chosen for the study based on the MRD and CNS disease status.

Results: Quantitation of IGH-variable sequences in cfDNA allowed us to detect clonal heterogeneity and track the response of individual B-ALL clones throughout treatment. cfDNA was detected in patient biofluids with clinical diagnoses of MRD and CNS disease, and leukemic clones could be detected even when diagnostic cell-count thresholds for MRD were not met. These data suggest that cfDNA assays may be useful in detecting the presence of ALL in the patient, even when blasts are not physically present in the biofluid sample.

Conclusions: The Nanopore IGH detection workflow to monitor cell-free DNA is a simple, rapid, and inexpensive assay that may ultimately serve as a valuable complement to traditional clinical diagnostic approaches for ALL.

KEYWORDS

B-cell acute lymphoblastic leukemia (B-ALL), central nervous system (CNS) disease, clonality, minimal residual disease (MRD), relapse, VDJ rearrangement

Introduction

Acute Lymphoblastic Leukemia (ALL) is the most common pediatric malignancy. Despite cure rates approaching 90%, relapsed ALL remains the second leading cause of cancer-related death in the pediatric population. Clinicians measure response to chemotherapy after the first round of treatment by assessing the number of leukemic blasts remaining after the first round of treatment. The presence or absence of minimal residual disease (MRD), or more than 0.01% of leukemic blasts remaining at the end of induction and consolidation chemotherapy, remains the most powerful prognostic indicator of patient outcome (1–4). The central nervous system (CNS) is also an important site of involvement in ALL and is a common site for ALL relapse (5, 6). The prevalence of CNS disease in ALL is high enough that every ALL patient receives prophylactic treatment involving multiple doses of intrathecal chemotherapy, which can have adverse and long-term side effects in pediatric patients. Better stratification of patients based on risk status and potential for relapse or CNS disease will rely on more precise diagnostics.

Current methods to diagnose MRD and CNS disease in ALL rely on detecting blasts in patient samples using flow cytometry or microscopy. Developing more sensitive assays that depend on the molecular detection of leukemic blasts *via* next-generation sequencing (NGS) has proven difficult since ALL has one of the lowest mutational burdens of any cancer (7, 8). This lack of common mutations precludes the design of targeted, cancer-specific sequencing probes commonly used in NGS assays for other types of cancers. Recently, Adaptive Biotechnologies developed the ClonoSEQ assay, an NGS assay that sequences VDJ rearrangements within B cell receptors instead of cancer-specific mutations (9, 10). This strategy is ideal for lymphocytic leukemias, as every T and B cell undergoes VDJ recombination to generate functional B and T cell receptors; the specific sequence of the rearrangement in the receptor is unique to an individual B or T cell. ALL results from the abnormal expansion of typically 1-5 B or T cell clones, each of which will have a unique VDJ sequence (11, 12). ClonoSEQ uses NGS methods to sequence the genomic DNA of cells isolated from patient blood and bone marrow samples to identify clonally expanded VDJ sequences and detect as few as one leukemic blast per million cells. ClonoSEQ has been implemented in Europe for MRD detection in B-cell lymphoid malignancies and is FDA-approved and in clinical trials in the US (13–15).

The major limitation of the ClonoSEQ method is its reliance on the collection of genomic DNA from leukemia cells within the patient sample. A significant concern for any cell-based assay is the accurate detection of CNS disease in ALL. Animal models showed that ALL cells often become embedded in the CNS tissue or attached to spinal nerves (16, 17). Approximately 85% of patients that succumbed to their disease had ALL blasts present in the brain or spinal cord at autopsy (18). However, only 11% of patients are clinically diagnosed as CNS disease positive, based on the detection of lymphoblasts in their cerebrospinal fluid (CSF) (5, 6). These findings highlight a critical need to develop more sensitive assays to complement cell-based pathology, flow cytometry, and ClonoSEQ assays, especially pertaining to ALL spread into the CNS.

Cell-free DNA as a cancer biomarker is transforming how patients are diagnosed and monitored for cancer progression. Cell-free DNA is constitutively released by cancer cells and is found free-floating in patient biofluids (19, 20). Tumor-specific cfDNA increases as tumors grow. The half-life of cfDNA is only 15-120 minutes, making it a valuable and proven biomarker for detecting cancer development in healthy individuals and monitoring tumor response to treatment in cancer patients (21). In 2020, FoundationOne's Liquid CDx cfDNA test was FDA-approved to detect *EGFR*, *BRCA1/2*, *ALK*, *ATM*, and *PIK3CA* mutations in cfDNA in ovarian, breast, prostate, and lung cancers to stratify patients into treatment regimens (22). Detection of tumor-specific VDJ rearrangements in cfDNA is used to monitor lymphoid lymphoma progression (23–25), and emerging evidence in myeloid malignancies suggests that cfDNA monitoring will be a useful diagnostic tool for leukemia patients as well. For example, in Acute Myelogenous Leukemia, cfDNA assays detected bone marrow relapse 30 days earlier than the standard flow cytometry-based methods (26). Finally, emerging evidence suggests that cfDNA may be more beneficial than cell-based assays in monitoring CNS tumors. For example, in leptomeningeal carcinomatosis, cancer-derived cfDNA was detectable in cases where microscopy did not reveal malignant cells in the CSF, and cfDNA fluctuated over time, correlating with CNS tumor burden (27). A comprehensive examination of several types of CNS malignancies showed that cfDNA isolated from the CSF was much more reliable than genomic DNA isolated from cells within the CSF in identifying tumor-associated mutations (28). These data suggest that cfDNA can identify CNS-associated cancers much more accurately than assays that rely on the presence of cancer cells within the CSF. To our knowledge, cfDNA has not been used to examine MRD status or CNS disease in ALL.

Our study outlines a method for isolation and detection of leukemia-derived cfDNA in the peripheral blood and CNS of pediatric B-ALL patients. We developed a simple and inexpensive workflow based on Nanopore MinION sequencing of PCR amplified VDJ rearrangements in cfDNA, which allowed us to analyze as little as 25 picograms of cfDNA per patient biofluid sample (Figure 1). We found that cfDNA can provide a more accurate assessment of B-ALL heterogeneity, as cfDNA sequencing could detect clones not present in the genomic DNA of bone marrow biopsy samples. Plasma cfDNA samples were used to monitor the response of specific clones to treatment and identified B-ALL clones present in MRD. Additionally, our

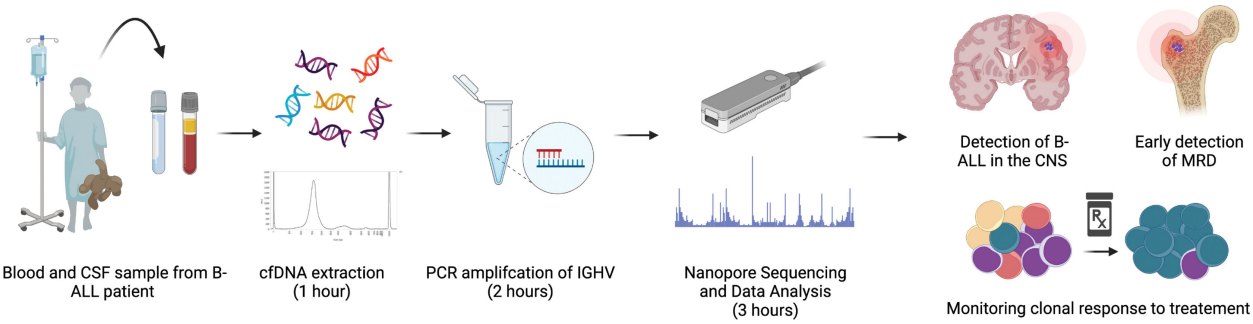

FIGURE 1
Workflow of IGHV sequencing. Diagrammatical overview of workflow and time input required for sequencing, from patient sample collection to read analysis.

Nanopore cfDNA sequencing workflow could detect B-ALL associated cfDNA in the CSF of patients that had been clinically diagnosed with CNS disease and in some patients diagnosed as CNS-negative. The clearance of CNS-associated clones was confirmed by the loss of cfDNA in the patient's CSF sample. Our data demonstrate the utility of cfDNA in assessing B-ALL heterogeneity and in monitoring B-ALL progression. The low cost and ease of use make the MinION cfDNA workflow ideal for cfDNA analysis in research settings, and the specificity and sensitivity of the assay in detecting MRD and CNS disease suggest that cfDNA may ultimately be a valuable complement to current cell-based clinical assays.

Materials and methods

Isolation and cryopreservation of mononuclear cells from bone marrow aspirate

Bone marrow aspirate was collected in Streck tubes (Streck, Cat # 218962) at the University of Kentucky's Pediatric Oncology clinic. Samples were diluted with an equal volume of room temperature 2% fetal bovine serum (FBS) in 1X PBS. The sample was slowly added to a 50mL Sepmate tube (Stem Cell Technologies, Cat # 85450) containing 15mL of Ficoll-Paque density gradient medium (Millipore Sigma, Cat # GE17-5446-52) and centrifuged at 2800rpm for 10 min. The top layer containing the mononuclear cells was poured into a new 50mL conical tube. The volume was brought up to 50mL with RPMI supplemented with 10% FBS and spun for 15 mins at 1,400 rpm at 4°C. Media was aspirated, cells were resuspended in 1mL RPMI, then counted with a hemocytometer. An additional 49 mL of complete RPMI was added to the cells, and cells were centrifuged for additional 10 mins at 1,400 rpm at 4°C for the second wash. The media was removed, and the cells were resuspended in 1ml of freezing medium (90% FBS + 10% DMSO) per 10^7 cells and added to a cryovial. Vials were placed in a CoolCell (Corning, Cat # 432003), cooled at -1°C/minute at -80°C then moved to liquid nitrogen for long-term storage.

Isolation of genomic DNA from banked mononuclear cells

Vials of banked mononuclear cells from patient bone marrow aspirate were warmed to 37°C and transferred to a sterile 15 mL conical tube. Pre-warmed, 25% fetal bovine serum (FBS) in Iscove's Modified Dulbecco's Media (IMDM) was added dropwise to the cells at a rate of approximately 2-3 seconds/ml for 10 mL. Cells were centrifuged at 1,000 rpm for 10 minutes, and the supernatant was gently aspirated. The addition of media, centrifugation, and removal of supernatant was repeated. Cells were then washed once in 1X PBS. gDNA was isolated using the Zymo Quick-gDNA Miniprep Kit (Zymo, Cat # D3025), using the manufacturer's instructions.

Isolation of cfDNA from Plasma and Cerebrospinal Fluid

Patient blood and CSF samples were collected into cell-free DNA collection tubes (Streck, Cat # 218962). Samples were stored at room temperature and processed within two weeks of collection. Blood samples were centrifuged at room temperature for 10 minutes at 1,600xg. After the initial spin, the plasma was removed, being careful not to disturb the buffy coat layer, transferred into a clean 1.5 mL Eppendorf tube, and centrifuged for 10 mins at 16,000xg at room temperature. The supernatant containing the cfDNA was carefully removed so as not to disturb the cell pellet and placed in a fresh tube. cfDNA from the plasma

was isolated using the Qiagen QIAmp MinElute ccfDNA Midi Kit (Qiagen, Cat # 55284) as per the manufacturer's instructions, except that the final elution occurs with nuclease-free water pre-warmed at 56°C for an enhanced yield of DNA from the column. cfDNA was isolated from CSF samples using the Zymo Research Quick-cfDNA Serum and Plasma Kit (Zymo, Cat # D4076) according to the manufacturer's instructions except with the following modifications: i) after adding proteinase K, the samples were incubated at 55°C for 1hr and ii) final elution step was carried out in 35 µl of nuclease-free water pre-warmed at 56°C. cfDNA samples were quantified using a Qubit Fluorometer using the high-sensitivity dsDNA quantification kit (Thermofisher Scientific, Cat # Q32851) according to the manufacturer's instructions and stored at -20°C.

PCR amplification of *IGH* regions in genomic and cell-free DNA

The IdentiClone *IGH* Gene Clonality gel detection kit (*In vivo*scribe, 91010020) was used to amplify the immunoglobulin heavy chain (*IGH*) region of genomic and cfDNA. The PCR was performed using the primer master mix labeled Tube A (*In vivo*scribe, Cat # 21010010CE) according to the manufacturer's directions, with 0.5ng of genomic DNA or cfDNA as input. Tonsil DNA (IVS-0000 polyclonal control, Cat # 40920010, supplied in the kit) was used as a negative control as well as for limit of DNA input detection. Amplitaq Gold Taq Polymerase (ThermoFisher Scientific, Cat # N8080240) was used for PCR amplification at 0.2ul per 50ul reaction, and PCR was run for 40 cycles with the cycling parameters of 95°C for 7 minutes of initial denaturation; 40 cycles of 95°C for 45 sec; 60°C for 45 sec; 72°C for 90 sec and final extension of 72°C for 10min. A portion (5µl) of the PCR reaction was run on agarose gel electrophoresis to confirm the amplification before proceeding with the library preparation.

Library preparation for MinION sequencing

Following the *IGH* clonality, PCR samples were measured on Qubit, and 50 ng of each sample was used as input for the library prep for the MinION sequencing. The PCR Barcoding Kit (Oxford, SQK-PBK004) was used for the library generation according to the manufacturer's protocol with the following modifications: i) since an amplicon was used as starting material, the initial fragmentation step of the protocol was omitted, ii) half-reaction volumes were used throughout the library generation procedure to conserve materials. Libraries were loaded onto the MinION Nanopore sequencer (Oxford) and were run until all barcodes had a minimum of 4000 reads, which averaged about 1-2 hours.

Illumina MiSeq analysis

IGH variable region was amplified from plasma cfDNA using the *Invivoscribe* kit as described above. The PCR reaction was size-selected using Ampure bead purification (Beckman Coulter, Cat # A63880) and eluted in nuclease-free water. The eluted DNA was sent to Genewiz for targeted amplicon-based sequencing under their "Amplicon EZ" category. Standard Illumina adapters were used in the library prep, and the final amplicon libraries were run on the Illumina MiSeq sequencing system. The merged Fastq files were then analyzed similarly to the files from the MinION, described below, to assess the *IGH* variable region clonal rearrangements and their abundance.

MinION analysis pipeline to identify *IGH* rearrangements

Sequencing reads were base-called and demultiplexed using the MinKNOW software package and built-in basecaller. Reads with a quality score of ≥ 7 were used to generate fastq files and for all downstream analyses. Fastq output files were concatenated into a single file per sample. Merged fastq files from MinION and those generated by MiSeq were then processed using the Galaxy server and available tools. Reads were mapped to hg38 using Minimap2 to generate BAM alignment files. Alignment files were then used as input for Feature Counts along with a gff reference file of the *IGH* locus on Chromosome 14. The output text file of how many reads mapped to each feature in the gff reference file was used for data analysis and graph creation. Read counts for each feature were normalized as a percentage of total reads for each patient. Major *IGHV* clones were identified in the diagnosis sample as those features that contained reads equal to or greater than 5% of the total reads for that sample. The select major clones were tracked through subsequent time points in each patient. All graphs were generated using Prism GraphPad

Results

Characteristics of B-ALL patients

Pediatric B-cell acute lymphoblastic leukemia (B-ALL) patients were admitted to the UK Healthcare Kentucky Children's Hospital at initial diagnosis of B-ALL and enrolled for sample collection. We retrospectively chose samples for use in this study based on CNS disease and MRD status after initial therapy. Our cohort consisted of five patients, out of which one patient (AAL-008) was MRD-positive at the end of induction. Patient AAL-004 had a few leukemic blasts noted but was MRD-negative as blast counts did not reach the threshold for a clinical

MRD diagnosis. Patients AAL-009, 010, and 012 were MRD-negative at the end of induction, and patients AAL-008 and 010 were positive for CNS disease at the time of diagnosis. Table 1 summarizes the complete characteristics of these patients. Genomic DNA was isolated from the bone marrow aspirate collected from each B-ALL patient at diagnosis. Cell-free DNA was isolated from plasma and cerebrospinal fluid (CSF) samples collected throughout treatment.

Identification of B cell clones *via* Nanopore sequencing of the recombined IGH gene

B cells recombine more than 85 gene segments in the immunoglobulin heavy chain (*IGH*) locus as part of their normal maturation. This locus is also enriched for single nucleotide variants, which further enhances the diversity of the sequence *IGH* region between individual B cells. Sequencing the *IGH* region in genomic DNA has been used to trace B cell lineages and track B-cell malignancies (29–31). We developed a novel experimental workflow that combines PCR amplification of the *IGH* region with the third-generation Oxford Nanopore MinION sequencer (ONT) (32) to detect B-ALL patient-specific *IGH* clonal rearrangements. We focused on analyses of the unique patient-specific variable region rearrangements (*IGHV*) and tracked these clones throughout the treatment. Ultimately, this method can be applied to genomic DNA isolated from blasts in patient samples or cfDNA collected from patient biofluids. In the first step, we used a commercially available PCR kit to amplify the *IGH* sequence between the conserved framework region 1 (FR1) and the conserved Joining (J) region, which allows for a complete representation of all variable regions within the *IGH* gene (referred to hereafter as *IGHV*) (33). PCR products were subjected to library preparation to add adapters and barcodes that allow for multiplexing, and then samples were run through the benchtop MinION Nanopore sequencer. We used a simple pipeline comprised of freely available software to analyze the output files: i) MinKNOW, which operates the sequencer and automatically performs simultaneous sequencing, demultiplexing, and barcode trimming using the built-in Guppy toolkit, ii) Minimap2 to map the merged fastq files to create BAM alignment files, and iii) Featurecounts to determine how many reads align with the *IGHV* region. We have provided step-by-step instructions for analysis using these tools in the Supplemental Methods. From sample collection to data analysis, the entire process takes approximately 6 hours, with most of that time hands-off, costs less than $30 per sample, and can be carried out by users with basic computer skills.

Limit of input DNA detection on Nanopore workflow

The recommended amount of input DNA for *IGH* PCR is 2 ng (34). As our ultimate goal was to adapt our workflow toward the detection of cfDNA, we determined the lowest level of input DNA that could be used in *IGH* PCR and Nanopore sequencing. We tested our workflow on 0.01 - 0.10 ng of genomic DNA isolated from healthy tonsils, which are enriched in B cells. The human *IGH* locus region is located on the long arm of Chromosome 14 (Chr14, Figure 2A), and we used the Nanopore generated reads that mapped to this locus over other locations as a readout of PCR specificity and sensitivity. Libraries of *IGH* PCR reactions from all DNA concentrations tested had reads that mapped to chromosome 14. Predictably, mapping frequency to Chr14 decreased with decreasing input DNA amount; however, we did observe reduced mapping in total mapped reads after we lowered DNA input to 0.025ng (Figure 2B). When we distributed mapped reads across all chromosomes, it became evident that non-specific mapping increased inversely with template amount. The signal-to-noise was indistinguishable at concentrations below 0.025ng, as reads mapping to Chr14 dropped below the levels of mapping to other chromosomes (Figure 2C). Nevertheless, even with the lowest input DNA amount, we could detect reads mapping to the identical *IGHV* clones identified with the highest DNA input amount (Figure 2D), suggesting that sensitivity with Nanopore sequencing can be maintained even when specificity decreases. This aspect of Nanopore sequencing is essential when working

TABLE 1 Patient characteristics.

Subject ID	Blast Count at Diagnosis (*10^9/L)	WBC Count at Diagnosis (*10^9/L)	Number of Days to Clear Circulating Blasts	EOI MRD Status	CNS Disease Status	Number of Days to Clear CSF
ALL-004	0.57	3.33	9	Negative*	Negative	N/A
ALL-008	1.53	4.79	9	Positive	Positive	8
ALL-009	14.92	19.38	11	Negative	Negative	N/A
ALL-010	1.58	6.32	13	Negative	Positive	9
ALL-012	23.88	31.84	11	Negative	Negative	N/A

*Negative MRD at the threshold of one blast per 10,000 cells by flow cytometry, but a few leukemic cells noted.
WBC, white blood cell; EOI, end of induction; MRD, minimal residual disease; CNS, central nervous system; CSF, cerebrospinal fluid.

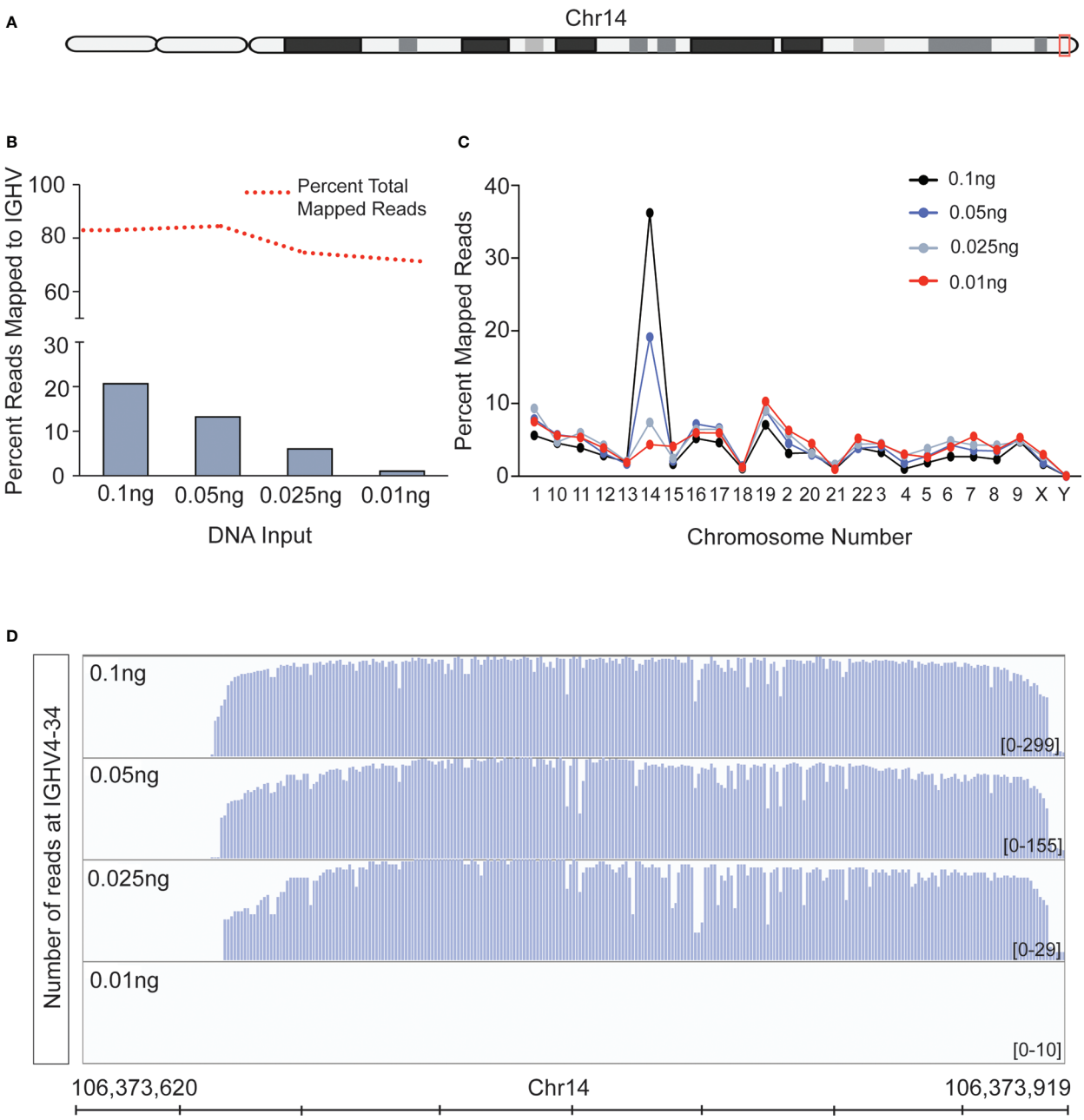

FIGURE 2
The MinION sequencing workflow can reliably detect IGHV reads in as little as 25 picograms of DNA. **(A)** Schematic of chromosome 14. The red box denotes the region containing the IGHV sequence to which all MinION reads were aligned. **(B)** The IGHV region was PCR amplified from the indicated input amount of normal tonsil DNA. Approximately 4,000 reads were obtained from the resulting libraries using nanopore MinION sequencing. The red dashed line shows the percent of all reads mapped to the human genome, and the bars denote the percentage of those mapped to the IGHV sequence. **(C)** The percent of all reads mapped from the samples in **(B)** are plotted across all chromosomes. **(D)** Alignment plots to a selected IGHV, V4-34, show accurate reads alignment when the input DNA is as little as 0.025ng, or a threshold of 20 reads mapped to IGHV over other location.

with patient samples after the treatment regimen to detect MRD when the genetic material obtained may be too low to quantify by standard means.

cfDNA from patient biofluids as input for Nanopore sequencing workflow

cfDNA is emerging as a robust prognostic biomarker that can assess tumor heterogeneity and tumor burden (35). Additionally, cfDNA is localized to patient biofluids (36), so sample collection is less invasive than tumor or tissue biopsy. cfDNA has not previously been assessed in the B-ALL disease setting. We assessed the Bioanalyzer traces of cfDNA samples isolated from the plasma of patients AAL-004 and AAL-010, and they matched the expected cfDNA sizes of ~150 base pairs (37, 38) (Supplemental Figure 1). We applied PCR and Nanopore sequencing of *IGH* to both the genomic DNA (gDNA) isolated from bone marrow aspirate and cfDNA isolated from the plasma at diagnosis. Only sequences that had an 80% or greater match to the *IGH* region of Chr14 were considered B-cell "clones" and included for further analyses. Clones that comprised ≥ 5% of the total mapped reads were considered significant clones in the sample (Supplemental Table 1). We reasoned that a ≥ 5% representation of a particular *IGHV* sequence in the sample would most likely be due to clonal expansion of the B-ALL. However, our methods record sequencing data from all clones. If a rare clone emerges as a dominant driver of B-ALL progression at later stages, we can retrospectively trace this clone in banked patient samples.

Clone distribution is consistent regardless of the sequencing platform

We used the same cfDNA PCR reaction from the plasma of two patients, AAL-004 and AAL-010, to determine if Nanopore sequencing is comparable to Illumina MiSeq analysis, a routinely used NGS platform for MRD monitoring. Both platforms detected similar clone identity and clonal abundance across treatment time points (Figure 3). These data indicate that the Nanopore sequencing workflow can assess the *IGH* clonal repertoire in B-ALL and identify clones in cfDNA, but with a faster turn-around time lower cost than Illumina.

Nanopore sequencing of *IGH* from cfDNA monitors therapeutic response

The half-life of cfDNA is 1-2 hours (39–41), making it an excellent biomarker for assessing leukemia burden and analyzing the response of individual clones to therapy. We analyzed the gDNA from bone marrow biopsy and the cfDNA from plasma collected from patients at diagnosis to identify the expanded clones comprising the B-ALL, as described above. These clones were then tracked in subsequent plasma cfDNA samples to assess the changes in clonal distribution throughout treatment. cfDNA samples were taken ~ 1 week into induction chemotherapy (denoted as Early-I in Figure 4), ~2 weeks into induction therapy (denoted Mid-I), and at the end of induction chemotherapy (denoted EOI). In some cases, we collected

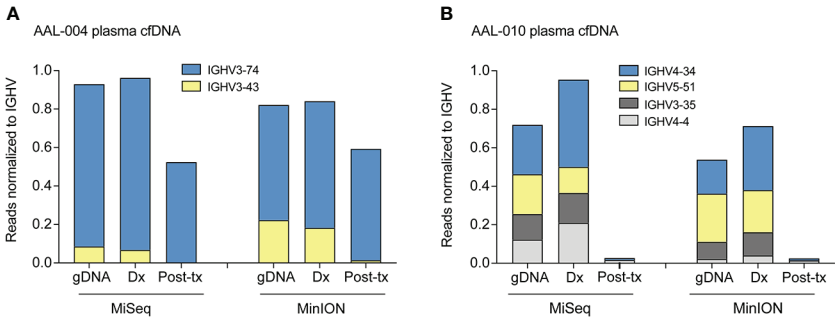

FIGURE 3
Comparison of clone distribution between Illumina and Nanopore MinION sequencing platforms. IGHV PCR of select time points from patients AAL-004 **(A)** and AAL-010 **(B)** was divided and sequenced with MinION (nanopore) or MiSeq (Illumina). V-region clones comprising more than 5% of the total clones in the sample taken at diagnosis were tracked across the two later time points and normalized to the total number of reads aligned to Chr14 per sample. Clone distribution across different time points within each patient is uniform regardless of the sequencing platform. Dx: sample taken at B-ALL diagnosis, post-tx: sample taken post-treatment.

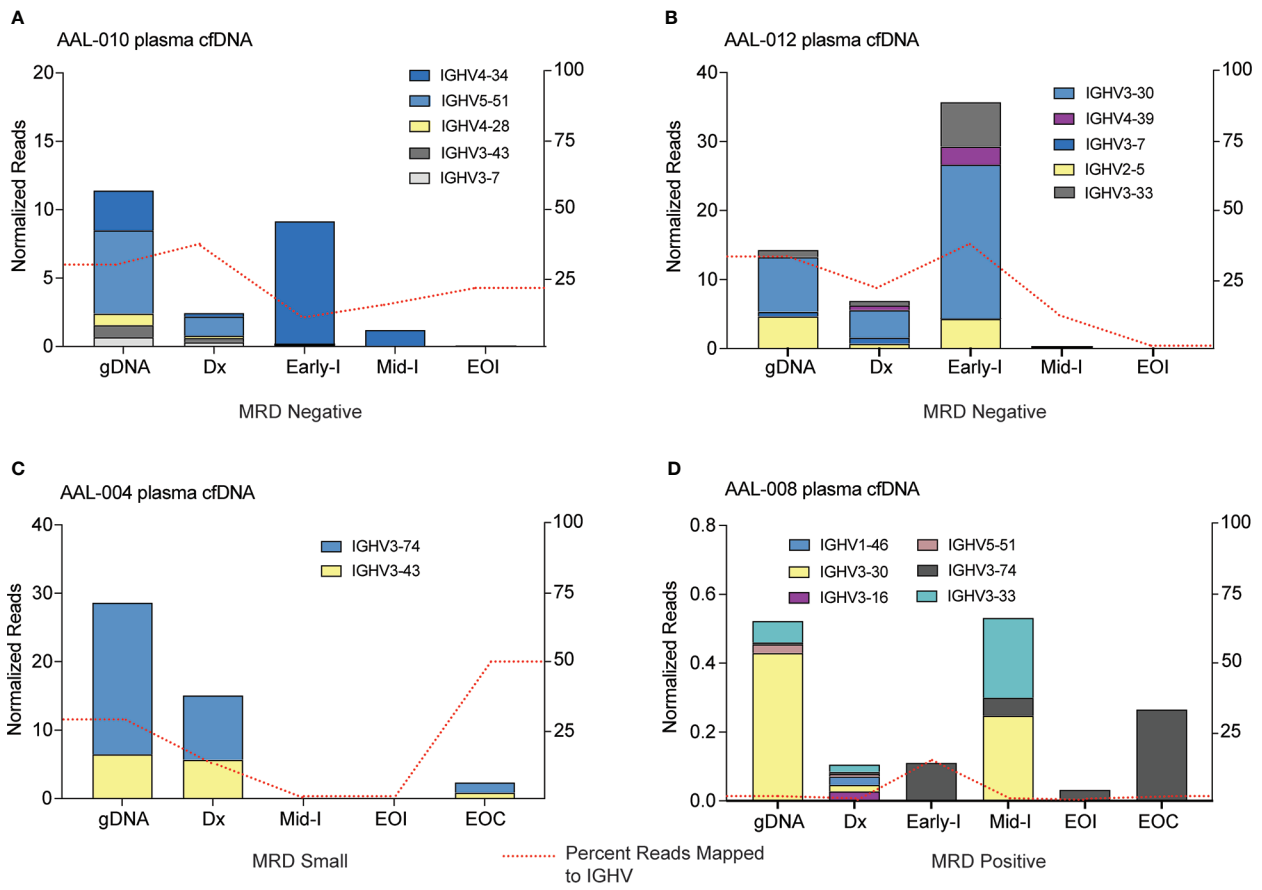

FIGURE 4
IGHV sequencing of cfDNA can define B-ALL heterogeneity and track clonal response throughout treatment. cfDNA was extracted from plasma samples of four patients, IGHV regions were PCR amplified, and resultant libraries were sequenced using MinION. Data were analyzed using Galaxy. Clones present in the genomic DNA (gDNA) and cell-free DNA plasma samples at diagnosis (Dx) that comprised at least 5% of total reads were tracked across treatment timepoints. Clone abundance is normalized to total mapped reads per library and shown on the left axis. The percentage of reads aligned to the IGHV region on Chr14 (red dashed line) is a relative indicator of leukocyte abundance at each timepoint/sample and is shown on the right axis. Patients in **(A, B)** were clinically diagnosed as MRD negative *via* flow cytometry. Patient **(C)** was MRD negative but had blasts present in the sample that did not reach the clinical cut-off of one blast per 10,000 cell thresholds for MRD diagnosis. Patient **(D)** was diagnosed as MRD positive.

cfDNA at the end of consolidation (EOC) therapy, which can occur several months after diagnosis.

Two patients, AAL-010 and AAL-012, were clinically diagnosed as MRD negative at the end of induction therapy. At their initial disease diagnosis, both patients had heterogenous B-ALL, with 5 distinct *IGHV* sequences present as ≥ 5% of the total mapped reads. Interestingly, in patient AAL-010 we observed a clonal population (*IGHV*4-34) that expanded at the onset of induction therapy (Figure 4A **Early-I**) and was eliminated by the end of induction, indicating clonal response to therapy. All identified clones were eliminated after treatment, consistent with this patient's clinical diagnosis of MRD-free (Figure 4A). However, we did detect reads mapping to chr14 within the cfDNA sample taken at the end of induction therapy, (red dashed line, Figure 4A), although none of these new clones mapped to any of the ALL clones present at diagnosis. This spike might be attributed to a clonal expansion of a B cell caused by an illness or other antibody response in the patient.

AAL-012 had a clone, *IGHV*4-39, not present in the diagnosis gDNA bone marrow biopsy sample but identified in the diagnosis cfDNA plasma sample (Figure 4B). Because every B-ALL clone release cfDNA into the plasma, cfDNA may ultimately be more accurate in detecting the actual clonal composition of the B-ALL than the bone marrow biopsy, which can only detect clones present at the site of biopsy. Additionally, early into both patient AAL-10's and AAL-012's treatment, we observed a sharp increase in cfDNA associated with these clones, which likely indicates leukemia cell death and release of DNA into the blood and may indicate a good response to treatment.

Two additional patients, AAL-004 and AAL-008, had blasts present in their clinical samples at the end of induction therapy. Patient AAL-004 was not diagnosed with MRD, as the blast count fell below the one blast per 10,000 cell thresholds for clinical MRD. Patient AAL-008 was MRD positive. In both patients, we detected heterogenous B-ALL comprised of several distinct *IGHV* sequences in the gDNA from bone marrow biopsy and the plasma cfDNA isolated at diagnosis. Patient AAL-004 appeared to clear their clones during induction therapy, as we could not detect reads linked with chr14 in the cfDNA samples. However, we observed clone *IGHV*3-74, a major clone present at diagnosis, re-emerge in cfDNA samples collected at the end of consolidation therapy (Figure 4C). Patient AAL-008 unfortunately never cleared the clones detected in the biopsy gDNA and cfDNA sample at diagnosis. Interestingly, we observed that some clones (*IGHV*3-30, *IGHV*3-33, *IGHV*3-74), which were equally distributed amongst the other clones at diagnosis, became enriched at later treatment stages (Figure 4D). Although reads from clone *IGHV*3-30 and *IGHV*3-33 drop off during the end of induction (EOI), clone *IGHV*3-74, remains unresponsive. Together, these data highlight the utility of cfDNA analysis as a method to track B-ALL patient-specific clonal dynamics during treatment. This workflow may be useful in identifying patients whose B-ALL does not respond well to therapy, such as patient AAL-008, which may allow them to be stratified into a high-risk category early into their treatment for better disease management. Additionally, cfDNA can be used as a non-invasive method to routinely assess patients for clone re-emergence after treatment *via* simple blood draw.

cfDNA can be detected in the CSF of B-ALL patients using the MinION sequencing workflow

Approximately 4% of B-ALL patients will have infiltration of ALL blasts into their CNS at diagnosis, and 30-40% of the patients will have pronounced CNS disease at relapse (5). CNS infiltration is a significant adverse prognostic indicator in B-ALL, but the only way to diagnose it is to detect blasts in the CSF sample. However, B-ALL cells can be embedded in the brain or associated with spinal neurons and not be freely floating and detectable in the CSF (5, 42, 43), meaning patients might have CNS disease but present clinically as negative for CNS infiltration. For this reason, every ALL patient is given intrathecal chemotherapy. We reasoned that since cfDNA is released by B-ALL cells into patient biofluids, it might be detectable in CSF samples even if the blasts themselves are not. We applied our MinION sequencing workflow to cfDNA isolated from CSF samples taken from patients diagnosed as CNS positive (AAL-008 and 010) and CNS negative (AAL-009 and 012). We detected *IGHV* reads in the cfDNA from CNS positive B-ALL patients (Figures 5A, B), and these clones were cleared by the end of induction therapy. Interestingly, we detected very low levels of *IGHV* sequence in the diagnosis CSF cfDNA sample from patient AAL-009 (Figure 5C), even though this patient was diagnosed as CNS negative. Finally, patient AAL-012 was diagnosed as CNS negative. However, we observed an *IGHV* clone *IGHV*3-21 in the cfDNA from the CSF of this patient at diagnosis that significantly expanded by the end of induction (Figure 5D). CSF is not drawn from patients after induction therapy when their initial diagnosis is CNS negative, so we could not follow up on the *IGHV* in the cfDNA in later CSF samples of AAL-012. However, their plasma cfDNA remained clear of *IGHV* reads throughout consolidation. Finally, across all patients, we observed that some of the *IGHV* reads in the cfDNA from the plasma were also present in the cfDNA in the CSF, indicating B-ALL clones were present at both locations. In other instances, clones were exclusively present in one location, suggesting that cfDNA analysis may be useful in research focused on ALL homing to the CNS.

Discussion

Despite advancements in the treatment of Acute Lymphoblastic Leukemia, relapsed leukemia remains the second leading cause of death in pediatric cancer patients (44). The current methods of MRD monitoring in patients' post-chemotherapy have room for improvement. For example, cell-based quantification *via* flow cytometry has poor resolution. ClonoSeq NGS analysis is costly, can take days to weeks to return results, and is not yet used to detect CNS disease in B-ALL (9, 45, 46). Early detection of MRD, better biomarkers to monitor treatment response in real-time, and a non-invasive, routine screening method to identify ALL recurrence could improve patient disease management. cfDNA analysis has emerged as a robust, minimally invasive prognostic biomarker that correlates well with the tumor heterogeneity and tumor burden. In this study we present a workflow for analyzing cfDNA in the blood and CSF of ALL patients, which, as far as we know, has previously not been applied to B-ALL. Our study demonstrates the utility of MinION-based Nanopore sequencing of *IGH* rearrangement from the cfDNA to quickly visualize B-ALL clonal heterogeneity and track clonal response to treatment from patient biofluids. Towards this end, our workflow is very amenable in terms of small input material for PCR, quick turnaround time, and is very cost-effective. Workflows from other NGS platforms routinely used for cfDNA or MRD detection, such as Illumina, require specialized instruments, batch runs, long wait/turnaround times, and complex pipelines for data analysis. The MinION sequencing device is inexpensive, and the data analysis we describe is an easy-to-use pipeline that utilizes freely available tools such as Nanopipe, Galaxy, and IGV genome browser. These features make the MinION sequencing

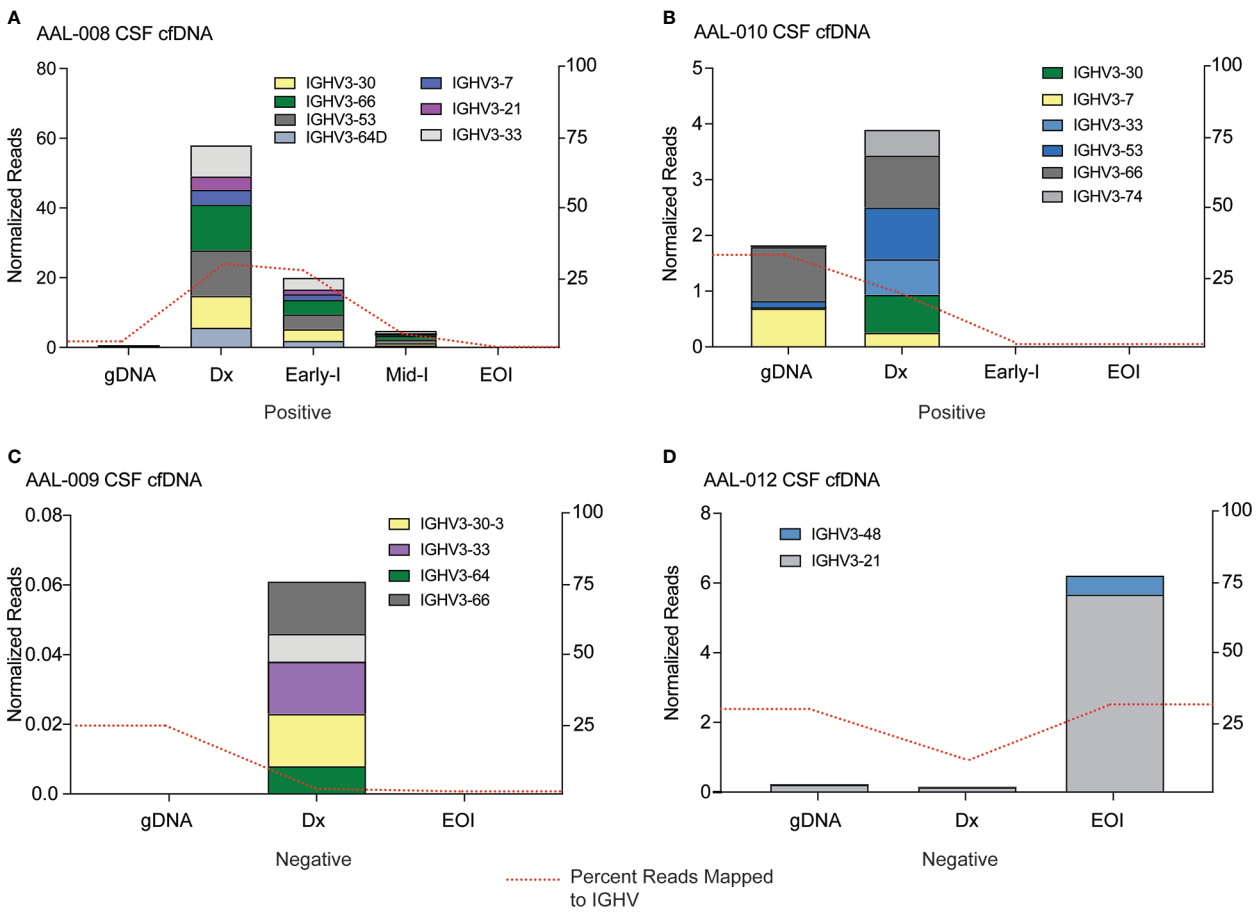

FIGURE 5
IGHV sequencing can detect cfDNA in the cerebrospinal fluid of B-ALL patients. cfDNA was extracted from CSF samples of four patients, IGHV regions were PCR amplified, and resultant libraries were sequenced using MinION. Data were analyzed using Galaxy. Clones in the genomic DNA (gDNA) of bone marrow biopsy and cell-free DNA (Dx) CSF samples at diagnosis that comprised at least 5% of total reads were tracked across all timepoints. Clone abundance is normalized to total mapped reads per library, shown on the left axis. The percentage of reads aligned to the IGHV region on Chr14 (red dashed line) is a relative indicator of leukocyte abundance at each timepoint/sample and is shown on the right axis. Patients in **(A)** and **(B)** were clinically diagnosed as CNS positive by flow cytometry, indicating infiltration of B-ALL cells into the CNS. Patients **(C)** and **(D)** were diagnosed as CNS negative, although IGHV reads from cfDNA were detectable in the CNS sample.

for the detection of cfDNA a promising platform in the clinical setting.

With a limit of detection as low as 25 picograms of DNA, this workflow is an ideal alternative for cell-based assays requiring genomic DNA from clinical samples limited in material (Figure 2). Our workflow identified similar clonal heterogeneity and abundance compared to routinely used and more expensive NGS platforms such as Illumina Miseq, indicating the robustness of our assay (Figure 3).

Nanopore sequencing revealed interesting B-ALL clonal dynamics from our patient cohort that had a clinical diagnosis of either MRD positive (ALL-008) or negative (AAL-010 and AAL-012) and MRD small (AAL-004). All the patients showed heterogenous B-ALL in that several distinct *IGHV* sequences were present. We were able to track the response of these individual clones throughout the treatment and identified clones that were either responded to or survived chemotherapy. In a research setting, these data could be combined with other NGS methods, such as single-cell RNAseq, and may provide new insights into mechanisms of chemotherapy resistance. Interestingly, analysis of cfDNA from plasma samples at patient diagnosis identified *IGHV* sequences and B-ALL clones that were not present in the cell-based analysis of the genomic DNA collected from the bone marrow biopsy sample (Figure 4). These data reiterate the ability of cfDNA to act as a biomarker that can capture the full extent of heterogeneity and clonal dynamics within a patient's leukemia. Although, we were able to detect multiple *IGHV* clones in each of the B-ALL patients, we realize our analysis may not completely capture the extent of *IGH*V-D-J rearrangements.

Since the hg38 reference genome does not include *IGH* recombinations, mapping of the shorter, *IGH* joining (J) or diversity (D), regions will be less accurate because they exist up hundreds of kilobases away from the variable regions (V). Thus, we focused on the longer *IGHV* regions since they would be the most likely to capture clonal heterogeneity. For a more quantitative analysis of possible rearrangements of *IGHV* clones with different J and D regions the raw read data from MinION can be used in other freely available VDJ analysis software such as IMGT/V-Quest (47, 48) or VDJServer (49).

Because ALLs have a low mutational burden, cell-based clonal analyses like ClonoSEQ are the only NGS methods available for sensitive detection of MRD. ClonoSEQ is currently completed only at the end of the induction chemotherapy. Longitudinal Nanopore analysis of cfDNA with every blood draw could provide a valuable complement to ClonoSEQ, allowing for a more complete assessment of ALL responses throughout a patient's treatment. For example, a caveat of our assay and ClonoSEQ is that it cannot distinguish between B-ALL and normal B cell expansion due to an antibody response, such as during an infection. We detected reads mapping to chr 14 in patient AAL-010 at EOI (Figure 4A). None of these reads mapped to any clones identified at diagnosis, suggesting an antibody response that presents during transient infection rather than B-ALL recurrence. Since we can run our workflow on the next blood sample from the patient, we can easily confirm whether this expansion was indeed an immune response or a cause for clinical concern.

Another important use of our workflow is the detection of CNS positive disease in B-ALL. Blasts can spread into the CNS during B-ALL development, and the CNS is a common site for ALL relapse (50). Outcomes in B-ALL patients with CNS positive disease are lower than those without evidence of CNS positivity. Patients typically have 16-20 lumbar punctures (LP) with administration of intrathecal chemotherapy. With each lumbar puncture (LP) CSF is assayed by cell count and cytospin to surveille for evidence of CNS relapse. Cytospin analysis requires a pathologist review a concentrated CSF prep under microscopy, manually enumerating the quantity of each cell type, which is an arduous process. A primary clinical concern is that current diagnostic methodologies may not be sensitive enough to detect CNS disease in ALL, as blasts may be embedded with CNS tissue and not present in CSF samples (43, 51). Interestingly, we detected cfDNA in the CSF of one patient diagnosed as CNS negative, meaning cells were not detected by flow cytometry of the CSF sample. This finding attests to the potential sensitivity of our cfDNA workflow in monitoring CNS disease. Two of our patients (AAL-008 and AAL-010) were diagnosed with CNS disease. Nanopore sequencing allowed us to identify which clones spread into the CNS versus those that remained in the blood. The absence of further cfDNA reads in CSF samples after the initial doses of intrathecal chemotherapy suggested that those clones were cleared from the CNS (Figure 5). CSF is removed from patients each time they receive intrathecal chemotherapy to prevent increased CSF volume when the treatment is injected. Instead of discarding this fluid, cfDNA analysis could provide valuable insights into CNS disease status and clonal response.

Although our conclusions are based on a very small sample study, the observed data on *IGHV* sequencing of cfDNA and MRD status suggests a possible correlation. Similarly, *IGHV* sequencing showed obvious contrasts between CNS-positive and CNS-negative patients. A future study with 20 to 30 patients will be sufficient for proof of concept to show that cfDNA assays may be useful in detecting the presence of ALL in patients when blasts are not in the biofluid sample.

In summary, our study demonstrates the utility of a Nanopore sequencing workflow as a simple, rapid, and low-cost method to visualize B-ALL patient-specific *IGHV* clonal heterogeneity and track these clones throughout treatment. We found that quantitation of *IGHV* reads from cfDNA samples provided insights into B-ALL heterogeneity in our patient cohort. The workflow could be scaled up for quickly and efficiently assessing the dynamics of B-ALL clones in response to treatment in large patient datasets, particularly in Consortia studying B-ALL. Similar Nanopore sequencing strategies could also be developed and applied to detect tumor-associated mutations in cfDNA in any cancer type.

Data availability statement

The raw read data from the MinION sequencing are uploaded to the Sequence Read Archive (NCBI) Project ID: PRJNA891254. Further inquiries can be directed to the corresponding author.

Ethics statement

The studies involving human participants were reviewed and approved by protocol 44672, approved by the University of Kentucky's Institutional Review Board. Written informed consent to participate in this study was provided by the participants' legal guardian/next of kin.

Author contributions

SS, YC, MH, TB, and JB designed experiments. SS and YC conducted experiments and acquired data; SS, YC, IS analyzed data. TT, BF, TB obtained patient consent and oversaw the collection of patient samples. MH, LM, AC, IS processed samples. SS, YC, MH, and IS drafted the manuscript. JB edited

the manuscript. JB provided supervision and funding. All authors contributed to the article and approved the submitted version.

Funding

Funding for this research was provided by a Kentucky Pediatric Cancer Research Trust Fund research grant to JB and TB, NIH grants DP2CA228043 and R37CA227656 to JB, and T32CA165990 to MH.

Conflict of interest

The authors declare that the research was conducted in the absence of any commercial or financial relationships that could be construed as a potential conflict of interest.

Publisher's note

Supplementary material

The Supplementary Material for this article can be found online at: https://www.frontiersin.org/articles/10.3389/fonc.2022.958673/full#supplementary-material

References

1. Hunger SP, Mullighan CG. Acute lymphoblastic leukemia in children. *N Engl J Med* (2015) 373(16):1541–52. doi: 10.1056/NEJMra1400972

2. Kato M, Manabe A. Treatment and biology of pediatric acute lymphoblastic leukemia. *Pediatr Int* (2018) 60(1):4–12. doi: 10.1111/ped.13457

3. Coustan-Smith E, Mullighan CG, Onciu M, Behm FG, Raimondi SC, Pei D, et al. Early T-cell precursor leukaemia: A subtype of very high-risk acute lymphoblastic leukaemia. *Lancet Oncol* (2009) 10(2):147–56. doi: 10.1016/S1470-2045(08)70314-0

4. Campana D, Pui CH. Minimal residual disease-guided therapy in childhood acute lymphoblastic leukemia. *Blood* (2017) 129(14):1913–8. doi: 10.1182/blood-2016-12-725804

5. Lenk L, Alsadeq A, Schewe DM. Involvement of the central nervous system in acute lymphoblastic leukemia: Opinions on molecular mechanisms and clinical implications based on recent data. *Cancer Metastasis Rev* (2020) 39(1):173–87. doi: 10.1007/s10555-020-09848-z

6. Ranta S, Nilsson F, Harila-Saari A, Saft L, Tani E, Söderhäll S, et al. Detection of central nervous system involvement in childhood acute lymphoblastic leukemia by cytomorphology and flow cytometry of the cerebrospinal fluid. *Pediatr Blood Cancer* (2015) 62(6):951–6. doi: 10.1002/pbc.25363

7. Waanders E, Gu Z, Dobson SM, Antić Ž, Crawford JC, Ma X, et al. Mutational landscape and patterns of clonal evolution in relapsed pediatric acute lymphoblastic leukemia. *Blood Cancer Discovery* (2020) 1(1):96–111. doi: 10.1158/0008-5472.Bcd-19-0041

8. Wu C, Li W. Genomics and pharmacogenomics of pediatric acute lymphoblastic leukemia. *Crit Rev Oncol Hematol* (2018) 126:100–11. doi: 10.1016/j.critrevonc.2018.04.002

9. Ching T, Duncan ME, Newman-Eerkes T, McWhorter MME, Tracy JM, Steen MS, et al. Analytical evaluation of the clonoseq assay for establishing measurable (Minimal) residual disease in acute lymphoblastic leukemia, chronic lymphocytic leukemia, and multiple myeloma. *BMC Cancer* (2020) 20(1):612. doi: 10.1186/s12885-020-07077-9

10. Monter A, Nomdedéu JF. Clonoseq assay for the detection of lymphoid malignancies. *Expert Rev Mol Diagn* (2019) 19(7):571–8. doi: 10.1080/14737159.2019.1627877

11. Mullighan CG, Phillips LA, Su X, Ma J, Miller CB, Shurtleff SA, et al. Genomic analysis of the clonal origins of relapsed acute lymphoblastic leukemia. *Science* (2008) 322(5906):1377–80. doi: 10.1126/science.1164266

12. Fries C, Adlowitz DG, Spence JM, Spence JP, Rock PJ, Burack WR. Acute lymphoblastic leukemia clonal distribution between bone marrow and peripheral blood. *Pediatr Blood Cancer* (2020) 67(6):e28280. doi: 10.1002/pbc.28280

13. Bal S, Costa LJ. Best practices for the assessment of measurable residual disease (Mrd) in multiple myeloma. *Clin Adv Hematol Oncol* (2020) 18 Suppl 1(1):1–20.

14. Hussaini MO, Srivastava J, Lee LW, Nishihori T, Shah BD, Alsina M, et al. Assessment of clonotypic rearrangements and minimal residual disease in lymphoid malignancies: A Large cancer center experience using clonoseq. *Arch Pathol Lab Med* (2022) 146(4):485–93. doi: 10.5858/arpa.2020-0457-OA

15. Clonoseq cleared for residual cancer testing. *Cancer Discovery* (2018) 8(12): Of6. doi: 10.1158/2159-8290.Cd-nb2018-136

16. Münch V, Trentin L, Herzig J, Demir S, Seyfried F, Kraus JM, et al. Central nervous system involvement in acute lymphoblastic leukemia is mediated by vascular endothelial growth factor. *Blood* (2017) 130(5):643–54. doi: 10.1182/blood-2017-03-769315

17. Yao H, Price TT, Cantelli G, Ngo B, Warner MJ, Olivere L, et al. Leukaemia hijacks a neural mechanism to invade the central nervous system. *Nature* (2018) 560(7716):55–60. doi: 10.1038/s41586-018-0342-5

18. Bojsen-Møller M, Nielsen JL. Cns involvement in leukaemia. an autopsy study of 100 consecutive patients. *Acta Pathol Microbiol Immunol Scand A* (1983) 91(4):209–16.

19. Wan JCM, Massie C, Garcia-Corbacho J, Mouliere F, Brenton JD, Caldas C, et al. Liquid biopsies come of age: Towards implementation of circulating tumour DNA. *Nat Rev Cancer* (2017) 17(4):223–38. doi: 10.1038/nrc.2017.7

20. Volik S, Alcaide M, Morin RD, Collins C. Cell-free DNA (Cfdna): Clinical significance and utility in cancer shaped by emerging technologies. *Mol Cancer Res* (2016) 14(10):898–908. doi: 10.1158/1541-7786.MCR-16-0044

21. Pessoa LS, Heringer M, Ferrer VP. Ctdna as a cancer biomarker: A broad overview. *Crit Rev Oncol Hematol* (2020) 155:103109. doi: 10.1016/j.critrevonc.2020.103109

22. Woodhouse R, Li M, Hughes J, Delfosse D, Skoletsky J, Ma P, et al. Clinical and analytical validation of foundationone liquid cdx, a novel 324-gene cfdna-based comprehensive genomic profiling assay for cancers of solid tumor origin. *PloS One* (2020) 15(9):e0237802. doi: 10.1371/journal.pone.0237802

23. Sarkozy C, Huet S, Carlton VE, Fabiani B, Delmer A, Jardin F, et al. The prognostic value of clonal heterogeneity and quantitative assessment of plasma circulating clonal ig-vdj sequences at diagnosis in patients with follicular lymphoma. *Oncotarget* (2017) 8(5):8765–74. doi: 10.18632/oncotarget.14448

24. Kwok M, Wu SP, Mo C, Summers T, Roschewski M. Circulating tumor DNA to monitor therapy for aggressive b-cell lymphomas. *Curr Treat Options Oncol* (2016) 17(9):47. doi: 10.1007/s11864-016-0425-1

25. Kubaczkova V, Vrabel D, Sedlarikova L, Besse L, Sevcikova S. Cell-free DNA - minimally invasive marker of hematological malignancies. *Eur J Haematol* (2017) 99(4):291–9. doi: 10.1111/ejh.12925

26. Zhong L, Chen J, Huang X, Li Y, Jiang T. Monitoring immunoglobulin heavy chain and T-cell receptor gene rearrangement in cfdna as minimal residual disease detection for patients with acute myeloid leukemia. *Oncol Lett* (2018) 16 (2):2279–88. doi: 10.3892/ol.2018.8966

27. De Mattos-Arruda L, Mayor R, Ng CKY, Weigelt B, Martínez-Ricarte F, Torrejon D, et al. Cerebrospinal fluid-derived circulating tumour DNA better

represents the genomic alterations of brain tumours than plasma. *Nat Commun* (2015) 6:8839. doi: 10.1038/ncomms9839

28. Shah M, Takayasu T, Zorofchian Moghadamtousi S, Arevalo O, Chen M, Lan C, et al. Evaluation of the oncomine pan-cancer cell-free assay for analyzing circulating tumor DNA in the cerebrospinal fluid in patients with central nervous system malignancies. *J Mol Diagn* (2021) 23(2):171–80. doi: 10.1016/j.jmoldx.2020.10.013

29. Shin S, Hwang IS, Kim J, Lee KA, Lee ST, Choi JR. Detection of immunoglobulin heavy chain gene clonality by next-generation sequencing for minimal residual disease monitoring in b-lymphoblastic leukemia. *Ann Lab Med* (2017) 37(4):331–5. doi: 10.3343/alm.2017.37.4.331

30. Wu D, Emerson RO, Sherwood A, Loh ML, Angiolillo A, Howie B, et al. Detection of minimal residual disease in b lymphoblastic leukemia by high-throughput sequencing of igh. *Clin Cancer Res* (2014) 20(17):4540–8. doi: 10.1158/1078-0432.CCR-13-3231

31. Gawad C, Pepin F, Carlton VE, Klinger M, Logan AC, Miklos DB, et al. Massive evolution of the immunoglobulin heavy chain locus in children with b precursor acute lymphoblastic leukemia. *Blood* (2012) 120(22):4407–17. doi: 10.1182/blood-2012-05-429811

32. Jain M, Olsen HE, Paten B, Akeson M. The Oxford nanopore minion: Delivery of nanopore sequencing to the genomics community. *Genome Biol* (2016) 17(1):239. doi: 10.1186/s13059-016-1103-0

33. Bruggemann M, Kotrova M, Knecht H, Bartram J, Boudjogrha M, Bystry V, et al. Standardized next-generation sequencing of immunoglobulin and T-cell receptor gene recombinations for mrd marker identification in acute lymphoblastic leukaemia; a euroclonality-ngs validation study. *Leukemia* (2019) 33(9):2241–53. doi: 10.1038/s41375-019-0496-7

34. Vergani S, Korsunsky I, Mazzarello AN, Ferrer G, Chiorazzi N, Bagnara D. Novel method for high-throughput full-length ighv-D-J sequencing of the immune repertoire from bulk b-cells with single-cell resolution. *Front Immunol* (2017) 8:1157. doi: 10.3389/fimmu.2017.01157

35. Heitzer E, Haque IS, Roberts CES, Speicher MR. Current and future perspectives of liquid biopsies in genomics-driven oncology. *Nat Rev Genet* (2019) 20(2):71–88. doi: 10.1038/s41576-018-0071-5

36. Jahr S, Hentze H, Englisch S, Hardt D, Fackelmayer FO, Hesch RD, et al. DNA Fragments in the blood plasma of cancer patients: Quantitations and evidence for their origin from apoptotic and necrotic cells. *Cancer Res* (2001) 61(4):1659–65.

37. Mouliere F, Chandrananda D, Piskorz AM, Moore EK, Morris J, Ahlborn LB, et al. Enhanced detection of circulating tumor DNA by fragment size analysis. *Sci Transl Med* (2018) 10(466). doi: 10.1126/scitranslmed.aat4921

38. Alcaide M, Cheung M, Hillman J, Rassekh SR, Deyell RJ, Batist G, et al. Evaluating the quantity, quality and size distribution of cell-free DNA by multiplex droplet digital pcr. *Sci Rep* (2020) 10(1):12564. doi: 10.1038/s41598-020-69432-x

39. Khier S, Lohan L. Kinetics of circulating cell-free DNA for biomedical applications: Critical appraisal of the literature. *Future Sci OA* (2018) 4(4):FSO295. doi: 10.4155/fsoa-2017-0140

40. Heitzer E, Perakis S, Geigl JB, Speicher MR. The potential of liquid biopsies for the early detection of cancer. *NPJ Precis Oncol* (2017) 1(1):36. doi: 10.1038/s41698-017-0039-5

41. Kustanovich A, Schwartz R, Peretz T, Grinshpun A. Life and death of circulating cell-free DNA. *Cancer Biol Ther* (2019) 20(8):1057–67. doi: 10.1080/15384047.2019.1598759

42. Wang Y, Springer S, Zhang M, McMahon KW, Kinde I, Dobbyn L, et al. Detection of tumor-derived DNA in cerebrospinal fluid of patients with primary tumors of the brain and spinal cord. *Proc Natl Acad Sci U.S.A.* (2015) 112 (31):9704–9. doi: 10.1073/pnas.1511694112

43. Frishman-Levy L, Izraeli S. Advances in understanding the pathogenesis of cns acute lymphoblastic leukaemia and potential for therapy. *Br J Haematol* (2017) 176(2):157–67. doi: 10.1111/bjh.14411

44. Terwilliger T, Abdul-Hay M. Acute lymphoblastic leukemia: A comprehensive review and 2017 update. *Blood Cancer J* (2017) 7(6):e577. doi: 10.1038/bcj.2017.53

45. Irving J, Jesson J, Virgo P, Case M, Minto L, Eyre L, et al. Establishment and validation of a standard protocol for the detection of minimal residual disease in b lineage childhood acute lymphoblastic leukemia by flow cytometry in a multi-center setting. *Haematologica* (2009) 94(6):870–4. doi: 10.3324/haematol.2008.000414

46. Gaipa G, Cazzaniga G, Valsecchi MG, Panzer-Grumayer R, Buldini B, Silvestri D, et al. Time point-dependent concordance of flow cytometry and real-time quantitative polymerase chain reaction for minimal residual disease detection in childhood acute lymphoblastic leukemia. *Haematologica* (2012) 97(10):1582–93. doi: 10.3324/haematol.2011.060426

47. Giudicelli V, Duroux P, Ginestoux C, Folch G, Jabado-Michaloud J, Chaume D, et al. Imgt/Ligm-db, the imgt comprehensive database of immunoglobulin and T cell receptor nucleotide sequences. *Nucleic Acids Res* (2006) 34(Database issue):D781–4. doi: 10.1093/nar/gkj088

48. Lefranc MP, Giudicelli V, Ginestoux C, Jabado-Michaloud J, Folch G, Bellahcene F, et al. Imgt, the international immunogenetics information system. *Nucleic Acids Res* (2009) 37(Database issue):D1006–12. doi: 10.1093/nar/gkn838

49. Christley S, Scarborough W, Salinas E, Rounds WH, Toby IT, Fonner JM, et al. Vdjserver: A cloud-based analysis portal and data commons for immune repertoire sequences and rearrangements. *Front Immunol* (2018) 9:976. doi: 10.3389/fimmu.2018.00976

50. Deak D, Gorcea-Andronic N, Sas V, Teodorescu P, Constantinescu C, Iluta S, et al. A narrative review of central nervous system involvement in acute leukemias. *Ann Transl Med* (2021) 9(1):68. doi: 10.21037/atm-20-3140

51. Thastrup M, Marquart HV, Levinsen M, Grell K, Abrahamsson J, Albertsen BK, et al. Flow cytometric detection of leukemic blasts in cerebrospinal fluid predicts risk of relapse in childhood acute lymphoblastic leukemia: A Nordic society of pediatric hematology and oncology study. *Leukemia* (2020) 34(2):336–46. doi: 10.1038/s41375-019-0570-1

frontiers | Frontiers in Oncology

TYPE Review
PUBLISHED 15 December 2022
DOI 10.3389/fonc.2022.1070479

OPEN ACCESS

EDITED BY
Rana Jahanban-Esfahlan,
Tabriz University of Medical Sciences, Iran

REVIEWED BY
Xinlei Li,
Nationwide Children's Hospital, United States
Adeleh Taghi Khani,
City of Hope, United States
Migara Jayasinghe,
National University of Singapore, Singapore

*CORRESPONDENCE
Taichiro Nonaka
taichiro.nonaka@lsuhs.edu

SPECIALTY SECTION
This article was submitted to Molecular and Cellular Oncology, a section of the journal Frontiers in Oncology

RECEIVED 14 October 2022
ACCEPTED 09 November 2022
PUBLISHED 15 December 2022

CITATION
Nonaka T (2022) Application of engineered extracellular vesicles to overcome drug resistance in cancer. *Front. Oncol.* 12:1070479. doi: 10.3389/fonc.2022.1070479

Application of engineered extracellular vesicles to overcome drug resistance in cancer

Taichiro Nonaka[1,2]*

[1]Department of Cellular Biology and Anatomy, Louisiana State University Health Sciences Center, Shreveport, LA, United States, [2]Feist-Weiller Cancer Center, Louisiana State University Health Shreveport, Shreveport, LA, United States

Targeted therapies have significantly improved survival rates and quality of life for many cancer patients. However, on- and off-target side toxicities in normal tissues, and precocious activation of the immune response remain significant issues that limit the efficacy of molecular targeted agents. Extracellular vesicles (EVs) hold great promise as the mediators of next-generation therapeutic payloads. Derived from cellular membranes, EVs can be engineered to carry specific therapeutic agents in a targeted manner to tumor cells. This review highlights the progress in our understanding of basic EV biology, and discusses how EVs are being chemically and genetically modified for use in clinical and preclinical studies.

KEYWORDS

extracellular vesicle, exosome, engineered EV, drug delivery, cancer

Introduction

Budding from the membranes of prokaryotic and eukaryotic cells, extracellular vesicles (EVs) act as intercellular messengers (1). They carry information in the form of proteins, lipids, RNA, and DNA to cells in the local environment and at distant sites, and retain many of the features of their parental cell of origin. Such information imprinting means that EVs can regulate processes during normal homeostasis; conversely, deregulation of EV function can translate to pathology in EV-targeted cells. This is exemplified by EV-dependent perturbations of the immune response, organ development, reproduction, and vasculogenesis (2, 3). EVs can also modulate the tumor microenvironment, leading to either enhanced or reduced tumorigenesis (4, 5). By understanding the fundamental biological processes that govern EV behavior, we will be able to exploit EVs to use them as conduits of anticancer therapeutics. By definition EVs are biocompatible, and researchers in the field are now fine-tuning EVs *via* chemical and genetic strategies to transform them into drug delivery systems (6). The pros and

cons of EVs in the context of cancer therapy is the main focus of this review. We draw upon examples from basic and translational research to highlight the advantages and limitations of EV use in the preclinical and clinical settings. Our aim is to provide a conceptual framework to spur on novel research approaches in the EV field, with the ultimate aim of improving survival rates in cancer patients.

Biochemical properties of EVs

EV secretion has been observed in virtually all kingdoms of life. EV biogenesis and cargo loading are tightly linked processes, and these steps are strictly regulated to ensure that the subsequent interaction with target cells produces the desired biological effects (7). Cargos as diverse as proteins, lipids, nucleic acids, cytokines and even organelles provide an information-rich payload that can be exploited to achieve downstream cellular effects (3). Indeed, the ExoCarta database contains 9,690 proteins, 3,300 mRNAs, and 1,010 different types of lipids that have been identified in exosomes, which underscores the complexity and heterogeneity of these nanostructures (8). Specific examples of select cargos are discussed below.

Small non-coding RNAs have been found within EVs, and may control molecular events in recipient cells by regulating the activity of target mRNAs, for example (9). These RNA cargos could be exploited as potential non-invasive biomarkers for multiple disorders such as those that affect the immune system (10). EV has been isolated from most cell types and body fluids, including saliva. Saliva diagnostics is a rapidly expanding field and the non-invasive saliva testing could greatly facilitate the early diagnosis of many diseases, including cancers (11, 12).

The lipid composition of EVs is very similar to that of their parental cells; this provides an ideal physical barrier to protect internal cargo from premature degradation. In addition to providing EV integrity, the large amounts of sphingomyelin and cholesterol prevent EV cargos from degradation by both nucleases and proteases (13). Such lipids also act as physiological buffers that ensure the pH and osmotic balance within EVs is maintained (14, 15). These properties could be exploited to effectively increase the amount of drug that is delivered to a particular tumor.

A suite of fatty acids in EVs provide the building blocks for the generation of signaling intermediates that regulate multiple physiological processes (16). Consistent with the coordinated regulation of EV biogenesis and function, the EVs also contain the enzymes required for conversion of fatty acids into bioactive products such as esterified fatty acids and eicosanoids (17). These features underlie the ability of EVs to regulate inflammatory processes involved in chronic tissue remodeling, cancer, asthma, rheumatoid arthritis and autoimmune disorders (18).

Strategies to functionalize EVs

Despite their advantageous small size and ability to cross the blood brain barrier, natural EVs require further optimization before they can be used for drug delivery. Major limitations include the lack of target cell specificity and an inability to store sufficient payload quantities. Great strides have been made with regard to improving the loading of heterogenous cargo (19). EV membranes can be decorated with a wide variety of molecules that increase target cell specificity and/or reduce the likelihood of EV destruction by host macrophages during immune surveillance (20, 21). Genetic and non-genetic manipulation can lead to a release of modified EVs by introducing targeting moieties such as bispecific antibody, single-domain antibody (nanobody), single-chain variable fragment (scFv), affibody, or targeting peptide that can bind to molecules on target cells (Figure 1).

Genetic manipulation of parental cells

Cellular nanoporation (CNP) is the method of choice for delivery of nucleic acids, including large mRNAs, to EVs (19). The mRNAs may encode tumor suppressor genes that comprise a therapeutic payload, or may encode fusion proteins that have a tumor cell-targeting domain and a bioactive domain. Portions of naturally occurring EV membrane proteins are often used in these fusion constructs; the N-terminus of Lamp2b and CD47 are two common examples. Peptides containing the Arg-Gly-Asp (RGD) integrin recognition motif have been fused to Lamp2b to increase the tumor homing capability of EVs (Figure 1). This has been used successfully to deliver the chemotherapeutic, doxorubicin, to tumor cells (22). In a similar approach, CDX and CREKA, two other tumor-targeting peptides, have been fused to CD47 to facilitate delivery of mRNA encoding the tumor suppressor, PTEN, to glioblastoma cells (19).

The single-chain transmembrane glycoprotein PDGFR has been exploited for breast cancer immunotherapy by Cheng et al., who designed nanoscale controllers termed synthetic multivalent antibody retargeted exosomes (SMART-Ex) (23). Using the PDGFR transmembrane domain as an anchor, single-chain variable fragments (scFv) that recognize either CD3, EGFR, or HER2 have been introduced to EV membranes (23, 24) (Figure 1). The CD8 transmembrane region has also been used to generate chimeric antigen receptor (CAR)-expressing EVs that target either EGFR or HER2; the CAR-EVs promoted tumor regression and did not elicit significant toxicity (25).

Interestingly, EV-type structures from non-mammalian organisms are also being evaluated for their potential as drug carriers. A case in point are bacterial outer membrane vesicles that have been engineered to express a HER2-specific antibody

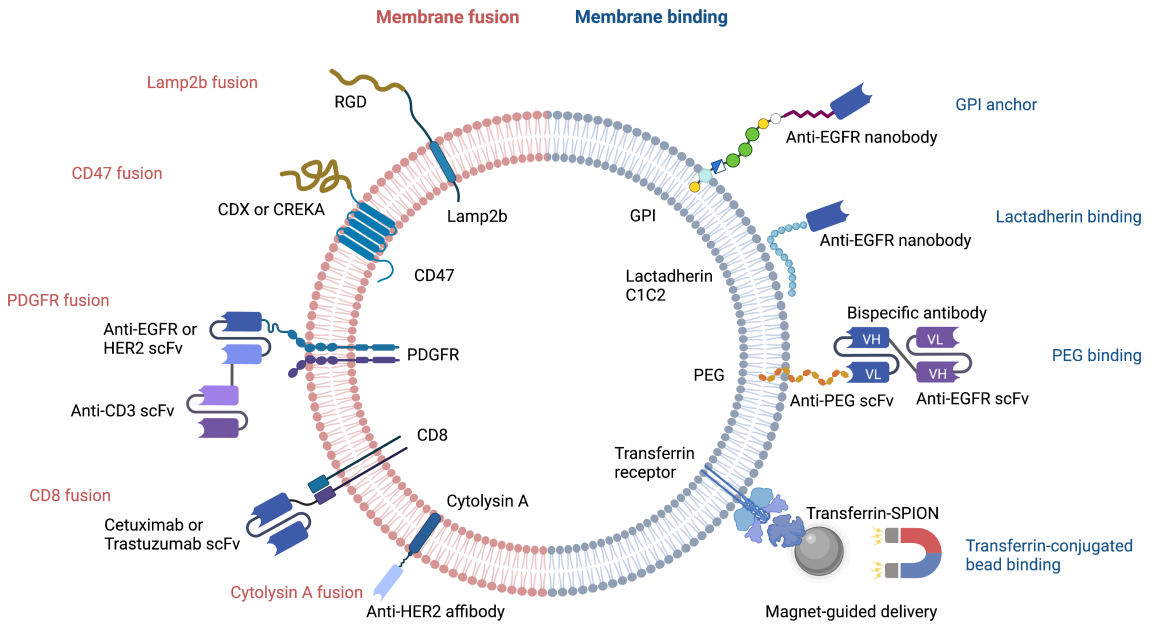

FIGURE 1
Strategies for targeted delivery of EVs. RGD, Arg-Gly-Asp peptide; CDX, d-peptide ligand of the nicotine acetylcholine receptor; CREKA, pentapeptide Cys-Arg-Glu-Lys-Ala; EGFR, epidermal growth factor receptor; HER2, human epidermal growth factor receptor 2; scFv, single-chain variable fragment; PDGFR, platelet-derived growth factor receptor; GPI, glycosylphosphatidylinositol; PEG, polyethylene glycol; Transferrin-SPION, transferrin-conjugated superparamagnetic iron oxide nanoparticle.

fused to the transmembrane region of the bacteria pore-forming protein, cytolysin A (26).

Modification of EV membranes

The therapeutic efficacy of EVs can be increased by bioconjugation of nanobodies or bispecific antibodies that bind to specific molecules and receptors on target cells. The ExoMAb approach exemplifies this strategy of engineering EVs to express non-natural antigens (27). Briefly, lactadherin contains a C1C2 domain which binds phosphatidylserine moieties in EV membranes. This provides the basis for decorating the EV membrane with exogenous proteins that are fused to C1C2 domain. This has been used to express tumor antigens at high-levels on EV membranes surface antigens, which could be exploited to generate tumor-specific antibodies. Anti-EGFR nanobodies have also been conjugated to glycosylphosphatidylinositol (GPI) anchor signal peptides or to the lactadherin C1C2 domain. This approach led to a remarkable improvement in selective cargo delivery to EGFR-positive cells (Figure 1) (28, 29).

Circulating EVs play a continuous 'cat and mouse' game with patrolling macrophages, which can phagocytose EVs upon recognition. This clearly reduces the effective half-life of EVs in the body. CD47 (mentioned above) can again be exploited here: by binding to signal regulatory protein alpha (SIRPα) on the surface of macrophages, CD47 sets up a 'don't eat me' signal (21, 30). Thus, CD47-decorated EVs have longer circulatory half-lives and are more likely to reach their target cancer cells to deliver a therapeutic payload (Figure 2). An extremely innovative approach builds on this by combining CD47-loaded red blood cell (RBC) membranes with membranes from cancer cells themselves (31). Since CD47 is overexpressed on the surface of RBC, chimeric EVs derived from RBC-MCF7 hybrid membrane protect EVs from phagocytosis. These hybrid EVs have a longer half-life, but also exploit antigens from the cancer cell membranes to re-target the original cancer cells (31). This has demonstrable therapeutic efficacy, as DOX-loaded hybrid EVs were able to induce tumor regression in a preclinical mouse model.

The EV membrane surface can be chemically or enzymatically modified to either increase EV half-life, or to alter its targeting selectivity. For example, polyethylene glycol (PEG) conjugation to the surface of EVs increases their half-life (32) (Figure 2). PEG can also be used as a 'recognition signal' for bispecific antibodies. Proof-of-concept is provided with a study using a PEG/EGFR bispecific antibody that increased specific targeting of PEG-loaded EVs to EGFR-positive tumors (33) (Figure 1). One can see here that PEG's effects on EV half-life and antibody targeting is a powerful combination. Altering the surface glycan composition of EVs *via* enzymatic removal of sialic acid moieties also changes their biodistribution (34);

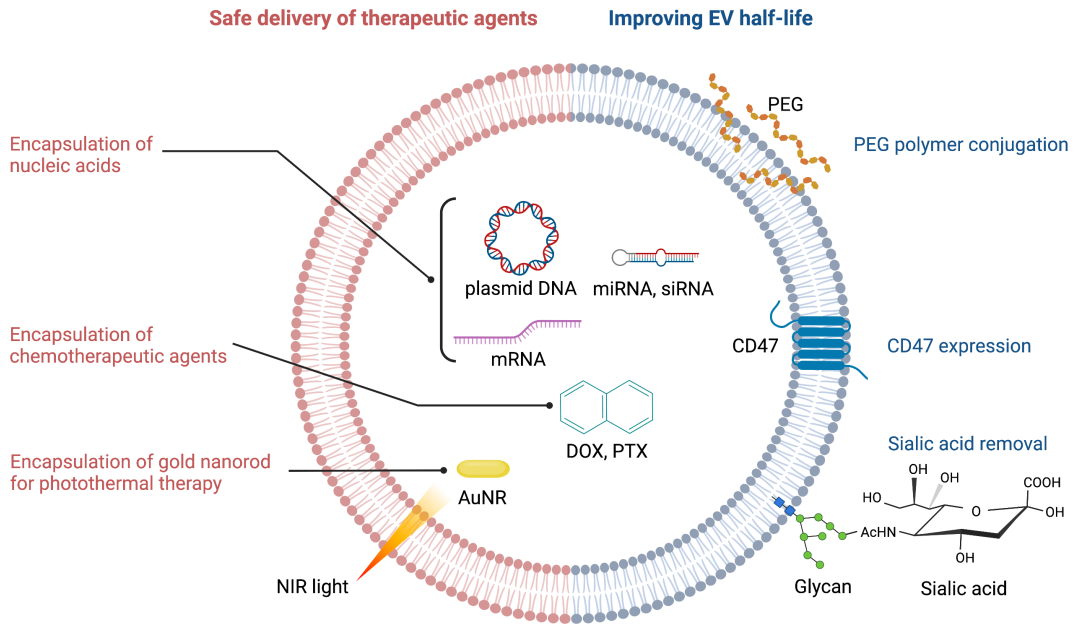

FIGURE 2
Strategies for improving therapeutic efficacy of EVs. PEG, polyethylene glycol; NIR, near infrared; AuNR, gold nanorod; DOX, doxorubicin; PTX, paclitaxel.

this could ultimately be exploited to achieve tumor-specific targeting of EVs (Figure 2).

Transferrin receptors are highly enriched on the surface of reticulocyte-derived EVs. This can be exploited to enrich and purify EVs during production, or to facilitate EV-dependent drug delivery. For example, transferrin-conjugated superparamagnetic iron oxide nanoparticles (SPIONs) have been used for targeted delivery of chemotherapeutic drugs (35) (Figure 1).

Fusion to liposomes or micelles offers an alternative to chemical modification of EV membranes. For example, fusion of EVs to liposomes using the freeze-thaw method increases the cellular uptake of these hybrid EVs (36). Micelles have been used to deliver PEG-conjugated EGFR single-chain Fab fragment (scFab) to EVs, thereby expanding the spectrum of therapeutics amenable to an EV approach (33).

Loading of exogenous molecules into EVs

Encapsulation of chemotherapeutic agents and safe delivery to the target tumor are the common challenges in EV-mediated cancer chemotherapy (Figure 2). Drugs such as nucleic acids can be loaded *via* passive methods, such as combining drugs with the lipid bilayer after incubation, or conjugating drugs to the EV surface. Alternatively, for drugs with high molecular weight (i.e. DOX, PTX, AuNR), active methods of loading such as mechanical or chemical opening of the EV membrane *via* sonication, electroporation, saponin treatment or freeze-thaw cycles can be employed (37). The active methods create temporary pores through which therapeutic payloads can enter. However, this is not without risk: the internal composition of EVs and their cargos can be compromised, which may reduce efficacy (32). Ultimately, the success of both the passive and active methods is determined by the source of EVs, the specific drug involved, and the experimental design (38).

For the evaluation of EVs in clinical trials, drug loading must be achieved using a robust protocol, and at an industrial scale to meet demands (39). These prerequisites have presented challenges, because EVs lack the intracellular structures of whole cells, and therefore are not amenable to approaches such as conventional transfection.

Sources of EVs

In this section, we describe the wide variety of systems from which EVs can be sourced. As will become evident, the precise choice of system will depend on the downstream application. We also provide several examples of the application of EVs to cancer therapy.

Despite their substantial contribution to cancer treatment, chemotherapeutic agents are prone to rapid clearance, are poorly

biocompatible, and suffer from low intra-tumoral delivery; they also induce systemic side effects and their efficacy is compromised by the onset of drug resistance (40). To overcome these challenges, various types of nanoscale delivery vehicles have been developed. These vehicles are associated with efficient drug delivery and tumor-specific targeting ability, and many have been evaluated in human clinical oncology trials (Table 1).

Tumor-derived EVs (TEX)

Tumor-derived EVs (TEX) preferentially home to and target the tumor cells from which they were derived (50) (Table 2). For example, accumulation of DOX in HT1080 xenografts was higher when the drug was delivered by HT1080-derived TEX rather than by those obtained from HeLa cells. Successful inhibition of tumor growth in other preclinical models using TEX carrying a chemotherapeutic payload has been independently confirmed (46). Furthermore, TEX have been used to deliver DOX-loaded porous silicon nanoparticles (PSiNPs) in mouse models of hepatocarcinoma, melanoma, and breast cancer (54). In each of these situations, beneficial attributes of EVs were observed. These included enhanced accumulation of drugs within tumors, more efficient extravasation and tissue penetration and striking anti-tumor activities.

Glioma is a devastating malignant brain tumor with a high mortality rate due to low penetration and efficacy of the available chemotherapeutics. TEX are already having an impact in this tumor type. For example, TEX-mediated delivery of IMV-001 (an antisense oligonucleotide against the transmembrane receptor, IGF1R) to patients with recurrent malignant glioma was more effective than other delivery methods due as it was associated with an increased number of tumor-infiltrating lymphocytes and enhanced anti-tumor immunity (57, 58). In glioblastoma, co-delivery of TEX with α-galactosylceramide enhanced the efficacy of a dendritic cell vaccine, likely due to

TABLE 1 Clinical trials for EV applications in human cancers.

Phase	Period	Location	N	EV source	EV cargo	Condition	Outcome	Clinical trial number and/or Reference
I	NA - 2002	USA	13	DEX	MAGE tumor antigen	NSCLC	2 stable diseases	(41)
I	2001 - 2004	France	15	DEX	MAGE tumor antigen	Melanoma	2 stable, 1 minor, 1 partial, 1 mixed responses	(42)
I	2006 - 2007	China	40	Malignant ascites	GM-CSF	Colorectal cancer	1 stable disease, 1 minor response	(43)
I	NA - 2008	France	15	DEX	NKG2D ligand	Melanoma	2 tumor regressions	(44)
I	2011 - recruiting	USA	35*	Plant	Curcumin	Colon cancer	NA	NCT01294072
I	2018 - recruiting	USA	28*	MSC	KRAS G12D siRNA	Pancreas cancer	NA	NCT03608631
I	2022 - recruiting	USA	30*	HEK293	STAT6 ASO	Hepatocellular carcinoma, gastric cancer, colorectal cancer	NA	NCT05375604
II	2010 - 2013	France	26	IFNg+ DEX	MAGE tumor antigen	NSCLC	7 stable diseases over 4 months	CSET 2008/1437 IDRCB 2008-A1171-54 (45)
II	2010 - 2015	France	41	DEX	MAGE tumor antigen	NSCLC	Progression free survival over 4 months	NCT01159288
II	2013 - 2014	China	30*	TEX	MTX, Cisplatin, PTX	Malignant pleural effusion, malignant ascites	NA	NCT01854866 (46)
II	2016 - 2019	China	90*	TEX	MTX	Malignant pleural effusion	NA	NCT02657460
NA	2013 - 2015	China	6	TEX	Cisplatin	End stage lung cancer	3 improved pleural effusions	(47)
NA	2015 - 2018	China	20	TEX	MTX	Cholangiocarcinoma	5 reliefs in biliary obstruction	ChiCTR-OIB-15007589 (48)
NA	2015 - 2019	China	62	TEX	MTX	Malignant pleural effusion	Decrease in MPE	ChiCTR-ICR-15006304 (49)

DEX, dendritic cell-derived EVs; MAGE, melanoma-associated antigen; NSCLC, non-small cell lung cancer; GM-CSF, granulocyte-macrophage colony-stimulating factor; ASO, antisense oligonucleotide; IFNg, interferon gamma; MTX, methotrexate; PTX, paclitaxel; NA, not applicable. *Estimated enrollment.

TABLE 2 Applications of TEX in murine tumor models.

EV source	EV cargo	Murine tumor model	Result	Reference
Rat C6 glioma cell line	Tumor peptide	Glioma	Inhibited tumor growth	(51)
Mouse J774A.1	DOX, c-Met binding peptide	Breast cancer	Inhibited tumor growth	(52)
Mouse Hepa1-6, 4T1, Panc02	HMGN1 adjuvant	Hepatocellular carcinoma	Inhibited tumor growth	(53)
Mouse H22	DOX-loaded porous silicon nanoparticles	Hepatocarcinoma, melanoma, breast cancer	Inhibited tumor growth	(54)
Mouse H22, human A2780	MTX, Cisplatin, PTX	Hepatocarcinoma, ovarian cancer	Inhibited tumor growth	(46)
Human HT1080, HeLa	DOX	Fibrosarcoma	Inhibited tumor growth	(50)
Human MCF-7	V_2C QDs, TAT peptide, PEG, RGD	Breast cancer	NIR laser irradiation almost completely killed tumor cells	(55)
Hybrid RBC and MCF-7 cell membranes	DOX	Breast cancer	Inhibited tumor growth	(31)
Human MDA-MB-231	PTX, CuB	Breast cancer	Inhibited tumor growth and lung metastasis	(56)

DOX, doxorubicin; c-Met, mesenchymal-epithelial transition factor; HMGN1, high mobility group nucleosome-binding protein 1; MTX, methotrexate; PTX, paclitaxel; V_2C QDs, vanadium carbide quantum dots; TAT, transactivator of transcription of human immunodeficiency virus; PEG, polyethylene glycol; RGD, Arg-Gly-Asp peptide; NIR, near infrared; RBC, red blood cell; CuB, cucurbitacin B.

its stimulation of immunomodulatory factor release into the tumor microenvironment (51).

In the liver cancer setting, administration of functionalized TEX loaded with an adjuvant, high mobility group nucleosome-binding protein 1 (HMGN1), reduced tumor size and potentiated immunogenicity in a mouse model of hepatocellular carcinoma (53) (Table 2). Furthermore, treatment of end-stage extrahepatic cholangiocarcinoma patients with malignant biliary obstruction with MTX-loaded TEX was efficacious and relieved biliary obstruction (48).

Pleural effusions and ascites are abnormal fluid collections within the thoracic and peritoneal cavity, respectively. They are frequent in terminal stage malignancies, and require aspiration and paracentesis to manage disease conditions. TEX may be particularly suited to drug delivery for pleural effusions. For example, A549 tumor cell-derived EVs loaded with methotrexate (MTX) induced neutrophil recruitment in the effusion fluid and improved primary malignant pleural effusion (MPE) in non-small cell lung cancer patients (49). Additionally, two clinical trials have been conducted in patients with MPE to explore the anti-tumor effects of methotrexate- or cisplatin-loaded TEX (NCT01854866, NCT02657460) (Table 1). End-stage lung cancer patients with metastatic malignant pleural effusion (MPE) and resistance to cisplatin were treated with cisplatin-loaded TEX (47). This led to a 95% reduction in the number of tumor cells in the malignant fluids, and was associated with increased survival rate without significant side effects.

In addition to tumor cells themselves, TEX are also present in ascites. These ascites-derived TEX can also be exploited for cancer treatment, as exemplified in a clinical trial (43) (Table 1). This study demonstrated that treatment of advanced colorectal cancer with TEX from malignant ascites plus GM-CSF induced a specific anti-tumor T cell response.

Mesenchymal stem cell-derived EVs (STEX)

Mesenchymal stem cell (MSC)-derived EVs (STEX) arise from different tissues in normal and disease conditions and have beneficial effects in wound healing (59), myocardial infarction (60), acute kidney injury (61), hepatic injury (62), neonatal lung injury (63) and optic nerve injury (64). STEX may be particularly suitable for therapeutic applications due to their excellent safety profile, low immunogenicity, and their ability to cross biological barriers (65). They have been used to successfully deliver both chemical and genetic payloads, as we discuss below.

Human umbilical cord STEX enhance drug-induced apoptosis of leukemic cells *in vitro* (66) and increase their sensitivity to the anticancer drug imatinib through caspase activation (67). STEX can also deliver genetic cargos. For example, STEX-mediated delivery of miR-379 significantly suppressed breast cancer growth *in vivo* by decreasing cyclooxygenase (COX)-2 expression (68) (Table 3). Furthermore, an ongoing phase I clinical trial in KRAS G12D-mutant pancreatic cancer is evaluating the optimal dose and adverse effects of STEX loaded with KRAS G12D siRNA (NCT03608631) (Table 1).

Adipose tissue-derived mesenchymal stromal cells (AD-MSCs) are one of the most studied STEX sources because they are easier to obtain and harvest through subcutaneous lipoaspiration; this is much less painful and less ethically sensitive than collecting bone marrow or embryonic stem

TABLE 3 Applications of MSC- and HEK293-derived EVs in murine tumor models.

EV source	EV cargo	Murine tumor model	Result	Reference
Mouse MSCs	TNFα, SPION	Melanoma	Inhibited tumor growth	(69)
Rat AD-MSCs	b-catenin	Hepatocellular carcinoma	Inhibited tumor growth	(70)
Mouse AD-MSCs	miR-16-5p	Breast cancer	Inhibited tumor growth	(71)
Human AD-MSCs	miR-101	Osteosarcoma	Inhibited lung metastasis	(72)
Human BM-MSCs	GRP78 siRNA	Hepatocellular carcinoma	Inhibited tumor growth and metastasis	(73)
Human BM-MSCs	miR-379	Breast cancer	Inhibited tumor growth	(68)
Human HEK293	ASO-STAT6	Colorectal cancer, hepatocellular carcinoma	Inhibited tumor growth	(74)
Human HEK293T	BCR-ABL siRNA, Imatinib, LAMP2B-IL3	Chronic myeloid leukemia	Inhibited CML	(75)
Human HEK293T	PSMA, EGFR, or Folate aptamer; Survivin siRNA	Prostate, breast, colorectal cancer	Inhibited tumor growth	(76)
Human HEK293T	DOX, lipHA	Breast cancer	Inhibited tumor growth	(77)
Human HEK293T	miR-21-sponge	Glioma	Inhibited tumor growth	(78)
Human HEK293T	miR-21 inhibitor, 5-FU, LAMP2-HER2 affibody	Colorectal cancer	Inhibited tumor growth	(79)

SPION, superparamagnetic iron oxide nanoparticle; GRP78, glucose regulatory protein 78; ASO-STAT6, antisense oligonucleotide targeting STAT6; BCR-ABL, fusion gene of breakpoint cluster region BCR and tyrosine-protein kinase ABL1; LAMP2B-IL3, fusion protein of LAMP2B and interleukin 3; CML, chronic myeloid leukemia; PSMA, prostate-specific membrane antigen; EGFR, epidermal growth factor receptor; lipHA, lipidomimetic chains-grafted hyaluronic acid; LAMP2-HER2 affibody, fusion protein of LAMP2 and anti-HER2 (human epidermal growth factor receptor 2) affibody.

cells (80, 81). In the first animal study of its kind, Ko et al. found that AD-MSC-derived EVs significantly increased the number of circulating NKT cells and inhibited HCC tumor growth (70). Following demonstrations that AD-MSCs have anti-tumor effects in bladder cancer (82), prostate cancer (83) and breast cancer (71) *via* induction of apoptosis, there has been a surge of interest in the use of AD-MSCs for cancer therapy. This is highlighted by the finding that delivery of miR-101 by AD-MSC-derived EVs downregulated BCL6 and inhibited the metastasis of osteosarcoma to the lungs in a preclinical mouse model (72) (Table 3).

Bone marrow-derived STEX carrying GRP78 siRNA enhanced sorafenib sensitivity in an HCC xenograft mouse model (73) (Table 3). Moreover, miR-125b-loaded EVs derived from AD-MSCs specifically reduced HCC cell proliferation *in vitro* by activation of the p53 tumor suppressor (84). STEX are currently under investigation in clinical trials beyond cancer, including those focused on neurological and cardiovascular diseases, and SARS-CoV-2 (85).

HEK293-derived EVs (HEX)

HEK293T cells have been widely used as EV producer cells due to their inherent rapid proliferation, high EV yield, and ease of genetic manipulation (86–90). HEK293-derived EVs (HEX) have been used to deliver gene therapies including miRNA for breast cancer (91) and both chemotherapeutics and therapeutic protein constructs in a schwannoma model (92). Notably, HEX are more readily taken up by human neural stem cells when compared to mature neurons, suggesting that they might be used to modulate undifferentiated neurons in future therapeutic applications (93).

Administration of HEX loaded with a miR-21 sponge construct (which prevents miR-21 binding to its natural target) significantly reduced tumor burden in a C6 glioma rat model (78) (Table 3). Since miR-21 is overexpressed in glioma, we infer that miR-21 sponge-loaded EVs will reduce the proliferation and malignant metastatic behavior of tumor cells in patients. Additionally, HEX loaded with an antisense oligonucleotide (ASO) targeting STAT6 selectively silenced expression of this transcription factor in colorectal cancer and HCC mouse models; combined with anti-PD1 immunotherapy, this led to greater than 90% inhibition of tumor growth (74) (Table 3). With the same strategy, an ongoing phase I clinical trial is evaluating the pharmacokinetics and pharmacodynamics of exoASO-STAT6 (CDK-004) in advanced HCC, colorectal cancer, and liver metastases from gastric cancer (NCT05375604) (Table 1).

Dendritic cell-derived EVs (DEX)

Cancer vaccines are used to boost the endogenous human immune response to cancer through enhanced recognition of tumor cell-related antigens. Adding to the therapeutic arsenal in this area are dendritic cell-derived EVs (DEX), which express MHC-I- and MHC-II-bound antigen peptides as well as other

adhesion molecules (94). Pioneering work demonstrated that EVs derived from tumor peptide-pulsed bone marrow dendritic cells (BMDC) could prime cytotoxic T cells and thereby facilitate tumor growth inhibition in syngeneic tumor mouse models (95) (Table 4).

DEX can activate CD4+ T cells by inducing Th1 and Th2 immune responses, irrespective of the maturity of the DCs (102). However, large and small DEX constructs differ in their capacity to induce a T cell response, favoring cytokine secretion by Th2 and Th1 cell subtypes, respectively. A Phase II clinical trial evaluating DEX loaded with tumor antigen in patients with unresectable non-small cell lung cancer has recently been completed. The trial revealed activation of both innate and adaptive immunity, and over 4 months of progression-free survival in 32% of patients (NCT01159288) (45) (Table 1). Another Phase I trial in this cancer type showed that DEX therapy was well-tolerated and elicited only minor adverse effects (41).

NK cell-derived EVs (NEX)

NK cell-derived EVs (NEX) can carry cargo such as cytotoxic proteins, miRNAs, and cytokines that employ multiple mechanisms to kill tumor cells (103). They also exhibit immunomodulatory activity by stimulating other immune cells. Prior studies have demonstrated that NEX contain not only FasL and perforin but also TNFα; these molecules can all trigger melanoma cell death (96, 104) (Table 4). NEX exposed to neuroblastoma cells can 'teach' naive NK cells to recognize and kill these cancer cells, thereby overcoming immune resistance (97). Moreover, tumor cell growth is blocked by NEX containing the tumor suppressor miR-186, and these NEX also derepress TGFβ1-dependent inhibition of NK cells (98). These findings suggest that, in addition to their role as drug carriers, NEX can act as immunotherapeutic agents.

Macrophage-derived EVs (MEX)

Macrophages can be categorized into anti-tumor M1 and protumor M2 subtypes, and reprogramming between these phenotypes has been exploited for anticancer therapy (74). Macrophage-derived EVs (MEX) derived from the M1 macrophage cell line, RAW264.7, accumulate at the tumor site and promote M2-to-M1 macrophage reprogramming (100). MEX loaded with DOX also induced apoptosis and suppressed the growth of xenografts in a murine model of breast cancer (101) (Table 4).

Plant-derived EVs (PEX)

Fruits and vegetables have been used historically as medicines to treat numerous diseases. Following the discovery of plant-derived EVs (PEX), which can be isolated by extracting apoptotic vesicles from leaf, sunflower seeds, and roots (105), it was a natural progression to investigate whether they could be harnessed for therapeutic benefit (106). The choice of a specific PEX is determined by the type of health-promoting molecule that is enriched within each plant; this selection must match the disease to be treated. Specific examples follow below.

The consumption of grapes may reduce the impact of risk factors associated with multiple diseases, including cancer (107). This has been attributed to the presence of anti-inflammatory flavonoids (107), phenolic acids and polyphenols that exert anti-cancer activity by scavenging reactive oxygen species (108). It is therefore not surprising that PEX from grapes and grapefruit exhibit anti-inflammatory properties (109, 110) and can reduce colitis in murine models (109, 111).

TABLE 4 Applications of DC-, NK-, and macrophage-derived EVs in murine tumor models.

EV source	EV cargo	Murine tumor model	Result	Reference
Mouse BMDCs	Tumor peptide	Mastocytoma, mammary adenocarcinoma	Inhibited tumor growth	(95)
Mouse imDCs	DOX, Lamp2b-RGD	Breast cancer	Inhibited tumor growth	(22)
Human NK92-MI	FasL, perforin, TNFa	Melanoma	Inhibited tumor growth	(96)
Human NK cells from healthy donor	NKG2D, NKp44, NKp30	Neuroblastoma	Inhibited tumor growth	(97)
Human NK cells from healthy donor	miR-186	Neuroblastoma	Inhibited tumor growth	(98)
Mouse RAW264.7	PTX	Lung cancer	Inhibited tumor growth and lung metastasis	(99)
Mouse RAW264.7	LFA-1	Colorectal cancer	Inhibited tumor growth	(100)
Mouse RAW264.7	DOX	Breast cancer	Inhibited tumor growth	(101)

BMDC, bone marrow-derived dendritic cell; imDC, mouse immature dendritic cell; RAW264.7, mouse macrophage cell line; Lamp2b-RGD, fusion protein of Lamp2b and Arg-Gly-Asp peptide; LFA-1, lymphocyte function-associated antigen 1.

Ginger contains gingerol, which has powerful antioxidant and anti-inflammatory properties (112); together with other compounds in ginger root, this may explain the ability of extracts from this plant to inhibit oxidative stress, arthritis, inflammation, and various types of infection (113). Ginger may also decrease the risk of cancer and diabetes (112, 114). As highlighted for grapes, ginger PEX are also able to attenuate inflammation (115) and reduce the pathologies associated with colitis (116).

Although their anti-inflammatory effects are well established, the evaluation of PEX as cancer therapeutics is still in the early stages. However, initial results are encouraging. For example, PEX from citrus lemons suppressed chronic myeloid leukemia xenograft growth by inducing TRAIL-mediated cell death (117) (Table 5). Additionally, an ongoing phase I clinical trial (NCT01294072) is evaluating whether PEX can be used to deliver curcumin (a constituent of the spice, turmeric) to perturb tumor cell metabolism and modulate the immune response in colon cancer patients (Table 1). There is a strong underlying preclinical evidence for this, because curcumin was reported to suppress colon cancer in a murine xenograft model by inhibiting Wnt/β-catenin signaling (122). A separate *in vitro* study showed that curcumin significantly arrested the growth of human colon cancer cells (123). These promising early data provide the rationale for further study of the therapeutic effects of PEX in diverse diseases.

Application of EVs in cancer therapy

Following the discussion of the sources of EVs above, we now present several examples of how EVs are being used to complement and enhance current anti-cancer approaches. It should become apparent from this discussion that the targeting potential of EVs, as well as some of their innate abilities to penetrate cell membranes, offers great promise in the realm of cancer therapy.

Tumor-specific targeting

A major obstacle to effective cancer chemotherapy is a lack of tumor-specific targeting, which is associated with toxicity in normal tissues. Superparamagnetic iron oxide nanoparticles (SPIONs) have great potential utility as magnetic nanoplatforms for targeted drug delivery (124), as they can be directed to the required tissue area through the use of external magnets. SPIONs conjugated with transferrin can readily be attached to EVs, which express high surface levels of the transferrin receptor (125). The SPION-decorated EVs can be loaded with a chemotherapeutic agent and then directed to the tumor site using magnets. This has been elegantly demonstrated by Zhang et al., who observed DOX-dependent tumor regression and increased survival in a preclinical model using this approach (120). The SPION approach has also been used to enhance the cytotoxic effect of the pro-apoptotic cytokine, TNFα, in melanoma cells (69).

An alternative to SPIONs with regard to tumor-specific targeting is the use of aptamers. Aptamers are short single-stranded DNA or RNA that can bind to a specific target molecule (126). Aptamers can be used for therapeutic purposes in the same way as monoclonal antibodies. For example, EVs loaded with siRNA against the anti-apoptotic molecule, survivin, have been specifically delivered to prostate cancer cells *in vivo* using prostate-specific membrane antigen (PSMA) aptamers (76) (Table 3). In a similar manner, EGFR aptamer-conjugated EVs loaded with survivin siRNA inhibited tumor growth in an orthotopic breast cancer mouse model (76). We believe that the aptamer approach could readily be exploited to treat other cancer types. For example, the interleukin-3 receptor (IL3R) is overexpressed on chronic myeloid leukemia (CML) cells, but is absent or expressed at low levels on normal hematopoietic stem cells. This suggests that IL3R could serve as a receptor target for EV-based cancer drug delivery systems (127–129).

TABLE 5 Applications of plant-derived and other EVs in murine tumor models.

EV source	EV cargo	Murine tumor model	Result	Reference
Grapefruit	Stat3 inhibitor JSI-124	Brain cancer	Inhibited tumor growth	(118)
Citrus limon	TRAIL-stimulating factor	Chronic myeloid leukemia	Inhibited CML	(117)
Mouse whole blood	Photosensitizer PpIX fused with NLS peptide	Breast cancer	630 nm He-Ne laser irradiation inhibited tumor growth	(119)
Human neutrophils from healthy donor	DOX, SPION	Colorectal cancer	Inhibited tumor growth	(120)
Human BJ foreskin fibroblast	KRAS G12D siRNA	Pancreatic cancer	Inhibited metastasis	(21)
Human H9 ES cell line	PTX, RGD	Brain cancer	Inhibited tumor growth	(121)

PpIX, Protoporphyrin IX; NLS, nuclear localization signal.

Overcoming drug resistance

Following several rounds of chemotherapy, the onset of drug resistance leads to reduced survival. Several lines of evidence suggest that EVs may offer breakthroughs in this challenging area. For example, HEX modified with lipidomimetic chain-grafted hyaluronic acid can efficiently deliver DOX and reverse multi-drug resistance in breast cancer cells (77) (Table 3). In a 5-FU-resistant HER2-positive colorectal cancer mouse model, co-delivery of an miR-21 inhibitor using EVs decorated with a LAMP2-HER2 affibody fusion significantly enhanced cytotoxicity and restored 5-FU sensitivity (79). Multidrug-resistant Madin-Darby canine kidney cells can be re-sensitized to paclitaxel when the drug is delivered *via* EVs (99). Finally, HEX loaded with imatinib and siRNA to the driver oncogene, BCR-ABL, have been used to re-sensitize CML xenografts to imatinib in a preclinical model (75).

Hard-to-treat tumors

Primary brain tumors and tumors that metastasize to the brain are difficult to treat due to poor drug penetrance across the blood brain barrier (BBB). EVs may offer a natural solution to this problem because they are nanosized membrane vesicles that can easily pass through the BBB. The combination of BBB penetration and tumor cell-selective targeting using EVs has been compellingly demonstrated in glioma. Specifically, EVs decorated with RGERPPR, a peptide ligand for neuropilin-1 which is highly expressed on glioma cells but not other neuronal cells (130, 131), were able to target glioma cells in an orthotopic mouse model (132). Another example of EV success in brain tumors is the selective targeting of glioblastoma cells, which overexpress integrin αVβ3 receptors (133). EVs loaded with paclitaxel (PTX) and conjugated with RGD peptides which have high affinity for αVβ3 receptors were able to target orthotopic glioblastomas and prolong survival in a mouse model (121).

Triple negative breast cancer (TNBC) has the worst prognosis of all breast cancers, primarily because it lacks estrogen and progesterone receptors, and has extremely low levels of HER2 (134, 135). However, TNBC cells express high levels of the c-Met tyrosine kinase oncogene, which is associated with poor prognosis and drug resistance (136, 137), and could be targeted by EVs. Proof-of-concept has been demonstrated *via* the delivery of DOX to TNBC xenografts using MEX coated with the c-Met binding peptide, CBP (52, 138).

Enhancing other therapeutic modalities

EVs can be used in combination with cutting edge drug delivery and activation technologies, such as photothermal and photodynamic therapies. Gold nanorods (AuNRs) have unique properties that make them attractive for applications in bioimaging, drug delivery, and photothermal therapy in cancer (139). Irradiating AuNRs with near-infrared light (NIR) produces a moderate temperature rise in the target region that leads to selective damage in tumor tissues (Figure 2). Since NIR lasers can be manipulated precisely, this activation mechanism provides an ideal and versatile platform to simultaneously deliver heat and anticancer drugs with control over the exposure area, time, and dosage. An alternative photothermal agent is the vanadium carbide quantum dot (V_2C QD). This compound has higher photothermal conversion efficiency than AuNRs, and V_2C QD-loaded EVs have superior biocompatibility and long circulation times combined with advanced antitumor activity (55) (Table 2).

Photodynamic therapy (PDT) requires light and a photosensitizing chemical substance that produces an oxygen radical to elicit cell death (140). EVs conjugated with the photosensitizer protoporphyrin IX (PpIX) and nuclear localization signal (NLS) peptide have good biocompatibility and the ability to target the nucleus. This subcellular targeting strategy and the cytotoxic reactive oxygen species generated by the photosensitizer enhances the efficacy of PDT, opening a new window for cancer therapy (119).

Conclusion and future perspective

There is great demand for safe, efficient, and versatile drug delivery systems for cancer therapy. Engineered EVs hold great promise in this regard, given their ability to specifically target and efficiently transfer therapeutic agents into cancer cells. However, more evaluation is required to produce and incorporate engineered EVs into clinically relevant systems, weighing the potential risks and benefits of this new approach. While the use of allogenic EVs appears feasible, the selection of parental cells, assessment of immunologic and oncogenic effects, and risk of viral contamination need to be carefully considered.

Successful clinical translation of EVs depends on the availability of reliable methods for large-scale production, isolation, and characterization to minimize lot-to-lot variations in drug-loaded EVs (141). A potential solution to many of these challenges is the use of EV mimics or artificial EV generated by chemical or genetic modification. Fusion of drug-loaded liposomes with EVs can enhance drug loading and targeting abilities (142), while customized production of EVs by exogenously implanted cells offers a new route for the production of engineered EVs *in vivo* (143). Although further studies are required to develop safer, more efficient, and cost-effective methods for generating engineered EVs for practical applications in oncology, the future is decidedly bright for this next-generation cancer therapy.

Author contributions

The author confirms being the sole contributor of this work and has approved it for publication.

Funding

The work was supported by National Institutes of Health Grants (R03 DE029272), Feist-Weiller Cancer Center Foundation Legacy Fund, and LSU Collaborative Cancer Research Initiative (CCRI) Fund to TN.

Acknowledgments

The work was supported by National Institutes of Health Grants (R03 DE029272), Feist-Weiller Cancer Center Foundation Legacy Fund, and LSU Collaborative Cancer Research Initiative (CCRI) Fund to TN. Figures were created with BioRender.com.

Conflict of interest

The author declares that the research was conducted in the absence of any commercial or financial relationships that could be construed as a potential conflict of interest.

Publisher's note

All claims expressed in this article are solely those of the authors and do not necessarily represent those of their affiliated organizations, or those of the publisher, the editors and the reviewers. Any product that may be evaluated in this article, or claim that may be made by its manufacturer, is not guaranteed or endorsed by the publisher.

References

1. Colombo M, Raposo G, Thery C. Biogenesis, secretion, and intercellular interactions of exosomes and other extracellular vesicles. *Annu Rev Cell Dev Biol* (2014) 30:255–89. doi: 10.1146/annurev-cellbio-101512-122326

2. Amabile N, Guerin AP, Leroyer A, Mallat Z, Nguyen C, Boddaert J, et al. Circulating endothelial microparticles are associated with vascular dysfunction in patients with end-stage renal failure. *J Am Soc Nephrol* (2005) 16(11):3381–8. doi: 10.1681/ASN.2005050535

3. Yanez-Mo M, Siljander PR, Andreu Z, Zavec AB, Borras FE, Buzas EI, et al. Biological properties of extracellular vesicles and their physiological functions. *J Extracell Vesicles* (2015) 4:27066. doi: 10.3402/jev.v4.27066

4. Kalluri R. The biology and function of exosomes in cancer. *J Clin Invest* (2016) 126(4):1208–15. doi: 10.1172/JCI81135

5. Tkach M, Thery C. Communication by extracellular vesicles: where we are and where we need to go. *Cell* (2016) 164(6):1226–32. doi: 10.1016/j.cell.2016.01.043

6. Kalluri R, LeBleu VS. The biology, function, and biomedical applications of exosomes. *Science* (2020) 367(6478). doi: 10.1126/science.aau6977

7. Valadi H, Ekstrom K, Bossios A, Sjostrand M, Lee JJ, Lotvall JO. Exosome-mediated transfer of mrnas and microrna is a novel mechanism of genetic exchange between cells. *Nat Cell Biol* (2007) 9(6):654–9. doi: 10.1038/ncb1596

8. Keerthikumar S, Chisanga D, Ariyaratne D, Saffar H, Anand S, Zhao K, et al. Exocarta: A web-based compendium of exosomal cargo. *J Mol Biol* (2015) 428. doi: 10.1016/j.jmb.2015.09.019

9. O'Brien K, Breyne K, Ughetto S, Laurent LC, Breakefield XO. Rna delivery by extracellular vesicles in mammalian cells and its applications. *Nat Rev Mol Cell Biol* (2020) 21(10):585–606. doi: 10.1038/s41580-020-0251-y

10. Turchinovich A, Drapkina O, Tonevitsky A. Transcriptome of extracellular vesicles: state-of-the-art. *Front Immunol* (2019) 10:202. doi: 10.3389/fimmu.2019.00202

11. Nonaka T, Wong DTW. Liquid biopsy in head and neck cancer: Promises and challenges. *J Dent Res* (2018) 97(6):701–8. doi: 10.1177/0022034518762071

12. Nonaka T, Wong DTW. Saliva diagnostics. *Annu Rev Anal Chem (Palo Alto Calif)* (2022) 15(1):107–21. doi: 10.1146/annurev-anchem-061020-123959

13. Niemelä P, Hyvönen MT, Vattulainen I. Structure and dynamics of sphingomyelin bilayer: Insight gained through systematic comparison to phosphatidylcholine. *Biophys J* (2004) 87(5):2976–89. doi: 10.1529/biophysj.104.048702

14. Fathali H, Dunevall J, Majdi S, Cans AS. Extracellular osmotic stress reduces the vesicle size while keeping a constant neurotransmitter concentration. *ACS Chem Neurosci* (2017) 8(2):368–75. doi: 10.1021/acschemneuro.6b00350

15. Parolini I, Federici C, Raggi C, Lugini L, Palleschi S, De Milito A, et al. Microenvironmental ph is a key factor for exosome traffic in tumor cells. *J Biol Chem* (2009) 284(49):34211–22. doi: 10.1074/jbc.M109.041152

16. Record M, Carayon K, Poirot M, Silvente-Poirot S. Exosomes as new vesicular lipid transporters involved in cell-cell communication and various pathophysiologies. *Biochim Biophys Acta* (2014) 1841(1):108–20. doi: 10.1016/j.bbalip.2013.10.004

17. Boilard E. Extracellular vesicles and their content in bioactive lipid mediators: more than a sack of microrna. *J Lipid Res* (2018) 59(11):2037–46. doi: 10.1194/jlr.R084640

18. Harizi H, Corcuff JB, Gualde N. Arachidonic-acid-derived eicosanoids: roles in biology and immunopathology. *Trends Mol Med* (2008) 14(10):461–9. doi: 10.1016/j.molmed.2008.08.005

19. Yang Z, Shi J, Xie J, Wang Y, Sun J, Liu T, et al. Large-scale generation of functional mrna-encapsulating exosomes *via* cellular nanoporation. *Nat BioMed Eng* (2020) 4(1):69–83. doi: 10.1038/s41551-019-0485-1

20. Alvarez-Erviti L, Seow Y, Yin H, Betts C, Lakhal S, Wood MJA. Delivery of sirna to the mouse brain by systemic injection of targeted exosomes. *Nat Biotechnol* (2011) 29(4):341–5. doi: 10.1038/nbt.1807

21. Kamerkar S, LeBleu VS, Sugimoto H, Yang S, Ruivo CF, Melo SA, et al. Exosomes facilitate therapeutic targeting of oncogenic kras in pancreatic cancer. *Nature* (2017) 546(7659):498–503. doi: 10.1038/nature22341

22. Tian Y, Li S, Song J, Ji T, Zhu M, Anderson GJ, et al. A doxorubicin delivery platform using engineered natural membrane vesicle exosomes for targeted tumor therapy. *Biomaterials* (2014) 35(7):2383–90. doi: 10.1016/j.biomaterials.2013.11.083

23. Cheng Q, Shi X, Han M, Smbatyan G, Lenz HJ, Zhang Y. Reprogramming exosomes as nanoscale controllers of cellular immunity. *J Am Chem Soc* (2018) 140(48):16413–7. doi: 10.1021/jacs.8b10047

24. Shi X, Cheng Q, Hou T, Han M, Smbatyan G, Lang JE, et al. Genetically engineered cell-derived nanoparticles for targeted breast cancer immunotherapy. *Mol Ther* (2020) 28(2):536–47. doi: 10.1016/j.ymthe.2019.11.020

25. Fu W, Lei C, Liu S, Cui Y, Wang C, Qian K, et al. Car Exosomes derived from effector car-t cells have potent antitumour effects and low toxicity. *Nat Commun* (2019) 10(1):4355. doi: 10.1038/s41467-019-12321-3

26. Gujrati V, Kim S, Kim SH, Min JJ, Choy HE, Kim SC, et al. Bioengineered bacterial outer membrane vesicles as cell-specific drug-delivery vehicles for cancer therapy. *ACS Nano* (2014) 8(2):1525–37. doi: 10.1021/nn405724x

27. Delcayre A, Estelles A, Sperinde J, Roulon T, Paz P, Aguilar B, et al. Exosome display technology: applications to the development of new diagnostics

and therapeutics. *Blood Cells Mol Dis* (2005) 35(2):158–68. doi: 10.1016/j.bcmd.2005.07.003

28. Kooijmans SA, Aleza CG, Roffler SR, van Solinge WW, Vader P, Schiffelers RM. Display of Gpi-anchored anti-egfr nanobodies on extracellular vesicles promotes tumour cell targeting. *J Extracell Vesicles* (2016) 5:31053. doi: 10.3402/jev.v5.31053

29. Kooijmans SAA, Gitz-Francois J, Schiffelers RM, Vader P. Recombinant phosphatidylserine-binding nanobodies for targeting of extracellular vesicles to tumor cells: a plug-and-play approach. *Nanoscale* (2018) 10(5):2413–26. doi: 10.1039/c7nr06966a

30. Koh E, Lee EJ, Nam GH, Hong Y, Cho E, Yang Y, et al. Exosome-sirpalpha, a cd47 blockade increases cancer cell phagocytosis. *Biomaterials* (2017) 121:121–9. doi: 10.1016/j.biomaterials.2017.01.004

31. Zhang K-L, Wang Y-J, Sun J, Zhou J, Xing C, Huang G, et al. Artificial chimeric exosomes for anti-phagocytosis and targeted cancer therapy. *Chem Sci* (2019) 10(5):1555–61. doi: 10.1039/C8SC03224F

32. Kooijmans SAA, Fliervoet LAL, van der Meel R, Fens M, Heijnen HFG, van Bergen En Henegouwen PMP, et al. Pegylated and targeted extracellular vesicles display enhanced cell specificity and circulation time. *J Control Release* (2016) 224:77–85. doi: 10.1016/j.jconrel.2016.01.009

33. Su Y-C, Burnouf P-A, Chuang K-H, Chen B-M, Cheng T-L, Roffler SR. Conditional internalization of pegylated nanomedicines by peg engagers for triple negative breast cancer therapy. *Nat Commun* (2017) 8(1):15507. doi: 10.1038/ncomms15507

34. Royo F, Cossío U, Ruiz de Angulo A, Llop J, Falcon-Perez JM. Modification of the glycosylation of extracellular vesicles alters their biodistribution in mice. *Nanoscale* (2019) 11(4):1531–7. doi: 10.1039/c8nr03900c

35. Qi H, Liu C, Long L, Ren Y, Zhang S, Chang X, et al. Blood exosomes endowed with magnetic and targeting properties for cancer therapy. *ACS Nano* (2016) 10(3):3323–33. doi: 10.1021/acsnano.5b06939

36. Sato YT, Umezaki K, Sawada S, S-a M, Sasaki Y, Harada N, et al. Engineering hybrid exosomes by membrane fusion with liposomes. *Sci Rep* (2016) 6(1):21933. doi: 10.1038/srep21933

37. Fuhrmann G, Serio A, Mazo M, Nair R, Stevens MM. Active loading into extracellular vesicles significantly improves the cellular uptake and photodynamic effect of porphyrins. *J Control Release* (2015) 205:35–44. doi: 10.1016/j.jconrel.2014.11.029

38. Doyle LM, Wang MZ. Overview of extracellular vesicles, their origin, composition, purpose, and methods for exosome isolation and analysis. *Cells* (2019) 8(7):727. doi: 10.3390/cells8070727

39. Armstrong JPK, Holme MN, Stevens MM. Re-engineering extracellular vesicles as smart nanoscale therapeutics. *ACS Nano* (2017) 11(1):69–83. doi: 10.1021/acsnano.6b07607

40. Senapati S, Mahanta AK, Kumar S, Maiti P. Controlled drug delivery vehicles for cancer treatment and their performance. *Signal Transduct Target Ther* (2018) 3:7. doi: 10.1038/s41392-017-0004-3

41. Morse MA, Garst J, Osada T, Khan S, Hobeika A, Clay TM, et al. A phase I study of dexosome immunotherapy in patients with advanced non-small cell lung cancer. *J Transl Med* (2005) 3(1):9–. doi: 10.1186/1479-5876-3-9

42. Escudier B, Dorval T, Chaput N, André F, Caby M-P, Novault S, et al. Vaccination of metastatic melanoma patients with autologous dendritic cell (dc) derived-exosomes: results of thefirst phase I clinical trial. *J Transl Med* (2005) 3(1):10–. doi: 10.1186/1479-5876-3-10

43. Dai S, Wei D, Wu Z, Zhou X, Wei X, Huang H, et al. Phase I clinical trial of autologous ascites-derived exosomes combined with gm-csf for colorectal cancer. *Mol Ther* (2008) 16(4):782–90. doi: 10.1038/mt.2008.1

44. Viaud S, Terme M, Flament C, Taieb J, Andre F, Novault S, et al. Dendritic cell-derived exosomes promote natural killer cell activation and proliferation: a role for nkg2d ligands and Il-15ralpha. *PloS One* (2009) 4(3):e4942. doi: 10.1371/journal.pone.0004942

45. Besse B, Charrier M, Lapierre V, Dansin E, Lantz O, Planchard D, et al. Dendritic cell-derived exosomes as maintenance immunotherapy after first line chemotherapy in nsclc. *Oncoimmunology* (2015) 5(4):e1071008-e. doi: 10.1080/2162402X.2015.1071008

46. Tang K, Zhang Y, Zhang H, Xu P, Liu J, Ma J, et al. Delivery of chemotherapeutic drugs in tumour cell-derived microparticles. *Nat Commun* (2012) 3(1):1282. doi: 10.1038/ncomms2282

47. Ma J, Zhang Y, Tang K, Zhang H, Yin X, Li Y, et al. Reversing drug resistance of soft tumor-repopulating cells by tumor cell-derived chemotherapeutic microparticles. *Cell Res* (2016) 26(6):713–27. doi: 10.1038/cr.2016.53

48. Gao Y, Zhang H, Zhou N, Xu P, Wang J, Gao Y, et al. Methotrexate-loaded tumour-cell-derived microvesicles can relieve biliary obstruction in patients with extrahepatic cholangiocarcinoma. *Nat Biomed Eng* (2020) 4(7):743–53. doi: 10.1038/s41551-020-0583-0

49. Xu P, Tang K, Ma J, Zhang H, Wang D, Zhu L, et al. Chemotherapeutic tumor microparticles elicit a neutrophil response targeting malignant pleural effusions. *Cancer Immunol Res* (2020) 8(9):1193–205. doi: 10.1158/2326-6066.CIR-19-0789

50. Qiao L, Hu S, Huang K, Su T, Li Z, Vandergriff A, et al. Tumor cell-derived exosomes home to their cells of origin and can be used as trojan horses to deliver cancer drugs. *Theranostics* (2020) 10(8):3474–87. doi: 10.7150/thno.39434

51. Liu H, Chen L, Liu J, Meng H, Zhang R, Ma L, et al. Co-delivery of tumor-derived exosomes with alpha-galactosylceramide on dendritic cell-based immunotherapy for glioblastoma. *Cancer Lett* (2017) 411:182–90. doi: 10.1016/j.canlet.2017.09.022

52. Li S, Wu Y, Ding F, Yang J, Li J, Gao X, et al. Engineering macrophage-derived exosomes for targeted chemotherapy of triple-negative breast cancer. *Nanoscale* (2020) 12(19):10854–62. doi: 10.1039/D0NR00523A

53. Zuo B, Qi H, Lu Z, Chen L, Sun B, Yang R, et al. Alarmin-painted exosomes elicit persistent antitumor immunity in large established tumors in mice. *Nat Commun* (2020) 11(1):1790. doi: 10.1038/s41467-020-15569-2

54. Yong T, Zhang X, Bie N, Zhang H, Zhang X, Li F, et al. Tumor exosome-based nanoparticles are efficient drug carriers for chemotherapy. *Nat Commun* (2019) 10(1):3838. doi: 10.1038/s41467-019-11718-4

55. Cao Y, Wu T, Zhang K, Meng X, Dai W, Wang D, et al. Engineered exosome-mediated near-infrared-ii region v(2)c quantum dot delivery for nucleus-target low-temperature photothermal therapy. *ACS Nano* (2019) 13(2):1499–510. doi: 10.1021/acsnano.8b07224

56. SWang K, Ye H, Zhang X, Wang X, Yang B, Luo C, et al. An exosome-like programmable-bioactivating paclitaxel prodrug nanoplatform for enhanced breast cancer metastasis inhibition. *Biomaterials* (2020) 257:120224. doi: 10.1016/j.biomaterials.2020.120224

57. Andrews DW, Resnicoff M, Flanders AE, Kenyon L, Curtis M, Merli G, et al. Results of a pilot study involving the use of an antisense oligodeoxynucleotide directed against the insulin-like growth factor type I receptor in malignant astrocytomas. *J Clin Oncol* (2001) 19(8):2189–200. doi: 10.1200/JCO.2001.19.8.2189

58. Andrews DW, Judy KD, Scott CB, Garcia S, Harshyne LA, Kenyon L, et al. Phase Ib clinical trial of igv-001 for patients with newly diagnosed glioblastoma. *Clin Cancer Res* (2021) 27(7):1912–22. doi: 10.1158/1078-0432.CCR-20-3805

59. Zhang Y, Liu Y, Liu H, Tang W. Exosomes: Biogenesis, biologic function and clinical potential. *Cell Bioscience* (2019) 9. doi: 10.1186/s13578-019-0282-2

60. Liu L, Jin X, Hu CF, Li R, Zhou Z, Shen CX. Exosomes derived from mesenchymal stem cells rescue myocardial ischaemia/reperfusion injury by inducing cardiomyocyte autophagy *Via* ampk and akt pathways. *Cell Physiol Biochem* (2017) 43(1):52–68. doi: 10.1159/000480317

61. van Koppen A, Joles JA, van Balkom BW, Lim SK, de Kleijn D, Giles RH, et al. Human embryonic mesenchymal stem cell-derived conditioned medium rescues kidney function in rats with established chronic kidney disease. *PloS One* (2012) 7(6):e38746. doi: 10.1371/journal.pone.0038746

62. Tan CY, Lai RC, Wong W, Dan YY, Lim SK, Ho HK. Mesenchymal stem cell-derived exosomes promote hepatic regeneration in drug-induced liver injury models. *Stem Cell Res Ther* (2014) 5(3):76. doi: 10.1186/scrt465

63. Willis GR, Mitsialis SA, Kourembanas S. "Good Things come in small packages": application of exosome-based therapeutics in neonatal lung injury. *Pediatr Res* (2018) 83(1-2):298–307. doi: 10.1038/pr.2017.256

64. Mead B, Tomarev S. Bone marrow-derived mesenchymal stem cells-derived exosomes promote survival of retinal ganglion cells through mirna-dependent mechanisms. *Stem Cells Transl Med* (2017) 6(4):1273–85. doi: 10.1002/sctm.16-0428

65. Gowen A, Shahjin F, Chand S, Odegaard KE, Yelamanchili SV. Mesenchymal stem cell-derived extracellular vesicles: challenges in clinical applications. *Front Cell Dev Biol* (2020) 8:149. doi: 10.3389/fcell.2020.00149

66. Phetfong J, Tawonsawatruk T, Kamprom W, Ontong P, Tanyong D, Borwornpinyo S, et al. Bone marrow-mesenchymal stem cell-derived extracellular vesicles affect proliferation and apoptosis of leukemia cells in vitro. *FEBS Open Bio* (2022) 12(2):470–9. doi: 10.1002/2211-5463.13352

67. Liu Y, Song B, Wei Y, Chen F, Chi Y, Fan H, et al. Exosomes from mesenchymal stromal cells enhance imatinib-induced apoptosis in human leukemia cells *via* activation of caspase signaling pathway. *Cytotherapy* (2017) 20. doi: 10.1016/j.jcyt.2017.11.006

68. O'Brien KP, Khan S, Gilligan KE, Zafar H, Lalor P, Glynn C, et al. Employing mesenchymal stem cells to support tumor-targeted delivery of extracellular vesicle (ev)-encapsulated microrna-379. *Oncogene* (2018) 37(16):2137–49. doi: 10.1038/s41388-017-0116-9

69. Zhuang M, Chen X, Du D, Shi J, Deng M, Long Q, et al. Spion decorated exosome delivery of tnf-α to cancer cell membranes through magnetism. *Nanoscale* (2020) 12(1):173–88. doi: 10.1039/C9NR05865F

70. Ko SF, Yip HK, Zhen YY, Lee CC, Lee CC, Huang CC, et al. Adipose-derived mesenchymal stem cell exosomes suppress hepatocellular carcinoma growth in a rat model: apparent diffusion coefficient, natural killer t-cell responses, and histopathological features. *Stem Cells Int* (2015) 2015:853506. doi: 10.1155/2015/853506

71. Li T, Zhou X, Wang J, Liu Z, Han S, Wan L, et al. Adipose-derived mesenchymal stem cells and extracellular vesicles confer antitumor activity in preclinical treatment of breast cancer. *Pharmacol Res* (2020) 157:104843. doi: 10.1016/j.phrs.2020.104843

72. Zhang K, Dong C, Chen M, Yang T, Wang X, Gao Y, et al. Extracellular vesicle-mediated delivery of mir-101 inhibits lung metastasis in osteosarcoma. *Theranostics* (2020) 10(1):411–25. doi: 10.7150/thno.33482

73. Li H, Yang C, Shi Y, Zhao L. Exosomes derived from sirna against grp78 modified bone-marrow-derived mesenchymal stem cells suppress sorafenib resistance in hepatocellular carcinoma. *J Nanobiotechnology* (2018) 16(1):103. doi: 10.1186/s12951-018-0429-z

74. Kamerkar S, Leng C, Burenkova O, Jang SC, McCoy C, Zhang K, et al. Exosome-mediated genetic reprogramming of tumor-associated macrophages by exoaso-stat6 leads to potent monotherapy antitumor activity. *Sci Adv* (2022) 8(7):eabj7002. doi: 10.1126/sciadv.abj7002

75. Bellavia D, Raimondo S, Calabrese G, Forte S, Cristaldi M, Patinella A, et al. Interleukin 3- receptor targeted exosomes inhibit in vitro and in vivo chronic myelogenous leukemia cell growth. *Theranostics* (2017) 7(5):1333–45. doi: 10.7150/thno.17092

76. Pi F, Binzel DW, Lee TJ, Li Z, Sun M, Rychahou P, et al. Nanoparticle orientation to control rna loading and ligand display on extracellular vesicles for cancer regression. *Nat Nanotechnol* (2018) 13(1):82–9. doi: 10.1038/s41565-017-0012-z

77. Liu J, Ye Z, Xiang M, Chang B, Cui J, Ji T, et al. Functional extracellular vesicles engineered with lipid-grafted hyaluronic acid effectively reverse cancer drug resistance. *Biomaterials* (2019) 223:119475. doi: 10.1016/j.biomaterials.2019.119475

78. Monfared H, Jahangard Y, Nikkhah M, Mirnajafi-Zadeh J, Mowla SJ. Potential therapeutic effects of exosomes packed with a mir-21-sponge construct in a rat model of glioblastoma. *Front Oncol* (2019) 9:782. doi: 10.3389/fonc.2019.00782

79. Liang G, Zhu Y, Ali DJ, Tian T, Xu H, Si K, et al. Engineered exosomes for targeted co-delivery of mir-21 inhibitor and chemotherapeutics to reverse drug resistance in colon cancer. *J Nanobiotechnology* (2020) 18(1):10. doi: 10.1186/s12951-019-0563-2

80. Gimble JM, Katz AJ, Bunnell BA. Adipose-derived stem cells for regenerative medicine. *Circ Res* (2007) 100(9):1249–60. doi: 10.1161/01.RES.0000265074.83288.09

81. Miana VV, Gonzalez EAP. Adipose tissue stem cells in regenerative medicine. *Ecancermedicalscience* (2018) 12:822. doi: 10.3332/ecancer.2018.822

82. Wang T, Yu X, Lin J, Qin C, Bai T, Xu T, et al. Adipose-derived stem cells inhibited the proliferation of bladder tumor cells by s phase arrest and wnt/beta-catenin pathway. *Cell Reprogram* (2019) 21(6):331–8. doi: 10.1089/cell.2019.0047

83. Rigotti G, Marchi A, Sbarbati A. Adipose-derived mesenchymal stem cells: past, present, and future. *Aesthetic Plast Surg* (2009) 33(3):271–3. doi: 10.1007/s00266-009-9339-7

84. Baldari S, Di Rocco G, Magenta A, Picozza M, Toietta G. Extracellular vesicles-encapsulated microrna-125b produced in genetically modified mesenchymal stromal cells inhibits hepatocellular carcinoma cell proliferation. *Cells* (2019). doi: 10.3390/cells8121560

85. Lee B-C, Kang I, Yu K-R. Therapeutic features and updated clinical trials of mesenchymal stem cell (msc)-derived exosomes. *J Clin Med* (2021) 10(4):711. doi: 10.3390/jcm10040711

86. Faruqu FN, Xu L, Al-Jamal KT. Preparation of exosomes for sirna delivery to cancer cells. *J Vis Exp* (2018). doi: 10.3791/58814

87. Ferguson S, Kim S, Lee C, Deci M, Nguyen J. The phenotypic effects of exosomes secreted from distinct cellular sources: a comparative study based on mirna composition. *AAPS J* (2018) 20(4):67. doi: 10.1208/s12248-018-0227-4

88. Johnsen KB, Gudbergsson JM, Skov MN, Pilgaard L, Moos T, Duroux M. A comprehensive overview of exosomes as drug delivery vehicles - endogenous nanocarriers for targeted cancer therapy. *Biochim Biophys Acta* (2014) 1846(1):75–87. doi: 10.1016/j.bbcan.2014.04.005

89. Liu Y, Li D, Liu Z, Zhou Y, Chu D, Li X, et al. Targeted exosome-mediated delivery of opioid receptor mu sirna for the treatment of morphine relapse. *Sci Rep* (2015) 5:17543. doi: 10.1038/srep17543

90. Zhu X, Badawi M, Pomeroy S, Sutaria DS, Xie Z, Baek A, et al. Comprehensive toxicity and immunogenicity studies reveal minimal effects in mice following sustained dosing of extracellular vesicles derived from hek293t cells. *J Extracell Vesicles* (2017) 6(1):1324730. doi: 10.1080/20013078.2017.1324730

91. Ohno S, Takanashi M, Sudo K, Ueda S, Ishikawa A, Matsuyama N, et al. Systemically injected exosomes targeted to EGFR deliver antitumor microrna to breast cancer cells. *Mol Ther* (2013) 21(1):185–91. doi: 10.1038/mt.2012.180

92. Mizrak A, Bolukbasi MF, Ozdener GB, Brenner GJ, Madlener S, Erkan EP, et al. Genetically engineered microvesicles carrying suicide mrna/protein inhibit schwannoma tumor growth. *Mol Ther* (2013) 21(1):101–8. doi: 10.1038/mt.2012.161

93. Jurgielewicz BJ, Yao Y, Stice SL. Kinetics and specificity of hek293t extracellular vesicle uptake using imaging flow cytometry. *Nanoscale Res Lett* (2020) 15(1):170. doi: 10.1186/s11671-020-03399-6

94. Pitt JM, Andre F, Amigorena S, Soria JC, Eggermont A, Kroemer G, et al. Dendritic cell-derived exosomes for cancer therapy. *J Clin Invest* (2016) 126(4):1224–32. doi: 10.1172/JCI81137

95. Zitvogel L, Regnault A, Lozier A, Wolfers J, Flament C, Tenza D, et al. Eradication of established murine tumors using a novel cell-free vaccine: dendritic cell-derived exosomes. *Nat Med* (1998) 4(5):594–600. doi: 10.1038/nm0598-594

96. Zhu L, Kalimuthu S, Gangadaran P, Oh JM, Lee HW, Baek SH, et al. Exosomes derived from natural killer cells exert therapeutic effect in melanoma. *Theranostics* (2017) 7(10):2732–45. doi: 10.7150/thno.18752

97. Shoae-Hassani A, Hamidieh AA, Behfar M, Mohseni R, Mortazavi-Tabatabaei SA, Asgharzadeh S. Nk cell-derived exosomes from nk cells previously exposed to neuroblastoma cells augment the antitumor activity of cytokine-activated nk cells. *J Immunother* (2017) 40(7):265–76. doi: 10.1097/cji.0000000000000179

98. Neviani P, Wise PM, Murtadha M, Liu CW, Wu CH, Jong AY, et al. Natural killer-derived exosomal mir-186 inhibits neuroblastoma growth and immune escape mechanisms. *Cancer Res* (2019) 79(6):1151–64. doi: 10.1158/0008-5472.Can-18-0779

99. Kim MS, Haney MJ, Zhao Y, Mahajan V, Deygen I, Klyachko NL, et al. Development of exosome-encapsulated paclitaxel to overcome mdr in cancer cells. *Nanomedicine* (2016) 12(3):655–64. doi: 10.1016/j.nano.2015.10.012

100. Choo YW, Kang M, Kim HY, Han J, Kang S, Lee JR, et al. M1 macrophage-derived nanovesicles potentiate the anticancer efficacy of immune checkpoint inhibitors. *ACS Nano* (2018) 12(9):8977–93. doi: 10.1021/acsnano.8b02446

101. Fan Z, Xiao K, Lin J, Liao Y, Huang X. Functionalized DNA enables programming exosomes/vesicles for tumor imaging and therapy. *Small* (2019) 15(47):1903761. doi: 10.1002/smll.201903761

102. Tkach M, Kowal J, Zucchetti AE, Enserink L, Jouve M, Lankar D, et al. Qualitative differences in t-cell activation by dendritic cell-derived extracellular vesicle subtypes. *EMBO J* (2017) 36(20):3012–28. doi: 10.15252/embj.201696003

103. Wu F, Xie M, Hun M, She Z, Li C, Luo S, et al. Natural killer cell-derived extracellular vesicles: novel players in cancer immunotherapy. *Front Immunol* (2021) 12:658698. doi: 10.3389/fimmu.2021.658698

104. Lugini L, Cecchetti S, Huber V, Luciani F, Macchia G, Spadaro F, et al. Immune surveillance properties of human nk cell-derived exosomes. *J Immunol (Baltimore Md 1950)* (2012) 189(6):2833–42. doi: 10.4049/jimmunol.1101988

105. Chen Y-S, Lin E-Y, Chiou T-W, Harn H-J. Exosomes in clinical trial and their production in compliance with good manufacturing practice. *Ci Ji Yi Xue Za Zhi* (2019) 32(2):113–20. doi: 10.4103/tcmj.tcmj_182_19

106. Rome S. Biological properties of plant-derived extracellular vesicles. *Food Funct* (2019) 10(2):529–38. doi: 10.1039/c8fo02295j

107. Vislocky LM, Fernandez ML. Biomedical effects of grape products. *Nutr Rev* (2010) 68(11):656–70. doi: 10.1111/j.1753-4887.2010.00335.x

108. Dinicola S, Cucina A, Antonacci D, Bizzarri M. Anticancer effects of grape seed extract on human cancers: a review. *J Carcinog Mutagen* (2014). doi: 10.4172/2157-2518.S8-005

109. Ju S, Mu J, Dokland T, Zhuang X, Wang Q, Jiang H, et al. Grape exosome-like nanoparticles induce intestinal stem cells and protect mice from dss-induced colitis. *Mol Ther* (2013) 21(7):1345–57. doi: 10.1038/mt.2013.64

110. Perez-Bermudez P, Blesa J, Soriano JM, Marcilla A. Extracellular vesicles in food: experimental evidence of their secretion in grape fruits. *Eur J Pharm Sci* (2017) 98:40–50. doi: 10.1016/j.ejps.2016.09.022

111. Wang B, Zhuang X, Deng ZB, Jiang H, Mu J, Wang Q, et al. Targeted drug delivery to intestinal macrophages by bioactive nanovesicles released from grapefruit. *Mol Ther* (2014) 22(3):522–34. doi: 10.1038/mt.2013.190

112. Mashhadi NS, Ghiasvand R, Askari G, Hariri M, Darvishi L, Mofid MR. Anti-oxidative and anti-inflammatory effects of ginger in health and physical activity: review of current evidence. *Int J Prev Med* (2013) 4(Suppl 1):S36–42.

113. Dugasani S, Pichika MR, Nadarajah VD, Balijepalli MK, Tandra S, Korlakunta JN. Comparative antioxidant and anti-inflammatory effects of [6]-gingerol, [8]-gingerol, [10]-gingerol and [6]-shogaol. *J Ethnopharmacol* (2010) 127(2):515–20. doi: 10.1016/j.jep.2009.10.004

114. Mao QQ, Xu XY, Cao SY, Gan RY, Corke H, Beta T, et al. Bioactive compounds and bioactivities of ginger (zingiber officinale roscoe). *Foods* (2019) 8(6). doi: 10.3390/foods8060185

115. Chen X, Zhou Y, Yu J. Exosome-like nanoparticles from ginger rhizomes inhibited nlrp3 inflammasome activation. *Mol Pharm* (2019) 16(6):2690–9. doi: 10.1021/acs.molpharmaceut.9b00246

116. Zhang M, Viennois E, Prasad M, Zhang Y, Wang L, Zhang Z, et al. Edible ginger-derived nanoparticles: a novel therapeutic approach for the prevention and treatment of inflammatory bowel disease and colitis-associated cancer. *Biomaterials* (2016) 101:321–40. doi: 10.1016/j.biomaterials.2016.06.018

117. Raimondo S, Naselli F, Fontana S, Monteleone F, Lo Dico A, Saieva L, et al. Citrus limon-derived nanovesicles inhibit cancer cell proliferation and suppress cml xenograft growth by inducing trail-mediated cell death. *Oncotarget* (2015) 6 (23):19514–27. doi: 10.18632/oncotarget.4004

118. Wang Q, Zhuang X, Mu J, Deng ZB, Jiang H, Zhang L, et al. Delivery of therapeutic agents by nanoparticles made of grapefruit-derived lipids. *Nat Commun* (2013) 4:1867. doi: 10.1038/ncomms2886

119. Cheng H, Fan J-H, Zhao L-P, Fan G-L, Zheng R-R, Qiu X-Z, et al. Chimeric peptide engineered exosomes for dual-stage light guided plasma membrane and nucleus targeted photodynamic therapy. *Biomaterials* (2019) 211:14–24. doi: 10.1016/j.biomaterials.2019.05.004

120. Zhang J, Ji C, Zhang H, Shi H, Mao F, Qian H, et al. Engineered neutrophil-derived exosome-like vesicles for targeted cancer therapy. *Sci Adv* (2022) 8(2): eabj8207. doi: 10.1126/sciadv.abj8207

121. Zhu Q, Ling X, Yang Y, Zhang J, Li Q, Niu X, et al. Embryonic stem cells-derived exosomes endowed with targeting properties as chemotherapeutics delivery vehicles for glioblastoma therapy. *Adv Sci* (2019) 6(6):1801899. doi: 10.1002/advs.201801899

122. Dou H, Shen R, Tao J, Huang L, Shi H, Chen H, et al. Curcumin suppresses the colon cancer proliferation by inhibiting wnt/beta-catenin pathways *via* Mir-130a. *Front Pharmacol* (2017) 8:877. doi: 10.3389/fphar.2017.00877

123. Mosieniak G, Adamowicz M, Alster O, Jaskowiak H, Szczepankiewicz AA, Wilczynski GM, et al. Curcumin induces permanent growth arrest of human colon cancer cells: link between senescence and autophagy. *Mech Ageing Dev* (2012) 133 (6):444–55. doi: 10.1016/j.mad.2012.05.004

124. Wahajuddin, Arora S. Superparamagnetic iron oxide nanoparticles: magnetic nanoplatforms as drug carriers. *Int J Nanomed* (2012) 7:3445–71. doi: 10.2147/IJN.S30320

125. Thery C, Zitvogel L, Amigorena S. Exosomes: composition, biogenesis and function. *Nat Rev Immunol* (2002) 2(8):569–79. doi: 10.1038/nri855

126. Keefe AD, Pai S, Ellington A. Aptamers as therapeutics. *Nat Rev Drug Discovery* (2010) 9(7):537–50. doi: 10.1038/nrd3141

127. Nievergall E, Ramshaw HS, Yong AS, Biondo M, Busfield SJ, Vairo G, et al. Monoclonal antibody targeting of il-3 receptor alpha with csl362 effectively depletes cml progenitor and stem cells. *Blood* (2014) 123(8):1218–28. doi: 10.1182/blood-2012-12-475194

128. Testa U, Pelosi E, Frankel A. Cd 123 is a membrane biomarker and a therapeutic target in hematologic malignancies. *biomark Res* (2014) 2(1):4. doi: 10.1186/2050-7771-2-4

129. Testa U, Riccioni R, Militi S, Coccia E, Stellacci E, Samoggia P, et al. Elevated Expression of Il-3ralpha in Acute Myelogenous Leukemia Is Associated with Enhanced Blast Proliferation, Increased Cellularity, and Poor Prognosis. *Blood* (2002) 100(8):2980–8. doi: 10.1182/blood-2002-03-0852

130. Chen L, et al. Inhibitory effect of neuropilin-1 monoclonal antibody (NRP-1 MAb) on glioma tumor in mice. *J BioMed Nanotechnol* (2013) 9(4):551–8. doi: 10.1166/jbn.2013.1623

131. Chen L, Zhang G, Shi Y, Qiu R, Khan AA. Neuropilin-1 (Nrp-1) and magnetic nanoparticles, a potential combination for diagnosis and therapy of gliomas. *Curr Pharm Des* (2015) 21(37):5434–49. doi: 10.2174/1381612821666150917092658

132. Jia G, Han Y, An Y, Ding Y, He C, Wang X, et al. Nrp-1 targeted and cargo-loaded exosomes facilitate simultaneous imaging and therapy of glioma in vitro and in vivo. *Biomaterials* (2018) 178:302–16. doi: 10.1016/j.biomaterials.2018.06.029

133. Zhong Y, Wang C, Cheng R, Cheng L, Meng F, Liu Z, et al. cRGD-directed, NIR-responsive and robust AuNR/PEG-PCL hybrid nanoparticles for targeted chemotherapy of glioblastoma in vivo. *J Control Release* (2014) 195:63–71. doi: 10.1016/j.jconrel.2014.07.054

134. Li X, Yang J, Peng L, Sahin AA, Huo L, Ward KC, et al. Triple-negative breast cancer has worse overall survival and cause-specific survival than non-triple-negative breast cancer. *Breast Cancer Res Treat* (2017) 161(2):279–87. doi: 10.1007/s10549-016-4059-6

135. Dent R, Trudeau M, Pritchard KI, Hanna WM, Kahn HK, Sawka CA, et al. Triple-negative breast cancer: clinical features and patterns of recurrence. *Clin Cancer Res* (2007) 13(15 Pt 1):4429–34. doi: 10.1158/1078-0432.CCR-06-3045

136. Sohn J, Liu S, Parinyanitikul N, Lee J, Hortobagyi GN, Mills GB, et al. Cmet activation and egfr-directed therapy resistance in triple-negative breast cancer. *J Cancer* (2014) 5(9):745–53. doi: 10.7150/jca.9696

137. Zagouri F, Bago-Horvath Z, Rossler F, Brandstetter A, Bartsch R, Papadimitriou CA, et al. High met expression is an adverse prognostic factor in patients with triple-negative breast cancer. *Br J Cancer* (2013) 108(5):1100–5. doi: 10.1038/bjc.2013.31

138. Wu Y, Fan Q, Zeng F, Zhu J, Chen J, Fan D, et al. Peptide-functionalized nanoinhibitor restrains brain tumor growth by abrogating mesenchymal-epithelial transition factor (met) signaling. *Nano Lett* (2018) 18(9):5488–98. doi: 10.1021/acs.nanolett.8b01879

139. Liao S, Yue W, Cai S, Tang Q, Lu W, Huang L, et al. Improvement o fgold nanorods in photothermal therapy: recent progress and perspective. *Front Pharmacol* (2021) 12:664123. doi: 10.3389/fphar.2021.664123

140. Li X, Lovell JF, Yoon J, Chen X. Clinical development and potential of photothermal and photodynamic therapies for cancer. *Nat Rev Clin Oncol* (2020) 17(11):657–74. doi: 10.1038/s41571-020-0410-2

141. Akuma P, Okagu OD, Udenigwe CC. Naturally occurring exosome vesicles as potential delivery vehicle for bioactive compounds. *Front Sustain Food Syst* (2019) 3.

142. Piffoux M, Silva AKA, Lugagne JB, Hersen P, Wilhelm C, Gazeau F. Extracellular vesicle production loaded with nanoparticles and drugs in a trade-off between loading, yield and purity: towards a personalized drug delivery system. *Adv Biosyst* (2017) 1(5):e1700044. doi: 10.1002/adbi.201700044

143. Kojima R, Bojar D, Rizzi G, Hamri GC, El-Baba MD, Saxena P, et al. Designer exosomes produced by implanted cells intracerebrally deliver therapeutic cargo for parkinson's disease treatment. *Nat Commun* (2018) 9(1):1305. doi: 10.1038/s41467-018-03733-8

frontiers | Frontiers in Oncology

TYPE Mini Review
PUBLISHED 22 December 2022
DOI 10.3389/fonc.2022.1069635

OPEN ACCESS

EDITED BY
Zohreh Amoozgar,
Massachusetts General Hospital and Harvard Medical School, United States

REVIEWED BY
Matthew Brendan O'Rourke,
University of Technology Sydney, Australia

*CORRESPONDENCE
Pouya Faridi
Pouya.Faridi@monash.edu
Ralf B. Schittenhelm
Ralf.Schittenhelm@monash.edu

SPECIALTY SECTION
This article was submitted to Molecular and Cellular Oncology, a section of the journal Frontiers in Oncology

RECEIVED 14 October 2022
ACCEPTED 05 December 2022
PUBLISHED 22 December 2022

CITATION
Tanuwidjaya E, Schittenhelm RB and Faridi P (2022) Soluble HLA peptidome: A new resource for cancer biomarkers.
Front. Oncol. 12:1069635.
doi: 10.3389/fonc.2022.1069635

Soluble HLA peptidome: A new resource for cancer biomarkers

Erwin Tanuwidjaya[1], Ralf B. Schittenhelm[1]* and Pouya Faridi[1,2]*

[1]Monash Proteomics & Metabolomics Facility, Department of Biochemistry and Molecular Biology, Monash Biomedicine Discovery Institute, Monash University, Clayton, VIC, Australia, [2]Department of Medicine, School of Clinical Sciences, Monash University, Clayton, VIC, Australia

Using circulating molecular biomarkers to screen for cancer and other debilitating disorders in a high-throughput and low-cost fashion is becoming increasingly attractive in medicine. One major limitation of investigating protein biomarkers in body fluids is that only one-fourth of the entire proteome can be routinely detected in these fluids. In contrast, Human Leukocyte Antigen (HLA) presents peptides from the entire proteome on the cell surface. While peptide-HLA complexes are predominantly membrane-bound, a fraction of HLA molecules is released into body fluids which is referred to as soluble HLAs (sHLAs). As such peptides bound by sHLA molecules represent the entire proteome of their cells/tissues of origin and more importantly, recent advances in mass spectrometry-based technologies have allowed for accurate determination of these peptides. In this perspective, we discuss the current understanding of sHLA-peptide complexes in the context of cancer, and their potential as a novel, relatively untapped repertoire for cancer biomarkers. We also review the currently available tools to detect and quantify these circulating biomarkers, and we discuss the challenges and future perspectives of implementing sHLA biomarkers in a clinical setting.

KEYWORDS

cancer biomarkers, liquid biopsy, immunopeptidomics, mass spectrometry, soluble HLA, HLA peptidome

Introduction

The pursuit of cancer biomarker discovery serves the purpose of identifying, characterizing, and monitoring specific molecules (or entire cells) in patients, allowing for early detection of cancer and/or its differentiation from non-cancerous tissue. There are three main types of biomarkers: 1) diagnostic, 2) prognostic and 3) predictive biomarkers (1). A diagnostic biomarker refers to a marker that allows for the detection and identification of a particular type of cancer. In contrast, a prognostic biomarker offers information on the likelihood of survival as well as on potential future disease progression, while a predictive biomarker informs clinicians and physicians about appropriate and suitable therapeutic treatments (1). Irrespective of the type of

biomarker, an ideal marker should be capable of reproducibly and robustly discriminating healthy individuals from patients (or subsequently the progress of diseases). In addition, it should be easy and inexpensive to assay with the possibility of high-throughput screening (2). Various types of biomarkers including cancer biomarkers have been extensively reviewed (1, 3), and the discovery and utilities of some of the most well-known cancer biomarkers have been discussed in great detail elsewhere (4).

Molecular profiling techniques to identify or screen biomarkers are typically initiated by acquiring tumor samples from patients using invasive surgeries, often referred to as tissue biopsies. Moreover, repeated surgeries are often required to observe the development of a specific tumor over time, especially in the case of metastasis (5). The cost of these surgeries in combination with the risk of conducting repeated invasive procedures on the same patient has created a pressing need for alternative methods to identify and screen biomarkers. One attractive solution is the use of liquid biopsies, which refers to a collection of techniques developed to detect, quantify and characterize circulating tumor cells (6) and/or cancer-related molecules in various, easily accessible body fluids. Measurement and analysis of biomarkers in such liquid biopsies allow for the prediction of cancer pathogenic processes *via* tumor-specific alterations in cancer (7–9).

Body fluids are fluids produced by the body for 1) normal bodily functions (e.g. blood), 2) as waste products (e.g. urine), or 3) in disease pathology (e.g. malignant pleural effusion, which results in the accumulation of exudative fluid in the lungs due to pathology-induced fluid imbalances) (10). The most commonly studied body fluid for human biomarker discovery is blood, which is readily accessible and contains circulating molecules from all over the body, including proteins and other biomolecules originating from the tumor(s). As such, blood – and its processed derivatives plasma and serum – are an attractive source for biomarker discovery translational research. Blood, however, contains a huge dynamic range of protein concentrations (13 orders of magnitude) with over half of the total protein mass made up of albumin (11). These highly abundant proteins complicate the detection of cancer-associated proteins, which are expected to be low in abundance. As of 2021, a total of 5,877 plasma proteins have been cataloged through the Human Plasma Proteome Project (HPPP) (12). This number, however, represents only one-fourth of the approximately 20,000 proteins characterized and annotated in the human proteome (13). Therefore characterizing protein biomarkers from blood will likely not provide a comprehensive view of the entire proteome expressed in tumors. Research on biomarker discovery is not only limited to blood. Cancer-associated proteins can also be present in other body fluids such as pleural effusion (14), saliva (15) and urine (16). For instance, soluble mesothelin-related peptide, which is an FDA-approved biomarker for clinical use in mesothelioma, has a high abundance in malignant pleural effusion (14). However, in contrast to blood, which contains proteins from all body organs, these body fluids predominantly contain proteins that are only released locally.

One additional major limitation of using proteins present in any body fluid as a source for biomarkers is that the array of proteins, which are present in these fluids, originated mostly from secreted and membrane-bound proteins. These two classes of proteins only represent around 35% of the whole proteome (17, 18). More importantly, only ~6% of known cancer-associated proteins are confirmed or predicted as secretory proteins and thus, cannot be detected in the intact form in body fluids (Supplementary Table S1) (19). As such, there is a clear need for alternative approaches if we want to use body fluids as a means to identify tumor-specific protein biomarkers.

Human Leukocyte Antigen (HLA) is a protein-product of the Major Histocompatibility Complex (MHC) gene in Humans and presents peptides on the cell surface for T cell recognition. The cargo of peptides bound to HLA proteins is termed the immunopeptidome (20). The immunopeptidome plays an essential role in immunomodulation as presented peptides may belong to either self or non-self (21). There are two main classes of HLA: 1) HLA class I (HLA-I) and 2) HLA class II (HLA-II). HLA-Is are expressed in the majority of nucleated cells and present peptides (typically between 8 to 12 amino acids long) from inside the cell, which are produced from proteasomal degradation (22). HLA-II molecules bind longer peptides (between 13 to 20 amino acids) and are expressed mostly by antigen presenting cells (APCs) (23). The peptide cargoes of HLA-II peptides are mostly of extracellular origin. As such, the collective immunopeptidome of HLA-I and HLA-II is not limited to secretory proteins, but rather represents snapshots of entire cellular proteomes including their surroundings.

Both HLA-I and HLA-II are predominantly membrane-bound (often termed mHLA), but intriguingly, a fraction of HLA molecules is released into body fluids where they are referred to as soluble HLAs (sHLAs) (24). In this review we discuss the potential to exploit the sHLA immunopeptidome of various body fluids as a novel, innovative and relatively untapped repertoire to identify circulating biomarkers derived from the entire cancer proteome. First, we broadly discuss the potential for sHLA immunopeptidome to be used as a source of cancer biomarkers including various concrete examples, and then we discuss our vision of analyzing these biomarkers at low cost in a high throughput manner in the context of translational clinical screening.

Sourcing biomarkers from soluble HLA: Current evidence and examples

The presence of HLA proteins in human plasma was first discovered by van Rood and colleagues in 1970 (25). Three soluble forms of HLA proteins have been discovered so far (26): 1) A ~35 kDa version corresponding to the extracellular domain of an mHLA molecule (27); 2) A ~39 kDa version originating from an alternative splicing event (28); and 3) the fully shed ~44 kDa mHLA molecule (24). There is increasing evidence linking the abundance of sHLA protein in serum to disease progression and immune evasion in cancer, particularly in protection from immune recognition and inhibition of destruction of the microenvironment (29). Additional studies have examined a potential link between sHLA levels and malignancy. While the majority of these studies agreed that elevated sHLA levels correlate with poorer prognosis, a few studies suggest otherwise (24, 30). It has to be noted however that these observations differ depending on the cancer type, and could therefore be explained by different immune reactions toward various cancer types. Regardless of the abundance of sHLA, several studies confirm their presence in different body fluids (Table 1) (31, 32, 34, 35, 37–42). Interestingly, peptides bound to these sHLA are derived from intra- and extracellular proteins expressed in the cell of origin. As such, the sHLA immunopeptidome acts as a reservoir of all proteins expressed in a cell including peptides derived from cancer-specific proteins in tumors (45).

This notion of exploring the sHLA immunopeptidome in the context of cancer biomarkers was initiated by Bassani-Sternberg and colleagues slightly more than a decade ago (33). In the seminal study comparing HLA immunopeptidomes in human plasma to hematological cancer cell lines, they aptly recognized that the sHLA complexes (consisting of the sHLA molecule themselves and their peptide ligands) remain stable in circulation for two days. More importantly, the peptide cargoes of the sHLAs were highly similar to those carried by their mHLA counterparts. These observations opened up the

TABLE 1 Summary of various body fluid in which presence of HLA has been validated *via* proteomics studies.

Body fluid	Origin of proteins	No. of proteins detected in the body fluid	Coverage for tumor-associated antigen[$]	Evidence of the presence of HLA in this body fluid
Amniotic fluid	Maternal blood	3025*	<3% (90/3025)	(31)
Aqueous humor	Eyes	1888**	<3% (50/1888)	(32)
Blood	Whole body organs	5877***	<3% (157/5877)	(33)
Cerebrospinal fluid	Brain	4364*	<3% (122/4364)	(34)
Milk	Whole body organs	2457*	<3% (67/2457)	(35)
Pleural effusion	Lungs	1519*	4% (62/1519)	(36)
Saliva	Oral cavity, whole body organs	2758*	3.3% (92/2758)	(37)
Seminal fluid	Male reproductive organs	4084*	3.6% (145/4084)	(38)
Sweat	Skin, whole body organs	1244*	3.1% (39/1244)	(39)
Synovial fluid	Joints, whole body organs	1637*	3.6% (59/1637)	(40)
Tears	Eyes	1882*	3.4% (64/1882)	(41)
Urine	Urinary organs, reproductive organs	7330*	<3% (196/7330)	(42)

*taken from Human Body Fluid Proteome database (43).
**taken from the latest available MS-based proteomics study with compiled database from all existing aqueous humor proteomics studies (44).
***taken from the latest Human Plasma Proteome Project-associated study article (12).
[$]data compiled in the Supplementary Table S1.

possibility of characterizing all proteins present in a tumor cell by studying peptides presented by sHLA complexes in body fluids.

At present, only a handful of studies exist describing sHLA immunopeptidomes, and many of those studies are centered around sHLA-I peptides isolated from blood (33, 46–48). The above-mentioned study by Bassani-Stenberg (33) identified a number of peptides derived from cancer-testis antigens (CTA) and tumor-associated antigens (TAA) in the blood of patients with hematological malignancies. More recent studies observed that sHLA complexes containing peptides derived from validated CTAs (macrophage inhibitory factor (49, 50) & NY-ESO-1 (51)) can be detected in the blood of breast cancer patients (52).

In 2016, Ritz and colleagues (46) conducted validation studies on the methodology for the current mHLA immunopeptidome extraction from cell lines. Once validated, the method was then implemented on the sera of melanoma patients and healthy individuals to assess its effectiveness in extracting sHLA immunopeptides. Their investigation identified a total of 22 peptides derived from validated melanoma-associated antigens (53), 15 of which were exclusively found in serum. Just one year later, the same laboratory successfully improved their sHLA peptidome characterization from a few hundred peptides in their original study (46) to about 2,000 peptides by adding an additional purification step (47). This number was further increased again to 26,841 peptides in 2019 (48), demonstrating a tremendous improvement in method development. In this study, Shraibman et al. managed to validate that the expression of potential biomarkers derived from plasma sHLA in glioblastoma patients change pre- vs post-surgical interventions, whilst most of the peptides remain constant during the same period of time (48).

In a more recent report, Khazan-Kost and colleagues discovered the potential of sHLA as a valuable source of biomarkers for lung cancers in pleural effusion (54). His work attempts to expand from the 2002 study in which Amirghofran and colleagues validated the presence of sHLA-I in malignant pleural effusion (36), to provide a comparison between malignant vs benign pleural effusions. Analysis of both the soluble and membrane HLA immunopeptidome resulted in the identification of a total of 32,970 unique HLA peptides derived from 11,305 proteins from both benign and malignant effusion with clear distinctions between them (19,294 and 1,784 peptides have been exclusively identified in the malignant and benign effusion, respectively). More importantly, unique sets of peptides derived from TAAs specific to lung adenocarcinoma were observed exclusively in pleural effusion and not in corresponding individual's plasma samples. The protein used as an example in the study, anaplastic lymphoma kinase (ALK), is not yet validated and classified as a CTA/TAA at present (55), but this protein has a potential to be a localized biomarker for lung cancer. Finally, while the study predominantly focused on pleural effusion, it also validated that the sHLA immunopeptidome can serve as a valuable source of TAAs as evidenced by the identification of several known TAAs (SAGE1, PBK and ODF2) in both pleural effusion and plasma samples of lung cancer patients.

The investigation of the sHLA-II immunopeptidome proved to be much more challenging than the HLA-I counterpart. At present, there is little progress on the identification and characterization of the peptide cargo of sHLA-II molecules (56). Combined with the lower abundance of sHLA-II in blood it is not surprising that only ~200 peptides have been identified from 3 mL of human plasma from healthy individuals (56). There are currently no HLA-II peptidome studies of cancer patients yet, either from blood nor any other body fluid.

Analysis of sHLA immunopeptides by using immunopeptidomics

Immunopeptidomics is the method of choice for the identification and quantification of sHLA-bound peptides and the pipeline is summarized in Figure 1. In brief, the body fluid of interest is collected from the patient *via* a minimally invasive procedure, and sHLA-peptide complexes are enriched *via* immunoaffinity purification (IP) using HLA-specific antibodies. Peptides are eluted from the sHLA protein by acidification and analyzed by liquid chromatography-tandem mass spectrometry (LC-MS/MS). The data is then analyzed against a human proteome reference database and/or a personalized database in the case of a proteogenomics approach (57). The peptides' source proteins are then typically mapped against the cancer testis antigen database (58).

Recent advances of the immunopeptidomic pipeline have resulted in significantly increased peptide identifications (IDs) as well as data accuracy and quality. This was predominantly accomplished by mitigating issues that have been plaguing earlier HLA peptidome studies. For example, earlier studies heavily relied on the extraction of mHLA-bound peptides directly from intact cancer cell lines using mild acid elution (MAE), which is highly prone to contamination (59). The implementation of antibody-based IP enrichments of HLA-peptide complexes after cell lysis resulted in a 6-fold increase in peptide numbers compared to the earlier MAE approach (60). Similarly, significant advances in the sensitivity, selectivity and speed of mass spectrometric instrumentation have led in the past 10 years to an increase in peptide IDs that can be identified from decreasing amounts of starting material (61). Just a decade ago, 10^{10} cells were required to identify approximately 3,000 peptides

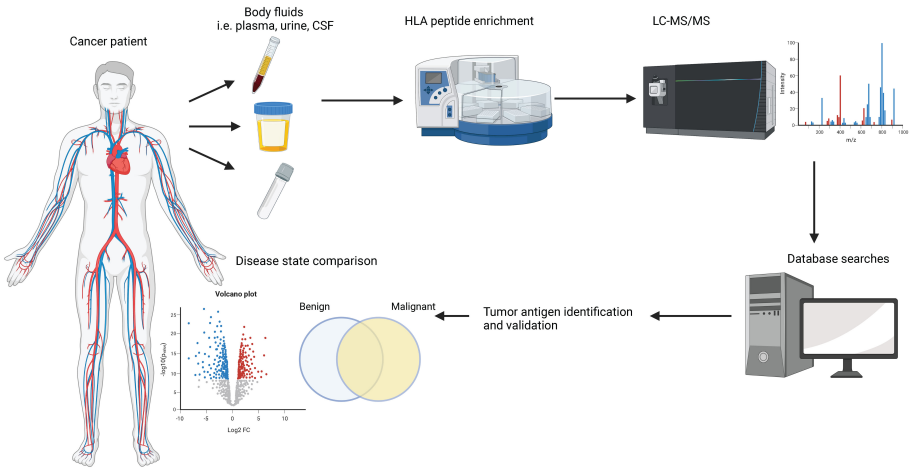

FIGURE 1
Commonly used pipeline to study HLA immunopeptidomes. Body fluids are extracted from cancer patients or healthy donors via minimally invasive procedures. sHLA-peptide complexes are enriched by immunoprecipitation assays and the peptide cargo is separated under mild acidic conditions. The peptides are analyzed by liquid chromatography-tandem mass spectrometry (LC-MS/MS) and various software packages are used to search the data against a human proteome database to obtain peptide sequence information. State-of-the-art bioinformatic analyses are employed to shortlist potential biomarkers.

(62). A similar number of peptides was identified with 100-fold less starting material (10^8 cells) just a few years later (63) and most recently, with as little as 10^7 cells (64). In the context of liquid biopsy analysis, current approaches have resulted in the identification of >20,000 peptides from human plasma derived from approximately 8,000 source proteins (48). Comparable numbers (32,970 peptides, derived from 11,305 source proteins) have also been identified in pleural effusion (54).

The classical MS acquisition method used for such studies is data-dependent acquisition (DDA) mass spectrometry, where abundant peptide sequences are obtained by searching the acquired mass spectra against existing protein databases (65, 66). However, such approaches usually suffer from a lack of reproducibility, and lower abundant peptide species are typically neglected. As a consequence, (DDA) mass spectrometry is increasingly replaced by the arguably superior data-independent acquisition (DIA) mass spectrometry, in which all peptides irrespective of their abundance are fragmented in the mass spectrometer (67–70). More recently, attempts to incorporate quantitative aspects into the historically purely qualitative field have gained traction, utilizing both label-free (71, 72) and label-based (73, 74) quantification approaches.

Challenges and future perspectives

In previous studies, similar sHLA peptidomes were observed for individuals sharing the HLA allotypes. Indeed, it is important to recognize that the HLA region is the most polymorphic region in the human genome (22, 75) and that HLA allo- and haplotypes determine the sHLA immunopeptidome (33). As a consequence, an analysis of two different populations has a high possibility of yielding two different sHLA immunopeptidomes. Because of the polymorphism of the HLA gene, the discovery of universal HLA-bound peptides biomarker is challenging. However, precision biomarkers (based on HLA types) would be an option. Another possibility is studying peptides present by non-classical HLAs, such as HLA-E and G, which are less polymorphic.

In order for biomarkers to be implemented in the clinical settings, they have to undergo a thorough validation study against a large cohort of samples from both cancer patients and healthy donors. This poses a significant technical challenge on the throughput capabilities of existing immunopeptidomics workflows, as emphasized by the Human Immunopeptidome Project (HIPP) (69). Many approaches have been attempted to overcome this challenge ranging from the use of multiplexing assays (73, 74) to establishing a 96-well format workflow applicable to both cell lines and tumor tissues (64). A promising recent study by Zhang and colleagues successfully incorporated the use of an automated liquid handling instrument (Assay MAP Bravo platform; Agilent Technologies) (76), which resulted in an overall improvement in speed, sensitivity, and also reproducibility. This automation has indeed created a standardized high-throughput workflow that eliminates human error and might pave the trend for future studies.

Another important challenge that has been plaguing immunopeptidomic studies is the amount of starting material needed. Considering the low abundance of sHLA-peptide complexes in body fluids, approximately 3-5 mL of plasma

(33, 56) and at least 10 mL of pleural effusion (54) are required for each analysis. In fact, some TAA-derived peptides are only found in a higher volume of starting material (54), posing a risk of losing valuable biomarkers when working with a lower volume. While the implementation of IP enrichments has allowed for significant improvement in peptide recovery, it comes with its limitation for reliable clinical biomarker screening. Varying quantities of peptides (from as low as 17.5% (77) up to 99% (78)) have been observed to be lost in the process, possibly due to the varying IP conditions employed in the literature (64). Therefore, the development of a standardized protocol for this method is paramount.

Lastly, all the current studies on sHLA immunopeptidomes used conventional proteome databases and only considered intact (not biologically modified) sequences which are present in the human reference proteome (79). However, recent studies suggest the high prevalence of post-translationally modified peptides (such as phosphorylated, deamidated and glycosylated peptides) as well as proteasomally spliced epitopes in the immunopeptidome (80–83). On the other hand, the rise of proteogenomic studies, which combine genomic and proteomic approaches, will accelerate the expansion of current databases with novel and variant peptide species (84–86). Taken together, these breakthroughs have created and will create superior approaches to investigate HLA immunopeptidomes at an unprecedented level, further elevating its potential as a repertoire for cancer biomarkers.

Conclusion

In summary, sHLA immunopeptidomes are a viable source of cancer biomarkers. sHLA complexes are present in most body fluids (31, 32, 34, 35, 37–42) and their peptide cargo contains many validated CTAs and TAAs (33, 46–48, 54). These peptides have the potential to be used as diagnostic, prognostic and/or predictive biomarkers for different cancer immunotherapy strategies such as immune checkpoint inhibitors, cancer vaccines and T-cell therapies. Continuous improvements in mass spectrometric instrumentation, bioinformatics and sample preparation over the past decade have allowed for more robust and comprehensive sHLA immunopeptidomics (57, 76, 77, 87, 88). However, we have to be acutely aware that there are currently very limited studies on liquid biopsy samples and a myriad of technical challenges to be overcome before its routine implementation in clinical settings (69). At this stage, developing standardized protocols for sHLA-based biomarker research would be an important initial step to ensure analytical validity and quality of future studies.

Author contributions

ET designed and drafted the manuscript. RS and PF critically revised the manuscript and contributed to writing the final manuscript. All authors contributed to the article and approved the submitted version.

Funding

PF was supported by the Victorian Department of Health and Human Services acting through the Victorian Cancer Agency.

Conflict of interest

The authors declare that the research was conducted in the absence of any commercial or financial relationships that could be construed as a potential conflict of interest.

Publisher's note

Supplementary material

The Supplementary Material for this article can be found online at: https://www.frontiersin.org/articles/10.3389/fonc.2022.1069635/full#supplementary-material

References

1. Henry NL, Hayes DF. Cancer biomarkers. *Mol Oncol* (2012) 6(2):140–6. doi: 10.1016/j.molonc.2012.01.010

2. Verma M, Patel P, Verma M. Biomarkers in prostate cancer epidemiology. *Cancers (Basel)* (2011) 3(4):3773–98. doi: 10.3390/cancers3043773

3. Strimbu K, Tavel JA. What are biomarkers? *Curr Opin HIV AIDS* (2010) 5 (6):463–6. doi: 10.1097/COH.0b013e32833ed177

4. Diamandis EP, Bast RC, Gold P, Chu TM, Magnani JL. Reflection on the discovery of carcinoembryonic antigen, prostate-specific antigen, and cancer

antigens CA125 and CA19-9. *Clin Chem* (2013) 59(1):22–31. doi: 10.1373/clinchem.2012.187047

5. McGranahan N, Swanton C. Clonal heterogeneity and tumor evolution: Past, present, and the future. *Cell* (2017) 168(4):613–28. doi: 10.1016/j.cell.2017.01.018

6. Pantel K, Alix-Panabières C. Circulating tumour cells in cancer patients: challenges and perspectives. *Trends Mol Med* (2010) 16(9):398–406. doi: 10.1016/j.molmed.2010.07.001

7. Liu Z, Wang L, Du M, Liang Y, Liang M, Li Z, et al. Plasm metabolomics study in pulmonary metastatic carcinoma. *Raghavamenon AC editor. J Oncol* (2022) 2022:1–14. doi: 10.1155/2022/9460019

8. Ulz P, Belic J, Graf R, Auer M, Lafer I, Fischereder K, et al. Whole-genome plasma sequencing reveals focal amplifications as a driving force in metastatic prostate cancer. *Nat Commun* (2016) 7(1):12008. doi: 10.1038/ncomms12008

9. Catalona WJ, Smith DS, Ratliff TL, Dodds KM, Coplen DE, Yuan JJJ, et al. Measurement of prostate-specific antigen in serum as a screening test for prostate cancer. *N Engl J Med* (1991) 324(17):1156–61. doi: 10.1056/NEJM199104253241702

10. Psallidas I, Kalomenidis I, Porcel JM, Robinson BW, Stathopoulos GT. Malignant pleural effusion: from bench to bedside. *Eur Respir Rev* (2016) 25 (140):189–98. doi: 10.1183/16000617.0019-2016

11. Anderson NL, Anderson NG. The human plasma proteome. *Mol Cell Proteomics* (2002) 1(11):845–67. doi: 10.1074/mcp.R200007-MCP200

12. Deutsch EW, Omenn GS, Sun Z, Maes M, Pernemalm M, Palaniappan KK, et al. Advances and utility of the human plasma proteome. *J Proteome Res* (2021) 20 (12):5241–63. doi: 10.1021/acs.jproteome.1c00657

13. Omenn GS, Lane L, Overall CM, Paik YK, Cristea IM, Corrales FJ, et al. Progress identifying and analyzing the human proteome: 2021 metrics from the HUPO human proteome project. *J Proteome Res* (2021) 20(12):5227–40. doi: 10.1021/acs.jproteome.1c00590

14. Creaney J, Robinson BWS. Malignant mesothelioma biomarkers. *Chest* (2017) 152(1):143–9. doi: 10.1016/j.chest.2016.12.004

15. Hu S, Arellano M, Boontheung P, Wang J, Zhou H, Jiang J, et al. Salivary proteomics for oral cancer biomarker discovery. *Clin Cancer Res* (2008) 14 (19):6246–52. doi: 10.1158/1078-0432.CCR-07-5037

16. Chakraborty A, Dasari S, Long W, Mohan C. Urine protein biomarkers for the detection, surveillance, and treatment response prediction of bladder cancer. *Am J Cancer Res* (2019) 9(6):1104–17.

17. Fagerberg L, Jonasson K, von Heijne G, Uhlén M, Berglund L. Prediction of the human membrane proteome. *Proteomics [Internet]*. (2010) 10(6):1141–9. doi: 10.1002/pmic.200900258

18. Uhlén M, Fagerberg L, Hallström BM, Lindskog C, Oksvold P, Mardinoglu A, et al. Tissue-based map of the human proteome. *Science* (1979) 347(6220). doi: 10.1126/science.1260419

19. Uhlén M, Karlsson MJ, Hober A, Svensson AS, Scheffel J, Kotol D, et al. The human secretome. *Sci Signal* (2019) 12(609). doi: 10.1126/scisignal.aaz0274

20. Vizcaíno JA, Kubiniok P, Kovalchik KA, Ma Q, Duquette JD, Mongrain I, et al. The human immunopeptidome project: A roadmap to predict and treat immune diseases. Molecular and cellular proteomics. *Am Soc Biochem Mol Biol Inc.;* (2020) 19:31–49. doi: 10.1074/mcp.R119.001743

21. Admon A, Barnea E, Ziv T. Tumor antigens and proteomics from the point of view of the major histocompatibility complex peptides. *Mol Cell Proteomics* (2003) 2(6):388–98. doi: 10.1074/mcp.R300004-MCP200

22. Rock KL, Reits E, Neefjes J. Present yourself! by MHC class I and MHC class II molecules. *Trends Immunol* (2016) 37(11):724–37. doi: 10.1016/j.it.2016.08.010

23. Unanue ER, Turk V, Neefjes J. Variations in MHC class II antigen processing and presentation in health and disease. *Annu Rev Immunol* (2016) 34 (1):265–97. doi: 10.1146/annurev-immunol-041015-055420

24. Tabayoyong WB, Zavazava N. Soluble HLA revisited. *Leuk Res* (2007) 31 (2):121–5. doi: 10.1016/j.leukres.2006.06.008

25. van ROOD JJ, van LEEUWEN A, van SANTEN MCT. Anti HL-A2 inhibitor in normal human serum. *Nature* (1970) 226(5243):366–7. doi: 10.1038/226366a0

26. Puppo F, Scudeletti M, Indiveri F, Ferrone S. Serum HLA class I antigens: markers and modulators of an immune response? *Immunol Today* (1995) 16 (3):124–7. doi: 10.1016/0167-5699(95)80127-8

27. Demaria S, Bushkin Y. Soluble HLA proteins with bound peptides are released from the cell surface by the membrane metalloproteinase. *Hum Immunol* (2000) 61(12):1332–8. doi: 10.1016/S0198-8859(00)00213-5

28. Krangel MS. Secretion of HLA-a and -b antigens *via* an alternative RNA splicing pathway. *J Exp Med* (1986) 163(5):1173–90. doi: 10.1084/jem.163.5.1173

29. Campoli M, Ferrone S. Tumor escape mechanisms: potential role of soluble HLA antigens and NK cells activating ligands. *Tissue Antigens* (2008) 72(4):321–34. doi: 10.1111/j.1399-0039.2008.01106.x

30. Kessler AL, Bruno MJ, Buschow SI. The potential of soluble human leukocyte antigen molecules for early cancer detection and therapeutic vaccine design. *Vaccines (Basel)* (2020) 8(4):775. doi: 10.3390/vaccines8040775

31. Sosa-Acosta P, Melani RD, Quiñones-Vega M, Melo A, Garcez PP, Nogueira FCS, et al. Proteomics of ZIKV infected amniotic fluids of microcephalic fetuses reveals extracellular matrix and immune system dysregulation. *Proteomics Clin Appl* (2022) 16(1):2100041. doi: 10.1002/prca.202100041

32. Wierenga APA, Gezgin G, van Beelen E, Eikmans M, Spruyt-Gerritse M, Brouwer NJ, et al. Soluble HLA in the aqueous humour of uveal melanoma is associated with unfavourable tumour characteristics. *Cancers (Basel)* (2019) 11 (8):1202. doi: 10.3390/cancers11081202

33. Bassani-Sternberg M, Barnea E, Beer I, Avivi I, Katz T, Admon A. Soluble plasma HLA peptidome as a potential source for cancer biomarkers. *Proc Natl Acad Sci* (2010) 107(44):18769–76. doi: 10.1073/pnas.1008501107

34. Karayel O, Virreira Winter S, Padmanabhan S, Kuras YI, Vu DT, Tuncali I, et al. Proteome profiling of cerebrospinal fluid reveals biomarker candidates for parkinson's disease. *Cell Rep Med* (2022) 3(6):100661. doi: 10.1016/j.xcrm.2022.100661

35. Zhu J, Garrigues L, van den Toorn H, Stahl B, Heck AJR. Discovery and quantification of nonhuman proteins in human milk. *J Proteome Res* (2018) 18(1): acs.jproteome.8b00550. doi: 10.1021/acs.jproteome.8b00550

36. Amirghofran Z, Sheikhi A, Kumar P, Firouzi MS. Soluble HLA class I molecules in malignant pleural and peritoneal effusions and its possible role on NK and LAK cytotoxicity. *J Cancer Res Clin Oncol* (2002) 128(8):443–8. doi: 10.1007/s00432-002-0371-0

37. Minagar A, Adamashvili I, Kelley RE, Gonzalez-Toledo E, McLarty J, Smith SJ. Saliva soluble HLA as a potential marker of response to interferon-β1a in multiple sclerosis: A preliminary study. *J Neuroinflamm* (2007) 4(1):16. doi: 10.1186/1742-2094-4-16

38. Samanta L, Parida R, Dias TR, Agarwal A. The enigmatic seminal plasma: a proteomics insight from ejaculation to fertilization. *Reprod Biol Endocrinol* (2018) 16(1):41. doi: 10.1186/s12958-018-0358-6

39. Yu Y, Prassas I, Muytjens CMJ, Diamandis EP. Proteomic and peptidomic analysis of human sweat with emphasis on proteolysis. *J Proteomics* (2017) 155:40–8. doi: 10.1016/j.jprot.2017.01.005

40. Lee JH, Jung JH, Kim J, Baek WK, Rhee J, Kim TH, et al. Proteomic analysis of human synovial fluid reveals potential diagnostic biomarkers for ankylosing spondylitis. *Clin Proteomics* (2020) 17(1):20. doi: 10.1186/s12014-020-09281-y

41. Aultman D, Adamashvili I, Yaturu K, Langford M, Gelder F, Gautreaux M, et al. Soluble HLA in human body fluids. *Hum Immunol* (1999) 60(3):239–44. doi: 10.1016/S0198-8859(98)00122-0

42. Ting YT, Coates PT, Marti HP, Dunn AC, Parker RM, Pickering JW, et al. Urinary soluble HLA-DR is a potential biomarker for acute renal transplant rejection. *Transplantation* (2010) 89(9):1071–8. doi: 10.1097/TP.0b013e3181d15492

43. Shao D, Huang L, Wang Y, Cui X, Li Y, Wang Y, et al. HBFP: a new repository for human body fluid proteome. *Database* (2021) 2021. doi: 10.1093/database/baab065/6395039

44. Yu M, Xie F, Liu X, Sun H, Guo Z, Liu X, et al. Proteomic study of aqueous humor and its application in the treatment of neovascular glaucoma. *Front Mol Biosci* (2020) 7:587677/full. doi: 10.3389/fmolb.2020.587677/full

45. Fritsche J, Rakitsch B, Hoffgaard F, Römer M, Schuster H, Kowalewski DJ, et al. Translating immunopeptidomics to immunotherapy-Decision-Making for patient and personalized target selection. *Proteomics* (2018) 18(12):1700284. doi: 10.1002/pmic.201700284

46. Ritz D, Gloger A, Weide B, Garbe C, Neri D, Fugmann T. High-sensitivity HLA class I peptidome analysis enables a precise definition of peptide motifs and the identification of peptides from cell lines and patients' sera. *Proteomics* (2016) 16 (10):1570–80. doi: 10.1002/pmic.201500445

47. Ritz D, Gloger A, Neri D, Fugmann T. Purification of soluble HLA class I complexes from human serum or plasma deliver high quality immuno peptidomes required for biomarker discovery. *Proteomics* (2017) 17(1–2):1600364. doi: 10.1002/pmic.201600364

48. Shraibman B, Barnea E, Kadosh DM, Haimovich Y, Slobodin G, Rosner I, et al. Identification of tumor antigens among the HLA peptidomes of glioblastoma tumors and plasma. *Mol Cell Proteomics* (2019) 18(6):1255–68. doi: 10.1074/mcp.RA119.001524

49. Grieb G, Merk M, Bernhagen J, Bucala R. Macrophage migration inhibitory factor (MIF): A promising biomarker. *Drug News Perspect* (2010) 23(4):257. doi: 10.1358/dnp.2010.23.4.1453629

50. Psallidas I, Kanellakis NI, Gerry S, Thézénas ML, Charles PD, Samsonova A, et al. Development and validation of response markers to predict survival and pleurodesis success in patients with malignant pleural effusion (PROMISE): a

multicohort analysis. *Lancet Oncol* (2018) 19(7):930–9. doi: 10.1016/S1470-2045(18)30294-8

51. Thomas R, Al-Khadairi G, Roelands J, Hendrickx W, Dermime S, Bedognetti D, et al. NY-ESO-1 based immunotherapy of cancer: Current perspectives. *Front Immunol* (2018) 9:947/full(MAY). doi: 10.3389/fimmu.2018.00947/full

52. Weidanz JA, Doll KL, Mohana-Sundaram S, Wichner T, Lowe DB, Gimlin S, et al. Detection of human leukocyte antigen biomarkers in breast cancer utilizing label-free biosensor technology. *J Visualized Experiments* (2015) 2015(97). doi: 10.3791/52159

53. Andersen RS, Thrue CA, Junker N, Lyngaa R, Donia M, Ellebæk E, et al. Dissection of T-cell antigen specificity in human melanoma. *Cancer Res* (2012) 72(7):1642–50. doi: 10.1158/0008-5472.CAN-11-2614

54. Khazan-Kost S, Cafri G, Melamed Kadosh D, Mooshayef N, Chatterji S, Dominissini D, et al. Soluble HLA peptidome of pleural effusions is a valuable source for tumor antigens. *J Immunother Cancer* (2022) 10(5):e003733. doi: 10.1136/jitc-2021-003733

55. Guo Y, Guo H, Zhang Y, Cui J. Anaplastic lymphoma kinase-special immunity and immunotherapy. *Front Immunol* (2022) 13:908894/full. doi: 10.3389/fimmu.2022.908894/full

56. Ritz D, Sani E, Debiec H, Ronco P, Neri D, Fugmann T. Membranal and blood-soluble HLA class II peptidome analyses using data-dependent and independent acquisition. *Proteomics* (2018) 18(12):1700246. doi: 10.1002/pmic.201700246

57. Nesvizhskii AI. Proteogenomics: concepts, applications and computational strategies. *Nat Methods* (2014) 11(11):1114–25. doi: 10.1038/nmeth.3144

58. Almeida LG, Sakabe NJ, deOliveira AR, Silva MCC, Mundstein AS, Cohen T, et al. CTdatabase: a knowledge-base of high-throughput and curated data on cancer-testis antigens. *Nucleic Acids Res* (2009) 37(Database):D816–9. doi: 10.1093/nar/gkn673

59. Storkus WJ, Zeh HJ, Salter RD, Lotze MT. Identification of T-cell epitopes: rapid isolation of class I-presented peptides from viable cells by mild acid elution. *J Immunother Emphasis Tumor Immunol* (1993) 14(2):94–103. doi: 10.1097/00002371-199308000-00003

60. Lanoix J, Durette C, Courcelles M, Cossette É, Comtois-Marotte S, Hardy MP, et al. Comparison of the MHC I immunopeptidome repertoire of b-cell lymphoblasts using two isolation methods. *Proteomics* (2018) 18(12):1700251. doi: 10.1002/pmic.201700251

61. Ramarathinam SH, Faridi P, Peng A, Szeto P, Wong NC, Behren A, et al. A peptide-signal amplification strategy for the detection and validation of neoepitope presentation on cancer biopsies. *bioRxiv* (2020). doi: 10.1101/2020.06.12.145276

62. Jarmalavicius S, Welte Y, Walden P. High immunogenicity of the human leukocyte antigen peptidomes of melanoma tumor cells. *J Biol Chem* (2012) 287(40):33401–11. doi: 10.1074/jbc.M112.358903

63. Gloger A, Ritz D, Fugmann T, Neri D. Mass spectrometric analysis of the HLA class I peptidome of melanoma cell lines as a promising tool for the identification of putative tumor-associated HLA epitopes. *Cancer Immunol Immunotherapy* (2016) 65(11):1377–93. doi: 10.1007/s00262-016-1897-3

64. Chong C, Marino F, Pak H, Racle J, Daniel RT, Müller M, et al. High-throughput and sensitive immunopeptidomics platform reveals profound interferonγ-mediated remodeling of the human leukocyte antigen (HLA) ligandome. *Mol Cell Proteomics* (2018) 17(3):533–48. doi: 10.1074/mcp.TIR117.000383

65. Hunt DF, Henderson RA, Shabanowitz J, Sakaguchi K, Michel H, Sevilir N, et al. Characterization of peptides bound to the class I MHC molecule HLA-A2.1 by mass spectrometry. *Science* (1992) 255(5049):1261–3. doi: 10.1126/science.1546328

66. Bassani-Sternberg M, Pletscher-Frankild S, Jensen LJ, Mann M. Mass spectrometry of human leukocyte antigen class I peptidomes reveals strong effects of protein abundance and turnover on antigen presentation. *Mol Cell Proteomics* (2015) 14(3):658–73. doi: 10.1074/mcp.M114.042812

67. Bruderer R, Bernhardt OM, Gandhi T, Miladinović SM, Cheng LY, Messner S, et al. Extending the limits of quantitative proteome profiling with data-independent acquisition and application to acetaminophen-treated three-dimensional liver microtissues. *Mol Cell Proteomics* (2015) 14(5):1400–10. doi: 10.1074/mcp.M114.044305

68. Ritz D, Kinzi J, Neri D, Fugmann T. Data-independent acquisition of HLA class I peptidomes on the q exactive mass spectrometer platform. *Proteomics* (2017) 17(19):1700177. doi: 10.1002/pmic.201700177

69. Caron E, Aebersold R, Banaei-Esfahani A, Chong C, Bassani-Sternberg M. A case for a human immuno-peptidome project consortium. *Immunity* (2017) 47(2):203–8. doi: 10.1016/j.immuni.2017.07.010

70. Caron E, Espona L, Kowalewski DJ, Schuster H, Ternette N, Alpízar A, et al. An open-source computational and data resource to analyze digital maps of immunopeptidomes. *Elife* (2015) 4. doi: 10.7554/eLife.07661

71. Murphy JP, Kim Y, Clements DR, Konda P, Schuster H, Kowalewski DJ, et al. Therapy-induced MHC I ligands shape neo-antitumor CD8 T cell responses during oncolytic virus-based cancer immunotherapy. *J Proteome Res* (2019) 18(6):2666–75. doi: 10.1021/acs.jproteome.9b00173

72. Jaeger AM, Stopfer L, Lee S, Gaglia G, Sandel D, Santagata S, et al. Rebalancing protein homeostasis enhances tumor antigen presentation. *Clin Cancer Res* (2019) 25(21):6392–405. doi: 10.1158/1078-0432.CCR-19-0596

73. Stopfer LE, Mesfin JM, Joughin BA, Lauffenburger DA, White FM. Multiplexed relative and absolute quantitative immunopeptidomics reveals MHC I repertoire alterations induced by CDK4/6 inhibition. *Nat Commun* (2020) 11(1):2760. doi: 10.1038/s41467-020-16588-9

74. Murphy JP, Yu Q, Konda P, Paulo JA, Jedrychowski MP, Kowalewski DJ, et al. Multiplexed relative quantitation with isobaric tagging mass spectrometry reveals class I major histocompatibility complex ligand dynamics in response to doxorubicin. *Anal Chem* (2019) 91(8):5106–15. doi: 10.1021/acs.analchem.8b05616

75. Robinson J, Halliwell JA, Hayhurst JD, Flicek P, Parham P, Marsh SGE. The IPD and IMGT/HLA database: allele variant databases. *Nucleic Acids Res* (2015) 43(D1):D423–31. doi: 10.1093/nar/gku1161

76. Zhang L, McAlpine PL, Heberling ML, Elias JE. Automated ligand purification platform accelerates immunopeptidome analysis by mass spectrometry. *J Proteome Res* (2021) 20(1):393–408. doi: 10.1021/acs.jproteome.0c00464

77. Stopfer LE, D'Souza AD, White FM. 1,2,3, MHC: a review of mass-spectrometry-based immunopeptidomics methods for relative and absolute quantification of pMHCs. *Immuno-Oncology Technol* (2021) 11:100042. doi: 10.1016/j.iotech.2021.100042

78. Hassan C, Kester MGD, Oudgenoeg G, de Ru AH, Janssen GMC, Drijfhout JW, et al. Accurate quantitation of MHC-bound peptides by application of isotopically labeled peptide MHC complexes. *J Proteomics* (2014) 109:240–4. doi: 10.1016/j.jprot.2014.07.009

79. Faridi P, Purcell AW, Croft NP. In immunopeptidomics we need a sniper instead of a shotgun. *Proteomics* (2018) 18(12). doi: 10.1002/pmic.201700464

80. Tran MT, Faridi P, Lim JJ, Ting YT, Onwukwe G, Bhattacharjee P, et al. T Cell receptor recognition of hybrid insulin peptides bound to HLA-DQ8. *Nat Commun* (2021) 12(1):5110. doi: 10.1038/s41467-021-25404-x

81. Mukherjee S, Sanchez-Bernabeu A, Demmers LC, Wu W, Heck AJR. The HLA ligandome comprises a limited repertoire of O-GlcNAcylated antigens preferentially associated with HLA-B*07:02. *Front Immunol* (2021) 12:796584/full. doi: 10.3389/fimmu.2021.796584/full

82. Mei S, Ayala R, Ramarathinam SH, Illing PT, Faridi P, Song J, et al. Immunopeptidomic analysis reveals that deamidated HLA-bound peptides arise predominantly from deglycosylated precursors. *Mol Cell Proteomics.* (2020) 19(7):1236–47. doi: 10.1074/mcp.RA119.001846

83. Solleder M, Guillaume P, Racle J, Michaux J, Pak HS, Müller M, et al. Mass spectrometry based immunopeptidomics leads to robust predictions of phosphorylated HLA class I ligands. *Mol Cell Proteomics* (2020) 19(2):390–404. doi: 10.1074/mcp.TIR119.001641

84. Laumont CM, Daouda T, Laverdure JP, Bonneil É, Caron-Lizotte O, Hardy MP, et al. Global proteogenomic analysis of human MHC class I-associated peptides derived from non-canonical reading frames. *Nat Commun* (2016) 7(1):10238. doi: 10.1038/ncomms10238

85. Chong C, Müller M, Pak H, Harnett D, Huber F, Grun D, et al. Integrated proteogenomic deep sequencing and analytics accurately identify non-canonical peptides in tumor immunopeptidomes. *Nat Commun* (2020) 11(1):1293. doi: 10.1038/s41467-020-14968-9

86. Olsson N, Heberling ML, Zhang L, Jhunjhunwala S, Phung QT, Lin S, et al. An integrated genomic, proteomic, and immunopeptidomic approach to discover treatment-induced neoantigens. *Front Immunol* (2021) 12. doi: 10.3389/fimmu.2021.662443

87. Faridi P, Li C, Ramarathinam SH, Vivian JP, Illing PT, Mifsud NA, et al. A subset of HLA-I peptides are not genomically templated: Evidence for cis- and trans-spliced peptide ligands. *Sci Immunol* (2018) 3(28). doi: 10.1126/sciimmunol.aar3947

88. Faridi P, Woods K, Ostrouska S, Deceneux C, Aranha R, Duscharla D, et al. Spliced peptides and cytokine-driven changes in the immunopeptidome of melanoma. *Cancer Immunol Res* (2020) 8(10):1322–34. doi: 10.1158/2326-6066.CIR-19-0894

frontiers | Frontiers in Oncology

TYPE Original Research
PUBLISHED 19 January 2023
DOI 10.3389/fonc.2022.1097816

OPEN ACCESS

EDITED BY
Zohreh Amoozgar,
Massachusetts General Hospital and Harvard Medical School, United States

REVIEWED BY
Michael Shafique,
Moffitt Cancer Center, United States
Zhenxiang Li,
Shandong Cancer Hospital, China

*CORRESPONDENCE
Tengfei Zhang
fcczhangtf@zzu.edu.cn
Yabing Du
fccduyb@zzu.edu.cn

SPECIALTY SECTION
This article was submitted to Molecular and Cellular Oncology, a section of the journal Frontiers in Oncology

RECEIVED 14 November 2022
ACCEPTED 29 December 2022
PUBLISHED 19 January 2023

CITATION
Wang H, Liu L, Yan J, Ma W, Du Y and Zhang T (2023) Folate receptor-positive circulating tumor cell count, lymphocyte count and derived neutrophil-to-lymphocyte ratio for diagnosing lung cancer relapse.
Front. Oncol. 12:1097816.
doi: 10.3389/fonc.2022.1097816

Folate receptor-positive circulating tumor cell count, lymphocyte count and derived neutrophil-to- lymphocyte ratio for diagnosing lung cancer relapse

Huanrong Wang, Lei Liu, Jiaqin Yan, Wang Ma, Yabing Du* and Tengfei Zhang*

Department of Oncology, The First Affiliated Hospital of Zhengzhou University, Zhengzhou, China

The folate receptor-positive circulating tumor cell (FR^+-CTC) count can be used to improve the diagnosis rate of lung cancer. The lymphocyte count (LC) and derived neutrophil-to-lymphocyte ratio (dNLR) are involved in inflammatory processes. Whether the FR^+-CTC count combined with the dNLR or LC is helpful for diagnosing lung cancer recurrence is not clear. Sixty-eight patients who were initially diagnosed with lung cancer and received first-line treatment were included. The clinicopathological characteristics, routine blood examination results and CTC examination results of the patients were collected. The role of the complete blood count and FR^+-CTC count in lung cancer treatment response and prognosis was analyzed. The FR^+-CTC count after treatment was significantly correlated with the T stage (p=0.005). Multivariate analysis showed that the pathological type and FR^+-CTC count were independent predictors of disease- or progression-free survival (DFS/PFS) in patients with lung cancer (p=0.010 and p=0.030, respectively). The FR^+-CTC count, LC and dNLR predicted the recurrence of lung cancer (sensitivity and specificity of the FR^+-CTC count, 69.2% and 71.4%; the LC, 50.0% and 88.5%; and the dNLR, 50.0% and 88.1%, respectively). The FR^+-CTC count combined with the LC or dNLR improved the diagnostic rate of lung cancer recurrence (sensitivity and specificity of the FR^+-CTC count plus the LC, 53.8% and 90.5%, and the FR^+-CTC count plus the dNLR, 73.1% and 73.8%, respectively). When these three indicators were combined to predict lung cancer recurrence, the AUC value was 0.817. The FR^+-CTC count combined with the dNLR and/or LC after treatment can improve the diagnostic rate of lung cancer recurrence. A higher FR^+-CTC count predicts worse DFS/PFS in patients with lung cancer.

KEYWORDS

folate receptor-positive circulating tumor cell, lymphopenia, derived neutrophil-to-lymphocyte ratio, lung cancer, relapse, prognosis, first-line treatment

Introduction

Lung cancer has the highest mortality rate of all cancers, according to the latest statistics from the American Cancer Society (1). According to the pathological type, lung cancer is divided into small cell lung cancer (SCLC) and non-small cell lung cancer (NSCLC), including lung squamous cell carcinoma (LUSC) and lung adenocarcinoma (LUAD). Although SCLC is sensitive to platinum-based chemotherapy agents, it has the highest mortality rate because of its recurrence and progression in a short time (2). Low-dose computed tomography (CT) is the primary means to screen lung cancer at present. In a multicenter study, low-dose CT screening for lung cancer reduced mortality by 20% compared with X-rays during follow-up (3). One study reported that circulating tumor cells (CTCs) were found in the peripheral blood of five patients with chronic obstructive pulmonary disease, and all five CTC-positive patients developed lung cancer during follow-up. The CTC count can be used to detect lung cancer one to four years earlier than chest CT (4). In addition, some studies have shown that identifying tyrosine kinase inhibitor resistance in NSCLC is significantly delayed, with a median lag time of 113 days (range, 45-169 days), based on CT compared with the CTC count (5).

CTCs are released into peripheral blood from primary tumors or during metastasis, and many studies have shown that the CTC count can be used to assist in the diagnosis of breast, gastric, and lung cancers (6–8). Initially, CTCs are epithelial types, but blood is not an ideal place for epithelial cells, so they enter an epithelial-mesenchymal cell change stage; notably, most detection methods cannot detect CTCs that develop this change (9). Folate receptor (FR) mediates folate transport into cells (10). Studies have shown that tumor cells need to absorb a large amount of folic acid for DNA synthesis in the process of proliferation. Hence, FR is highly expressed in most human tumor cells, such as lung cancer, endometrial cancer, and ovarian cancer cells (11–13). By injecting a tumor-specific fluorescent ligand recognition FR *in vivo*, CTCs can be counted by multiphoton fluorescence imaging of surface vessels, and the presence of CTCs can be detected a few weeks before metastatic lesions are observed by other methods (14). Thus, scientists can detect CTCs that undergo epithelial-mesenchymal transition using the ligand-targeted polymerase chain reaction method, which has been approved by the China Food and Drug Administration to detect the number of CTCs (15).

Inflammation is considered to be the main driver of tumorigenesis and progression. The inflammatory cells related to tumor progression are mainly neutrophils (NEs), macrophages and myeloid-derived suppressor cells (16–18). Myelopoiesis in the tumor is associated with defects in myeloid cell differentiation, resulting in the accumulation of immature myeloid cells such as myeloid-derived suppressor cells and NEs in the circulation (16). Lymphocytes are one of the important components of the immune system and are indispensable in the antitumor immune response. A study has shown that a low lymphocyte count (LC) induced by radiation therapy reduces survival in patients with stage III lung cancer (19). In addition, platelets (PLTs) are involved in the development of inflammation; most patients with tumors have higher PLT levels than patients without tumors (20). The neutrophil-to-lymphocyte ratio (NLR) and platelet-to-lymphocyte ratio (PLR) are important in the diagnosis and prognosis of lung cancer and other tumors, such as liver cancer and ovarian cancer (21, 22). In addition, the derived neutrophil-to-lymphocyte ratio (dNLR) is an essential factor in predicting the effect of immunotherapy in NSCLC patients (23). Investigators have demonstrated that the dNLR is associated with the prognosis of metastatic NSCLC, and these results were not affected by treatment plans (24). Thus, we speculated that the folate receptor-positive circulating tumor cell (FR^+-CTC) count combined with other serological markers, such as the LC, NLR, PLR, and dNLR, during first-line therapy in patients with lung cancer have the potential to be used as biomarkers to predict patient recurrence or progression. Moreover, these indicators are routinely measured in clinical practice. Compared with high invasive and inaccessible markers, it's more significant to explore these regular hematological tests for tumor diagnosis and prognosis.

Patients and methods

Patient recruitment and data collection

In this retrospective study, we enrolled patients who had just been diagnosed with lung cancer and treated between July 2018 and September 2021. We collected their clinicopathological characteristics, including age, sex, pathological type, treatment regimen, and maximum tumor diameter. TNM staging was determined based on the American Joint Committee on Cancer guidelines. Hematological parameters included NE, leukocyte, lymphocyte, PLT and FR^+-CTC counts. The study followed the guidelines of the Declaration of Helsinki. The study protocol was approved by the Ethics Committee of the First Affiliated Hospital of Zhengzhou University (2002-KY-2021-002).

Assessments

The inclusion criteria included the following: patients with lung cancer diagnosed by cytology and pathology; patients who had not received any antineoplastic therapy; and complete blood count and FR^+-CTC count were tested on admission and during treatment. Patients who received treatment only once or had incomplete follow-up data were excluded. Imaging was performed according to RECIST 1.1 to assess stable disease (SD) and progressive disease (PD). Assessments were performed every 1-2 months for the first year of lung cancer ascertainment and every 3-6 months thereafter. Progression-free survival (PFS) referred to the time from randomization to the first occurrence of disease progression or death from any cause. Disease-free survival (DFS) corresponded to the length of time after the operation during which a patient survives with no signs of disease. The follow-up time was up to July 2, 2022.

In this study, the posttreatment hematological indicators of the 68 patients were assessed. For patients who only received surgical treatment and targeted therapy, the indicators were collected within 3 months after treatment, and for patients treated with chemotherapy, indicators were collected at the end of two courses of treatment. The

FR^+-CTC number was detected with the CytoploRare Human Lung Cancer Circulating Tumor Cell Assay Kit (Geno). There are two steps in FR^+-CTC detection: enrichment by immunomagnetic beads and ligand-targeted polymerase chain reaction to detect and quantify FR^+-CTCs (25). The FR^+-CTC count was specified as the number of FR^+-CTCs detected in a 3 mL blood sample. Because of the heterogeneity of tumors and individual differences in patients, we used a receiver operating characteristic (ROC) curve to find the best optimal value (9.75 FU/3 mL, area under the curve (AUC)=0.744) associated with progression between a high FR^+-CTC count and a low FR^+-CTC count. The NLR was defined as the neutrophil count/lymphocyte count, the PLR was defined as the platelet count/lymphocyte group count, and the dNLR was defined as the absolute neutrophil count/white blood cell count-absolute neutrophil count.

Statistical analysis

The FR^+-CTC count and other categorical variables were compared with Pearson's chi-square test. An ROC curve was utilized to analyze the AUC and the corresponding 95% confidence interval (CI), sensitivity, and specificity for each diagnostic variable. The log-rank hazard regression model was used for univariate analysis, and the Kaplan–Meier method was used to draw survival curves. Cox's proportional hazards regression model was used for multivariate analysis to calculate hazard ratios (HRs) and 95% CIs. Figures in the article were drawn with PRISM 8. $P<0.05$ was considered statistically significant.

Results

Patient characteristics

Sixty-eight patients (35 males and 33 females) who met the criteria were included in our research. The average age at initiation of treatment was 58, with a maximum of 83 and a minimum of 32. We chose the maximum diameter of the tumor to record tumor size. The average tumor size was 2.79 cm, with a minimum of 0.63 cm and a maximum of 7.20 cm. Pathological types included LUAD (n=54), LUSC (n=7) and SCLC (n=7). All patients were initially diagnosed with lung cancer and received first-line treatment in the hospital. Sixteen people received surgical treatment. Fifteen people received chemotherapy with platinum-based single- or double-drug therapy. Three received targeted therapy with oral tyrosine kinase inhibitors. Thirty-four people received two or more combination treatments. By the end of follow-up, 26 patients had disease recurrence or progression. The clinicopathological characteristics of all patients are shown in Table 1.

TABLE 1 Clinical and pathological characteristics of the 68 patients.

Characteristics	Total (N=68)
Age (average, range), years	58 (32, 83)
Sex (male/female)	35/33
Pathologic	
LASC	7
LUSC	54
SCLC	7
Tumor size (average, range), cm	2.79(0.63, 7.20)
LC (average, range), $\times10^9$/L	1.5(0.49, 3.05)
NE (average, range), $\times10^9$/L	5.34(1.65, 10.67)
PLT (average, range), $\times10^9$/L	251 (88, 462)
NLR (average, range)	4.01(0.74, 14.28)
PLR (average, range)	183.1(76.0, 578.5)
dNLR (average, range)	2.20(0.49, 5.08)
Treatment	
Surgical only	16
Chemotherapy only	15
Targeted therapy only	3
Combined treatment	34
State of treatment (relapse/no relapse)	26/42

Association between the FR$^+$-CTC count and clinical characteristics

We analyzed the correlation between the posttreatment FR$^+$-CTC count and the clinicopathological characteristics of patients. As mentioned, we used 9.75 FU/3 mL as a cutoff value to classify high and low FR$^+$-CTC counts. For other clinical characteristics, the average value was used as the dividing line. The FR$^+$-CTC count of patients in the T3 and T4 stages was significantly higher than that of patients in the T1 and T2 stages (p=0.005). In addition, the CTC value of patients treated with systemic therapy was significantly higher than that of patients treated with surgery (p=0.019). However, other indicators were not significantly different from the FR$^+$-CTC count (Table 2).

Survival analysis

To study the factors affecting the DFS/PFS of lung cancer patients in depth, we included indicators such as sex, age, pathological type, tumor size, TNM stage, treatment regimen and FR$^+$-CTC count, NE count, LC, PLT count, dNLR, PLR, and NLR after treatment. Univariate analysis showed that pathological type, T classification, clinical stage, treatment regimen, FR$^+$-CTC count, LC, dNLR, and NLR were factors influencing PFS (Table 3).

Next, we performed survival analysis of different groups stratified by the first-line treatment regimen and pathological classification. For patients in the surgery group, the median disease-free survival (mDFS) of patients with a low FR$^+$-CTC count was significantly longer than that of patients with a high FR$^+$-CTC count (p=0.046,

TABLE 2 Correlation between the FR$^+$-CTC count and clinical characteristics.

Characteristics	CTC expression level		$\chi2$	p	Characteristics	CTC expression level		$\chi2$	p
	Low (n=38)	**High(n=30)**				**Low (n=38)**	**High(n=30)**		
Age(years)			1.36	0.243	**Clinical stage**			3.51	0.061
<58	18(47.4%)	10(33.3%)			I	20(52.6%)	9(30.0%)		
≥58	20(52.6%)	20(66.7%)			II+III+IV	18(47.4%)	21(70.0%)		
Sex			0.5	0.481	**PLT (×10^9/L)**			1.56	0.211
Male	21(55.2%)	14(46.6%)			<251	21(55.3%)	12(40.0%)		
Female	17(44.8%)	16(53.4%)			≥251	17(44.7%)	18(60.0%)		
Tumor size(cm)			0.68	0.411	**NE(×10^9/L)**			0.002	0.965
<2.79	19(50.0%)	18(60.0%)			<5.34	23(60.5%)	18(60.0%)		
≥2.79	19(50.0%)	12(40.0%)			≥5.34	15(39.5%)	12(40.0%)		
Pathologic type			3.76	0.053	**NLR**			0.14	0.712
NSCLC	37(97.4%)	24(80.0%)			<4.01	25(65.8%)	21(70.0%)		
SCLC	1(2.6%)	6(20.0%)			≥4.01	13(34.2%)	9(30.0%)		
Treatment			5.46	**0.019**	**PLR**			1.09	0.297
Surgery	13(34.2%)	3(10.0%)			<183.1	25(65.8%)	16(53.3%)		
Systemic therapy	25(65.8%)	27(90.0%)			≥183.1	13(34.2%)	14(46.7%)		
T classification			7.84	**0.005**	**dNLR**			1.19	0.276
T1+T2	33(86.8%)	17(56.7%)			<2.2	24(63.2%)	15(50.0%)		
T3+T4	5(13.2%)	13(43.3%)			≥2.2	14(36.8%)	15(50.0%)		
N classification			1.73	0.189	**LC(×10^9/L)**			0.19	0.666
N0	25(65.8%)	15(50.0%)			<1.5	17(44.7%)	15(50.0%)		
N1+N2+N3	13(34.2%)	15(50.0%)			≥1.5	21(55.3%)	15(50.0%)		
Metastasis tatus			0.66	0.416					
Yes	31(81.6%)	22(73.3%)							
No	7(18.4%)	8(26.7%)							

Values in bold mean p<0.05.

TABLE 3 Univariate and multivariate analyses of disease- or progression-free survival (N = 68, 26 progression events).

	DFS/PFS					
	Univariate Analysis			Multivariate Analysis		
Characteristic	HR	95% CI	*p*	HR	95% CI	*p*
Male (vs. female)	0.570	0.258-1.259	0.164	0.362	0.122-1.073	0.067
Age (per year)	2.267	0.952-5.397	0.064	0.784	0.214-2.872	0.713
SCLC (vs. NSCLC)	12.482	4.440-35.095	**0.000**	5.516	1.510-20.140	**0.010**
Tumor size(cm) ≥2.79(vs. <2.79)	1.596	0.734-3.470	0.238			
T3+T4 (vs. T1+T2)	2.695	1.231-5.899	**0.013**	0.612	0.142-2.645	0.511
Lymph node metastatic yes (vs. no)	1.937	0.893-4.201	0.094	0.816	0.228-2.918	0.755
Metastasis yes (vs. no)	1.040	0.416-2.597	0.933			
Clinical stage others (vs. I)	3.014	1.202-7.554	**0.019**	3.070	0.457-20.634	0.249
Systemic therapy (vs. surgery)	8.476	1.147-62.611	**0.036**	2.986	0.351-25.417	0.317
NE($x10^9$/L) ≥6.65 (vs. <6.65)	0.616	0.231-1.641	0.333			
LC($x10^9$/L) ≥1.72 (vs. <1.72)	0.206	0.062-0.686	**0.010**	0.383	0.101-1.455	0.159
PLT($x10^9$/L) ≥190 (vs. <190)	2.192	0.656-7.314	0.202			
dNLR≥2.46 (vs. <2.46)	5.105	2.235-11.661	**<0.001**	1.852	0.672-5.100	0.233
PLR≥171.5 (vs. <171.5)	2.149	0.972-4.751	0.059	1.965	0.673-5.738	0.217
NLR≥1.93 (vs. <1.93)	4.388	1.035-18.609	**0.045**	2.220	0.420-11.725	0.348
FR^+-CTC(Fu/3ml) ≥9.75(vs. <9.75)	3.861	1.674-8.908	**0.002**	3.039	1.111-8.310	**0.030**

Values in bold mean p<0.05.

Figure 1A, Table 4A). According to the cutoff value of the ROC curve, the LC and dNLR were used to divide patients into high and low groups, and we found that there was no significant difference in DFS between the two groups. For the systemic treatment group, we found that the median progression-free survival (mPFS) of patients with a low FR^+-CTC count was significantly longer than that of patients with a high FR^+-CTC count (23.53 months vs. 12.03 months, p=0.003, Figure 1A, Table 4A). Patients with a high LC were more likely than those with a low LC to experience a significantly prolonged mPFS (not reach (NR) vs. 14.8 months, p=0.029, Figure 1B, Table 4A). Patients with low dNLR values had a significantly longer mPFS than patients with high dNLR values (23.53 months vs. 8.033 months, p<0.001, Figure 1C, Table 4A). There was no significant difference in the prognosis of high NLR and low NLR in different treatment groups (Supplementary Figure 1). In addition, we divided patients into two groups according to NSCLC and SCLC. For the NSCLC group, the mDFS/mPFS of those with a low FR^+-CTC count was significantly longer than that of patients with a high FR^+-CTC count (NR vs. 20.1 months, p=0.014, Figure 2A, Table 4B). Patients with a low LC had a significantly shorter mDFS/mPFS than patients with a high LC (20.10 months vs. NR, p=0.029, Figure 2B, Table 4B), and patients with low dNLR values had a significantly longer mDFS/mPFS than patients with high dNLR values (NR vs. 13.9 months, p<0.001, Figure 2C, Table 4B). For the SCLC group, there was no significant difference in mPFS based on different blood markers (Figure 2, Table 4B).

According to the results of univariate analysis, variables with p<0.2 were included in multivariate analysis. We found that the FR^+-CTC count and pathological type were independent predictors of DFS/PFS (Table 3).

ROC analysis of the FR^+-CTC count, LC and dNLR and the diagnostic yield of joint diagnostic models

Next, we investigated whether the FR^+-CTC count, NE count, LC, PLT count, dNLR, PLR and NLR could predict recurrence or progression after first-line treatment of lung cancer. According to our analysis, the optimal cutoff value of the FR^+-CTC count for differentiating disease recurrence from disease stabilization was 9.75 FU/3 mL, with a sensitivity of 69.2% and a specificity of 71.4% (AUC=0.744). Similarly, the LC and

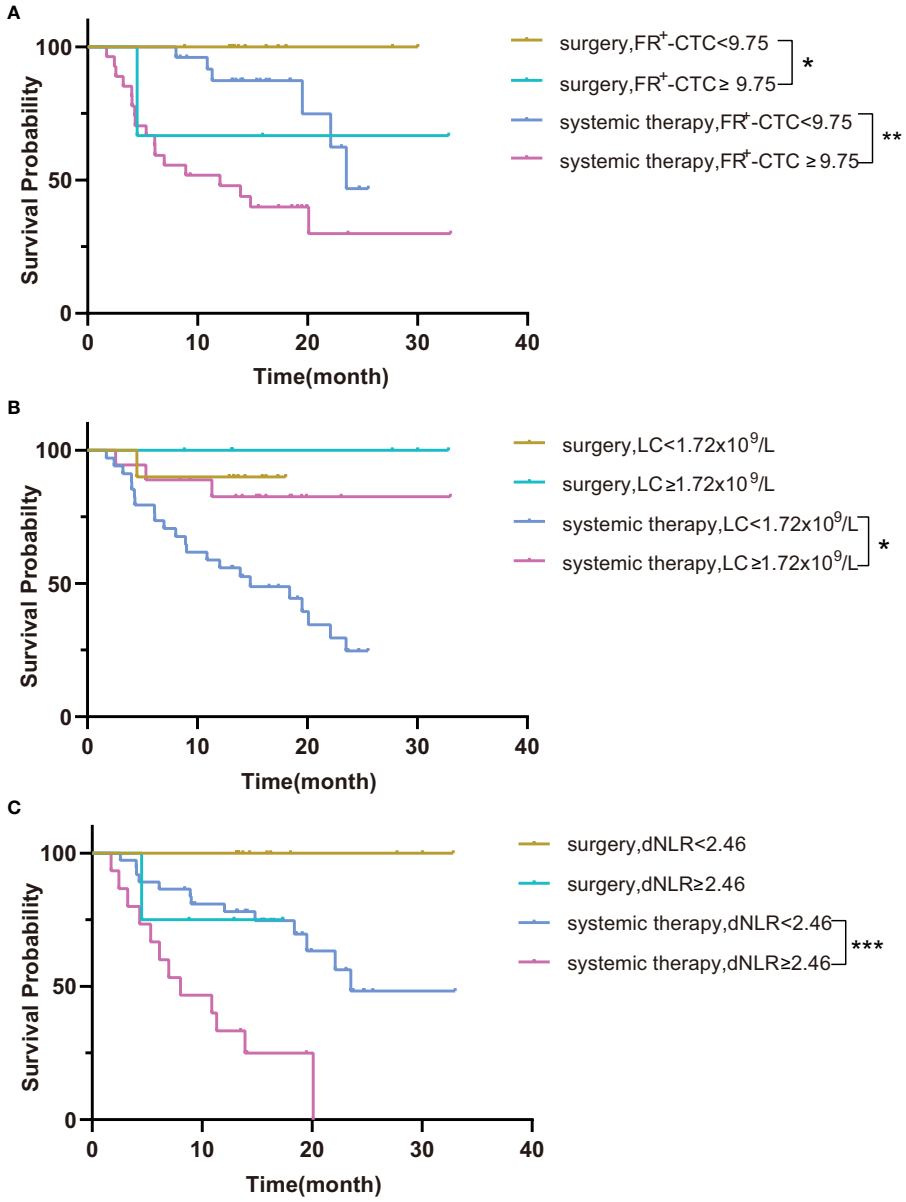

FIGURE 1
(A) Kaplan–Meier curves for survival probability according to the FR$^+$-CTC count between surgery and systemic therapy. **(B)** Kaplan–Meier curves for survival probability according to the LC between surgery and systemic therapy. **(C)** Kaplan–Meier curves for survival probability according to the dNLR between surgery and systemic therapy. *P < 0.05, **P < 0.01, ***P < 0.001.

dNLR significantly differentiated disease recurrence (sensitivity=50.0%, specificity=88.5%, AUC= 0.674 and sensitivity=50.0%, specificity=88.1%, AUC=0.675, respectively; Figure 3, Table 5).

Interestingly, by combining the FR$^+$-CTC count with the LC or dNLR, we found that the combined AUC was more significant than the AUC of either one alone (sensitivity and specificity of the FR$^+$-CTC count plus LC, 53.8% and 90.5%, AUC=0.759, Figure 4A, Table 5; sensitivity and specificity of the FR$^+$-CTC count plus the dNLR, 73.1% and 73.8%, AUC=0.762, Figure 4B, Table 5). When these three indicators were combined to diagnose lung cancer recurrence, the AUC value was higher than when any two were combined (sensitivity=73.1%, specificity= 78.6%, AUC=0.817, Figure 4C, Table 5). The above results indicated that the FR$^+$-CTC count combined with the LC and/or dNLR could improve the diagnosis rate of relapse in lung cancer. To present the overall predictive effect of the data, we divided all patients into two categories: relapse and no relapse. The confusion matrix for each hematological marker for predicting lung cancer relapse in patients is shown in Figure 5.

We found that the NE count, PLT count, PLR and NLR were not very useful for diagnosing lung cancer recurrence, so we do not show them here (Supplementary Figure 2).

Discussion

Although oncological research on lung cancer has been progressing yearly, recurrence or progression during treatment is still the most direct cause of lung cancer treatment failure. Over the

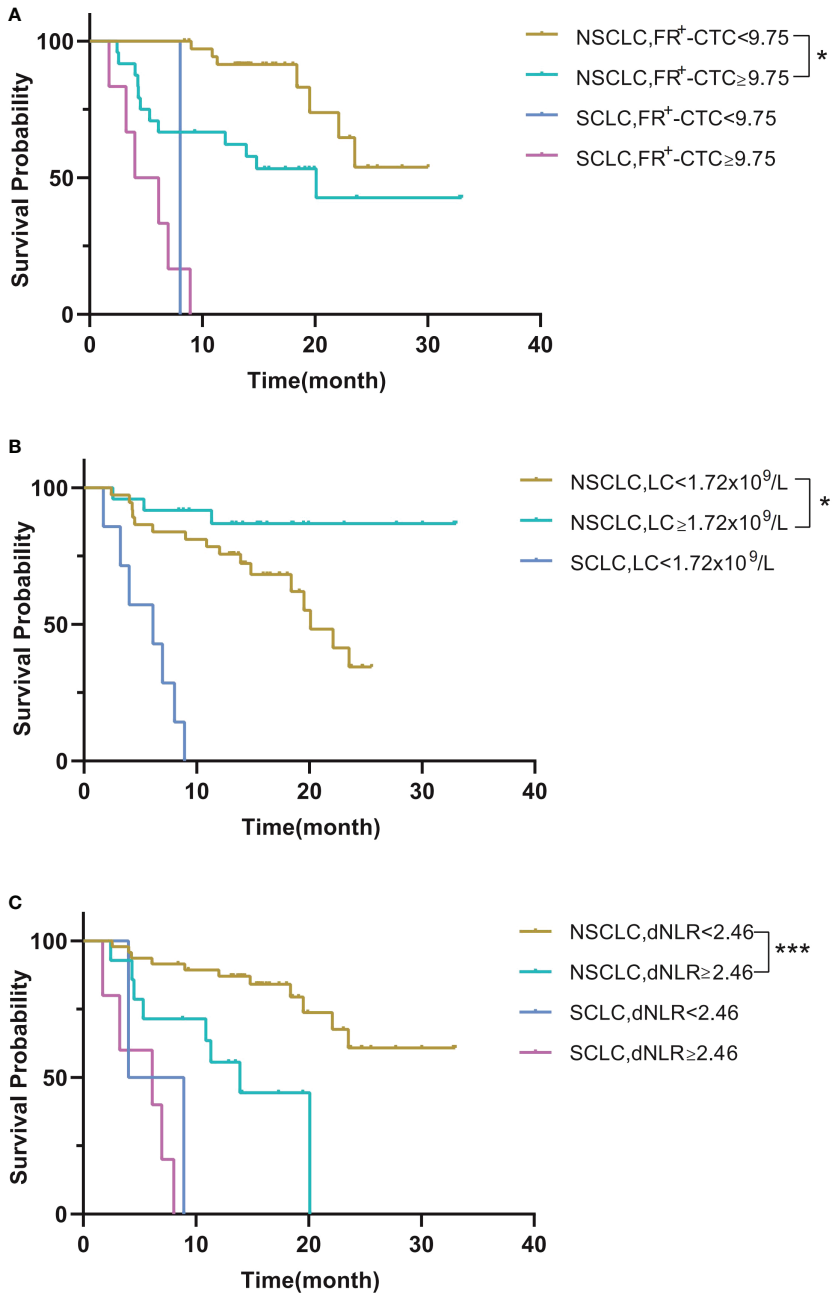

FIGURE 2
(A) Kaplan–Meier curves for survival probability according to the FR^+-CTC count between NSCLC and SCLC. **(B)** Kaplan–Meier curves for survival probability according to the LC between NSCLC and SCLC. **(C)** Kaplan–Meier curves for survival probability according to the dNLR between NSCLC and SCLC. *P < 0.05, **P < 0.01, ***P < 0.001.

past 20 years, researchers have demonstrated that CTCs play an essential role in the diagnosis and prognosis of malignant tumors (26, 27). However, the search for an efficient method to isolate and detect CTCs remains controversial, and oncologists are just beginning to understand how the information obtained from CTC detection and analysis can be used in patient care. In this study, we designed a diagnosis-treat-relapse model to investigate the significance of CTCs and other hematological markers for diagnosing lung cancer recurrence. We aimed to use these clinical hematological markers to detect lung cancer recurrence and adjust the treatment plan in time to bring the greatest clinical benefit to the patients.

Researchers have reported that the FR^+-CTC count can predict prognosis in breast cancer, gastrointestinal tumors, melanoma and prostate cancer (6, 28–31). A prospective, single-center clinical study showed that a lower FR^+-CTC count could be a predictor of first-line chemotherapy in SCLC patients (HR=0.656, p=0.049) (15). Hiltermann et al. found that the CTC count after the first cycle of chemotherapy predicted overall survival (HR=5.7, p=0.004) (32). All of the above findings suggest that the CTC count has important value in lung cancer predictions. In this study, we demonstrated a significant correlation between CTC levels and T stage. Patients with a high T stage had higher FR^+-CTC count after treatment

TABLE 4A Survival probability according to the FR$^+$-CTC count, LC and dNLR between surgery and systemic therapy.

		Median (months)	*p*
FR$^+$-CTC(FU/3ml) <9.75 vs. ≥9.75	surgery	NR	0.046
	systemic therapy	23.53vs.12.03	0.003
LC(x10^9/L) <1.72 vs.≥1.72	surgery	NR	0.480
	systemic therapy	14.8vs. NR	0.029
dNLR <2.46 vs.≥2.46	surgery	NR	0.097
	systemic therapy	23.53vs.8.033	<0.001

TABLE 4B Survival probability according to the FR+-CTC count, LC and dNLR between NSCLC and SCLC.

		Median (months)	*p*
FR$^+$-CTC(FU/3ml) <9.75 vs. ≥9.75	NSCLC	NRvs.20.1	0.014
	SCLC	8.033vs.5.067	0.569
LC(x10^9/L) <1.72 vs.≥1.72	NSCLC	20.1vs.NR	0.029
	SCLC	6.133vs.-	–
dNLR <2.46 vs.≥2.46	NSCLC	NRvs.13.9	<0.001
	SCLC	6.467vs.6.133	0.338

than those with a low T stage, indicating that similar to T stage, CTC levels may negatively affect patient survival. In addition, since patients with early-stage lung cancer received surgical treatment, while patients with advanced lung cancer received systemic treatment, patients treated with surgery had significantly lower CTCs than patients treated with systemic treatment.

Early recurrence in patients with resectable NSCLC ranges from 10-19% (33, 34). Although imaging tests have been used as the standard for tumor response assessment, they can only be used to detect space-occupying lesions and not minimal residual disease. A study of 26 early-stage lung cancer patients showed that after standard surgical treatment, the descending slope and daily decline in CTCs in recurrent lung cancer patients were lower than those in nonrecurring patients (35). We found that patients with systemic treatment and high FR$^+$-CTC values had the fastest decline in the survival curve and the worst prognosis. In addition, we also found that within 22 months after treatment, the mortality rate of patients with early-stage lung cancer with high postoperative FR$^+$-CTC was even higher than that of patients with advanced lung cancer with low FR$^+$-CTC. The survival curves of the low LC group and high dNLR group of advanced lung cancer decreased rapidly, and the prognosis was poor. Among the patients with a higher dNLR after systemic treatment, the last patient developed progression by the end of follow-up, and PFS was 20.1 months. This finding suggests that patients with higher FR$^+$-CTC count after treatment may have occult metastases and that systemic therapy is necessary for better disease control.

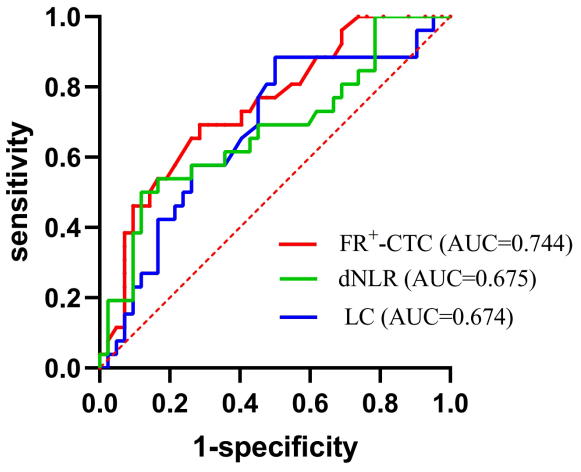

FIGURE 3
ROC curves of the FR$^+$-CTC count, dNLR, and LC in the diagnosis of lung cancer recurrence.

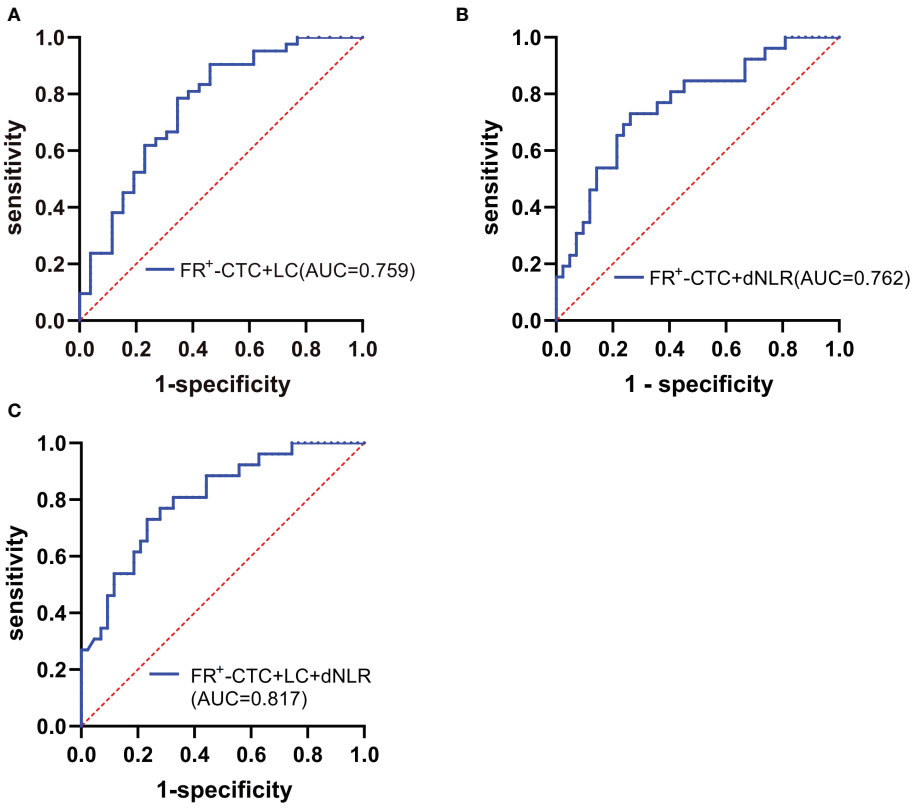

FIGURE 4
(A) ROC curve of the FR$^+$-CTC count plus LC in the diagnosis of lung cancer recurrence. **(B)** ROC curve of the FR$^+$-CTC count plus dNLR in the diagnosis of lung cancer recurrence. **(C)** ROC curve of the FR$^+$-CTC count combined with the LC and dNLR in the diagnosis of lung cancer recurrence.

Investigators have previously reported that the FR$^+$-CTC count can be used to diagnose stage I LUAD and LUSC patients with sensitivities of 66.7% and 69.2%, respectively (25). A recent study showed that in SCLC patients, a lower lymphocyte count was associated with worse overall survival (17.4 vs. 15.7 months, p=0.029) (36). A study of 211 patients who received first-line pembrolizumab treatment demonstrated that a dNLR < 2.6 significantly prolonged patients' mPFS (10.4 vs. 3.4 months, p< 0.001) (37). To investigate the diagnostic value of the FR$^+$-CTC count, dNLR, LC, PLR and NLR in recurrence, we performed ROC curve analysis of individual and combined indicators. We found that the FR$^+$-CTC count, dNLR and LC could be used as indicators for diagnosing lung cancer recurrence. In addition, when the FR$^+$-CTC count was combined with the dNLR and/or LC, it had a larger AUC than the indicators alone. This demonstrates that the combination of the FR$^+$-CTC count and dNLR and/or LC can improve the diagnosis rate at the time of recurrence of lung cancer.

Our study supports the evidence proposed by Chen et al. (38). This is the first study to use the FR$^+$-CTC count combined with the dNLR and/or LC to diagnose relapse rates after first-line therapy for lung cancer.

There are several limitations in this study. The research data were mainly entered manually, although no clinicopathological, hematological or survival data were missing. In addition, we established a cutoff value for the FR$^+$-CTC count based on our previous results rather than using a positive/negative threshold for the FR$^+$-CTC count (8.7 FU/3 mL positive) (39). However, this count was verified as appropriate for diagnosing patients who relapsed during treatment. Furthermore, because the FR$^+$-CTC examination was not included in the routine examination of lung cancer patients, the number of SCLC patients included in this study was relatively small, and most of them had high FR$^+$-CTC counts. The impact

TABLE 5 The diagnostic efficiency of models in patients with lung cancer.

Diagnostic Group	AUC	95% CI	Sensitivity (%)	Specificity (%)	*p*
FR$^+$-CTC	0.744	0.625-0.863	69.2	71.4	0.001
LC	0.674	0.540-0.807	50.0	88.5	0.017
dNLR	0.675	0.540-0.811	50.0	88.1	0.016
FR$^+$-CTC + LC	0.759	0.638-0.881	53.8	90.5	<0.001
FR$^+$-CTC + dNLR	0.762	0.645-0.879	73.1	73.8	<0.001
FR$^+$-CTC + LC +dNLR	0.817	0.715-0.919	73.1	78.6	<0.001

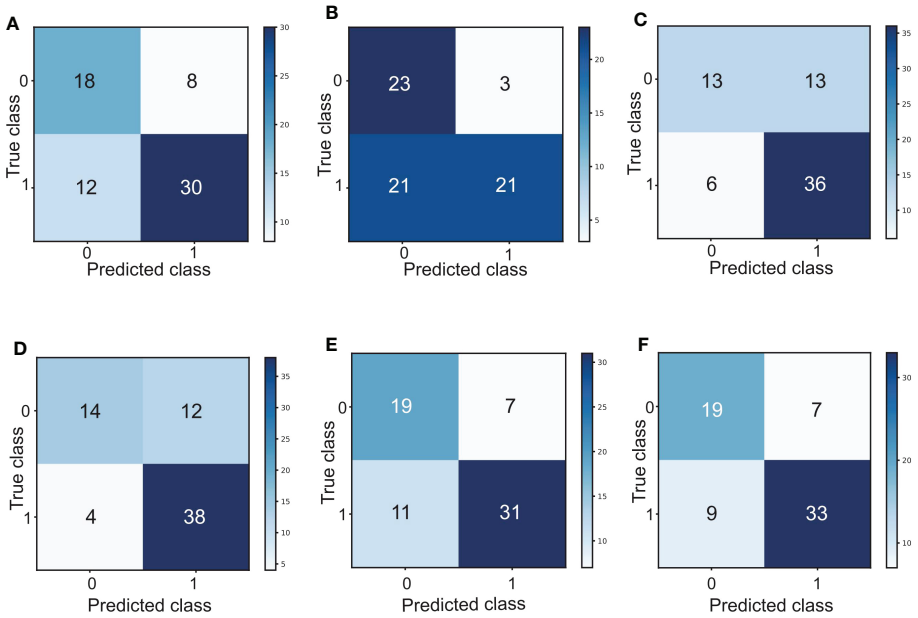

FIGURE 5
(A) Confusion matrix for predicting lung cancer relapse in patients based on the FR^+-CTC count. **(B)** Confusion matrix for predicting lung cancer relapse in patients based on the LC. **(C)** Confusion matrix for predicting lung cancer relapse in patients based on the dNLR. **(D)** Confusion matrix of the FR^+-CTC count combined with the LC to predict lung cancer relapse in patients. **(E)** Confusion matrix of the FR^+-CTC count combined with the dNLR to predict lung cancer relapse in patients. **(F)** Confusion matrix of the FR^+-CTC count combined with the LC and dNLR to predict lung cancer relapse in patients. 0: relapse; 1: no relapse.

of FR^+-CTC count on the survival rate of SCLC patients may not have been fully analyzed. However, SCLC patients with a higher FR^+-CTC count had a faster decline in the survival curve and a lower survival rate, which is also consistent with clinical significance.

In conclusion, the FR^+-CTC count, dNLR and LC are useful biomarkers. A high posttreatment FR^+-CTC count, dNLR and LC are indicators that predict whether a patient will progress, and the combined indicators had a better prediction effect. In addition, a higher FR^+-CTC count was significantly associated with shorter patient survival.

Data availability statement

The raw data supporting the conclusions of this article will bemade available by emailing corresponding authors.

Ethics statement

The studies involving human participants were reviewed and approved by Ethics Committee of the First Affiliated Hospital of Zhengzhou University. Written informed consent for participation was not required for this study in accordance with the national legislation and the institutional requirements.

Author contributions

HW was responsible for conceptualization, methodology, software, formal analysis, original draft preparation, review and editing; LL was responsible for validation, formal analysis, review and editing; JY and WM were responsible for supervision; YD was responsible for formal analysis, resources, investigation, supervision, review and editing; TZ was responsible for formal analysis, data curation, review and editing, supervision, project administration and funding acquisition. All authors contributed to the article and approved the submitted version.

Funding

This research was funded by the Natural Science Foundation of Henan Province (Grant No. 212300410398) and the National Key Research and Development Program of China (2021YFC2501005).

Acknowledgments

The authors would like to thank all study patients and their family members.

Conflict of interest

The authors declare that the research was conducted in the absence of any commercial or financial relationships that could be construed as a potential conflict of interest.

Publisher's note

Supplementary material

The Supplementary Material for this article can be found online at: https://www.frontiersin.org/articles/10.3389/fonc.2022.1097816/full#supplementary-material

SUPPLEMENTARY FIGURE 1
Kaplan–Meier curves for survival probability according to the NLR between surgery and systemic therapy.

SUPPLEMENTARY FIGURE 2
ROC curves of the NE count, PLT count, NLR and PLR in the diagnosis of lung cancer recurrence.

References

1. Siegel RL, Miller KD, Fuchs HE, Jemal A. Cancer statistics, 2022. *CA: Cancer J Clin* (2022) 72(1):7–33. doi: 10.3322/caac.21708

2. van Meerbeeck JP, Fennell DA, De Ruysscher DK. Small-cell lung cancer. *Lancet (London England)* (2011) 378(9804):1741–55. doi: 10.1016/s0140-6736(11)60165-7

3. Aberle DR, Adams AM, Berg CD, Black WC, Clapp JD, Fagerstrom RM, et al. Reduced lung-cancer mortality with low-dose computed tomographic screening. *New Engl J Med* (2011) 365(5):395–409. doi: 10.1056/NEJMoa1102873

4. Vasseur A, Kiavue N, Bidard FC, Pierga JY, Cabel L. Clinical utility of circulating tumor cells: An update. *Mol Oncol* (2021) 15(6):1647–66. doi: 10.1002/1878-0261.12869

5. Jiang T, Zhao J, Zhao C, Li X, Shen J, Zhou J, et al. Dynamic monitoring and predictive value of circulating tumor cells in egfr-mutated advanced non-Small-Cell lung cancer patients treated with first-line egfr tyrosine kinase inhibitors. *Clin Lung Cancer* (2019) 20(2):124–33.e2. doi: 10.1016/j.cllc.2018.11.014

6. Qian H, Zhang Y, Xu J, He J, Gao W. Progress and application of circulating tumor cells in non-small cell lung cancer. *Mol Ther oncolytics* (2021) 22:72–84. doi: 10.1016/j.omto.2021.05.005

7. Abdallah EA, Braun AC, Flores B, Senda L, Urvanegia AC, Calsavara V, et al. The potential clinical implications of circulating tumor cells and circulating tumor microemboli in gastric cancer. *oncologist* (2019) 24(9):e854–e63. doi: 10.1634/theoncologist.2018-0741

8. Wu Q, Zheng H, Gu J, Cheng Y, Qiao B, Wang J, et al. Detection of folate receptor-positive circulating tumor cells as a biomarker for diagnosis, prognostication, and therapeutic monitoring in breast cancer. *J Clin Lab Anal* (2022) 36(1):e24180. doi: 10.1002/jcla.24180

9. Brozos-Vázquez EM, Díaz-Peña R, García-González J, León-Mateos L, Mondelo-Macía P, Peña-Chilet M, et al. Immunotherapy in nonsmall-cell lung cancer: Current status and future prospects for liquid biopsy. *Cancer immunology immunotherapy CII* (2021) 70(5):1177–88. doi: 10.1007/s00262-020-02752-z

10. O'Shannessy DJ, Yu G, Smale R, Fu YS, Singhal S, Thiel RP, et al. Folate receptor alpha expression in lung cancer: Diagnostic and prognostic significance. *Oncotarget* (2012) 3(4):414–25. doi: 10.18632/oncotarget.489

11. Toffoli G, Russo A, Gallo A, Cernigoi C, Miotti S, Sorio R, et al. Expression of folate binding protein as a prognostic factor for response to platinum-containing chemotherapy and survival in human ovarian cancer. *Int J Cancer* (1998) 79(2):121–6.

12. Iwakiri S, Sonobe M, Nagai S, Hirata T, Wada H, Miyahara R. Expression status of folate receptor alpha is significantly correlated with prognosis in non-Small-Cell lung cancers. *Ann Surg Oncol* (2008) 15(3):889–99. doi: 10.1245/s10434-007-9755-3

13. Li W, Tan G, Ma Y, Li H, He G. Inhibition of α folate receptor resulting in a reversal of taxol resistance in nasopharyngeal carcinoma. *Otolaryngology–head Neck Surg Off J Am Acad Otolaryngology-Head Neck Surg* (2012) 146(2):250–8. doi: 10.1177/0194599811426260

14. He W, Wang H, Hartmann LC, Cheng JX, Low PS. *In vivo* quantitation of rare circulating tumor cells by multiphoton intravital flow cytometry. *Proc Natl Acad Sci United States America* (2007) 104(28):11760–5. doi: 10.1073/pnas.0703875104

15. Shen J, Zhao J, Jiang T, Li X, Zhao C, Su C, et al. Predictive and prognostic value of folate receptor-positive circulating tumor cells in small cell lung cancer patients treated with first-line chemotherapy. *Oncotarget* (2017) 8(30):49044–52. doi: 10.18632/oncotarget.17039

16. Diakos CI, Charles KA, McMillan DC, Clarke SJ. Cancer-related inflammation and treatment effectiveness. *Lancet Oncol* (2014) 15(11):e493–503. doi: 10.1016/s1470-2045(14)70263-3

17. Yuan A, Hsiao YJ, Chen HY, Chen HW, Ho CC, Chen YY, et al. Opposite effects of M1 and M2 macrophage subtypes on lung cancer progression. *Sci Rep* (2015) 5:14273. doi: 10.1038/srep14273

18. Gabrilovich DI, Ostrand-Rosenberg S, Bronte V. Coordinated regulation of myeloid cells by tumours. *Nat Rev Immunol* (2012) 12(4):253–68. doi: 10.1038/nri3175

19. Matiello J, Dal Pra A, Zardo L, Silva R, Berton DC. Impacts of post-radiotherapy lymphocyte count on progression-free and overall survival in patients with stage iii lung cancer. *Thorac Cancer* (2020) 11(11):3139–44. doi: 10.1111/1759-7714.13621

20. Stone RL, Nick AM, McNeish IA, Balkwill F, Han HD, Bottsford-Miller J, et al. Paraneoplastic thrombocytosis in ovarian cancer. *New Engl J Med* (2012) 366(7):610–8. doi: 10.1056/NEJMoa1110352

21. Valero C, Lee M, Hoen D, Weiss K, Kelly DW, Adusumilli PS, et al. Pretreatment neutrophil-to-Lymphocyte ratio and mutational burden as biomarkers of tumor response to immune checkpoint inhibitors. *Nat Commun* (2021) 12(1):729. doi: 10.1038/s41467-021-20935-9

22. Templeton AJ, Ace O, McNamara MG, Al-Mubarak M, Vera-Badillo FE, Hermanns T, et al. Prognostic role of platelet to lymphocyte ratio in solid tumors: A systematic review and meta-analysis. *Cancer epidemiology Biomarkers Prev Publ Am Assoc Cancer Research cosponsored by Am Soc Prev Oncol* (2014) 23(7):1204–12. doi: 10.1158/1055-9965.Epi-14-0146

23. Takada K, Takamori S, Yoneshima Y, Tanaka K, Okamoto I, Shimokawa M, et al. Serum markers associated with treatment response and survival in non-small cell lung cancer patients treated with anti-Pd-1 therapy. *Lung Cancer (Amsterdam Netherlands)* (2020) 145:18–26. doi: 10.1016/j.lungcan.2020.04.034

24. Kazandjian D, Gong Y, Keegan P, Pazdur R, Blumenthal GM. Prognostic value of the lung immune prognostic index for patients treated for metastatic non-small cell lung cancer. *JAMA Oncol* (2019) 5(10):1481–5. doi: 10.1001/jamaoncol.2019.1747

25. Yu Y, Chen Z, Dong J, Wei P, Hu R, Zhou C, et al. Folate receptor-positive circulating tumor cells as a novel diagnostic biomarker in non-small cell lung cancer. *Trans Oncol* (2013) 6(6):697–702. doi: 10.1593/tlo.13535

26. Li XY, Dong M, Zang XY, Li MY, Zhou JY, Ma JJ, et al. The emerging role of circulating tumor cells in cancer management. *Am J Trans Res* (2020) 12(2):332–42.

27. Hong B, Zu Y. Detecting circulating tumor cells: Current challenges and new trends. *Theranostics* (2013) 3(6):377–94. doi: 10.7150/thno.5195

28. Khoja L, Lorigan P, Zhou C, Lancashire M, Booth J, Cummings J, et al. Biomarker utility of circulating tumor cells in metastatic cutaneous melanoma. *J Invest Dermatol* (2013) 133(6):1582–90. doi: 10.1038/jid.2012.468

29. Cohen SJ, Punt CJ, Iannotti N, Saidman BH, Sabbath KD, Gabrail NY, et al. Relationship of circulating tumor cells to tumor response, progression-free survival, and overall survival in patients with metastatic colorectal cancer. *J Clin Oncol Off J Am Soc Clin Oncol* (2008) 26(19):3213–21. doi: 10.1200/jco.2007.15.8923

30. Matsusaka S, Chìn K, Ogura M, Suenaga M, Shinozaki E, Mishima Y, et al. Circulating tumor cells as a surrogate marker for determining response to chemotherapy in patients with advanced gastric cancer. *Cancer Sci* (2010) 101(4):1067–71. doi: 10.1111/j.1349-7006.2010.01492.x

31. Scher HI, Jia X, de Bono JS, Fleisher M, Pienta KJ, Raghavan D, et al. Circulating tumour cells as prognostic markers in progressive, castration-resistant prostate cancer: A reanalysis of Immc38 trial data. *Lancet Oncol* (2009) 10(3):233–9. doi: 10.1016/s1470-2045(08)70340-1

32. Hiltermann TJN, Pore MM, van den Berg A, Timens W, Boezen HM, Liesker JJW, et al. Circulating tumor cells in small-cell lung cancer: A predictive and prognostic factor. *Ann Oncol Off J Eur Soc Med Oncol* (2012) 23(11):2937–42. doi: 10.1093/annonc/mds138

33. Wu CY, Fu JY, Wu CF, Hsieh MJ, Liu YH, Wu YC, et al. Survival prediction model using clinico-pathologic characteristics for nonsmall cell lung cancer patients after curative resection. *Medicine* (2015) 94(45):e2013. doi: 10.1097/md.0000000000002013

34. Thornblade LW, Mulligan MS, Odem-Davis K, Hwang B, Waworuntu RL, Wolff EM, et al. Challenges in predicting recurrence after resection of node-negative non-small cell lung cancer. *Ann Thorac Surg* (2018) 106(5):1460–7. doi: 10.1016/j.athoracsur.2018.06.022

35. Wu CY, Lee CL, Wu CF, Fu JY, Yang CT, Wen CT, et al. Circulating tumor cells as a tool of minimal residual disease can predict lung cancer recurrence: A longitudinal, prospective trial. *Diagnostics (Basel Switzerland)* (2020) 10(3):144. doi: 10.3390/diagnostics10030144

36. Suzuki R, Wei X, Allen PK, Cox JD, Komaki R, Lin SH. Prognostic significance of total lymphocyte count, neutrophil-to-Lymphocyte ratio, and platelet-to-Lymphocyte ratio in limited-stage small-cell lung cancer. *Clin Lung Cancer* (2019) 20(2):117–23. doi: 10.1016/j.cllc.2018.11.013

37. Alessi JV, Ricciuti B, Alden SL, Bertram AA, Lin JJ, Sakhi M, et al. Low peripheral blood derived neutrophil-to-Lymphocyte ratio (Dnlr) is associated with increased tumor T-cell infiltration and favorable outcomes to first-line pembrolizumab in non-small cell lung cancer. *J immunotherapy Cancer* (2021) 9(11):e003536. doi: 10.1136/jitc-2021-003536

38. Chen X, Zhou F, Li X, Yang G, Zhang L, Ren S, et al. Folate receptor-positive circulating tumor cell detected by Lt-Pcr-Based method as a diagnostic biomarker for non-Small-Cell lung cancer. *J Thorac Oncol Off Publ Int Assoc Study Lung Cancer* (2015) 10(8):1163–71. doi: 10.1097/jto.0000000000000606

39. Wang L, Wu C, Qiao L, Yu W, Guo Q, Zhao M, et al. Clinical significance of folate receptor-positive circulating tumor cells detected by ligand-targeted polymerase chain reaction in lung cancer. *J Cancer* (2017) 8(1):104–10. doi: 10.7150/jca.16856

frontiers | Frontiers in Oncology

TYPE Mini Review
PUBLISHED 04 April 2023
DOI 10.3389/fonc.2023.1103797

OPEN ACCESS

EDITED BY
Zohreh Amoozgar,
Massachusetts General Hospital and
Harvard Medical School, United States

REVIEWED BY
Monika Ulamec,
University of Zagreb, Croatia
Mingzhi Ye,
Beijing Genomics Institute (BGI), China

*CORRESPONDENCE
Warwick J. Locke
warwick.locke@csiro.au
Kim Y. C. Fung
kim.fung@csiro.au

†These authors have contributed equally to this work

SPECIALTY SECTION
This article was submitted to Molecular and Cellular Oncology, a section of the journal Frontiers in Oncology

RECEIVED 21 November 2022
ACCEPTED 23 March 2023
PUBLISHED 04 April 2023

CITATION
Johnston AD, Ross JP, Ma C, Fung KYC and Locke WJ (2023) Epigenetic liquid biopsies for minimal residual disease, what's around the corner?
Front. Oncol. 13:1103797.
doi: 10.3389/fonc.2023.1103797

Epigenetic liquid biopsies for minimal residual disease, what's around the corner?

Andrew D. Johnston, Jason P. Ross, Chenkai Ma, Kim Y. C. Fung*† and Warwick J. Locke*†

Human Health, Health and Biosecurity, CSIRO, Westmead, NSW, Australia

Liquid biopsy assays for minimal residual disease (MRD) are used to monitor and inform oncological treatment and predict the risk of relapse in cancer patients. To-date, most MRD assay development has focused on targeting somatic mutations. However, epigenetic changes are more frequent and universal than genetic alterations in cancer and circulating tumor DNA (ctDNA) retains much of these changes. Here, we review the epigenetic signals that can be used to detect MRD, including DNA methylation alterations and fragmentation patterns that differentiate ctDNA from noncancerous circulating cell-free DNA (ccfDNA). We then summarize the current state of MRD monitoring; highlight the advantages of epigenetics over genetics-based approaches; and discuss the emerging paradigm of assaying both genetic and epigenetic targets to monitor treatment response, detect disease recurrence, and inform adjuvant therapy.

KEYWORDS

MRD, epigenetics, liquid biopsy, ccfDNA (circulating cell-freeDNA), cancer, ctDNA (circulating tumor DNA), DNA methylation, fragmentomics

1 Introduction

Minimal residual disease (MRD) refers to a small number of cancer cells remaining in a patient's body after oncological treatment with curative intent. MRD does not cause clinical symptoms and is not detectable by traditional methods such as imaging (e.g., CT, MRI, PET, ultrasound, X-ray, etc.) or abnormal blood serum protein levels. MRD assays must be sensitive enough to detect as little as 1 cancerous cell in a background of 1 million noncancerous cells. This extreme sensitivity makes MRD assay development complex, but overcoming this barrier imbues MRD assays with the potential for much earlier detection of cancer recurrence than traditional methods, and thus earlier intervention with adjuvant chemotherapy or second and third-line treatments.

Detection of MRD indicates the failure of treatment to eliminate all cancerous cells which implies greater probability of future disease recurrence. Monitoring MRD signals during the remission period allows early detection of disease progression (1). Assaying for MRD, therefore, offers a means to monitor, predict, and detect cancer recurrence, as well as stratify patients for adjuvant therapy and predict their response to treatment (Figures 1A-

C) (2, 3). However, with the lack of a solid tumor to sample, traditional biopsy methods cannot be applied to MRD assays. Instead, MRD detection must make use of circulating tumor-derived entities such as circulating tumor cells (CTCs), extracellular vesicles, and circulating tumor DNA (ctDNA). These circulating molecules and cells shed by tumors are a rich source of information on cancer biology, featuring much of the genetic and epigenetic abnormalities that drive tumorigenesis and treatment response (Figure 1D) (4, 5). Such assays can be used to match patients to effective treatments by detecting clinically actionable variations (e.g., drug resistance) within the detected cancer cells and their molecular products, thus avoiding invasive procedures and the morbidities of ineffectual therapies. These novel diagnostic assays have utility in predicting both MRD and cancer recurrence. A positive MRD test after surgery can inform the decision for: (i) further surgery with curative intent; (ii) adjuvant chemotherapy; and/or (iii) increased surveillance, including imaging such as an FGD-PET scan. Whereas positive recurrence indicated by a quantitatively increasing signal over time can inform the decision for: (i) increased surveillance; and (ii) a switch to secondary/tertiary therapy based on the clonal evolution of the tumor burden, as determined by the assayed biomarkers being tracked (i.e., somatic mutations).

2 Epigenetics in oncology

2.1 DNA methylation

DNA methylation is a covalent modification of the DNA strand that, in mammals, occurs almost exclusively within the sequence context of cytosine followed by guanosine (CpG) dinucleotides. The genomic acquisition of DNA methylation is an essential developmental process with diverse roles including repressive associations at gene promoters and mobile genetic elements or, conversely, increased transcriptional activity when found within gene bodies [reviewed in Greenberg & Bourc'his (6)]. Genome wide deregulation of DNA methylation is a universal feature of cancer development, typified by global loss of methylation (particularly in repetitive sequences) (7) and localized foci of hypermethylation (8). While genetic alterations have proved useful in liquid biopsy and cancer management (including early cancer detection, prognosis, monitoring therapeutic response and detecting MRD), epigenetic alterations occur more frequently in cancer development and are typically more universal across tumors than specific somatic mutations (9–13). Aberrant DNA methylation is an early event in carcinogenesis that can both drive and be driven by tumor biology/treatments, is associated with a diverse range of biological impact, and can be targeted by liquid biopsies to detect specific cancers (Figure 1E) (14). Moreover, DNA methylation profiling in cancer has demonstrated an epigenetic role in hormone receptor signaling and response to endocrine therapy (15), prognosis (16, 17), metastasis (18), response to chemotherapy (19), and key aspects of tumor biology (20).

Most DNA methylation-based liquid biopsies target cancer-specific aberrations that separate cancer from its normal tissue counterpart. However, within healthy tissues DNA methylation exhibits highly cell type specific patterns across the genome (21). This untapped layer of epigenomic information provides a unique signature that can be targeted without the need for detectable cancer-specific aberrations. Despite the significant alteration of the epigenome during carcinogenesis, the underlying tissue-specific methylation patterns linked to cellular identity are still detectable (22). Applications of this approach have focused on the identification of tumor type, particularly in cases of cancer of unknown primary (23). However, the presence of circulating cell-free DNA (ccfDNA) originating from a source other than haemopoietic cells, blood vessel endothelial cells, or liver hepatocytes is exceeding rare in healthy individuals and thus indicative of pathology on its own (21, 24). Therefore, tissue-specific biomarkers could potentially be used in MRD assays to detect signals that span molecular subtypes of tumors that share a tissue of origin. Importantly, these targets are also unlikely to diminish due to tumor adaptation in response to treatment. To this point, recent academic research has begun to focus on exploiting tissue specificity along with ccfDNA originating outside the cancer. The process of cancer growth is highly disruptive to the organ/tissue in which it occurs. This results in elevated levels of cell death in the surrounding "healthy" tissues due to increased stresses causing inflammation and/or deformation of normal tissue structures (25–27). Further development of these methods is required before clinical application extends beyond the research domain; however, such novel approaches show significant promise in the management of advanced/recurrent disease.

2.2 Fragmentomics

The term "fragmentomics" describes the study of ccfDNA fragmentation patterns and the use of these patterns to decern biologically relevant information such as nucleosome positioning. Although few assays to-date utilize ccfDNA fragmentation patterns, numerous properties of ctDNA compared to healthy ccfDNA instill fragmentomics with the potential for use in oncological assays (Figure 1F). These properties include: (i) region-specific differences in ctDNA fragments lengths (28); (ii) shorter ctDNA fragment length distributions (29); (iii) fragment end sequence alterations in ctDNA (30); and (iv) altered nucleosome positioning in cancer (31). The most notable applications of fragmentomics so far reside around ctDNA fragment lengths. Mouliere et al. (29) demonstrated that selecting shorter ccfDNA fragments (between 90–150) greatly enriches for ctDNA and improves detection of clinically actionable mutations and copy number alterations. This enrichment technique should be a key consideration in MRD design going forward, given the extreme sensitivity required by assays to detect MRD. Beyond enrichment, Cristiano et al. (28) accurately discriminated 215 healthy individuals from 208 cancer patients (AUC = 0.94) using a machine learning model trained on ccfDNA fragment size and coverage across the genome, thus demonstrating the potential for region-specific ctDNA fragment lengths to be used as cancer biomarkers. Delfi Diagnostics is currently pursuing commercialization of this

10.3389/fonc.2023.1103797

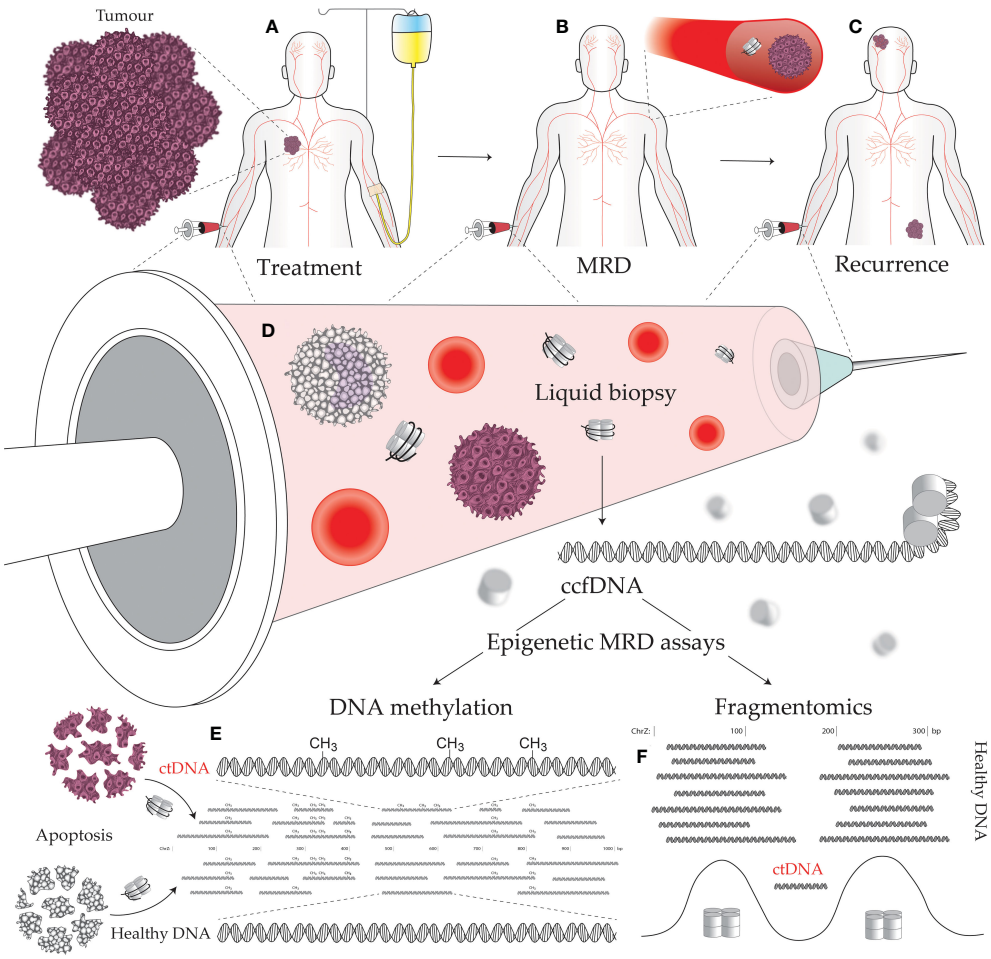

FIGURE 1
Minimal residual disease (MRD) epigenetic assays and their use across a cancer patient journey. **(A)** Establishing the molecular targets for MRD assays can be performed prior to treatment initiation. A decline in the level of the assayed biomarker suggests efficacious treatment and reduced tumor burden. **(B)** The continued presence of a tumor biomarker after curative intent treatment, accompanied by no visible signs of a tumor, indicates the presence of MRD. **(C)** Tracking with an MRD assay over time is useful for early detection of cancer recurrence, as the level of the assayed biomarker will increase as a tumor remerges. **(D)** Liquid biopsies can be performed on a variety of bodily fluids including blood, urine, saliva, lymph, and cerebrospinal fluid. Circulating tumor DNA (ctDNA) contains epigenetic alterations that can separate it from the cancer's normal tissue counterpart and circulating cell-free DNA (ccfDNA) derived from noncancerous sources. Cancer-specific epigenetic alterations include: **(E)** aberrant DNA methylation, and **(F)** altered fragmentomic signals (i.e., changes in ctDNA fragment lengths, end sequences, and nucleosome-associated genomic positioning).

technology with a focus on lung cancer and is in the process of recruiting 15,000 individuals for their CASCADE-LUNG clinical validation study.

As for nucleosome positioning, ccfDNA fragmentation patterns downstream of transcription start sites have been shown to reflect differential nucleosome positioning between expressed and unexpressed genes (32). These ccfDNA read depth coverage patterns match with gene expression signatures of hematopoietic cells (33). Similarly, ccfDNA-derived nucleosome spacing footprints around DNase I hypersensitive sites (e.g., occupied transcription factor binding sites) match most strongly with hematopoietic cell lines (31). These results are consistent with ccfDNA methylation analyses, which show that ccfDNA from healthy donors originates from white blood cells (55%), erythrocyte progenitors (30%), vascular endothelial cells (10%) and liver hepatocytes (1%) (21). In cancer, high levels of ctDNA can create a nucleosome footprint that diverges from these healthy sources and instead corresponds to a cancer's tissue of origin. For example, ccfDNA-derived nucleosome spacing has been used to infer the tissues of origin of late-stage tumors (31) and ccfDNA coverage patterns have been used to accurately classify expression levels of genes with somatic copy number gains in metastatic cancer patients (33). These findings demonstrate the potential for ctDNA fragmentation signatures to be used as cancer biomarkers. Moreover, nucleosome positioning is cell-type specific (34, 35), and nucleosome linker DNA lengths are up to 7 base pairs shorter in transcriptionally active chromatin versus inactive genes/compartments (31, 36). We envisage regions of the genome that are active in noncancerous ccfDNA contributing tissues and inactive in a tumor's tissue of origin, and vice versa. Such regions should possess a subset of nucleosome positions that are out-of-phase between these two sources due to differences in nucleosome spacing, thus producing a subpopulation of ctDNA fragments positioned at the breakpoints of "healthy" ccfDNA. In which case,

future MRD assays could potentially exploit tissue-specific nucleosome positioning to identify an underlying cancer signal at low ctDNA concentrations.

Going forward, the most sensitive and universal MRD assays will likely combine these epigenomic approaches. Until recently, the combination of DNA methylation and fragmentomics in a single assay was not possible due DNA methylation detection relying on bisulfite conversion (37). Bisulfite conversion causes DNA damage that erodes the fragmentomic signals embedded within ccfDNA fragments. However, the recent advent of enzymatic methylation conversion technology allows highly accurate methylation detection to be performed without this damage and the resulting loss of fragmentomic signals (38). Therefore, it is now possible to use next-generation methylation sequencing to detect both DNA methylation and fragmentomic biomarkers. At the very least, this means ctDNA sized-based enrichment can now be used to improve the detection sensitivity of DNA methylation-based MRD assays. However, enzymatic conversion also means differentially methylated regions, region-specific fragment length changes, and nucleosome positioning biomarkers can now all be incorporated into a single hybridization capture-seq panel.

3 MRD assays: Products on-market, clinical trials, and emerging technologies

The marketplace for MRD liquid biopsy assays is new, but several MRD diagnostic tests have now received early regulatory approvals (Table 1). In 2021, the Natera Signatera test for MRD was granted Breakthrough Device Designation (BDD) status by the FDA for an intended use in Stage I-IV colorectal cancer. This approach uses whole-exome sequencing of primary tumors along with matched normal blood samples to prepare bespoke personalized multiplex PCR assays. In total, 16 patient-specific somatic variants are selected to track using next-generation sequencing (NGS) (39, 40). The Inivata RaDaR test for residual disease and recurrence has received a Conformité Européenne (CE) mark for use in Europe and was granted FDA BDD status in 2021 (41, 42). Again, exome-sequencing informs the design of a secondary somatic mutation PCR panel and tracks up to 48 mutations in blood using NGS. These two-staged approaches are stated by their respective companies to take between 2 and 4 weeks for assay design and up to 1 week turnaround on subsequent blood draws. Finally, the FoundationOne Tracker test was awarded BDD status in 2022 and combines Foundation Medicine's patient-specific NGS tumor profiling with the multiplex PCR design of Natera (43). This test is used to detect and track MRD, assess a patient's response to therapy, and monitor for relapse following curative intent therapy.

While there are only a few somatic mutation-based MRD panels in the marketplace, there are a host currently in development and undergoing clinic trials. For example, Strata Oncology are also exploring a two-staged tumor-informed panel design in their Sentinel trial for cancer recurrence (44). Burning Rock Biotech has developed brPROPHET, a personalized capture panel-based approach for MRD detection and are currently working with BeiGene to progress this assay to clinical studies (45). Foresight Diagnostics (46) claims that Phased Variant Enrichment & Detection Sequencing (PhasED-seq), where two or more mutations occur on the same strand of DNA, offers more sensitivity for MRD. The company intends to develop a CLIA validated assay and market the assay as a lab-development test (LDT). Exact Sciences is running the 750 patient CORRECT-MRD II study to validate their MRD and recurrence test for stage II and III colorectal cancer. This is based on the Target Digital Sequencing (TARDIS) approach that Exact Sciences licensed from The Translational Genomics Research Institute (47).

Notably, genetic mutations are not broadly shared across cancers and the two-stage solutions to this shortcoming are limited by tumor heterogeneity and the volume of a tissue biopsy. That is, because only a subset of a tumor is sequenced there is still a high probability that mutations will be missed. However, a multi-omics approach can augment this shortcoming. The greater frequency and universality of epigenetic changes makes them more sensitive and universal markers for evidence of cancer after curative intent treatment, and somatic mutation testing highlights actionable variants that can inform subsequent treatment. This promise of MRD assays that incorporate epigenetics with somatic mutation testing is being realized. Guardant Health has combined somatic mutations, DNA methylation and fragmentomics into their LUNAR panel, which they have progressed into clinical trials for both primary detection and MRD of early-stage colorectal cancer (48).

Multiple companies are also progressing purely epigenetic-based MRD panel approaches. MethylGene is undertaking a clinical trial on multiple myeloma patients that will utilize DNA methylation sequencing of ctDNA for MRD detection (49). While GRAIL has concentrated on bringing the DNA methylation-based Galleri test to market for early detection of cancer, in 2021 the company also formed a deal with Amgen, AstraZeneca, and Bristol Myers Squibb to evaluate its technology for the detection of MRD and early recurrences (50). This expansion of use case by GRAIL points to the versatility of ultra-sensitive liquid biopsy assays. Fast turnaround and inexpensive serial epigenetic tests can identity MRD and recurrence early. A positive result provides the evidence to undertake imaging and to order large NGS panels to study clonal evolution of the tumor and indicate modes of treatment.

While most product development for MRD is concentrated around sequencing large panels of markers, simple DNA methylation-based PCR tests can also be highly efficacious. Colvera, developed by Clinical Genomics, is available as an LDT in the USA and has Medicare coverage for MRD and recurrence monitoring of colorectal cancer. This methylated ctDNA test detected 66.0% of recurrence, significantly higher than the 31.9% sensitivity of carcinoembryonic antigen (CAE), the current standard of care (51), and also has potential for identifying MRD due to treatment failure (52). Another PCR test is Bladder EpiCheck offered by Nucleix. This multiplex DNA methylation-based PCR assay is for monitoring of tumor recurrence in conjunction with

TABLE 1 Tests for mininmal residual disease currently avaliable or in development.

Test/Company	Technology/method	Clinical Applications	Development Stage/Regulatory Approval	Citations
Signatera Company: Natera	Somatic mutation detection in ctDNA using multiplex-PCR NGS assays Personalised targets from whole-exome sequencing of primary tumors	MRD and recurrence in: - Colorectal cancer (Stage I-IV) - Epithelial ovarian cancer (Stage I-IV)	BDD status (USA)	(39, 40)
RaDaR Company: Inivata	Somatic mutation detection in ctDNA using multiplex-PCR NGS assays Personalised targets from whole-exome sequencing of primary tumors	MRD and recurrence in: - Breast cancer	CE mark (Europe) BDD status (USA)	(41, 42)
FoundationOne Tracker Company: Foundation Medicine	Somatic mutation detection in ctDNA using bespoke multiplex-PCR NGS assays Personalised targets from whole-exome sequencing of primary tumors	MRD, treatment response and recurrence in: - Colorectal cancer - Bladder cancer	BDD status (USA)	(43)
Sentinel Trail Company: Strata Oncology	Somatic mutation detection in ctDNA using bespoke multiplex-PCR NGS assays Personalised targets from whole-exome sequencing of primary tumors	Treatment response and recurrence in: - Stage 1-3 solid tumors	Clinical Trial (NCT05082701)	(44)
brPROPHET Company: Burning Rock Biotech	Somatic mutation detection in ctDNA using bespoke hybridzation capture poanels and NGS. Personalised targets from whole-exome sequencing of primary tumors	MRD and recurrence in: - Colorectal cancer	Ungoing clinical studies	(45)
PhasED-seq Company: Foresight Diagnostics	Detection of phased varients (PVs), where two or more mutations on the same sequenced fragment of ctDNA PV panel assembled from whole-genome sequences of 2,538 tumors	MRD and recurrence in: - B-cell lymphomas	Developing as LDT	(46)
CORRECT-MRD II Company: Exact Sciences	Highly sensitive variaent detection using targeted linear pre-amplification of ccfDNA, UMI ligation, then somatic mutation detection using bespoke multiplex-PCR NGS assays. Personalised targets from whole-genome sequencing of primary tumors.	MRD and recurrence in: - Colorectal cancer (Stage II & III)	Clinical Trial (NCT05210283)	(47)
ECLIPSE Company: Guardant Health	Somatic mutation, DNA methylation and fragmentomic profiling of ccfDNA. 500 kB hybridization capture panel (LUNAR) for cancer detection using NGS.	Early detection, MRD and recurrence in: - Colorectal cancer	Clinical Trial (NCT04136002)	(48)
ctDNA Methylation Sequencing for Myeloma Company: MethylGene Tech	ctDNA methylation sequencing	MRD and recurrence in: - Multiple myeloma	Clinical Trial (NCT05578625)	(49)
Targeted methylation platform Company: GRAIL	ctDNA targeted methylation detection	MRD and recurrence	In development	(50)
Colvera Company: Clinical Genomics	real-time PCR test for detecing DNA methylation of BCAT1 and IKZF1 genes	MRD and recurrence in: - Colorectal cancer	Currently offered as an LDT	(51, 52)
Bladder EpiCheck Company: Nucleix	Multiplex DNA methylation-based PCR assay	Tumor recurrence in: - Bladder cancer	CE mark (Europe)	(53, 54)
ColonAiQ Company: Singlera Genomics	Six-plex methylation PCR test	MRD, treatment response and recurrence in: - Colorectal cancer	Clinical Trial (NCT05444491) Clinical Trial (NCT05536089)	(55)

cystoscopy in patients previously diagnosed with bladder cancer (53, 54). Also in development, Singlera Genomics is recruiting colorectal cancer patients to run clinical trials on their ColonAiQ six-plex methylation PCR test for MRD and cancer recurrence (55).

Interestingly, a simple well-designed PCR test can have adequate diagnostic power when compared to a large NGS panel. This is illustrated when comparing the rates of primary detection of colorectal cancer across the GRAIL-sponsored circulating cell-free genome atlas (CCGA) (27) study (Trial identifiers: NCT02889978 and NCT03085888) and Colvera trial data (56) (Trial identifier: ACTRN12611000318987). Both are large prospective observational studies and both report similar rates of detection across the four cancer stages, despite the GRAIL technology sequencing the entire ccfDNA repertoire and the Clinical Genomics test being only a two-gene PCR assay. This suggests the liquid biopsy detection of cancer, including MRD detection, may be primarily limited by the presence of any ctDNA in the peripheral blood, not the features nor breadth of the detection technology.

4 Conclusion

Liquid biopsy is a powerful, multifaceted, and minimally invasive method for MRD detection and hence for monitoring therapeutic response, disease recurrence, or patient resistance to therapy. Although a relatively new field, liquid biopsy assays are showing promising results when compared to current standards of care. Two-staged somatic mutation approaches, where tumor sequencing informs MRD assay targets, allow clinicians to track actionable mutations and monitor for signs of treatment resistance. However, the time required to establish theses assays does not fit well with the patient journey, as clinicians need to know sooner than 5-6 weeks whether a patient is not responding to treatment. Therefore, epigenetic-based MRD assays are preferable at treatment onset, as epigenetic changes are typically more widespread and likely to be shared among a greater number of cancers than somatic mutations. With the recent advent of enzymatic methylation conversion, targeted sequencing approaches combining DNA methylation, fragmentomics and machine learning will likely come to predominate. However, DNA methylation-based PCR tests currently offer the most cost-effective solution within this niche. In fact, a compelling paradigm may be the combination of inexpensive serial testing with a DNA methylation-based assay, then following a positive MRD/recurrence result with a broad NGS-based somatic mutation panel to identify actionable mutations.

Author contributions

AJ, JR, CM, KF, and WL wrote and revised this review. All authors contributed to the article and approved the submitted version.

Conflict of interest

The authors declare that the research was conducted in the absence of any commercial or financial relationships that could be construed as a potential conflict of interest.

Publisher's note

References

1. Tie J, Wang Y, Tomasetti C, Li L, Springer S, Kinde I, et al. Circulating tumor DNA analysis detects minimal residual disease and predicts recurrence in patients with stage II colon cancer. *Sci Transl Med* (2016) 8(346):346ra92. doi: 10.1126/scitranslmed.aaf6219

2. Tie J, Cohen JD, Wang Y, Christie M, Simons K, Lee M, et al. Circulating tumor DNA analyses as markers of recurrence risk and benefit of adjuvant therapy for stage III colon cancer. *JAMA Oncol* (2019) 5(12):1710–7. doi: 10.1001/jamaoncol.2019.3616

3. IJzerman MJ, de Boer J, Azad A, Degeling K, Geoghegan J, Hewitt C, et al. Towards routine implementation of liquid biopsies in cancer management: it is always too early, until suddenly it is too late. *Diagnostics* (2021) 11(1):103. doi: 10.3390/diagnostics11010103

4. Bettegowda C, Sausen M, Leary RJ, Kinde I, Wang Y, Agrawal N, et al. Detection of circulating tumor DNA in early-and late-stage human malignancies. *Sci Transl Med* (2014) 6(224):224ra24. doi: 10.1126/scitranslmed.3007094

5. Wan J, Massie C, Garcia-Corbacho J, Mouliere F, Brenton JD, Caldas C, et al. Liquid biopsies come of age: towards implementation of circulating tumour DNA. *Nat Rev Cancer* (2017) 17(4):223–38. doi: 10.1038/nrc.2017.7

6. Greenberg MV, Bourc'his D. The diverse roles of DNA methylation in mammalian development and disease. *Nat Rev Mol Cell Biol* (2019) 20(10):590–607. doi: 10.1038/s41580-019-0159-6

7. Ross JP, Rand KN, Molloy PL. Hypomethylation of repeated DNA sequences in cancer. *Epigenomics* (2010) 2(2):245–69. doi: 10.2217/epi.10.2

8. Skvortsova K, Stirzaker C, Taberlay P. The DNA methylation landscape in cancer. *Essays Biochem* (2019) 63(6):797–811. doi: 10.1042/EBC20190037

9. Keller L, Belloum Y, Wikman H, Pantel K. Clinical relevance of blood-based ctDNA analysis: mutation detection and beyond. *Br J Cancer* (2021) 124(2):345–58. doi: 10.1038/s41416-020-01047-5

10. Feinberg AP, Koldobskiy MA, Göndör A. Epigenetic modulators, modifiers and mediators in cancer aetiology and progression. *Nat Rev Genet* (2016) 17(5):284–99. doi: 10.1038/nrg.2016.13

11. Zhang J, Huang K. Pan-cancer analysis of frequent DNA co-methylation patterns reveals consistent epigenetic landscape changes in multiple cancers. *BMC Genom* (2017) 18(1):1–14. doi: 10.1186/s12864-016-3259-0

12. Chang MT, Bhattarai TS, Schram AM, Bielski CM, Donoghue MT, Jonsson P, et al. Accelerating discovery of functional mutant alleles in cancer. *Cancer Discovery* (2018) 8(2):174–83. doi: 10.1158/2159-8290.CD-17-0321

13. Chang MT, Asthana S, Gao SP, Lee BH, Chapman JS, Kandoth C, et al. Identifying recurrent mutations in cancer reveals widespread lineage diversity and mutational specificity. *Nat Biotechnol* (2016) 34(2):155. doi: 10.1038/nbt.3391

14. Locke WJ, Guanzon D, Ma C, Liew YJ, Duesing KR, Fung KYC, et al. DNA Methylation cancer biomarkers: translation to the clinic. *Front Genet* (2019) 10:1150. doi: 10.3389/fgene.2019.01150

15. Stone A, Zotenko E, Locke WJ, Korbie D, Millar EK, Pidsley R, et al. DNA Methylation of oestrogen-regulated enhancers defines endocrine sensitivity in breast cancer. *Nat Commun* (2015) 6(1):1–9. doi: 10.1038/ncomms8758

16. Schmitt M, Wilhelm OG, Noske A, Schricker G, Napieralski R, Vetter M, et al. Clinical validation of PITX2 DNA methylation to predict outcome in high-risk breast cancer patients treated with anthracycline-based chemotherapy. *Breast Care* (2018) 13 (6):425–33. doi: 10.1159/000493016

17. Stirzaker C, Zotenko E, Song JZ, Qu W, Nair SS, Locke WJ, et al. Methylome sequencing in triple-negative breast cancer reveals distinct methylation clusters with prognostic value. *Nat Commun* (2015) 6(1):1–11. doi: 10.1038/ncomms6899

18. Mathe A, Wong-Brown M, Locke WJ, Stirzaker C, Braye SG, Forbes JF, et al. DNA Methylation profile of triple negative breast cancer-specific genes comparing lymph node positive patients to lymph node negative patients. *Sci Rep* (2016) 6(1):1–15. doi: 10.1038/srep33435

19. Meyer B, Clifton S, Locke W, Luu P-L, Du Q, Lam D, et al. Identification of DNA methylation biomarkers with potential to predict response to neoadjuvant chemotherapy in triple-negative breast cancer. *Clin Epigenet* (2021) 13(1):1–7. doi: 10.1186/s13148-021-01210-6

20. Wang Z, Yang B, Zhang M, Guo W, Wu Z, Wang Y, et al. lncRNA epigenetic landscape analysis identifies EPIC1 as an oncogenic lncRNA that interacts with MYC and promotes cell-cycle progression in cancer. *Cancer Cell* (2018) 33(4):706–20.e9. doi: 10.1016/j.ccell.2018.03.006

21. Moss J, Magenheim J, Neiman D, Zemmour H, Loyfer N, Korach A, et al. Comprehensive human cell-type methylation atlas reveals origins of circulating cell-free DNA in health and disease. *Nat Commun* (2018) 9(1):5068. doi: 10.1038/s41467-018-07466-6

22. Barefoot ME, Loyfer N, Kiliti AJ, McDeed APIV, Kaplan T, Wellstein A. Detection of cell types contributing to cancer from circulating, cell-free methylated DNA. *Front Genet* (2021) 12:671057. doi: 10.3389/fgene.2021.671057

23. Moran S, Martínez-Cardús A, Sayols S, Musulén E, Balañá C, Estival-Gonzalez A, et al. Epigenetic profiling to classify cancer of unknown primary: a multicentre, retrospective analysis. *Lancet Oncol* (2016) 17(10):1386–95. doi: 10.1016/S1470-2045(16)30297-2

24. Liu X, Ren J, Luo N, Guo H, Zheng Y, Li J, et al. Comprehensive DNA methylation analysis of tissue of origin of plasma cell-free DNA by methylated CpG tandem amplification and sequencing (MCTA-seq). *Clin Epigenet* (2019) 11(1):1–13. doi: 10.1186/s13148-019-0689-y

25. Kang S, Li Q, Chen Q, Zhou Y, Park S, Lee G, et al. CancerLocator: non-invasive cancer diagnosis and tissue-of-origin prediction using methylation profiles of cell-free DNA. *Genome Biol* (2017) 18(1):1–12. doi: 10.1186/s13059-017-1191-5

26. Lehmann-Werman R, Neiman D, Zemmour H, Moss J, Magenheim J, Vaknin-Dembinsky A, et al. Identification of tissue-specific cell death using methylation patterns of circulating DNA. *Proc Natl Acad Sci USA* (2016) 113(13):E1826–E34. doi: 10.1073/pnas.1519286113

27. Liu MC, Oxnard GR, Klein EA, Swanton C, Seiden MV, Liu MC, et al. Sensitive and specific multi-cancer detection and localization using methylation signatures in cell-free DNA. *Ann Oncol* (2020) 31(6):745–59. doi: 10.1016/j.annonc.2020.02.011

28. Cristiano S, Leal A, Phallen J, Fiksel J, Adleff V, Bruhm DC, et al. Genome-wide cell-free DNA fragmentation in patients with cancer. *Nature* (2019) 570(7761):385–9. doi: 10.1038/s41586-019-1272-6

29. Mouliere F, Chandrananda D, Piskorz AM, Moore EK, Morris J, Ahlborn LB, et al. Enhanced detection of circulating tumor DNA by fragment size analysis. *Sci Transl Med* (2018) 10(466):eaat4921. doi: 10.1126/scitranslmed.aat4921

30. Markus H, Chandrananda D, Moore E, Mouliere F, Morris J, Brenton JD, et al. Refined characterization of circulating tumor DNA through biological feature integration. *Sci Rep* (2022) 12(1):1–11. doi: 10.1038/s41598-022-05606-z

31. Snyder MW, Kircher M, Hill AJ, Daza RM, Shendure J. Cell-free DNA comprises an in vivo nucleosome footprint that informs its tissues-of-origin. *Cell* (2016) 164(1-2):57–68. doi: 10.1016/j.cell.2015.11.050

32. Ivanov M, Baranova A, Butler T, Spellman P, Mileyko V. Non-random fragmentation patterns in circulating cell-free DNA reflect epigenetic regulation. *BMC Genom* (2015) 16(13):S1. doi: 10.1186/1471-2164-16-S13-S1

33. Ulz P, Thallinger GG, Auer M, Graf R, Kashofer K, Jahn SW, et al. Inferring expressed genes by whole-genome sequencing of plasma DNA. *Nat Genet* (2016) 48 (10):1273. doi: 10.1038/ng.3648

34. Teif VB. Nucleosome positioning: resources and tools online. *Brief Bioinform* (2016) 17(5):745–57. doi: 10.1093/bib/bbv086

35. Oruba A, Saccani S, van Essen D. Role of cell-type specific nucleosome positioning in inducible activation of mammalian promoters. *Nat Commun* (2020) 11(1):1–18. doi: 10.1038/s41467-020-14950-5

36. Norouzi D, Katebi A, Cui F, Zhurkin VB. Topological diversity of chromatin fibers: Interplay between nucleosome repeat length, DNA linking number and the level of transcription. *AIMS Biophys* (2015) 2(4):613. doi: 10.3934/biophy.2015.4.613

37. Clark SJ, Harrison J, Paul CL, Frommer M. High sensitivity mapping of methylated cytosines. *Nucleic Acids Res* (1994) 22(15):2991. doi: 10.1093/nar/22.15.2990

38. Vaisvila R, Ponnaluri VC, Sun Z, Langhorst BW, Saleh L, Guan S, et al. Enzymatic methyl sequencing detects DNA methylation at single-base resolution from picograms of DNA. *Genome Res* (2021) 31(7):1280–9. doi: 10.1101/gr.266551.120

39. Reinert T, Henriksen TV, Christensen E, Sharma S, Salari R, Sethi H, et al. Analysis of plasma cell-free DNA by ultradeep sequencing in patients with stages I to III colorectal cancer. *JAMA Oncol* (2019) 5(8):1124–31. doi: 10.1001/jamaoncol.2019.0528

40. Loupakis F, Sharma S, Derouazi M, Murgioni S, Biason P, Rizzato MD, et al. Detection of molecular residual disease using personalized circulating tumor DNA assay in patients with colorectal cancer undergoing resection of metastases. *JCO Precis Oncol* (2021) 5):1166–77. doi: 10.1200/po.21.00101

41. Lipsyc-Sharf M, de Bruin EC, Santos K, McEwen R, Stetson D, Patel A, et al. Circulating tumor DNA and late recurrence in high-risk hormone receptor–positive, human epidermal growth factor receptor 2–negative breast cancer. *J Clin Onco* (2022) 40(22):2408–19. doi: 10.1200/JCO.22.00908

42. Turner NC, Swift C, Jenkins B, Kilburn L, Coakley M, Beaney M, et al. Results of the c-TRAK TN trial: a clinical trial utilising ctDNA mutation tracking to detect molecular residual disease and trigger intervention in patients with moderate and high-risk early stage triple negative breast cancer. *Ann Oncol* (2022) 34(2):200–11. doi: 10.1016/j.annonc.2022.11.005

43. *Foundation medicine. foundation medicine's ctDNA monitoring assay, FoundationOne®Tracker, granted breakthrough device designation by U.S. food and drug administration* (2022). Available at: https://www.foundationmedicine.com/press-releases/af7bb7df-2dcf-411f-bc7d-ebb8ab90d788 (Accessed Feb 09, 2023).

44. Strata Oncology. *Evaluation of a personalized liquid biopsy test to detect cancer recurrence across solid tumors* (2022). Available at: https://strataoncology.com/sentinel (Accessed Nov 16, 2022).

45. Cao D, Wang F-L, Li C, Zhang R-X, Wu X-J, Li L, et al. Patient-specific tumor-informed circulating tumor DNA (ctDNA) analysis for molecular residual disease (MRD) detection in surgical patients with stage I-IV colorectal cancer (CRC). *J Clin Oncol* (2023) 41(4_suppl):213. doi: 10.1200/JCO.2023.41.4_suppl.213

46. Kurtz DM, Soo J, Co Ting Keh L, Alig S, Chabon JJ, Sworder BJ, et al. Enhanced detection of minimal residual disease by targeted sequencing of phased variants in circulating tumor DNA. *Nat Biotechnol* (2021) 39(12):1537–47. doi: 10.1038/s41587-021-00981-w

47. McDonald BR, Contente-Cuomo T, Sammut S-J, Odenheimer-Bergman A, Ernst B, Perdigones N, et al. Personalized circulating tumor DNA analysis to detect residual disease after neoadjuvant therapy in breast cancer. *Sci Transl Med* (2019) 11 (504):eaax7392. doi: 10.1126/scitranslmed.aax7392

48. Montañá JR, Martini G, Baraibar I, Villacampa G, Comas R, Ciardiello D, et al. Patient and tumor characteristics as determinants of overall survival (OS) in BRAF V600 mutant (mt) metastatic colorectal cancer (mCRC) treated with doublet or triplet targeted therapy. *J Clin Oncol* (2020) 38(15_suppl):4112. doi: 10.1200/JCO.2020.38.15_suppl.4112

49. ClinicalTrials.gov. *ctDNA methylation sequencing for myeloma* (2022). Available at: https://clinicaltrials.gov/ct2/show/NCT05578625 (Accessed Nov 5, 2022).

50. Grail Inc. *GRAIL announces collaborations with amgen, AstraZeneca, and Bristol Myers Squibb to evaluate cancer early detection technology for minimal residual disease* (2021). Available at: https://grail.com/press-releases/grail-announces-collaborations-with-amgen-astrazeneca-and-bristol-myers-squibb-to-evaluate-cancer-early-detection-technology-for-minimal-residual-disease (Accessed Nov 5, 2022).

51. Symonds EL, Pedersen SK, Murray D, Byrne SE, Roy A, Karapetis C, et al. Circulating epigenetic biomarkers for detection of recurrent colorectal cancer. *Cancer* (2020) 126(7):1460–9. doi: 10.1002/cncr.32695

52. Symonds EL, Pedersen SK, Yeo B, Al Naji H, Byrne SE, Roy A, et al. Assessment of tumor burden and response to therapy in patients with colorectal cancer using a quantitative ctDNA test for methylated BCAT1/IKZF1. *Mol Oncol* (2022) 16(10):2031–41. doi: 10.1002/1878-0261.13178

53. Territo A, Gallioli A, Diana P, Boissier R, Fontana M, Gaya JM, et al. DNA Methylation urine biomarkers test in the diagnosis of upper tract urothelial carcinoma: results from a single-center prospective clinical trial. *J Urol* (2022) 208(3):570–9. doi: 10.1097/JU.0000000000002748

54. Pierconti F, Martini M, Fiorentino V, Cenci T, Racioppi M, Foschi N, et al. Upper urothelial tract high-grade carcinoma: comparison of urine cytology and DNA methylation analysis in urinary samples. *Hum Pathol* (2021) 118:42–8. doi: 10.1016/j.humpath.2021.09.007

55. Cai G, Cai M, Feng Z, Liu R, Liang L, Zhou P, et al. A multilocus blood-based assay targeting circulating tumor DNA methylation enables early detection and early relapse prediction of colorectal cancer. *Gastroenterology* (2021) 161(6):2053–6.e2. doi: 10.1053/j.gastro.2021.08.054

56. Pedersen SK, Symonds EL, Baker RT, Murray DH, McEvoy A, Van Doorn SC, et al. Evaluation of an assay for methylated BCAT1 and IKZF1 in plasma for detection of colorectal neoplasia. *BMC Cancer* (2015) 15(1):654. doi: 10.1186/s12885-015-1674-2

frontiers | Frontiers in Oncology

TYPE Original Research
PUBLISHED 06 April 2023
DOI 10.3389/fonc.2023.1098128

OPEN ACCESS

EDITED BY
Zohreh Amoozgar,
Massachusetts General Hospital, Harvard Medical School, United States

REVIEWED BY
Monika Ulamec,
University of Zagreb, Croatia
Chuanbo Xie,
Sun Yat-sen University Cancer Center (SYSUCC), China

*CORRESPONDENCE
Changhong Liu
434503278@qq.com

SPECIALTY SECTION
This article was submitted to Molecular and Cellular Oncology, a section of the journal Frontiers in Oncology

RECEIVED 14 November 2022
ACCEPTED 20 February 2023
PUBLISHED 06 April 2023

CITATION
Zhang X, Zhang Y, Zhang S, Wang S, Yang P and Liu C (2023) Investigate the application of postoperative ctDNA-based molecular residual disease detection in monitoring tumor recurrence in patients with non-small cell lung cancer——A retrospective study of ctDNA. *Front. Oncol.* 13:1098128. doi: 10.3389/fonc.2023.1098128

Investigate the application of postoperative ctDNA-based molecular residual disease detection in monitoring tumor recurrence in patients with non-small cell lung cancer——A retrospective study of ctDNA

Xuefei Zhang[1], Youguo Zhang[1], Shanli Zhang[2], Sha Wang[2], Peng Yang[2] and Changhong Liu[1]*

[1]Department of Thoracic Surgery, The Second Hospital of Dalian Medical University, Dalian, Liaoning, China, [2]Geneseeq Research Institute, Nanjing Geneseeq Technology Inc., Nanjing, Jiangsu, China

Purpose: To evaluate whether postoperative circulating tumor DNA (ctDNA) in plasma of patients with non-small cell lung cancer (NSCLC) can be used as a biomarker for early detection of molecular residual disease (MRD) and prediction of postoperative recurrence.

Methods: This study subjects were evaluated patients with surgical resected non-small cell lung cancer. All eligible patients underwent radical surgery operation followed by adjuvant therapy. Tumor tissue samples collected during operation were used to detect tumor mutation genes, and blood samples collected from peripheral veins after operation were used to collect ctDNA. Molecular residue disease (MRD) positive was defined as at least 1 true shared mutation identified in both the tumor sample and a plasma sample from the same patient was.

Results: Positive postoperatively ctDNA was associated with lower recurrence-free survival (RFS).The presence of MRD was a strong predictor of disease recurrence. The relative contribution of ctDNA-based MRD to the prediction of RFS is higher than all other clinicopathological variables, even higher than traditional TNM staging. In addition, MRD-positive patients who received adjuvant therapy had improved RFS compared to those who did not, the RFS of MRD-negative patients receiving adjuvant therapy was lower than that of patients not receiving adjuvant therapy.

Conclusions: Post-operative ctDNA analysis is an effective method for recurrence risk stratification of NSCLC, which is beneficial to the management of patients with NSCLC.

KEYWORDS

NSCLC1, ctDNA2, molecular residual disease (MRD)3, postoperative 4, recurrence risk 5

1 Introduction

Lung cancer is one of the most common malignancies in the world. According to the epidemiological statistics, lung cancer has ranked sixth among the top 20 major causes of death in the world, and is the malignant tumor with the highest morbidity and mortality among males (1–3). Only about 25% of all patients with non-small cell lung cancer (NSCLC) survived more than five years. The 5-year survival rate for patients with NSCLC was about 25%. The ratio was decreased to less than 6% for metastatic NSCLC even after cytotoxic chemotherapy (4). Up to now, the prognosis of NSCLC is mainly evaluated based on clinicopathological parameters such as TNM stage, pathological subtype and tumor differentiation degree (5). The 2020 edition of the National Comprehensive Cancer Network Guidelines (NCCN) recommends adjuvant chemotherapy after radical surgery for the patients with stage IB-IIIA NSCLC who have high risk for recurrence (6).

However, a significant proportion of patients with low risk of recurrence based on these prognostic indicators experienced tumor recurrence, while some patients with high risk of recurrence still remained recurrence-free after long-time follow-up. At the same time, the outcome of some patients with high recurrence risk was not improved by adjuvant therapy (7). Clinicians urgently need a more effective method to identify patients at high risk of tumor recurrence and who are likely to benefit from adjuvant therapy.

In recent years, liquid biopsy has been introduced into clinical practice as a valuable tool for early diagnosis of recurrence and metastasis of non-small cell lung cancer (NSCLC) (8–12). Circulating tumor DNA (ctDNA) mainly comes from the small fragments of DNA released by apoptotic or necrotic tumor cells in tumor tissues into the blood system and the DNA released by the lysis of circulating tumor cells or micrometastases in the blood (13). Plasma ctDNA analysis can increase the chance of identifying targeted mutations, and is considered as an alternative to tissue biopsy. It has been widely used for early diagnosis, prognostic stratification, disease monitoring and treatment response assessment in different cancer types (14–16). Liquid biopsy techniques based on plasma ctDNA analysis can monitor and track personalized disease-related markers at the molecular level, and can be used to detect molecular residual desease (MRD) after treatment (10, 17, 18). In the TRACERx study, Addosh et al (19) found that ctDNA test after surgery could detect tumor recurrence or metastasis earlier than imaging. Recent trials using personalized mutation detection or CAPP-seq have also demonstrated the potential of ctDNA for MRD detection and early recurrence prediction, especially in post-surgical patients awaiting adjuvant therapy (20, 21). These studies were helpful to evaluate the prognostic value of post-operative ctDNA status in NSCLC. In addition, previous studies mainly focused on detecting MRD after the completion of adjuvant therapy. Few reports have discussed about whether the MRD detection based on the definition of post-operative ctDNA status could guide post-operative adjuvant therapy for NSCLC patients. Also, the utility of dynamic changes in serial ctDNA to predict the risk of relapse during disease surveillance has not been well characterized.

This study collected tumor pathological diagnosis information, post-operative plasma ctDNA detection results, post-operative adjuvant therapy and recurrence status of 73 patients with NSCLC who received radical surgery. The role of MRD detection based on post-operative plasma ctDNA in the prediction of recurrence and metastasis was retrospectively analyzed. It is expected that this study could provide some guidance on personalized treatment according to the molecular characteristics of NSCLC patients.

2 Materials and methods

2.1 Patients and samples

We enrolled 108 stage I–III NSCLC patients to evaluate the clinical utility of serial ctDNA monitoring from May 2016 to October 2021. Thirty-five patients were excluded due to pathologic diagnosis of stage IV or double/multiple primary lung cancer, the remaining 73 patients were included in the study. According to the latest version of the National Comprehensive Cancer Network (NCCN) guidelines and the patient's pathologic diagnosis, all patients eligible for postoperative adjuvant therapy are recommended for postoperative adjuvant therapy: (1) For absolutely resected level II to III NSCLC, 4 cycles of adjuvant chemotherapy after operation are recommended; (2) Adjuvant chemotherapy is suggested for sufferers in level IB with high-risk factor after operation. Chest computed tomography (CT) examination was performed at the first, third, sixth, and twelfth months of the first year after discharge, and at least once a year thereafter.

The primary cancer tissues of 73 patients obtained during the operation were pathologically diagnosed in the Department of Pathology, the Second Hospital of Dalian Medical University. 10 ml of whole blood was collected for separation plasma samples in these patients after radical lung cancer surgery and adjuvant therapy. All patients eligible for postoperative adjuvant therapy are recommended for postoperative adjuvant therapy. Chest computed tomography (CT) examination was performed at the first, third, sixth, and twelfth months of the first year after discharge, and at least once a year thereafter. Patients with multiple primary foci, prior malignancy, and incomplete clinicopathological data were excluded from the study. One patient was lost to follow-up, so they were not included in monitoring the efficacy of postoperative adjuvant therapy. The study was approved by the Ethics Review Committee of the Second Hospital of Dalian Medical University, and each patient signed an informed consent.

2.2 DNA extraction and targeted next generation sequencing

Genomic DNA from FFPE samples and white blood cells were extracted using the QIAamp DNA FFPE Tissue Kit (Qiagen). Plasma was extracted from about 10 ml whole blood in EDTA coated tubes within 2 h of blood withdrawing, and circulating cell free DNA

(cfDNA) was extracted using the QIAamp Circulating Nucleic Acid Kit (QIAGEN). Genomic DNA from white blood cells was extracted using DNeasy Blood & Tissue Kit (Qiagen,Germany) and used as normal control. All DNA concentration and purity were qualified by Nanodrop2000 (Thermo Fisher Scientific). All DNA samples were also quantified by Qubit 3.0 using the dsDNA HS Assay Kit (Life Technologies) according to the manufacturer's protocol.

Sequencing libraries were constructed using KAPA Hyper Prep kit (KAPA Biosystems) with an optimized manufacturer s instructions. In brief, cfDNA or DNA was experienced with endrepairing, A-tailing, adapter ligation and size selection using Agencourt AMPure XP beads (Beckman Coulter). Libraries were then subjected to PCR amplification and purification before targeted enrichment. The size distribution of libraries was measured by Agilent Technologies 2100 Bioanalyzer (Agilent Technologies). The enriched libraries were sequenced on Illumina Hiseq 4000 NGS platforms to cover mean depths of at least 1,000, 3,000, and 100, for FFPE, cfDNA, and blood, respectively (22).

Single nucleotide variants (SNVs) and short insertions/deletions (indels) were identified using VarScan2 2.3.9 (23) with minimum variant allele frequency threshold set at 0.01 and p-value threshold for calling variants set at 0.05 to generate Variant Call Format (VCF) files. All SNVs/indels were annotated with ANNOVAR, and each SNV/indel was manually checked with the Integrative Genomics Viewer (IGV). Copy number variations (CNVs) were identified using ADTEx 1.0.4 (24).

For each patient, 1 true variant detected in the tumor tissue was measured for its presence in the plasma. At least 1 true shared mutation identified in both the tumor sample and a plasma sample from the same patient was defined as positive for ctDNA. ctDNA levels were quantifiedas the fraction of mutant alleles ×100.

2.3 Statistical analysis

The primary outcome looked at was recurrence-free survival (RFS), defined as the period between the patient's surgery operation and the first confirmation of local or distant tumor recurrence, or death from any cause. The data were analyzed by SPSS 25.0 software. The chi-square test was used to assess the association of clinical characteristics and overall recurrence between postoperative ctDNA positive and negative subgroups, and the independent sample T test was used to compare quantitative data. Kaplan-meier analysis was used to investigate the relationship between progression-free survival (PFS) and postoperative plasma ctDNA status, TNM stage, tumor pathological type, degree of differentiation, and adjuvant therapy.

Cox regression analysis of statistically significant variables was used to analyze the correlation between tumor recurrence, progression-free survival (RFS) and postoperative plasma ctDNA status, TNM stage, tumor pathological type, degree of differentiation, and adjuvant therapy. Thus, the application value of postoperative plasma ctDNA status in the evaluation of prognosis of patients with NSCLC was obtained. P value < 0.05 was defined as statistically significant difference.

3 Results

3.1 Patient characteristics

The clinicopathological features of the enrolled 73 patients were shown in Table 1. The mean age of patients at diagnosis was 59 years (range: 47-84 years). Among all the patients, 35.6% were male, 64.4% were female, 95.9% were pathological type of lung adenocarcinoma, 30 patients (41.1%) had disease stage IB or above, and 21 patients (28.8%) had ctDNA detected in postoperative blood samples. Thirty-one patients (42.5%) received adjuvant therapy. All patients were followed for 4 to 67 months, with a median of 29 months. At the last follow-up, 21 patients (28.8%) had relapsed, and 51 patients (69.9%) had not relapsed or metasasized, except one patient who was lost to follow-up. The median pretreatment ctDNA level was 0 (range 0–38.2), and the median ctDNA level ctDNA after chemotherapy was 0 (range 0–31.6).

3.2 Prognostic value of the post-operative ctDNA

Univariate and multivariate analysis were performed to evaluate the relationship between RFS and clinicopathological variables (Table 2). The result showed that only pTNM stage and adjuvant therapy were correlated with RFS (P<0.05). We further evaluated the relationship between postoperative ctDNA status and tumor recurrence/metastasis in NSCLC. Data analysis showed that 71.4% (15 of 21) of patients who were postoperative ctDNA-positive experienced recurrence compared with those who were ctDNA-negative (6 of 52, 11.5%) (Table 2). We get the same results as before, post-operative ctDNA-based MRD status is a strong predictor of NSCLC recurrence. The postoperative ctDNA status was significantly correlated with RFS (Table 2). The ctDNA-positive patients had significantly worse RFS (HR 8.84, 95% CI 3.41-22.90; P<0.001) (Figure 1A). After adjusting for clinicopathological risk factors, postoperative ctDNA status remained an independent risk factor for RFS (HR 7.757, 95%CI 2.787-21.592; P <0.01) (Table 2). Survival curves showed that positive MRD was correlated with RFS in both stage IA (HR 39.49, 95%CI 4.72-330.75; P=0.001) (Figure 1B)and stage IB-III patients (HR 3.21, 95%CI 1.06-9.71; P=0.039) (Figure 1C).

In current clinical practice, patients with stage IB-III NSCLC based on clinicopathological factors are usually advised to receive adjuvant therapies after radical surgery, but only a small percentage of patients benefit from adjuvant therapies (6, 25, 26) . In this study, we explored the possibility that ctDNA-based MRD testing could help select eligible NSCLC patients for adjuvant therapy. One patient was excluded in the adjuvant therapy analysis because of loss of follow-up. First, we stratified the patients according to traditional TNM staging. Recurrence was detected in 43 of stage IA patients (16.27%) and of stage IB-III patients (45.16%), respectively. Of the 43 stage IA patients, 3 who received post-operative adjuvant therapy (ADT) did not experience recurrence, while 7 (18%) of those who did not receive ADT. Recurrence was

TABLE 1 Patient clinicopathological characteristics.

Characteristics	All patients (N = 73)
Gender (%)	
Male	26 (35.6)
Female	47 (64.4)
Age (years)	
Median (range)	59 (37-84)
Smoking status (%)	
Yes	14 (19.2)
No	59 (80.8)
Hypertension (%)	
Yes	19 (26)
No	54 (74)
Diabetes (%)	
Yes	10 (13.7)
No	63 (86.3)
Histology (%)	
Adenocarcinoma	70 (95.9)
Squamous cell carcinoma	3 (4.1)
Differentiation (%)	
Microinvasive	5 (6.8)
High	5 (6.8)
Moderately	43 (58.9)
Low	17 (23.3)
Mucous	3 (4.1)
pTMN stage (%)	
IA	43 (58.9)
IB	9 (12.3)
IIA	1 (1.4)
IIB	8 (11.0)
IIIA	11 (15.1)
IIIB	1 (1.4)
T stage (%)	
T1	52 (71.2)
T2	19 (26.0)
T3	1 (1.4)
T4	1 (1.4)
N stage (%)	
N0	53 (72.6)
N1	7 (9.6)
N2	13 (17.8)
ctDNA, pretreatment	
Median (range)	0 (0-38.2)
ctDNA after chemotherapy	
Median (range)	0 (0-31.6)
Adjuvant therapy (%)	
Yes	31 (42.5)
No	41 (56.2)
ctDNA Status,after chemotherapy (%)	
ctDNA Positive	13 (17.8)
ctDNA Negative	56 (76.7)
Undeteced	4 (5.5)
Recurrence (%)	
Yes	21 (28.8)
No	51 (69.9)

(Continued)

detected in 30 of stage IB-III patients (46.67%) respectively. Of the 30 stage IB-III patients who received ADT (28 patients), 14(50%) experienced tumor recurrence/metastasis, while 2 patients who did not receive ADT remained disease-free (Table 3).

When the effect of ADT on tumor recurrence/metastasis was analyzed in terms of post-operative ctDNA status, 9 (75%) of the 12 patients who were post-operative ctDNA-positive in the stage IB-III patients experienced recurrence. Among the patients with post-operative ctDNA-negative, recurrence was observed in 5 of 19 patients (26.3%) who received ADT (Table 3), compared with only 1 of 33 patients who did not receive adjuvant therapy.

For the patients who were post-operative ctDNA-positive, adjuvant therapy could significantly improve RFS (mean RFS: 18.5 months vs. 12.3 months; HR 0.63, 95% CI 0.22-1.81; P=0.394) (Figure 1D). In contrast, in the post-operative ctDNA-negative patients, those receiving adjuvant therapy had significantly shorter RFS (mean RFS 32.2 months versus 64.8 months; HR 0.09, 95% CI 0.01-0.77; P=0.028) (Figure 1E). However, when stratified the patients according to traditional TNM staging, there was no significant difference in PFS of both stage IA (P=0.48) and IB-III (P=0.21) patients who received ADT and those who did not. After adjustment for other clinicopathological variables, adjuvant therapy bring significant benefit to RFS in the MRD-negative population.

4 Discussion

There are correlations between plasma ctDNA and tumor burden, metabolism, proliferative indices, lymphovascular invasion, and the risk of disease recurrence/progression in patients with non-small cell lung cancer (NSCLC) (25). It is

TABLE 2 Recurrence-free survival (RFS) analysis of clinicopathological variables and postoperative ctDNA status in NSCLC patients.

Variables	Univariate analysis			Multivariate analysis		
	HR	95% CI	P value	HR	95% CI	P value
Postoperative ctDNA (n = 72)						
ctDNA status (Positive vs. Negative)	8.765	3.385 - 22.698	< 0.001	7.757	2.787 - 21.592	< 0.001
Age	1.041	0.988 - 1.097	0.131			
Gender (Female vs. Male)	0.764	0.322 - 1.816	0.543			
Smoking status(Yes vs. No)	1.653	0.641 - 4.265	0.299			
Hypertension (Yes vs. No)	0.902	0.330 - 2.463	0.840			
Diabetes (Yes vs. No)	0.930	0.273 - 3.160	0.907			
Histology(Adenocarcinoma vs. Squamous cell carcinoma)	0.698	0.093 - 5.226	0.726			
pTMN stage (IA vs. IB-III)	2.767	1.116 - 6.865	0.023	1.047	0.073 - 14.972	0.973
Adjuvant therapy (Yes vs. No)	2.859	1.151 - 7.100	0.024	1.313	0.092 - 18.775	0.841

possible to use ctDNA profiling to quantify MRD, a disease state associated with medically occult residual disease that can be detected using ctDNA, and inferior disease-free survival (DFS) (26). Plasma ctDNA monitoring has become a new method for prognosis prediction and post-operative monitoring of NSCLC. At present, various methods have been developed for ctDNA detection in solid tumors (3, 21, 27). However, it is difficult to determine the proportion of ctDNA by direct cfDNA quantification. Indirect quantification is based on the sequencing of cfDNA and the abundance of tumor-specific mutations carried in cfDNA (28). One study of 230 lung cancer patients found a positive correlation between postoperative ctDNA and late recurrence rates (27). Based on plasma samples, researchers determined the correlation between ctDNA status and postoperative RFS of patients using ctDNA quantified by highest mutation allele fraction (MAF), ctDNA status has a greater effect on RFS than any one or combination of clinicopathologic risk factors. In this prospective cohort study, we examined 73 NSCLC patients treated with surgical resection with adjuvant therapy to evaluate the utility of ctDNA in disease monitoring and treatment determination.

Several previous studies have shown that positive plasma ctDNA after surgical resection is associated with poor prognosis in lung cancer patients (20, 25, 29, 30). ctDNA serves as a robust biomarker for postsurgical and post-adjuvant chemotherapy risk stratification and early detection of recurrence in NSCLC (31). According to Wu, the prognostic value of MRD detection in patients with NSCLC after definitive surgery was confirmed, especially in those with longitudinal undetectable MRD (32), subgroup analysis suggested that adjuvant therapy may be unnecessary for patients with undetectable MRD. During surgery, ctDNA analysis can detect recurrence and MRD risk stratification of NSCLC. Adjuvant treatment is an independent factor in recurrence-free survival in MRD-positive population (33), Investigators confirmed MRD is a strong predictor for disease relapse, and whether receiving adjuvant therapies is an independent factor for RFS in the MRD-positive population. In this retrospective study, we examined 73 NSCLC patients undergoing radical surgical resection to assess the utility of ctDNA in disease surveillance and treatment determination. In our study, there were several situations: 4 patients who were ctDNA-negative 1-3 days after surgery, but their lessions recurred during subsequent monitoring. Among these 4 patients, one died of acute renal failure in 1 year after surgery, and 2 patients had ctDNA detected in blood tests after recurrence. One patient with brain metastasis did not detect ctDNA at any time point before and after recurrence, or even during the entire post-operative monitoring period. That could be explained by the fact that the blood brain barrier may deter ctDNA from brain lesions releasing into the circulation (31). Another reason for the negative ctDNA test may be the heterogeneity of the primary tumor, as the mutated gene sequence of the recurrent tumor may not be included in the sequencing region of the tumor biopsy and the range of test sequences used in this study.

The majority of patients in our study cohort were in stage I (58.9%). In contrast, most of the previous studies mainly enrolled patients with stage IB and the above stages (26, 34). Our cohort may more closely reflect the real-world distribution of NSCLC patients undergoing radical surgical treatment (32, 35). Currently, tumor recurrence is monitored mainly by imaging techniques. However, some studies have demonstrated the value of longitudinal ctDNA analysis to predict recurrence earlier than imaing (36–38). Our results suggest that post-operative ctDNA-positive is a strong predictor of NSCLC recurrence, and patients with post-operative positive MRD are more likely to relapse than patients with negative MRD. Multivariate Cox analysis also showed that MRD status was an independent factor of RFS. These results suggest that post-operative MRD status can be a powerful indicator of patient prognosis stratification.

In this study, most patients in stage IB and II-III received ADT, while most patients in stage IA did not. Therefore, it is acceptable that adjuvant therapy is associated with shorter RFS across the entire cohort (average ADT PFS 27.3 months vs. average non-ADT PFS 55.7 months). However, in subgroup analysis, two subgroups showed opposite trends: for MRD-positive patients, ADT is favorable to longer RFS, while for MRD-negative patients who

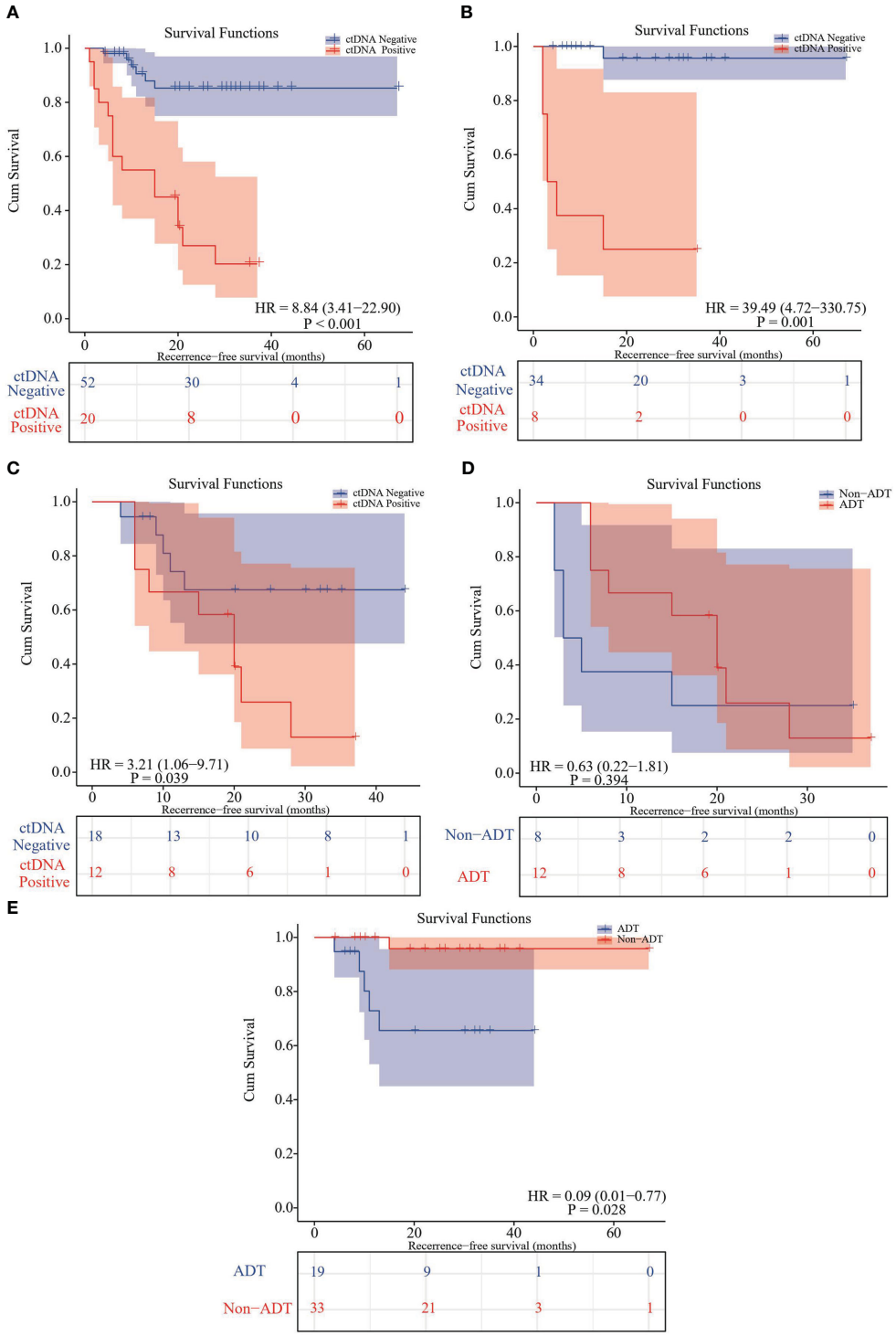

FIGURE 1
Kaplan–Meier curve in patients stratified by postsurgical ctDNA status. **(A)** Kaplan-Meier curve displaying RFS stratified by ctDNA-based MRD status. **(B)** Kaplan-Meier curve comparing RFS stratified of MRD-positive and MRD-negative subsets in TNM stage IA patients. **(C)** Kaplan-Meier curve comparing RFS stratified of MRD-positive and MRD-negative subsets in TNM stage IB-III patients. **(D)** Kaplan-Meier analysis comparing RFS between MRD-positive patients receiving adjuvant therapies and not receiving adjuvant therapy. **(E)** Kaplan-Meier analysis comparing RFS between MRD-negative patients receiving adjuvant therapies and not receiving adjuvant therapy.

received ADT had shorter RFS. The results held true when the analysis was further limited to a subgroup of stage IB-III patients. These results clearly indicate that MRD testing can be a powerful tool in screening patients for ADT.

To sum up, the key findings of this study includes: (1) ctDNA can be used as a biomarker for the prognosis of NSCLC after radical surgery; (2) Early prediction of tumor recurrence can be made by ctDNA-based MRD detection after NSCLC surgery; (3) MRD

TABLE 3 Relationship between postoperative ctDNA-based MRD and tumor recurrence and adjuvant therapy.

MRD			
Tumor recurrence/metastasis	positive	negative	
Yes (%)	15	6	21 (29.2)
No (%)	5	46	51 (70.8)
	20 (27.8)	52 (72.2)	
Adjuvant therapy			
Yes (%)	12	19	31 (43.1)
No (%)	8	33	41 (56.9)
	20 (27.8)	52 (72.2)	

positive patients will benefit from adjuvant therapy, while adjuvant therapy is not beneficial or even harmful to MRD-negative patients. These findings suggested that ctDNA quantification is a more sensitive monitoring technique than traditional imaging.

There are still some limitations to our study. First, our study is limited by a modest sample size and an absence of validation cohorts. However, the results of our study are consistent with those of others that have shown the potential clinical use of ctDNA analysis as a prognostic predictor. Future studies are still needed to further validate whether ctDNA detection can be adopted in routine clinical care. Secondly, the adoption of negative results needs further verification. Multiple factors may lead to false negative results of ctDNA. Thirdly, Some patients failed to complete the blood test in time for some reasons, resulting in missing genetic test results before and after recurrence.

In conclusion, in this retrospective study, we demonstrate that post-operative ctDNA testing can effectively detect MRD and identify NSCLC patients at high risk of recurrence. Adjuvant therapy based on MRD grouping can achieve greater survival benefit for patients with NSCLC. Our findings reveal the potential clinical use of postoperative ctDNA-based MRD testing in NSCLC patients.

Data availability statement

The datasets used and/or analyzed during the current study are available from the corresponding author on reasonable request.

Ethics statement

Written informed consent was obtained from the individual(s) for the publication of any potentially identifiable images or data included in this article.

Author contributions

CL and XZ conceived the study. CL and XZ provided project management and supervision. XZ, YZ and SZ provided or facilitated the accrual of patient samples, pathology, and/or clinical data. PY and SW performed bioinformatics and genomic analyses. XZ performed statistical analyses. XZ wrote the original draft, with input from all authors. All authors contributed to the article and approved the submitted version.

Funding

This work was supported by the Special Fund for Clinical Research of Wu Jieping Medical Foundation under Grant 320.6750.2021-16-8; Science and Technology funds from Liaoning Education Department under Grant LZ2019053, “1+X” program for Clinical Competency enhancement-Clinical Research Incubation Project, The Second Hospital of Dalian Medical University under Grant 2022LCYJYB09.

Acknowledgments

We thank Dr. CL and Dr. Dai Zhaoxia for their support of this paper. Thanks to Dr. XZ for his support in the statistical analysis of the paper. We thank the patients and their families for participation.

Conflict of interest

Authors SZ, SW, PY were employed by Nanjing Geneseeq Technology Inc.

The remaining authors declare that the research was conducted in the absence of any commercial or financial relationships that could be construed as a potential conflict of interest.

Publisher’s note

References

1. Cheng T, Gu Z, Song D, Liu S, Tong X, Wu X, et al. Genomic and clinical characteristics of MET exon14 alterations in a large cohort of Chinese cancer patients revealed distinct features and a novel resistance mechanism for crizotinib. *J Cancer*. (2021) 12(3):644–51. doi: 10.7150/jca.49391

2. Barta JA, Powell CA, Wisnivesky JP. Global epidemiology of lung cancer. *Ann Glob Health* (2019) 85(1). doi: 10.5334/aogh.2419

3. Parikh AR, Van Seventer EE, Siravegna G, Hartwig AV, Jaimovich A, He Y, et al. Minimal residual disease detection using a plasma-only circulating tumor DNA assay in patients with colorectal cancer. *Clin Cancer Res* (2021) 27(20):5586–94. doi: 10.1158/1078-0432.CCR-21-0410

4. Mattiuzzi C, Lippi G. Current cancer epidemiology. *J Epidemiol Glob Health* (2019) 9(4):217–22. doi: 10.2991/jegh.k.191008.001

5. Torre LA, Islami F, Siegel RL, Ward EM, Jemal A. Global cancer in women: Burden and trends. *Cancer Epidemiol Biomarkers Prev* (2017) 26(4):444–57. doi: 10.1158/1055-9965.EPI-16-0858

6. Ettinger DS, Wood DE, Aggarwal C, Aisner DL, Akerley W, Bauman JR, et al. NCCN guidelines insights: Non-small cell lung cancer, version 1. *2020. J Natl Compr Canc Netw* (2019) 17(12):1464–72. doi: 10.6004/jnccn.2019.0059

7. Postmus PE, Kerr KM, Oudkerk M, Senan S, Waller DA, Vansteenkiste J, et al. Early and locally advanced non-small-cell lung cancer (NSCLC): ESMO clinical practice guidelines for diagnosis, treatment and follow-up. *Ann Oncol* (2017) 28:iv1–iv21. doi: 10.1093/annonc/mdx222

8. Rolfo C, Mack PC, Scagliotti GV, Baas P, Barlesi F, Bivona TG, et al. Liquid biopsy for advanced non-small cell lung cancer (NSCLC): A statement paper from the IASLC. *J Thorac Oncol* (2018) 13(9):1248–68. doi: 10.1016/j.jtho.2018.05.030

9. Guibert N, Pradines A, Favre G, Mazieres J. Current and future applications of liquid biopsy in nonsmall cell lung cancer from early to advanced stages. *Eur Respir Rev* (2020) 29(155). doi: 10.1183/16000617.0052-2019

10. Sardarabadi P, Kojabad AA, Jafari D, Liu CH. Liquid biopsy-based biosensors for MRD detection and treatment monitoring in non-small cell lung cancer (NSCLC). *Biosensors (Basel)* (2021) 11(10):394. doi: 10.3390/bios11100394

11. Esagian SM, Grigoriadou G, Nikas IP, Boikou V, Sadow PM, Won JK, et al. Comparison of liquid-based to tissue-based biopsy analysis by targeted next generation sequencing in advanced non-small cell lung cancer: a comprehensive systematic review. *J Cancer Res Clin Oncol* (2020) 146(8):2051–66. doi: 10.1007/s00432-020-03267-x

12. Del Re M, Crucitta S, Gianfilippo G, Passaro A, Petrini I, Restante G, et al. Understanding the mechanisms of resistance in EGFR-positive NSCLC: From tissue to liquid biopsy to guide treatment strategy. *Int J Mol Sci* (2019) 20(16):3951. doi: 10.3390/ijms20163951

13. Rolfo C, Castiglia M, Hong D, Alessandro R, Mertens I, Baggerman G, et al. Liquid biopsies in lung cancer: the new ambrosia of researchers. *Biochim Biophys Acta* (2014) 1846(2):539–46. doi: 10.1016/j.bbcan.2014.10.001

14. Nagasaka M, Uddin MH, Al-Hallak MN, Rahman S, Balasubramanian S, Sukari A, et al. Liquid biopsy for therapy monitoring in early-stage non-small cell lung cancer. *Mol Cancer*. (2021) 20(1):82. doi: 10.1186/s12943-021-01371-1

15. Krug AK, Enderle D, Karlovich C, Priewasser T, Bentink S, Spiel A, et al. Improved EGFR mutation detection using combined exosomal RNA and circulating tumor DNA in NSCLC patient plasma. *Ann Oncol* (2018) 29(3):700–6. doi: 10.1093/annonc/mdx765

16. Stinchcombe TE, Doebele RC, Wang X, Gerber DE, Horn L, Camidge DR. Preliminary clinical and molecular analysis results from a single-arm phase 2 trial of brigatinib in patients with disease progression after next-generation ALK tyrosine kinase inhibitors in advanced ALK + NSCLC. *J Thorac Oncol* (2021) 16(1):156–61. doi: 10.1016/j.jtho.2020.09.018

17. Coakley M, Garcia-Murillas I, Turner NC. Molecular residual disease and adjuvant trial design in solid tumors. *Clin Cancer Res* (2019) 25(20):6026–34. doi: 10.1158/1078-0432.CCR-19-0152

18. De Silva S, Tennekoon KH, Karunanayake EH. Overview of the genetic basis toward early detection of breast cancer. *Breast Cancer (Dove Med Press)*. (2019) 11:71–80. doi: 10.2147/BCTT.S185870

19. Abbosh C, Birkbak NJ, Wilson GA, Jamal-Hanjani M, Constantin T, Salari R, et al. Phylogenetic ctDNA analysis depicts early-stage lung cancer evolution. *Nature*. (2017) 545(7655):446–51. doi: 10.1038/nature22364

20. Ulrich B, Pradines A, Mazieres J, Guibert N. Detection of tumor recurrence *via* circulating tumor DNA profiling in patients with localized lung cancer: Clinical considerations and challenges. *Cancers (Basel)*. (2021) 13(15):3759. doi: 10.3390/cancers13153759

21. Chaudhuri AA, Chabon JJ, Lovejoy AF, Newman AM, Stehr H, Azad TD, et al. Early detection of molecular residual disease in localized lung cancer by circulating tumor DNA profiling. *Cancer Discovery* (2017) 7(12):1394–403. doi: 10.1158/2159-8290.CD-17-0716

22. Zhao Z, Fu T, Gao J, Xu Y, Wu X, Chen W, et al. Identifying novel oncogenic RET mutations and characterising their sensitivity to RET-specific inhibitors. *J Med Genet* (2021) 58(2):79–86. doi: 10.1136/jmedgenet-2019-106546

23. Koboldt DC, Zhang Q, Larson DE, Shen D, McLellan MD, Lin L, et al. VarScan 2: somatic mutation and copy number alteration discovery in cancer by exome sequencing. *Genome Res* (2012) 22:568–76. doi: 10.1101/gr.129684.111

24. Amarasinghe KC, Li J, Hunter SM, Ryland GL, Cowin PA, Campbell IG, et al. Inferring copy number and genotype in tumour exome data. *BMC Genomics* (2014) 15:732. doi: 10.1186/1471-2164-15-732

25. Blakely CM, Weder W, Bubendorf L, He J, Majem M, Shyr Y, et al. Primary endpoints to assess the efficacy of novel therapeutic approaches in epidermal growth factor receptor-mutated, surgically resectable non-small cell lung cancer: a review. *Lung Cancer* (2023). doi: 10.1016/j.lungcan.2023.01.002

26. Abbosh C, Birkbak NJ, Swanton C. Early stage NSCLC–challenges to implementing ctDNA-based screening and MRD detection[J]. *Nat Rev Clin Oncol* (2018) 15(9):577–86. doi: 10.1038/s41571-018-0058-3

27. Tie J, Wang Y, Tomasetti C, Li L, Springer S, Kinde I, et al. Circulating tumor DNA analysis detects minimal residual disease and predicts recurrence in patients with stage II colon cancer. *Sci Transl Med* (2016) 8(346):346ra92. doi: 10.1126/scitranslmed.aaf6219

28. Liang W, Zhao Y, Huang W, Gao Y, Xu W, Tao J, et al. Non-invasive diagnosis of early-stage lung cancer using high-throughput targeted DNA methylation sequencing of circulating tumor DNA (ctDNA). *Theranostics*. (2019) 9(7):2056–70. doi: 10.7150/thno.28119

29. Newman AM, Bratman SV, To J, Wynne JF, Eclov NC, Modlin LA, et al. An ultrasensitive method for quantitating circulating tumor DNA with broad patient coverage. *Nat Med* (2014) 20(5):548–54. doi: 10.1038/nm.3519

30. Tie J, Wang Y, Cohen J, Li L, Hong W, Christie M, et al. Circulating tumor DNA dynamics and recurrence risk in patients undergoing curative intent resection of colorectal cancer liver metastases: A prospective cohort study. *PLoS Med* (2021) 18(5):e1003620.

31. Qiu B, Guo W, Zhang F, Lv F, Ji Y, Peng Y, et al. Dynamic recurrence risk and adjuvant chemotherapy benefit prediction by ctDNA in resected NSCLC. *Nat Commun* (2021) 12(1):6770. doi: 10.1038/s41467-021-27022-z

32. Zhang JT, Liu SY, Gao W, Liu SYM, Yan HH, Ji L, et al. Longitudinal undetectable molecular residual disease defines potentially cured population in localized non-small cell lung cancer [J]. *Cancer Discov* (2022) 12(7):1690–701. doi: 10.1158/2159-8290.CD-21-1486

33. Xia L, Mei J, Kang R, Deng S, Chen Y, Yang Y, et al. Perioperative ctDNA-based molecular residual disease detection for non-small cell lung cancer: A prospective multicenter cohort study (LUNGCA-1). *Clin Cancer Res* (2021) 28(15):3308–17. doi: 10.1158/1078-0432.CCR-21-3044

34. Oliveira KCS, Ramos IB, Silva JMC, Barra WF, Riggins GJ, Palande V, et al. Current perspectives on circulating tumor DNA, precision medicine, and personalized clinical management of cancer. *Mol Cancer Res* (2020) 18(4):517–28. doi: 10.1158/1541-7786.MCR-19-0768

35. Herbreteau G, Vallee A, Charpentier S, Normanno N, Hofman P, Denis MG. Circulating free tumor DNA in non-small cell lung cancer (NSCLC): clinical application and future perspectives. *J Thorac Dis* (2019) 11(Suppl 1):S113–S26. doi: 10.21037/jtd.2018.12.18

36. Song Y, Hu C, Xie Z, Wu L, Zhu Z, Rao C, et al. Circulating tumor DNA clearance predicts prognosis across treatment regimen in a large real-world longitudinally monitored advanced non-small cell lung cancer cohort. *Transl Lung Cancer Res* (2020) 9(2):269–79. doi: 10.21037/tlcr.2020.03.17

37. Huang K, Dahele M, Senan S, Guckenburger M, Rodrigues G, Ward A, et al. Radiographic changes after lung stereotactic ablative radiotherapy (SABR) – can we distinguish fibrosis from recurrence? a systematic review of the literature. *Pract Radiat Oncol* (2013) 3(2 Suppl 1):S11–2. doi: 10.1016/j.prro.2013.01.039

38. Hopstaken JS, de Ruiter JC, Damhuis RAM, de Langen AJ, van Diessen JNA, Klomp HM, et al. Stage I non-small cell lung cancer: Treatment modalities, Dutch daily practice and future perspectives. *Cancer Treat Res Commun* (2021) 28:100404. doi: 10.1016/j.ctarc.2021.100404

Frontiers in Oncology

Advances knowledge of carcinogenesis and tumor progression for better treatment and management

The third most-cited oncology journal, which highlights research in carcinogenesis and tumor progression, bridging the gap between basic research and applications to imrpove diagnosis, therapeutics and management strategies.

Discover the latest Research Topics

See more →

Frontiers

Avenue du Tribunal-Fédéral 34
1005 Lausanne, Switzerland
frontiersin.org

Contact us

+41 (0)21 510 17 00
frontiersin.org/about/contact